Imperial College London
Department of Mechanical Engineering

Non-linear System Identification in Structural Dynamics:

Advances in Characterisation of Non-linearities and Non-linear Modal Analysis

Václav Ondra

September 2017

This thesis is submitted for the degree of
Doctor of Philosophy

Lucince

Abstract

Many new methods for theoretical modelling, numerical analysis and experimental testing have been developed in non-linear dynamics in recent years. Although the computational power has greatly improved our ability to predict non-linear behaviour, non-linear system identification, a central topic of this thesis, still plays a key role in obtaining and quantifying structural models from experimental data.

The first part of the thesis is motivated by the industrial needs for fast and reliable detection and characterisation of structural non-linearities. For this purpose a method based on the Hilbert transform in the frequency domain is proposed. The method detects and characterises structural non-linearities from a single frequency response function and does not require a priori knowledge of the system.

The second part of the thesis is driven by current research trends and advances in non-linear modal analysis and adaptive time series processing using the Hilbert-Huang transform. Firstly, the alternatives of the Hilbert transform, which is commonly used in structural dynamics for the estimation of the instantaneous frequency and amplitude despite suffering from a number of numerical issues, are compared to assess their potential for non-linear system identification. Then, a possible relation between the Hilbert-Huang transform and complex non-linear modes of mechanical systems is investigated. Based on this relation, an approach to experimental non-linear modal analysis is proposed. Since this approach integrates the Hilbert-Huang transform and non-linear modes, it allows not only to detect and characterise structural non-linearities in a non-parametric manner, but also to quantify the parameters of a selected model using extracted non-linear modes. Lastly, a new method for the identification of systems with asymmetric non-linear restoring forces is proposed. The application of all proposed methods is demonstrated on simulated and experimental data.

Acknowledgements

First of all, I would like to thank my supervisor Dr Christoph W. Schwingshackl for giving me the opportunity to work and study in an excellent research environment, managing the funding, and supporting me during my stay at Imperial College London. I would also like to express my gratitude to Dr Ibrahim A. Sever from Rolls-Royce plc for giving his comments on numerous issues.

I own thanks to many researches, colleagues and friends from Vibration University Technology Centre, some of them for their constructive criticism of my early work by which they, maybe unknowingly, motivated me to pursue this research, some of them for creating a pleasant working environment that made my studies enjoyable experience.

I would like to also mention my six-week stay at Non-linear Mechanics and Dynamics Research Institute supported by Sandia National Laboratory in New Mexico. I am grateful to Dr Matthew R. W. Brake for inviting me to participate and to all the great people I met there for sharing this amazing experience with me.

I would like to thank Dr Luca Pesaresi for sharing the experimental data from an under-platform damper test rig used in chapter 2, and Dr Pavel Polunin and researchers from Stanford University for providing the experimental data from a micro-electro-mechanical resonator used in chapter 6.

I would also like to express my gratitude to Professor Gaëtan Kerschen from University of Liège and Professor Peter Cawley from Imperial College London for being my examiners, taking time to review this thesis and for their valuable comments.

Special thanks belong to my whole family, especially to my parents for supporting me in all my decisions.

Lastly, I would like to express my most sincere love and gratitude to my wife, Lucy. Without her kindness, support and patience, this thesis would not have been possible. She has always been there for me when I needed and I am proud that I can be there for her.

Declaration of originality

I hereby declare that except where specific reference is made to the work of others, the contents of this thesis are original and have not been submitted in whole or in part for consideration for any other degree or qualification at this or any other university. This thesis is my own work and contains nothing which is the outcome of work done in collaboration with others, except as specified in the text and Acknowledgements.

Václav Ondra
September 2017

Table of contents

List of figures

List of tables

Nomenclature

Roman symbols

$a(t)$	Instantaneous amplitude
a_0	Initial amplitude
$A(\omega)$	Accelerance
$\mathbf{A}(\lambda)$	Dynamic stiffness matrix
b	Clearance threshold
b_1, b_2	Off-centre clearance thresholds
c_{nl}	Non-linear damping coefficient
$c(t)$	Intrinsic mode function
$\mathbf{c}_0$	Coefficients of the zeroth harmonic
$\mathbf{c}_k$	Coefficients of the cosine part of the k-th harmonic
$d(t)$	Logarithm of the instantaneous amplitude
e_{min}, e_{max}	Upper and lower envelope
E	Young's modulus
$f(t)$	Instantaneous frequency
f_{nl}, $\mathbf{f}_{\mathrm{nl}}$	Non-linear force and vector of non-linear forces
f_{s}	Sampling frequency
$F(t)$, $\mathbf{F}(t)$	Excitation force and vector of excitation forces
$\mathbf{F}_{\mathrm{e}}$	Vector of excitation force amplitudes
F_{el}, F_{d}	Elastic and dissipative restoring force
$G(\omega)$	Difference between a receptance and its Hilbert transform
$G(\mathbf{u})$, $\mathbf{G}(\mathbf{u})$	Objective function and a set of objective functions
$h(t)$	Proto-mode function

$H(\omega)$	Receptance
k_1, k_2	Bilinear stiffness coefficients
k_{nl}	Non-linear stiffness coefficient
l	Subscript of the lower part of a signal
L, W	Length of a beam and width of its cross section
m, c, k	Mass, damping and stiffness coefficients
M	Spectral moment of a frequency response function
$\mathbf{M}$, $\mathbf{C}$, $\mathbf{K}$	Mass, damping and stiffness matrix
n	Number of degree-of-freedom
N_{f}	Normal force
N_{h}	Number of harmonics
N_{HVD}	Number of components in the Hilbert vibration decomposition
N_{IMF}	Number of intrinsic mode functions
N_{N}	Number of neurons in the hidden layer
N_{sl}	Number of spectral lines
N_t	Number of time samples
O	Index of orthogonality
q	Modal amplitude
q_s, q_c	Normalisation amplitude of the sine and cosine part
$r(t)$	Residuum
$R_{H\tilde{H}}$	Cross-correlation between a receptance and its Hilbert transform
s	Continuation step
$\mathbf{s}_k$	Coefficients of the sine part of the k-th harmonic
$\mathbf{S}$	Scatter matrix
T	Period of vibration
t	Time
$\mathbf{t}$	Complex vector for phase normalisation
u	Subscript of the upper part of a signal
$\mathbf{u}$	Vector of unknowns
w	Weights

$x(t)$, $\dot{x}(t)$, $\ddot{x}(t)$	Displacement, velocity and acceleration
$\mathbf{x}(t)$, $\dot{\mathbf{x}}(t)$, $\ddot{\mathbf{x}}(t)$	Vectors of displacement, velocity and acceleration
$\mathbf{y}$	Extended vector of unknowns
$Y(\omega)$	Mobility
$z(t)$	Analytic signal
$\mathbf{z}$	Vector of unknown Fourier coefficients

Greek symbols

α, β	Coefficients of viscous proportional damping
γ	Function describes
$\mathbf{\Gamma}(\omega)$	Operator of the Fourier transform
δ	Damping rate
$\Delta\omega$	Frequency shift
ϵ	Small dimensionless parameter
ζ	Damping ratio
$\theta(t)$	Phase
$\Theta(t)$	Slow phase
$\kappa(t)$	Frequency modulation
λ	Complex fundamental eigenfrequency
λ_{W}	Smoothing parameter in the Whittaker smoother
μ	Friction coefficient
$\boldsymbol{\nu}$	Manifold
ρ	Density or length density
φ	Phase angle
$\phi(t)$	Fast phase
$\phi_{\mathrm{e}}(t)$	Excitation phase
$\boldsymbol{\phi}$	Estimated non-linear modes
$\mathbf{\Psi}$	Complex eigenvector
ω	Angular frequency
$\omega_{\min}$, $\omega_{\max}$	Minimal and maximal frequency of a frequency response function
Ω	Excitation frequency

Ω_{IFM}	Angular frequency of intra-wave frequency modulation

Other symbols

i	Imaginary unit
pv	Cauchy principal value of the integral
std($\bullet$)	Standard deviation
sgn($\bullet$)	Signum function
$\mathbb{I}_n$	Identity matrix of the size $n \times n$
$\nabla(\lambda)$	Differential operator
$\mathscr{H}\{\bullet\}$	Hilbert transform operator
$\Im\{\bullet\}$	Imaginary part
$\Re\{\bullet\}$	Real part
$\lvert\bullet\rvert$	Absolute value
$\lVert\bullet\rVert$	Euclidean norm
$(\,\cdot\,)$	Dot product
$(\,,\,)$	Interval boundaries
$\langle\,,\,\rangle$	Operator of generalised Fourier coefficients
$\otimes$	Kronecker tensor product
$\bullet^{+}$	Moore-Penrose pseudo-inverse
$\bullet^{\dagger}$	Organised vector of the time samples
$\bullet^{\mathrm{H}}$	Hermitian (conjugate) transpose
$\bullet^{\mathrm{T}}$	Transpose
$\hat{\bullet}$	Estimated functions
$\tilde{\bullet}$	Hilbert transform
$\bullet^{*}$	Complex conjugate
$\bar{\bullet}$	Mean value

Acronyms

AFT	Alternating frequency-time procedure
AM	Amplitude modulation
ANN	Artificial neural network
CEEMDAN	Complete ensemble empirical mode decomposition with adaptive noise

CNM	Complex non-linear mode
CRP	Conditioned reverse path
CxA	Complexification-averaging
DEO	Differential energy operator
DIC	Digital image correlation
DOF	Degree-of-freedom
DQ	Direct quadrature
EEMD	Ensemble empirical mode decomposition
EMA	Experimenal modal analysis
EMD	Empirical mode decomposition
FE	Finite element
FEM	Finite element method
FFT	Fast Fourier transform
FM	Frequency modulation
FNSI	Frequency domain non-linear subspace identification
FORSE	Force response suite
FRF	Frequency response function
GZC	Generalised zero-crossing method
HBM	Harmonic balance method
HEO	Higher-order energy operator
HHSA	Holo-Hilbert spectral analysis
HHT	Hilbert-Huang transform
HT	Hilbert transform
HTD	Hilbert transform describers
HVD	Hilbert vibration decomposition
IA	Instantaneous amplitude
IF	Instantaneous frequency
IFM	Intra-wave frequency modulation
IMF	Intrinsic mode function
IMO	Intrinsic modal oscillations

LDV	Laser Doppler vibrometry
MAC	Modal assurance criterion
MDOF	Multi-degree-of-freedom
MEMS	Micro-electro-mechanical system
NARMAX	Nonlinear autoregressive moving average model with exogenous inputs
NHT	Normalised Hilbert transform
NIFO	Non-linear identification through feedback of the output
NLI	Non-linearity index
NNM	Non-linear normal mode
NPR	Non-causal power ratio
OMA	Operational modal analysis
PC	Principal component
PCA	Principal component analysis
PCS	Principal component scores
RFS	Restoring force surface
ROM	Reduced order model
SDOF	Single-degree-of-freedom
SNR	Signal-to-noise ratio
STFT	Short-time Fourier transform
TEO	Teager energy operator
TNSI	Time domain non-linear subspace identification
WGC	Weighted global criterion method
WT	Wavelet transform
ZC	Zero-crossing method
ZC	Zero-crossing
ZCA	Zero-crossing method for systems with asymmetric restoring forces

Introduction

It is widely acknowledged that non-linearity is an important and often inherent feature of a large majority of engineering structures while linear behaviour is a rare exception. It is of a paramount importance to distinguish between linear and non-linear systems because non-linear systems usually possess a wide range of phenomena which are completely unknown in linear theory. These phenomena can either lead to potentially catastrophic consequences if unexpected resonances emerge or bring major improvements to dynamic performance of structures if, for instance, an increase in damping or change in stiffness reduces the response amplitude or shifts the resonance frequency. Therefore, should the modern designs meet the ever-increasing demand for reliable performing structures, the effect of structural non-linearities on vibration behaviour must be systematically and thoroughly considered.

In recent decades, non-linear structural dynamics has been a fruitful research area in which many new methods for theoretical modelling, numerical analysis and experimental testing of non-linear systems have been developed. It is therefore rather surprising that non-linear dynamics is not commonly used to design new technologies. Linear behaviour is almost always taken for granted and the presence of non-linearity is often ignored. This is arguably given by the complexity of non-linear problems, limited understanding of physical nature of structural non-linearities and by the lack of a widespread universal methodology to model, analyse and experimentally test non-linear systems.

Whilst recent advances in the theoretical modelling and numerical analysis greatly improve our ability to predict non-linear vibration behaviour in a timely and inexpensive fashion, the experimental testing and associated system identification still play a key role in the process of creating and validating numerical models. The non-linear system identification refers not only to the estimation of model coefficients, but also to a development (or improvement) of a mathematical (structural) model with no a priori knowledge of non-linearities. Due to the complicated nature of non-linear systems, difficulties of their experimental testing and the fact that it is an inverse problem, the non-linear system identification is most likely one of the most challenging tasks in non-

linear dynamics. The non-linear system identification is usually structured in three parts - detection of structural non-linearity, its characterisation and quantification. The aim of detection is to find out whether any structural non-linearity exists in a system and ideally to give an indication of its strength, i.e. whether it has weak or strong effects on the dynamic behaviour of the structure. The aim of characterisation is to specify the type, spatial location and functional (mathematical) form of the detected non-linearity. The characterisation is probably the most challenging step in non-linear system identification since non-linearities can originate from multiple different sources. Once this crucial step has been performed, quantification, the last step in the identification process, estimates the coefficients of the non-linearities while ideally considering the uncertainty of the model and measured data. If non-linear system identification is successful, a structural model with a good predictive accuracy is obtained.

Although a significant effort has been made to develop a reliable non-linear system identification methodology, there is no method applicable to all possible non-linear systems and excitation types. A central topic of this thesis is the development of new methods for non-linear system identification, with a particular focus on detection and characterisation of structural non-linearities, and advances in non-linear modal analysis.

Objectives

Two main objectives of the thesis are

1. *Enable robust and fast detection and characterisation of non-linearity from a single frequency response function in an industrial environment*

   A large amount of data is usually collected in industry during the experimental testing of mechanical components. These data are often obtained in terms of frequency response functions to allow their convenient analysis using well-established methods of experimental modal analysis. It is often assumed that the system is linear even if non-linear behaviour is suspected based on the engineering knowledge of the problem, but no systematic detection of non-linearity is usually carried out. Therefore, the first objective of the thesis is to develop a method for detection of structural non-linearities that could be used as a pre-step of linear modal analysis to verify the assumption of the linear behaviour. If a non-linearity has been detected, the method should also provide an insight into the type of this non-linearity. To comply with compatibility requirements, the method must operate on a single frequency response function and it must be robust against measured

noise. In addition, the method should be suitable for an industrial use, avoiding expertise decision making and minimising the processing time. The versatility of the developed method should be demonstrated on a number of numerical and experimental cases.

2. *Develop an approach to experimental non-linear modal analysis by investigating the use of time-frequency methods based on instantaneous frequency and amplitude and their possible relation to one of the concepts of non-linear modal analysis*

   A more general concept of time-frequency analysis offers a broader range of possibilities than the processing of frequency response functions, especially due to the adaptive processing of measured time domain data that requires no a priori knowledge of the system. The Hilbert-Huang transform is arguably the most popular and successful method for instantaneous frequency and amplitude estimation. However, it still possesses several limitations, including a lack of rigorous mathematical background and its practical inability to identify systems with asymmetric restoring forces. The second objective of this thesis is to examine the possibilities of the Hilbert-Huang transform for non-parametric non-linear system identification and to remove some of its limitations. In particular, it should be attempted to connect the Hilbert-Huang transform with one of the available concept of non-linear modal analysis. If such connection is possible, an approach to non-linear modal analysis which uses the Hilbert-Huang transform to estimate the non-linear modes of the structure should be developed, numerically verified and experimentally demonstrated.

The first objective of the thesis addresses the current industrial needs for a quick and reliable detection and characterisation of structural non-linearities. The second objective, on the other hand, is driven by the desire for a scientific progress and is motivated by current research trends in the fields of non-linear system identification and non-linear modal analysis.

Outline of the thesis

A state-of-the-art review is conducted in chapter 1. Firstly, the field of non-linear structural dynamics is briefly introduced and current approaches in theoretical modelling, numerical analysis and experimental testing are reviewed. Subsequently, the focus is on non-linear system identification, where several groups of methods are distinguished and the relevant ones are described in more detail to build a background for the rest of the

thesis. A particular focus is on detection and characterisation of structural non-linearities in the frequency domain, time-frequency analysis, and theoretical and experimental non-linear modal analysis. The limitations of the current approaches that are addressed in this thesis are identified at the end of chapter 1.

In chapter 2 a method for detection and characterisation of structural non-linearities from a frequency response function (FRF) is proposed. The robustness of the method against measured noise is investigated and the method is also applied to a simulated multi-degree-of-freedom system. Then, the method is used to detect and characterise non-linear behaviour from a number of experimentally obtained FRFs of a cantilever beam with a clearance non-linearity, an under-platform damper test rig and the ECL benchmark. Chapter 2 concludes by discussing advantages and disadvantages of the proposed method.

Chapter 3 firstly discusses why the frequency domain and frequency response functions do not necessary have to be the right approach to non-linear system identification. It also introduces concepts of time-frequency analysis in detail. A particular focus is on the group of methods concerned with the estimation of instantaneous frequency (IF) and amplitude (IA), especially on the Hilbert-Huang transform (HHT). Both parts of the HHT, i.e. the empirical mode decomposition (EMD) and methods for instantaneous frequency and amplitude estimation, are described. The main problems of the EMD are discussed in detail and several approaches to overcome these problems are introduced. It is also shown how the frequency resolution of the EMD can be investigated before applying the EMD. This also allows closely spaced vibration modes to be defined. Traditionally, the estimation of instantaneous frequency and amplitude is carried out using the Hilbert transform. However, the Hilbert transform suffers from a number of mathematical and numerical issues, and can be sometimes replaced by different methods. These methods are assessed in detail and it is shown that while all the methods provide equivalent results after low-pass filtering or other smoothing, each method has unique features that can be used to detect and characterise the non-linearity. Based on this assessment, a method for characterisation of stiffness non-linearities based on the intra-wave frequency modulation is proposed at the end of chapter 3.

The lack of mathematical background of the Hilbert-Huang transform is addressed in chapter 4. It is discussed that the physics-based foundation was already established by showing the correspondence between the intrinsic mode functions (IMFs) and slow-flow dynamics. However, no connection to one of the concepts of non-linear modal analysis has been proposed yet. This chapter attempts to provide the missing link by showing the relation between complex non-linear modes (CNMs) and the HHT. The approximative

relation is highlighted by investigating the correspondence between the IMFs and reduced order model of slow-flow dynamics derived from the CNMs. As this link cannot be proven analytically, it is evidenced using a number of numerical studies. It is found that the relation between the HHT and CNMs is only approximative, i.e. the HHT is unable to recover correct non-linear modes from transient data. This finding limits the accuracy of non-linear modal analysis approach described in the following chapter.

Chapter 5 proposes an approach to non-linear modal analysis in which non-linear modes are used to detect, characterise and quantify the non-linearity. The method firstly detects and characterises the type of structural non-linearity using the Hilbert-Huang transform. The quantification of non-linearity is then carried out through the optimisation of a selected structural model. The final output of the method is a model of the structure with fully identified linear and non-linear parameters. The validity and limitations of the suggested approach are examined on several numerical cases. The method is then demonstrated on the experimental data obtained from the ECL benchmark.

The inability of the Hilbert-Huang transform to deal with systems with asymmetric non-linearities is addressed in chapter 6. A proposed method, named zero-crossing method for systems with asymmetric restoring forces (ZCA), is an extension of zero-crossing method of the instantaneous frequency and amplitude estimation. This method treats the upper and lower part of the resonant decay response separately and allows identification of amplitude-dependent natural frequency, damping and restoring forces. The ZCA is demonstrated on a number of numerical validation cases for which it is shown that the results are equivalent to those obtained by the Hilbert vibration decomposition (HVD). The proposed method and the HVD are also applied to experimental measurement obtained from a micro-electro-mechanical system.

The last chapter summarises the thesis, revisits the most important findings and evaluates the research objectives. It also states the main original contributions of the presented research work. Lastly, the avenues of the future research in non-linear system identification that directly relate to this thesis are suggested.

The thesis is accompanied by three appendices. Appendix A aims to provide a complete list of non-linear system identification methods with their functions (detection, characterisation or quantification) and a few relevant references. Appendix B describes the numerical implementation of the complex non-linear modes whose theoretical background is presented in chapter 4. Appendix C describes the Whittaker smoother that is used throughout the thesis for the smoothing of experimental data.

Chapter 1

Literature review

Abstract

This chapter provides a brief, non-mathematical introduction to non-linear dynamics and non-linear system identification. Firstly, non-linear dynamics is introduced and the effects and sources of structural non-linearities are discussed. Then, the basic skills and processes that are required for a successful solution of structural vibration problems, i.e. theoretical modelling, numerical analysis and experimental testing, are briefly reviewed. However, the main objective of the chapter is to review the available methods and approaches to non-linear system identification and to identify possible avenues of the development with regards to the objectives of the thesis. Firstly, the non-linear system identification is structured into detection, characterisation and quantification and the most important methods and concepts are surveyed. Then, non-linear system identification methods are categorised based on their features. The main focus is on the frequency domain methods, time-frequency analysis and non-linear modal analysis, because these groups of methods will be used in other chapters. At the end of this chapter, the limitations of the existing approaches that are addressed in this thesis are summarised.

1.1 Non-linear structural dynamics

Non-linear structural dynamics is a study of mechanical motion, forces and their relations in a non-linear structure. The subject of non-linear dynamics is externally broad with a vast mathematical theory [89, 158] and applications ranging from biology to engineering [258]. Mathematically, the non-linear dynamics could be regarded as a study of any set of non-linear differential equations that model a system [271, 281]. In structural engineering the mathematical models, often called structural modes, have a certain, well established form consisting of mass, damping and stiffness matrices, which represent an underlying linear system, accompanied by non-linear restoring forces [63, 119, 158]. The non-linear restoring forces can depend on the displacement or velocity and can be described by many parameters. It is widely acknowledged that non-linearity is an important and often inherent feature of a large majority of systems. In contrast, linear behaviour is a rare exception, which, however, is often assumed due to its mathematical elegance. The non-linear effects are often neglected in practical applications, owing partly to the complexity of non-linear dynamics. However, it is important to distinguish between linear and non-linear systems because non-linear systems possess a number of features unknown in linear theory, for instance

- The dynamics of non-linear systems may be much richer, featuring phenomena that cannot be observed in linear systems. For instance, several stable equilibrium positions, sudden changes in overall dynamics with a small perturbation of parameters (jumps, bifurcations) or internal resonances (transfer of energy between modes).

- The non-linear system can respond in a number of ways depending on the initial conditions. For example, a simple experimental set-up from [273] (essentially a Duffing oscillator) was shown to exhibit limit cycles, bifurcations, chaotic behaviour and a strong dependence of steady state responses on the initial conditions.

- Fundamental properties of linear systems are lost, including the principle of superposition and the force invariance (or even a rigorous definition) of frequency response functions. All of such properties are discussed in more detail in section 1.2.1 while reviewing methods for detection of structural non-linearities based on the violation of these fundamental principles.

- The modal properties (frequency, damping and mode shapes) that are widely used for the analysis of linear systems are no longer invariant to vibration amplitude. This is a very important feature of non-linear systems that prevents linear modal analysis. The amplitude-dependence of modal properties is a direct consequence

of the principle of frequency-energy dependence [119], which is also responsible for non-existence of analytical solutions of damped non-linear vibration [186] or non-linear mode localisation in arrays of oscillators [267].

- Chaotic behaviour can occur even in systems with simple configurations, such as a double pendulum or Duffing oscillator. Deterministic chaos is seemingly unpredictable, irregular and random-like motion extremely sensitive to initial conditions. At the same time, however, the system is deterministic in a sense that there are no stochastic variables or effects. Although the chaotic systems are also studied in mechanical engineering [154, 258], no chaotic behaviour is further considered in this thesis.

There are many sources of non-linearities in mechanical systems [119, 289], including

- *Geometric non-linearity* originates from the potential energy as a consequence of large displacements, often observable in highly flexible structures, such as beams, cables, plates or shells [179]. The geometric non-linearity can generally occur anywhere in a system, i.e. it is not localised in a specific spatial coordinate(s), but rather distributed in the structure. However, studying such a type of non-linearity is extremely difficult and time-consuming, so it is often avoided by modelling the effect of the distributed non-linearity using localised non-linear elements. Geometric non-linearities are described by polynomial models that are often based on the Taylor series approximation of a more complicated non-linearity. In particular, the cubic hardening stiffness is often studied, because while it is described by a relatively simple polynomial model, it gives a rise to many complex phenomena [273].

- *Non-linear material properties* are often inherent properties of materials. Unlike the geometric non-linearity that becomes relevant under high loading, these non-linearities can be activated under arbitrary loading conditions. Non-linear material behaviour is commonly exhibited, for example, by rubbers and foams [246, 280]. The dynamic analysis of these non-linearities has not received so much attention in the past because the behaviour can be commonly approximated by simpler non-linear models that can introduce very comparable effects.

- *Non-linear dissipative effects* are responsible for the loss of energy so that the vibration is eventually damped if no external force is acting in the system. In linear systems, all dissipative effects, which can originate from air resistance or material dissipation, are usually included in the damping matrix. However, the dissipative mechanisms are not well understood even in the linear domain where

several damping models exist [63]. The proportional viscous damping is the most commonly used model, which assembles the damping matrix as a linear combination of the mass and stiffness matrices. In non-linear dynamics, the linear damping is still present, but in addition to it, there may be many non-linear dissipative effects. Non-linear dissipation can be an inherent characteristic of the material, but is also exhibited in frictional interfaces and joints. The energy dissipation in joints and interfaces is arguably the most frequent cause of non-linearity in real-life structures. Even without bolts, the structures must have some connections or assemblies that experience some level of friction between them. Despite intensive research, many challenges in reliable modelling of joints remain and some of them appear to be almost unsolvable. This fact led to suggestions to change the philosophy of joint modelling completely [64].

- *Non-linearities from external sources* include all non-linearities which are not properties of the structure, but still influence its behaviour. For example, boundary conditions can be non-linear due to presence of the fluid or other objects. In addition, there may exist external fields, such as electromagnetic field, which can cause non-linear behaviour of otherwise linear structure.

- *Non-linearities in the measurement chain* may be associated with the experimental testing of structures. They can arise from a shaker-structure interaction, bolt looseness, unwanted pre-stresses effects or poor transducer mounting. In practice, as much effort as possible should be invested into avoiding them or minimising their consequences. In laboratory testing, this type of non-linearities should be avoided completely by using state-of-the-art equipment and acquisition software [289].

The non-linearity can often generate negative and unwanted effects. For example, in a vehicle brake squeal problem the steady sliding frictional interface can become unstable, generating vibration and noise in the process [122]. On the other hand, the same effect, called friction-induced vibration, generates sound in musical stringed instruments [149]. There are also some important applications where the non-linearity is essential for the proper function and is purposefully introduced [27]. For example, under-platform dampers in aircraft engines [198] are designed to dissipate energy through frictional interfaces and to cause a frequency shift of the resonance frequency. It can be assumed that to meet the increasing demand for better performing structures, the non-linearities will have to be more and more utilised in the future.

The basic skills required for a successful solution of a structural problem have been reviewed in [64] and are summarised in Fig. 1.1. Three basic skills are *theoretical*

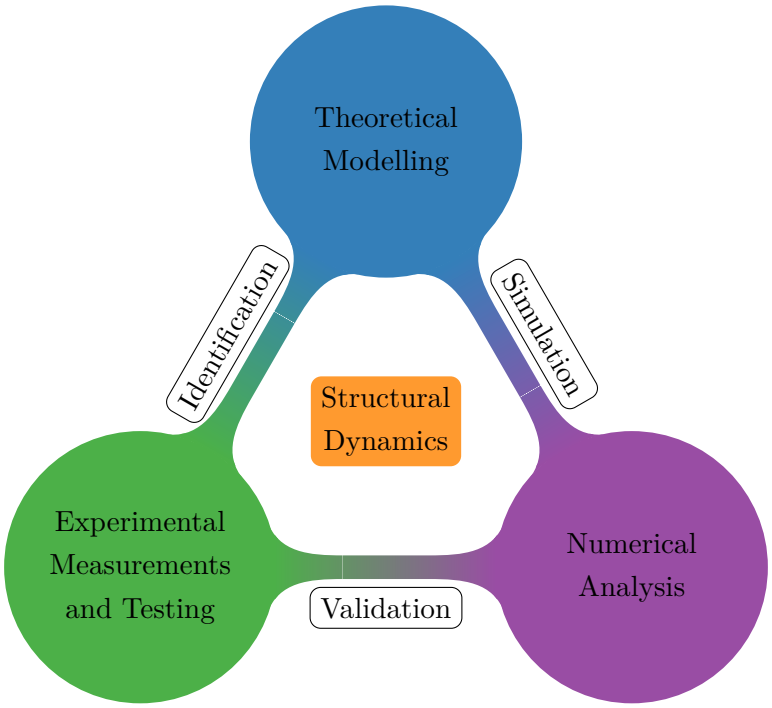

Figure 1.1 Three basic skills and procedures required for a successful solution of a structural problem

modelling, *numerical analysis* and *experimental modelling*, but for the successful solution of a dynamical problem, they cannot be exercised separately. The combination of theoretical modelling and numerical analysis is often referred to as a *simulation* and the simulated results should always be *validated* to ensure that the analysis provided desired and reasonably accurate results. In contrast to verification, which ensures that applied mathematical procedures generated mathematically correct results regardless of their relevance to reality, the validation always requires experimental measurements. The experimental testing is also related to the theoretical modelling through the *non-linear system identification*. Non-linear system identification is sometimes considered as the internal part of validation and verification [119]. However, this classification is not accurate, because the main focus of non-linear system identification is on the development (or providing the information necessary for the development) of structural models from experimental measurements. Non-linear system identification in structural dynamics is a central theme of this thesis and is reviewed in detail in section 1.2. However, to give a wider background of non-linear dynamics three basic skills are firstly briefly reviewed.

1.1.1 Theoretical modelling

Theoretical modelling of non-linear systems usually requires a deep understanding of the physics of the problem and the ability to define a set of equations that describes the structure. In structural dynamics, the basic form of the governing equations of motion is well established, consisting of mass, damping and stiffness matrices that model the underlying linear system, a matrix of non-linear restoring forces that accounts for the effects of structural non-linearities and a vector of excitation forces. These matrices describe discretised structures, but some simpler geometries, such as beam, plate or shells can also be adequately modelled by continuous models [179].

Besides the classical lumped parameters models for simpler structures, the *finite element method* (FEM) has emerged as a dominant means of high fidelity modelling. This method allows discretisation of the geometry of a structure using the finite number of elements which are used to assemble the mass and stiffness matrices. The FEM is used in virtually every branch of engineering and many commercial packages exist, allowing a wide range of numerical solutions and analyses. However, very few of them allow dynamical analysis of non-linear systems, thereby contributing to a limited number of applications of non-linear dynamics in practice. In order to deal with non-linear dynamical problems, the FEM is usually used to assemble the model of the underlying linear system (mass and stiffness matrices) and linear dissipative effects (damping) and non-linearity are modelled separately. The complete set of equations is then solved by numerical methods (section 1.1.2) which are usually implemented in in-house software.

The crucial problem arises when trying to describe the non-linearity via mathematical models. Each source of non-linearity is represented by a different model and in some cases, such as joints and interfaces, many competitive models have been developed. There are several common models of localised non-linearities:

- *Polynomial approximation* [12, 119, 289] is the simplest functional form that can describe many non-linearities accurately. However, there are classes of non-linearities, such as non-smooth ones, which can be approximated by the polynomial expressions only if very high order polynomials are used which requires many coefficients to be identified. The polynomial approximation does not necessary have to be always the best choice because it might not represent the physical mechanism of non-linearity.

- *Non-integer exponent-type models* have been used in some cases as an alternative to polynomial approximation to describe the restoring forces with higher accuracy [218]. Such models were used for the modelling of rubber isolators [219], visco-elastic materials [231, 246, 280] or the ECL benchmark in [115, 139]. Besides these

models, *cubic splines* [51, 56, 165] can also offer very high flexibility in cases where polynomial approximation is not sufficient.

- *Black-box models* are used in situations where no information about the system is available. These general models can describe practically any (linear or non-linear) behaviour of a system based on its inputs and outputs. However, the key limitation is a lack of any information about the physics that governs the dynamics of the problem. The black-box models are often used in system identification via machine learning [286], in particular the artificial neural networks (ANN) has been successfully applied [21, 35, 287]. Unlike black-box models, the *gray-box models* combine a partial theoretical knowledge of the system with measured data to identify the most appropriate model. Thus, most of the models used in non-linear system identification could be regarded as gray-box models, because almost always some knowledge of the non-linearity is available from the physical understanding of the problem and the existence of underlying linear system is assumed. To complete the list, it should be mentioned that sometimes the term *white models* is used for models that are purely theoretical so they do not build on, nor are supported by any experimental data.

- *Hysteresis models* describe behaviour of structures with inelastic restoring forces. These restoring forces cannot be defined through the instantaneous state variables of the system, because there is a lag in the arrival of the output with respect to input or the output depends on the history of the input [272]. A number of models describing the hysteresis effects in mechanical systems has been developed [7, 105, 247] and corresponding system identification methods have also emerged [282, 285].

- *Models of joints and interfaces* have received substantial attention of a research community due to their presence virtually in any mechanical system. Since bolted joints and interfaces are understood to have system-level dependencies, and because there has not been an established methodology for joints modelling, there is great diversity in joint models [24, 88, 93]. These include detailed finite element models of joint components [120, 213], continuum element approaches using zero-thickness elements [111, 259], and thin-layer elements [52, 240], lumped models [81, 87, 230], whole-joint modelling using hysteresis elements [106, 236, 249], and node-to-node coupling with friction contact elements [196, 202, 235]. It was also argued in [64] that since no joint model has a required predictive capability that could be used during a design process of new products, the way of how the joints are designed and modelled might have to be radically re-thought in the future.

- *Specific models* of non-linearity are developed when it is required by a specific application and supported by a good understanding of the physics of the problem [27]. For example, *models of time-dependent degradation* [34] in a presence of seismic loading are used to assess the safety of structures during earthquakes and *models of breathing cracks* [79, 143] are used during structural health monitoring.

The creation of the underlying linear model using the FEM is nowadays well established and verified process. It does not usually present any significant challenge and the predictive capability of linear models is guaranteed. A good theoretical model of a non-linear system should be predictive as well, it should also reflect the true nature of the system and be described by the parameters that can be easily measured or estimated from measured data. Unfortunately, these premises are very rarely achieved, because the physical understanding of many non-linear phenomena is not yet sufficient. This is one of the reasons why non-linear system identification, a central topic of this thesis, is still very important at this time when the computational modelling is so widely spread.

1.1.2 Numerical analysis

The numerical analysis is concerned with the solution of the set of equations, which has been obtained by theoretical modelling, in order to provide required insight into the problem in a reasonable time. Many analytical, approximative and numerical procedures have been developed to reflect very rich nature of non-linear systems. It would be ideal to solve dynamical problems analytically, thereby obtaining close-form exact or approximative solutions. Unfortunately, the approximative close-form solutions are available only for a small subset of conservative non-linear systems under quite restrictive conditions. The methods used for the analytical solution include *harmonic balance method*, *method of multiple scales* and *perturbation methods* [61, 89, 158].

The numerical methods have become absolutely dominant in recent years. One of the most intuitive, albeit very time consuming, numerical procedure is the *direct time domain integration* of equations of motions. This is generally not very appealing method due to the extremely long time required to obtain the time domain response which might not be very informative. On the other hand, it is not restricted to periodic excitation and any system with smooth or non-smooth non-linearities can be solved. In this thesis, numerically simulated data via direct time domain integration are used to replace the data from experimental measurements. Non-linear system identification methods can then be tested on such data to evaluate whether they were able to estimate the original model.

Most of the numerical methods in mechanical engineering are concerted with the computation of periodic solutions, including *time domain shooting technique* [257], *simulated stepped-sine experiment* [63] or *orthogonal collocation method* [112]. One of the most popular methods for the computation of steady state periodic forced responses is, however, the *harmonic balance method* (HBM) [158], also known as the *Fourier–Galerkin method* [54]. The method approximates the steady state solution using the Fourier series in which a specific number of harmonics can be retained and coefficients of these harmonics are then computed. Due to its long use, the numerical implementation has been well optimised, including the condensation of equations of motion into non-linear degrees of freedom [156, 202] (one of the reason why localised non-linearities are often used), alternating frequency-time procedure [29, 227] which allows effective evaluation of any non-linear forces in the frequency domain, and the analytical computation of Jacobian matrices to reduce the number of numerical operations [201]. The HBM is also coupled with a *numerical continuation* [178, 239] (also known as *path-following methods*) which allows to track the evolution of the periodic solutions with respect to the frequency or other parameter. The numerical continuation uses a predictor to approximate the next solution, a corrector to accurate the predicted solution and a means of controlling the distance between solution points. The HBM has been extensively used for gas turbine structures [129, 202, 203, 228], joint and contact problems [107, 198, 274] or satellite structure [53, 54]. The HBM is also used throughout this thesis to generate frequency response functions (FRFs).

A modified version of the harmonic balance method is also adopted for the computation of non-linear modes of non-conservative autonomous dynamical systems in [127, 134, 135] and chapter 4. A considerable number of other numerical methods for a different concepts of non-linear modal analysis (reviewed in section 1.3.3) was recently reviewed in [215]. Because the complex non-linear modal analysis is one of the central topics of this thesis and because it has not yet been so widely used, its numerical implementation based on a modified version of the harmonic balance method is described in appendix B.

1.1.3 Experimental measurements and testing

Whilst the theoretical modelling and numerical analysis greatly improve our ability to predict behaviour of structures in timely fashion, the experimental measurements and testing still play a key role in the process of creating and validating numerical models. The experimental vibration testing is conducted on daily basis in both experimental (laboratory) and operational environment. The goal of the laboratory testing is to provide data to create and validate the structural model, whereas operational testing provides

data mostly for structural health monitoring. A wide range of hardware and software is available and many test procedures have been developed [26, 63, 273, 289].

Traditionally, the vibration data are acquired using contact accelerometers or strain gauges [170]. These technologies are relatively cheap, accurate, easy to use and set up. On the other hand, they have the disadvantage of being contact measurements, so they might sometimes influence the structure which is being tested. Also, it does not have to be always possible to connect them to the structure.

More recently, a range of other measurement methods has been utilised to acquire time domain data of vibrating structures. For example, the use of laser Doppler vibrometry (LDV) is already quite common [33]. It offers precise velocity measurements that are performed in a non-contact manner so there is no influence of the dynamics. The LDV has been used for modal analysis [251, 252] or investigation of joint structures [55, 224], including under-platform damper measurements [196–198] presented in section 2.5.

The digital image correlation (DIC) which processes a series of quick snapshots of the movement has gained some popularity too. The lasers are replaced by cameras or high speed cameras whose records are processed to obtain relevant information about vibration behaviour. This type of measurements shows a great potential and have been used in a number of applications, including modal analysis [90], structural model updating [276] or non-linear dynamics [58, 199]. Both lasers and cameras are contact-less measurements so they do not influence the structure. However, their application in an operational environment is very limited due to their high price and the fact that the structure must be clearly visible to them.

Regardless of measurement hardware the experiments must be designed in such a way that all unwanted effects are reduced as much as possible [55]. Besides the best practices of modal analysis, such as sensor placing or excitation attachment [63], particular care must be taken in non-linear dynamics to set-up a test rig very accurately [273]. Even seemingly small discrepancies can significantly influence non-linear behaviour. For example, the ECL benchmark [261] has been used by many research groups and despite being very simple, it was observed that the smallest changes in the design can alter the dynamic of the structure. A slight pre-stress can change a typical hardening behaviour to softening at low amplitudes [85, 168].

Leaving aside the design and manufacturing of the test rigs in which many uncertainties can arise, the problems with the excitation and boundary conditions must be considered. For the experimental testing of non-linear systems, the choice of excitation heavily influences the quality of acquired data and system identification possibilities. For example, for the testing of steady state responses, the sine wave excitation is preferable.

While this can produce high quality steady state responses, it is not suitable for the estimation of modal properties of the structure. The choice of boundary conditions is also important and is often discussed in books about experimental testing [63]. As a rule, the attention should be paid to minimise the influence of any external effects on the structure so that the phenomenon of interest can be isolated and studied.

In general, it seems that the acquisition of vibration data does not present a challenging task any more if appropriate hardware and software are available. A large amount of data can be easily obtained even for complex structures, such as aircraft engines [238]. On the other hand, the processing, interpretation and system identification based on the measured data still appear to be very difficult tasks. The data used in this thesis are frequency response functions measured using a stepped-sine excitation and time domain free decays, i.e. no random excitation has been used.

1.2 Non-linear system identification in structural dynamics

Non-linear system identification refers to not only estimation of model parameters, but also to establishment (or improvement) of the model with no a priori knowledge of the system [119]. Some of the methods, therefore, require a model of the structure to be defined beforehand. Such methods are sometimes referred to as *parametric*, whereas methods that do not require a model are termed *non-parametric*. The non-parametric methods attempt to create a model of a non-linear system based on the data without any a priori knowledge of the non-linear mechanism. Once the model of the structure has been found, it can be quantified in the same way as in parametric methods.

A wide range of methods for non-linear system identification have been developed to address the different nature of structural non-linearities, loading conditions and meet specific requirements. Non-linear system identification is usually divided into three main stages that are executed in a sequence. These are *detection*, *characterisation* and *quantification* as shown in Fig. 1.2. Detection aims to detect the presence of structural non-linearities in a structure and optimally to indicate to what extent these non-linearities influence the vibration behaviour of the structure. If no non-linearity is detected or if the non-linearity is very weak (in a sense that it does not have a significant influence on otherwise linear behaviour), the structure can be treated as linear and linear system identification can be used. If the non-linearity has been detected, it is further characterised. Firstly, the type of the non-linearity, which relates to the underlying non-linear mechanism, is established, then the spatial location of the non-linearity is

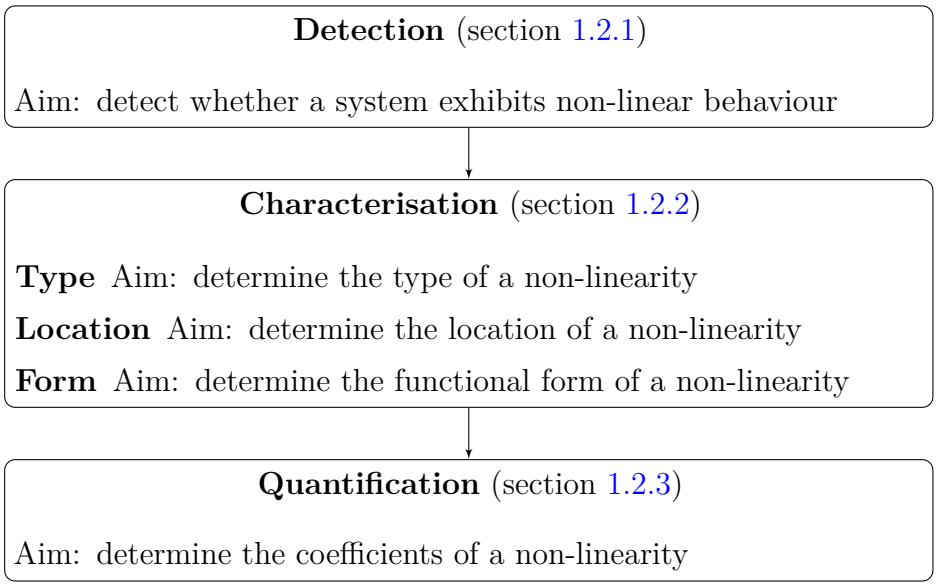

Figure 1.2 Identification process: detection, characterisation and quantification

found and a functional form which is used for a mathematical description is selected. Having detected and characterised the non-linearity, the model of the structures can be created and subsequently the parameters of the model can be quantified. It is also beneficial to consider the uncertainty of the obtained model. In parametric methods, detection and characterisation are not necessary since the model of the structure, including non-linearities, is already known.

Several books and review papers about non-linear system identification have recently been published, highlighting the active research interest in the field [2, 20, 30, 31, 119, 164, 289]. A brief review of the most relevant methods is conducted in the following. A more complete list of methods with their range of applicability and relevant references can be found in appendix A.

1.2.1 Detection

Detection of structural non-linearities is the first step in the identification process. It aims to discover non-linear behaviour in a structure and, optimally, to indicate (or quantify) to what extent this non-linearity influences the vibration behaviour of the structure. If no or very week non-linearity has been found, the structure can be treated as linear and well-established methods for linear system identification can be used instead. Numerous methods for detection can be found in the review papers [2, 30, 31, 119, 164] and also in in-depth survey papers focusing closely on detection [97, 269].

The available detection methods can be grouped into the methods which look for the violation of basic linear principles, methods based on the linear modal analysis, and methods operating in the frequency domain. The first two groups of methods are briefly reviewed in the following. The third group is described in more detail in section 1.3.1. All methods from that group can be applied directly to a frequency response function and do not require modal analysis to be performed. The last group of methods is described separately in detail because it provides a background for chapter 2 that proposes a new method for detection and characterisation from a single frequency response function in order to achieve the first objective of the thesis.

The methods based on the violation of basic linear principles

Various concepts for the dynamic analysis of linear systems do not apply to non-linear systems so the violation of these basic principles enables detection of non-linearities. If a linear system is excited by a single frequency sine wave and is allowed to reach a steady state, it responses with a sine wave of the same frequency, but with a different amplitude. The distortion of the output sine wave indicates non-linear behaviour. The method which seeks such a distortion is sometimes referred to as the *harmonic distortion* test [289]. The distortion is caused by the presence of higher harmonics in the response and the *harmonic detection method* [150] can be used to assess the harmonic content of the output. If the output spectrum contains higher harmonics, in addition to the excitation frequency, the system is non-linear.

The *principle of superposition* is one of the fundamental principles of linear systems. It states that the response at a given place and time caused by two or more excitation forces is equal to the sum of the responses that would be caused by each excitation force individually. Despite the fact that the principle of superposition defines linear systems, its practical applicability to investigate whether the system is linear or not is limited as explained in [289]. In order to conclusively establish the linearity of the system, all possible combinations of excitation forces would need to be tried, which is clearly impossible. On the other hand, to show that the system is non-linear, only one combination that disproves the principle of superposition must be found, which might be less demanding task. Although the principle of superposition is a definite means of detecting the non-linearity, it is not usually applied. Instead, its modified version called homogeneity method, described in section 1.3.1, which can be used with conventionally measured frequency response functions is frequently applied.

The simplest test of linearity which is available in all commercial software packages for the experimental modal analysis or a frequency response measurement is the *Coherence*.

A detailed description of this method can be found in many signal processing books, for instance [19, 26, 63, 242]. Essentially, the coherence captures the quality of the transfer function estimated for a linear system. In an ideal case, the coherence is equal to one for all measured frequencies so its drop is considered as a sign of non-linearity. Unfortunately, a major issue is that the coherence is also strongly influenced by measured noise and there is no way to distinguish whether its drop was caused by measured noise or non-linearity.

The methods based on the experimental modal analysis

A number of detection methods is based directly on the experimental modal analysis (EMA) [268]. Such methods detect the presence of a non-linearity from the evolution of the modal parameters for different levels, types of excitation or amplitude of vibration. This underlying idea is utilised via so called *Linearity plot* [82] which is any visualisation of the independence of modal properties on a relevant factor, either type or level of excitation, amplitude of vibration or their combination. If the extracted modal properties are not independent to aforementioned factors, a non-linearity is present in the structure. The acquisition and processing of the data for this detection method can be unnecessary time-consuming because the complete experimental modal analysis must be performed in order to establish the presence of the non-linearity, which, however, renders the modal analysis irrelevant.

If the modal damping is estimated using the circle fit method then the so called *Carpet plot* can be constructed [63]. A carpet plot is a surface that depicts the dependency of the estimated damping on two frequencies, one before and one after the resonance, which were used for the damping estimation. If the damping is independent on these two frequencies, the surface is flat and the structure is deemed to be linear in damping. On the other hand, the variation of the surface indicate a damping non-linearity. The circle fit method requires the vibration modes of the structure to be well separated and the damping model to be selected.

The modal properties of closely spaced modes can be identified by well-established subspace identification methods [216] that are applied for the experimental and operational modal analysis. Often, the so called *stabilisation diagram* is used to find an appropriate order of the linear system. If the system is non-linear, the stabilisation diagram can be difficult to interpret and therefore can be used as an indication of non-linearity. The use of stabilisation diagrams to non-linear system identification was introduced as a part of the *frequency domain non-linear subspace identification* (FNSI) [162, 163] and *time domain non-linear subspace identification* (TNSI) methods [146, 169]. As both of these methods allow quantification of the non-linearity they are reviewed later in section 1.2.3.

If the mode shapes have already been estimated (by any EMA method), they can be used for detection using the *reciprocal modal vector* [41]. The reciprocal modal vectors are defined as the product of the mode shape vector and the mass matrix and it was shown, both numerically and experimentally, that estimated mode shapes and their corresponding reciprocal modal vectors are orthogonal to each other. Based on this orthogonality, a detection matrix, which is equal to an identity matrix for a linear, noise-free system, can be defined. Any deviations from an identity matrix may be caused by the non-linearity, but unfortunately, by any other analysis errors as well. As a consequence, this detection method may not be reliable in practical applications.

Indication of the strength of the non-linearity

Sometimes, it may be important to know to what extent the non-linearity influence the behaviour of the structure. If the influence is minor, the system is almost linear and can be treated accordingly. On the other hand, when the non-linearity significantly influences the system behaviour, the use of linear approaches is bound to fail. Terms such as "weak non-linearity" and "strong non-linearity" are often used in publications without any definition. Although some methods which provide an insight into the strength of the non-linearity are available, the definition of the strength of non-linearity is generally impossible since this quantification is application- and non-linearity type-dependent.

The most straightforward way to assess the strength of the non-linearity is to compare the measured characteristic to its known linear counterpart. Subsequently, a non-linearity index (NLI) which is usually zero for a linear system and non-zero (positive or negative) for a non-linear system can be defined. The strength of the non-linearity can be assessed from the absolute value of this index. The review of several non-linearity indexes based on the distortion of the frequency domain and time domain linear characteristics can be found in [97]. These include *coherence*, *bicoherence* and *higher order spectra* and their performance is compared on the Duffing oscillator. It is concluded in [97] that although the higher order spectra and associated statistics theoretically offer greater possibilities, their application is limited in a presence of measured noise.

The non-linearity index, termed *Non-linear modal grade* [244], is applicable to a single non-linear mode of vibration and it is defined as the ratio of the peak magnitude of the non-linear modal force and linear modal force. The ranges of the non-linear modal grade that determine weak, moderate and strong non-linear behaviour were proposed in [244]. Unfortunately, despite being suggested in line with an engineering practice, the thresholds are basically arbitrary without any support in theory. The non-linear modal

grade was proposed as a co-product of a more complex topic so its range of applicability has not been further investigated.

The *correlation-based indication functions* [289] can be used to compute the correlation matrices from measured time domain signals. These matrices are equal to zero for linear systems and the non-zero values are indicators of non-linear behaviour. Although the principle of the method is simple, the excitation must be a sine wave with an uncorrelated Gaussian noise which is a very restrictive requirement.

A non-linearity index which can be used in combination with the harmonic detection method is called the *Sig-function* [150]. This index is the ratio of the energy of the output harmonics and the total energy of the output for each frequency. It is claimed that a high harmonic content at low frequencies (high Sig-function) indicates a strong non-linearity, but no other information (such as the type of non-linearity) can be obtained. The Sig-function is amplitude-dependent so it might be difficult to establish its statistical significance.

The *linearity J-factor* [123] quantifies the strength of a non-linearity using a J-factor. Unlike most of non-linearity indexes the J-factor lies in the range 0 to 1, where 1 stands for the linear system. The J-factor is defined as a multiplication of three sub-factors that relate to the difference between the linear and non-linear FRFs qualified using bias errors. The excitation amplitude influences the size of this factor. With the exception of [123], no use of this factor can be found in literature.

Several non-linearity indexes can be proposed to quantify the difference between FRFs and their Hilbert transform. These indexes are reviewed in detail in section 1.3.1 and further discussed in chapter 2 where a few new indexes are proposed as well.

1.2.2 Characterisation

The aim of characterisation is to specify the type, spatial location and functional form of the non-linearities which have been previously detected in a structure (see Fig. 1.2). This step is necessary for the development of a structural model with a good predictive capability because it should provide a precise understanding of non-linear phenomena. Characterisation is arguably the most challenging step in the identification process since the non-linearity may be caused by many different mechanisms. A large number of characterisation methods exits and some of the most important are described in the following sections. A more complete list of methods can be found in the appendix A. This step might not be necessary if a model is known beforehand or a model can simply be created based on the physical understanding of the problem and its results compared to the measurements. If the match is not satisfactory, then the model can be changed and

validated again until the required accuracy is reached. Using this brute force procedure, the correct model of a structure can be eventually found. However, such a process may be very time-consuming and in general the procedure does not lead to a good predictive model since it might ignore all underlying physical mechanics.

Type characterisation

The first part of the characterisation process tries to establish the type of the non-linearity, i.e. to identify the underlying mechanics that causes the non-linear behaviour. Most of the methods in this group are based on subjective judgement, so in most cases, previous experience is required to characterise the non-linearity correctly.

Usually, the distortion of the measured data provides an insight into the type of non-linearity. For example, the distortion of *frequency response functions* [234, 268], *Volterra series* [36], *higher order FRFs* [28, 256] or *higher-order spectra* [44] can be used for a judgement about the non-linearity type. From all these possibilities, the FRFs are measured most often and when coupled with the *Hilbert transform in the frequency domain*, they provide a reliable means of type characterisation. This is reviewed in section 1.3.1 in detail since it creates a part of the method proposed in chapter 2.

Regardless of the measured function, the vast experience in the field is required to distinguish among possible types of non-linearities. To remove the need for this experience, a footprint library [83] (a collection of typical shapes) can be used. In addition, the idea of a footprint library presented in [83] utilised shape matching algorithms for a comparison of computed restoring force surfaces with the measured counter-pairs. This procedure avoids the subjective judgement, but measured noise has to be handled very carefully otherwise a very time-consuming matching algorithm might fail.

The methods that estimate non-linear modes can be often used for type characterisation too. These are reviewed separately in section 1.3.3 in mode detail because they are used later in the thesis.

Localisation of non-linearity

Localisation tries to find the spatial position of a non-linearity in a structure. Although the location of the non-linearity is clearly an important element for successful identification, very few methods for this task have been proposed.

The *type-analysis correlation* [141] locates the non-linearity via the correlation of a non-linear analytical model and measured vibration data. The model has to be known i.e. mass and stiffness matrices must be estimated or theoretically assembled and the measured data must be acquired in the coordinate of the non-linearity. If possible at

all, the latter may require the measurement of many coordinates to ensure that required non-linear data are obtained.

Some methods for non-linearity localisation are based on *damage localisation* [145] because the damage, such as a crack, introduces non-linear behaviour as well. The method locates the non-linearity between sensors if the sensor is not directly at the place of the damage. However, operational mode shapes of the structure are needed and the density of the measured points has to be sufficient. Moreover, the method works well only for weak non-linearities.

The non-linearity can be also localised using a pattern recognition, also called classification, such as using *nearest neighbour pattern recognition* procedure [264] or *artificial neural networks* [125, 126]. However, the pattern recognition may require a full spatial model of the structure with different locations and types of non-linearities. Therefore, this type of classification, which is essentially a brute force approach, may be very time-consuming task.

Generally, the location of the non-linearity is often clear from the geometry of the structure. For example, it may be expected that shell-like structure will exhibit geometrically distributed non-linearities, whereas the non-linearity of a bolted structure will originate from bolts and joints. Some of the methods that have originally been proposed for quantification (reviewed in section 1.2.3) allow localisation by a brute force approach as well.

Functional form characterisation

The selection of the functional form of non-linearity, i.e. the mathematical expression that is used for the modelling of the non-linearity, is closely related to the non-linearity type. Any function form discussed in section 1.1.1 can be theoretically used. However, if no a priori insight into the non-linear mechanism is available, the selection of the functional form might be very complicated.

Often, the *polynomial approximation* [12, 119] is used since it can describe many types of non-linearities and is mathematically simple. However, there are classes of non-linearities, such as non-smooth ones, which cannot be accurately approximated by the polynomial expressions of a reasonable order. The method used for an assessment of the quality of the polynomial approximation is called the *significance factor* [12]. It defines the percentage contribution of one element to the model variance. A single element of the polynomial expression is used to fit the non-linearity and the difference between the coefficient of this element and the coefficients of the complete polynomial is calculated.

This process requires many iterations, but the terms with the small contribution can eventually be discarded.

The non-linearities which cannot be accurately described by the polynomial approximation may be modelled by other series such as *non-integer exponent-type* [219] or *fractional derivatives* [231]. In addition, *cubic splines* [51, 56] can offer very high flexibility in cases where polynomials are not sufficient. Very sophisticated models can also be used to describe the functional form when it is required by an application (see section 1.1.1). Unfortunately, these models cannot be selected solely based on measured data so a priori knowledge of the system and underlying physical phenomena are necessary. On the other hand, if selected appropriately, these models should be predictive and capture the dynamics of the problem for a wide range of loading conditions.

In contrast, when little is known about the system, *non-linear black-box models* [110, 194, 248] can be used. The black-box models, for instance *NARMAX models* [20, 262], *neural networks* [66], *fuzzy sets* [302] or *genetic algorithms* [260], are the most versatile group of functional forms that can represent practically any type of non-linearity. Most of these models are defined as the discrete time models which look for a relationship between past and future observations. The biggest disadvantage of these models is that they do not provide an insight into the physical properties of an investigated system so their coefficients do not have a physical interpretation.

1.2.3 Quantification

Quantification is the last step in the identification process. At this stage, the non-linear behaviour has been detected and the type of the non-linearity, its location and the functional form have been characterised. Only the numerical quantification of the model parameters is now required. A number of methods to quantify these parameters exists, some of which are reviewed in this section. A more complete list of available methods is given in appendix A.

The approach which was originally proposed for the quantification but can be used for characterisation as well is called the *restoring force surface method* (RFS) [148] or *force-state mapping method* [48]. If the excitation, displacement, velocity and acceleration are measured and the mass is known (or estimated), the non-linear restoring force of a SDOF system can be constructed and displayed as a function of displacement and velocity. The resulting surface has a characteristic shape given by the type of non-linearity, thereby allowing detection and type characterisation. Under an assumption that the non-linearity is described by a polynomial expression, this expression can be used to fit the surface to quantify the non-linearity numerically. Various combinations of elements

in the polynomials can be tried in order to find the best combination which represents the measured data. The RFS has been mainly used for the identification of a single mode of vibration, but its extension to MDOF systems, using a transformation from the physical to modal space, has also been proposed [8, 23]. If all data in all degrees of freedom have been measured, the RFS can also be used for localisation. The restoring force surface has been successfully used for many applications, ranging from spacecraft structures [166] through experimental benchmarks [113, 116] to micro-electro-mechanical systems [9, 173]. Probably the main limitation of the restoring force method is that it requires a lot of data to be measured and some preliminary knowledge of the system (mass matrix) is required.

Similarly, *direct parameter estimation* [153] (also called *singular value decomposition* method [31]) requires all data to be measured in all degrees of freedom and a full model of the system to be known. If all data are available, the parameters (both linear and non-linear) of the selected model can be obtained by fitting this model to the data. Generally, the number of measured time samples is much higher than the number of fitted parameters so the model must be fitted in a least-square sense. Theoretically, this method can obtain exact (to the level of numerical errors) parameters for any excitation, but every kind of measured response (displacement, velocity, acceleration and excitation forces) is needed, making the method impractical to use [31].

The *reverse path method* [217] is a spectral method that estimates the frequency response of the linear and non-linear part of the system. It can be applied to any system excited by any random excitation. The method requires the excitation at the location of non-linearity. This significant limitation is removed in the *conditioned reverse path method* (CRP) [144]. The CRP computes conditioned frequency responses of the underlying linear system with no influence of non-linearities. The non-linearities are then quantified in the second step and the coefficients of the non-linearities are frequency-dependent. The CRP was successfully used in a number of applications, including the ECL benchmark [115], the VTT benchmark [80] and a folding wing model [293]. The method can be also used for the localisation of non-linearity [108, 301].

The *non-linear identification through feedback of the output* (NIFO) [3, 4] treats the non-linearities as internal non-linear feedback forces acting on the underlying linear system. This method attempts to simultaneously estimate the linear and non-linear frequency response of the system that has been excited by random excitation. Similarly to the reverse path method, the NIFO identifies frequency-dependent coefficients of non-linearities which are averaged for the final estimate. The method can be used for multi-degrees-of-freedom systems, but it may sometimes suffer from numerical issues [119].

The extension of subspace identification methods used in the operational modal analysis (OMA) [187, 270] to non-linear system identification is called*time domain non-linear subspace identification* (TNSI) [132, 146, 169]. The non-linearities are treated in the same way as in the NIFO, i.e. as additional forces applied to the underlying linear structure. The TNSI is suitable for any random excitation and uses robust numerical tools. It is said [168] that the method is superior in accuracy compared to the NIFO and CRP methods. A frequency domain version of the TNSI was introduced in [163] and named as the *frequency domain non-linear subspace identification* (FNSI). It applies the same principal idea as the TNSI, i.e. non-linearities are treated as forces applied to the underlying linear system. However, unlike the TNSI, the data are processed in the frequency domain which allows the frequency range of interest to be selected. Consequently, the processing time and computation requirements are reduced, while the accuracy is retained. Both TNSI and FNSI methods have a potential to identify large industrial structures with complex non-linearities [162, 167], which, if unknown, can be approximated by flexible cubic splines [56, 165].

1.3 Review of relevant groups of methods

A number of non-linear system identification methods have been very briefly described based on the identification process in Fig. 1.2. However, the methods do not have to be sorted according to Fig. 1.2, but can be grouped into several categories based on similar features instead [119, 164]. Three of these categories are described in more detail since the methods discussed therein will be used in other chapters of the thesis. The rest of the groups are briefly introduced:

- *Linearisation* attempts to treat the structure as if it were linear. Because the linear modal analysis has been extremely popular for a long time, there have been many attempts to apply it to non-linear systems without modifications [289]. This can be achieved by approximating the non-linear systems by a best linear model with equivalent mass, damping and stiffness. Unfortunately, this approach to the identification (and the analysis alike) is bound to fail for strong non-linear behaviour. Moreover, any linearisation is valid only for one excitation type and level. The linearisation is often achieved by random excitation, because the random excitation is the only type of forcing that generates frequency response functions that appear like linear ones. Examples of the methods that can be used for the linearisation using the random excitation include *equivalent linearisation* and *statistical linearisation* that are both based on the probability theory [289]. For

harmonic excitation, *describing function* [15, 177] can be used to approximate FRFs of a non-linear system based on its model. Then, these approximative FRFs can be fitted to the measured data. The linearisation via the describing function is equivalent to the linearisation using the *harmonic balance method* (HBM) [54, 158] in which only the fundamental harmonic is retained.

- *Time domain methods* operate solely on time domain data in order to recover physical phenomena presented in the structure. The computation of the time domain data using the direct numerical approaches is very time consuming and brings relatively low amount of information. On the other hand, the measurement of time domain data is much faster than the acquisition of complete frequency response functions. More importantly, the time domain data carry full information about the system that is not distorted by any signal processing. Therefore, the time domain data offer better possibilities for non-linear system identification. The difference between the time domain and frequency domain data is revisited in detail in chapter 3. The methods that operate on the time domain data include the *restoring force surface* (section 1.2.3), *time-frequency analysis* methods (section 1.3.2), *NARMAX models* [20] or *black-box models*.

- *Machine learning* does not assume any specific form of non-linearity, but uses the *black-box models* instead. Instead, these methods attempt to obtain very general models that can describe practically any (linear or non-linear) behaviour of a system based on its inputs and outputs. The machine learning methods are native to computational science and its applications [57, 91, 94], but have also been extensively used in mechanical systems as surveyed in [286]. There is a range of methods, but the *artificial neural networks* (ANNs) have received the greatest attention because it has been shown that they can approximate virtually any mapping between inputs and outputs. The use of ANNs in mechanical research is extensive [286] and also includes the identification of vibration structural systems [21, 35, 287]. The black-box models are very versatile so they can be applied to a wide range of systems with continuous and discontinuous non-linearities. However, the key limitation is a lack of any information about the physics that underlines the dynamics of the problem. This is quite significant issue because it limits the use of black-box models to one specific system configuration and operational conditions. Often, the predictive capabilities (which is called generalisation in the machine learning) of the model cannot be guaranteed and the parameters of the network cannot be associated with any physical values.

- *Structural model updating* is a process that is used for the correction (improvement) of a structural model to match an experimental response. In theory, non-linear system identification should be able to provide a model that does not have to be corrected and that can predict non-linear behaviour correctly. Unfortunately, it can be often found that due to a number of errors in modelling and testing [119], some subsequent correction and validation are necessary. As the models are usually created using the finite element method, the updating is often called *finite element model updating* [78]. The updating is achieved either by manual adjustments of relevant parameters or by minimisation of an objective function based on the difference between measured and computed vibrational characteristics. Any kind of optimisation (single or multi-objective optimisation, global or local, iterative or heuristics methods) can be used and the objective function may be defined by means of time domain data [95, 232], frequency response functions [83, 151, 244], instantaneous frequencies and amplitude [278], non-linear principal component analysis [113, 114] or any other feature of interest (even multi-physical one [160]). The updating is generally non-linear optimisation problem, often with constrains and limited ranges of coefficients. A successful and time-feasible solution of optimisation problem requires not only reliable model with the characterised non-linearities, but also a good starting guess and an appropriately constrained domain of coefficients. The reliable models as well as initial coefficients should be ideally obtained by non-linear system identification. However, if non-linear system identification cannot provide any information about the character of the non-linearity, a concept of *model upgrading* can be used [32, 65]. The model upgrading starts with a linear model and attempts to modify it as little as possible, but in such a way that it captures non-linear behaviour. This process has not yet been extensively used. However, it seems that it is suitable only for weak non-linearities. Structural model updating and upgrading can also be used as brute force approaches where no or very little system identification is conducted so the correct response of the system is re-constructed based on the trial-error process. Obviously, this can be computationally very expensive and may lead to the model that does not capture required physics of the systems.

The other three groups of methods - *frequency domain methods*, *time-frequency analysis methods* and *non-linear modal analysis* are introduced in detail in the following sections. The background of these methods is required to understand the concepts proposed in the thesis. The following literature review also highlights limitations of the current methods that are addressed in this thesis.

1.3.1 Frequency domain detection and characterisation

A number of methods for detection and characterisation of structural non-linearities from frequency response functions can be found in literature [31, 97, 119, 164, 269, 289]. These methods may be employed as a pre-step of linear modal analysis to verify the linear behaviour of the structure. As the modal analysis is dominantly used with frequency response functions, the methods described in this section operate solely on the FRFs and require no model of a tested structure. This group of methods is reviewed in detail to identify a prospective method or methods that could serve as a starting point for the method that needs to be developed to achieve the first objective of the thesis, i.e. enable fast and reliable detection and characterisation of structural non-linearities from a single frequency response function.

One of the important properties of the FRF matrix of a linear system is that it is symmetric [63]. This property is called reciprocity and, if violated, it is an indication of a non-linearity. In a *reciprocity test*, an FRF is measured and then the locations of the excitation and response sensors are switched while other parameters of the testing set-up remain unchanged. If the two FRFs are significantly different, the system is conclusively non-linear, whereas if they are the same, the system is probably linear. Unfortunately, some symmetrical non-linear systems may also hold the reciprocity even if they do not satisfy the principle of superposition [289]. The reciprocity test can be time-consuming and difficult to perform because it requires to switch the location of the excitation and response. This can be a tedious process that does not have to be possible due to the design of the tested structure.

Unlike the reciprocity test, the *homogeneity test* [130] does not require to change the experimental set-up. The homogeneity test relies on the fact that FRFs of the linear system are independent of the excitation amplitude, which is a direct consequence of the superposition principle. Therefore, several FRFs measured for different levels of excitation should overlay if the system is linear. On the contrary, if the FRFs are significantly different, the system is non-linear. Although the homogeneity test does not require the change of the experimental setting, it can still be time-consuming since several FRFs must be acquired.

If only one FRF is measured, detection and characterisation are possible based on the *FRF distortion*. All linear FRFs have a typical shape, so if a significantly distorted FRF is observed, it indicates a presence of non-linearity. Moreover, the shape of this distortion is known to be a characteristic of non-linearity. The distortion of FRFs may be assessed by eye. However, this simple visual inspection can be subjective, can require a vast experience to characterise the non-linearity correctly, and it is not very precise. There are

several tools that can help to decide about the presence and character of non-linearity. Because FRFs are complex functions, they can be visualised differently and the visual inspection performed from different plots which can simplify the final judgement. For instance, it is widely known that the FRF of the linear system produces a circle in the *Nyquist plot* so the distortion of the circle is a clear sign of a non-linearity. Likewise, the absolute value of an *inverse receptance* of a linear system plotted as a function of time is a straight line and any significant deviation from this line indicates a non-linearity. In addition, a collection of FRFs in a footprint library [83] can be helpful to decide about the type of non-linearity.

The visual inspection of a single measured FRF does not have to be sufficient to provide enough information to reliably detect and characterise the non-linearity. *The Hilbert transform in the frequency domain* [245] greatly simplifies the identification process by providing more information from a single FRF. This method explores the fact that the linear FRFs are invariant to the Hilbert transform. On the contrary, the Hilbert transform of non-linear FRFs produces distorted FRFs whose shapes are unique for different types of non-linearities. The Hilbert transform in the frequency domain is an effective and often used method to obtain more information to detect and characterise non-linearity. However, it still has several limitations. There are several numerical issues when evaluating the Hilbert transform of general non-linear FRFs and the visual inspection is still necessary. The footprint libraries can again assist in this visual inspection [289].

It should be noted that, strictly speaking, the Hilbert transform does not detect non-linearity, but non-causality. The non-causality does not refer to the fact that the system is non-causal in the sense that an effect precedes its cause. It refers to the fact that the inverse Fourier transform of an FRF cannot be interpreted as the impulse response because it has non-zero values for negative time. The non-zero values are not caused by numerical errors but are usually a consequence of non-linearity [289]. It has not been proven that all non-linear FRFs are always non-causal [119]. Therefore, there might theoretically exist a class of non-linear systems whose non-linearity cannot be detected by the Hilbert transform. However, no such behaviour of the Hilbert transform has ever been reported in literature. The non-zero amplitudes for negative time in the inverse Fourier transform of an FRF can directly be used for detection of non-linearity using the *non-causal power ratio* (NPR) method [121]. The NPR is the ratio of the power of the non-causal part to the power of the whole signal. It was shown that the NPR depends on an excitation level and differs with the type of non-linearity. However, due to its sensitivity to measured noise it is not commonly used.

Several scalar coefficients have been proposed to describe the difference between the FRFs and its Hilbert transform. These coefficients could be called *non-linearity indexes*. They are usually equal to zero for a linear system and non-zero (positive or negative) for non-linear systems [97]. The *correlation coefficient* was proposed in [130] and so called *Hilbert transform describes* in [263]. The former describes the similarities between the FRFs and its Hilbert transform using a cross-correlation coefficient, whereas the latter uses spectral (statistical) moments up to third order. Both non-linearity indexes could be theoretically used to assess the strength of non-linear behaviour. However, because the strength of non-linearity is case-dependent and generally undefined term, it is not usually attempted. Despite the fact that non-linearity indexes can simplify the decision about the presence of non-linearity, a subjective judgement is still needed to decide about the type.

From the literature review above, it appears that the Hilbert transform in the frequency domain is one of the most powerful methods. While it does not require multiple measurements, it provides a great amount of information to detect and characterise non-linearity. It appears to be suitable as a pre-step of modal analysis in an industrial framework where the time of measurement and processing must be minimised as much as possible. However, the main limitation associated with this method is the lack of an established methodology to determine if the distortion observed in an FRF is significant. If the FRF is influenced by measured noise, detection and characterisation using visual inspection can be very problematic. These limitations are overcome by the method proposed in chapter 2.

1.3.2 Time-frequency analysis

It is widely recognised that the frequency domain representation of measured signals possesses certain limitations with regards to non-linear system identification. The methods that are applied directly to measured time series generally offer better possibilities to estimate a greater amount of information about the system, which may eventually lead to a better structural model. Many methods for time-frequency analysis have been developed and used in countless fields [76, 101, 161]. All these methods attempt to reconstruct a time-frequency-amplitude map of a measured signal. However, each method leads to a map with a different time and frequency resolution, and even with a different definition of frequency. Several groups of methods can be distinguished - *time-frequency methods*, *time-scale methods* and methods based on *instantaneous amplitude and frequency*. This part of the literature review is conducted with regards to the second objective of the thesis, i.e. investigation of the time-frequency methods, and it aims to select the most

promising group of time-frequency analysis methods that will be further developed in this thesis.

Time-frequency methods are methods that seek a time-frequency-amplitude map of a signal using a fixed kernel function that does not change with time. The well-known *short-time Fourier transform* (STFT), also called *spectrogram* after its output, belongs to this group. The STFT is entirely based on the discrete *fast Fourier transform* (FFT) that estimates a frequency spectrum of the analysed signal. For the computation of a spectrogram the FFT is applied to short, windowed blocks of the original signal and the resulting spectra are plotted as a function of time. The STFT is a well developed tool that has been used in many areas of science and engineering, for instance for the modal analysis [140, 157], non-linear system identification [131, 161] or structural health monitoring [223]. One of the fundamental problems of the STFT is its fixed time and frequency resolution, i.e. no matter how the analysed signal changes, the resolution of results remain unchanged. Moreover, there is a fundamental trade-off between the resolution in time (the time at which frequency changes) and frequency resolution (frequencies that can be distinguished). If a wide window is used, the time resolution is poor, but better frequency resolution is achieved and vice versa. This trade-off indirectly relates to Heisenberg uncertainty principle and can be mathematically derived [43, 176, 242]. The limit of this trade-off when the best resolutions in time and frequency are reached simultaneously is called the *Gabor transform* [77, 250]. Probably the most intuitive way how to improve the resolution issue of the STFT is to vary the size of the sliding time window, i.e. the size of signal blocks that are analysed [131]. However, this would no longer be time-frequency method, but rather a time-scale method because the kernel would change in time.

Time-scale methods, also termed *wavelet transform* (WT) [76], improve the resolution in both frequency and time domain. The wavelet transform is essentially an adjustable sliding window Fourier analysis, in which, however, the frequency and amplitude are not defined, but a frequency scale is used instead. The time-scale methods yield a *scalogram* which represents the energy of a signal on a given frequency scale and at given time. A very appealing feature of the wavelet analysis is that it can provide a uniform resolution for all the scales so it is very useful in analysing data with gradual frequency changes [103]. However, the wavelet transform is not adaptive, i.e. it does not adjust the form of the wavelet based on the data, so the whole data set must be analysed by a single selected wavelet. Many wavelet forms with a wide range of properties exist [76], but a Fourier based Morlet wavelet is used the most. The WT has been used in many applications as

a better alternative of the STFT, in particular for modal analysis in [136, 225], damping estimation [22] and non-linear system identification [253, 254]

Both time-frequency and time-scale methods are based on the representation of the measured time series using the Fourier series. However, this representation can be often misleading as argued in [101–103], especially when it is used for the system identification. A minor concern is that the Fourier transform requires stationarity in the data. This requirement is, however, removed by the application of the FFT and WT to short blocks of the data. By doing so, even non-stationary data can be well analysed, assuming that the stationary exists in a block. A more serious concern is that the Fourier transform has a specific physical interpretation for non-linear time series which does not have to be suitable for non-linear system identification. The Fourier series is an excellent and elegant mathematical tool that can approximate any series, but in order to describe non-linear processes, several harmonic components (commonly called harmonics) are needed. For example, when analysing a distorted sine-wave, which is a well-known consequence of a cubic hardening non-linearity [289], the Fourier transform reveals the presence of several harmonics. However, while observing the particle moving on the distorted sine wave, the harmonics cannot be seen in the movement, but only in the Fourier spectrum. On the other hand, the movement of the participle can be easily interpreted as a vibration motion with an almost constant frequency which fluctuates slightly. The interpretation of signals using an almost constant (correctly called narrow-band) frequency that fluctuates in time is a basic concept of the methods based on instantaneous frequency and amplitude. The instantaneous frequency and amplitude are both functions of time and are not, therefore, the same frequency and amplitude that can be obtained by the Fourier or wavelet transform. The concept of instantaneous frequency and amplitude has been known for some time [43, 176]. However, it has not been so dominant due to a lack of established mathematical background and the collision with the established predictive methods that are mostly based on the Fourier transform, such as harmonic balance method (HBM). This concept offers many different possibilities and it allows to interpret vibration signal in more natural framework [103]. The difference between the time-frequency/time-scale methods and instantaneous frequency and amplitude concept will be revisited in chapter 3.

The instantaneous frequency (IF) and amplitude (IA) have been used for non-linear systems identification for over two decades. Probably the most well-known method for resonant decay processing is the *Freevib* algorithm [67]. It applies the Hilbert transform to estimate the IF and IA and subsequently computes modal properties. If the system is forced, a modified version of the Freevib called the *Forcevib* can be applied. Both

methods use the Hilbert transform to estimate the IF and IA. Unfortunately, the Hilbert transform suffers from a number of mathematical and numerical issues. To remove some of these limitations and offer enhanced features, alternative methods have been developed in different fields, for instance, zero-crossing methods [142, 173, 207], direct quadrature [103], energy operators [226] or conjugate-pair decomposition [181]. These methods will be compared in chapter 3 on simulated data to evaluate their potential for non-linear system identification.

The Freevib has been successfully used in many applications. The method is non-parametric, so it does not require any model of the system beforehand. However, the basic assumption is that the identified system possesses symmetric restoring forces. However, asymmetric elastic and dissipative restoring forces appear in practical applications as well. The systems with the asymmetric restoring forces cannot be identified using the Freevib, but the recently proposed *Hilbert vibration decomposition* (HVD) [71, 73] can be used instead. The HVD can identify amplitude-dependent backbones, damping curves, dissipative and elastic restoring forces. The HVD is relatively complex method that is influenced by a number of signal processing issues. A method which can obtain equivalent results, but with higher accuracy and does not suffer from the signal processing issues is proposed in chapter 6.

The Freevib must be applied to a mono-component function, i.e. the signal that can be described by one narrow-band frequency. The multi-component signals can also be analysed, but a direct decomposition method must be firstly applied. The most popular method of the direct decomposition of time signals is the *Hilbert-Huang transform*. The Hilbert-Huang transform (HHT) [101–103, 195] is potentially better than any time-frequency analysis method as it does use a priori chosen basis for the decomposition. It is therefore fully adaptive, thereby requiring no a priori knowledge of the system or observed non-linearity. The HHT maps a time series into a time-frequency-amplitude distribution by a two-step procedure. In the first step a complicated multi-component, non-linear and non-stationary time signal is decomposed into oscillatory functions, termed intrinsic mode functions (IMFs), by the empirical mode decomposition (EMD). Consequently, the instantaneous frequency and amplitude are estimated from IMFs by the Hilbert transform (HT) [71] or an equivalent method. The HHT is a versatile tool which has attracted a widespread interest in many fields, including structural dynamics where it has been used for experimental and operational modal analysis [210, 295, 296], structural health monitoring [38], and parametric and non-parametric identification of non-linear systems [25, 72, 182–184, 265]. Despite not having a rigorous mathematical background, the method has a solid logical justification as evidenced by a number of successful

studies. In addition, physics-based foundations of the EMD were derived in [118, 138]. Specifically, it was shown that IMFs relate to the slow-flow dynamics derived by the complexification-averaging (CxA). No connection between the HHT and non-linear modal analysis has so far been demonstrated in literature. In this thesis an attempt to connect the HHT and non-linear modal analysis is made in chapter 4.

1.3.3 Non-linear modal analysis

The linear modal analysis is a well-established method for the analysis of linear dynamic structures. Many sophisticated, highly accurate and precise methods for experimental (EMA) and operational modal analysis (OMA) have been developed in both frequency and time domain [26, 63], for instance, *least-squares complex estimators* [187, 270] (also called *polyMAX* [188]), *subspace identification methods* [216] or *eigenvalue realization algorithm* [109]. However, the extension of modal analysis concepts to non-linear structures has proven to be much more problematic for several reasons. The decoupling of equations of motion using a modal transformation, which is an essence of modal analysis and leads to an important model reduction, is no longer possible for non-linear systems. Moreover, frequency response functions and the modal properties (natural frequencies, damping ratios and mode shapes) become amplitude-dependent and the superposition is lost. It is argued in [283, 288] that there are three possibilities of how of to extend linear modal analysis to non-linear systems: (1) learn how to apply unchanged basic linear theory and philosophy to non-linear systems in a particular way so that the resulting modal properties are amplitude-dependent, (2) retain the philosophy of modal analysis but develop an appropriate theory that includes amplitude invariant properties of non-linear systems, or (3) change the paradigm, do not attempt to apply modal analysis and develop new theories for non-linear systems. The concepts of non-linear modal analysis, and associated experimental methods, are often a combination of these three options. The purpose of this part of the literature review is to briefly introduce the available concepts of non-linear modal analysis in order to provide motivation and background for chapter 4 and chapter 5.

A number of viewpoints on non-linear modal analysis exists, each of which tries to preserve a subset of properties of the original linear modal analysis. The non-linear modes have been actively studied for several decades so a range of methods for their numerical computation [215] as well as experimental investigation [164] has been developed, and a number of reviews written [14, 117, 152, 204, 266, 267].

Non-linear normal modes (NNMs) were originally defined as motions in unison of a conservative system [222]. Such definition requires all points of the system to reach their

extreme values and pass through zero simultaneously. However, this definition could not capture modal interactions during which the periodic motion consists of at least two interacting modes of different frequencies so the system does not vibrate in unison and the original definition cannot be applied. To account for modal interactions, the original definition must have been later extended, defining an NNM as a non-necessarily synchronous periodic motion of a conservative mechanical system. This definition has been adopted in a number of studies [59, 117, 190–192], partly because it enables an effective numerical computation of the NNMs [215]. The NNMs can generally undergo bifurcations, stability changes and experience internal resonances. However, they are not defined in the presence of damping (although the dynamics of lightly damped non-linear systems may be sometimes still interpreted using the NNMs of underlying conservative systems [117]). At the same time, however, complex damping mechanisms can occur in engineering assemblies, for instance in form of joints and interfaces, and even linear viscous damping of components may sometimes significantly change the dynamics of a structure.

An alternative definition of NNMs for damped systems, often called as *Shaw-Pierre definition of NNMs*, was proposed in [241]. Any form of dissipative effects (linear, non-linear, proportional or non-proportional) can be encompassed. An NNM is defined as a two-dimensional surface, termed invariant manifold, in the phase space. This manifold is obtained using a set of partial differential equations and is parametrised using a single pair of state-space variables (displacement and velocity). The trajectories of motions that started on this manifold remain on it for all time so the system effectively behaves as a non-linear SDOF system on this manifold. It was also shown that the modes hold approximate superposition so they can be approximately combined to obtain a physical motion [200, 283]. The evaluation of the invariant manifold is computationally expensive compared to the direct computation of a trajectory (a motion) on this manifold that can be found using complex non-linear modes.

Complex non-linear modes (CNMs) have recently been proposed in [135] and their use has been extended for non-linear modal synthesis, harmonically forced and self-excited systems in [127]. A complex non-linear mode of motion is defined as an oscillation of the autonomous system with (potentially) a phase different between its degrees of freedom. The CNMs allow direct computation of amplitude-dependent frequency, damping and mode shape at the resonance in a timely fashion. Moreover, the numerical implementation of the CNMs does not require significant modifications to conventional harmonic balance solvers. The ability of CNMs to deal with large non-conservative systems and general types of non-linearities led to their application to bladed disks coupled by mechanical

joints with friction interfaces [129, 134, 135]. In [128] the CNMs were used for the derivation of a *reduced order model* (ROM) of slow-flow dynamics of the system. The concept of the CNMs with the associated ROM is used in chapter 4 to investigate a possible connection between the Hilbert-Huang transform and non-linear modes and in chapter 5 for a development of non-linear system identification method.

Experimentally, non-linear modes are often investigated using *phase resonance testing* (also known as *force appropriation*) [59, 190, 191, 291]. This testing procedure has essentially two steps. In the first step the structure is excited using a multipoint, multi-harmonic excitation in such a way that it vibrates on a single non-linear mode of interest and specific amplitude (energy level). The isolation of one non-linear mode can generally be achieved using a force appropriation where the phase lag between the response and the applied force is used as a measure of a quality of the excited mode. In the second step, the excitation is turned off or removed and the system is allowed to decay on a single mode of vibration. The acquired signal is termed a resonant decay response and it is equivalent to the free decay response of a SDOF non-linear system. Such a resonant decay response may then be investigated by a number of appropriate non-linear system identification methods. However, in order to recover modal frequency, damping and mode shapes, the time-frequency analysis methods (section 1.3.2) are most suitable. The phase resonance testing has successfully been used for the experimental identification of symmetric non-linearities in the ECL benchmark [190, 191], clamped–clamped flat beam [59] or a sliding mass [142], and it is also used to obtain data from a MEMS device with an asymmetric restoring force in [173, 174] and chapter 6. Although the phase resonance testing is based on a solid framework of NNMs, it is an challenging procedure. For example, the set-up of a suitable multi-point excitation pattern that would isolate a single mode of vibration at specific amplitude level can be extremely difficult. In addition, the problem of turning off the shaker suddenly without influencing the structure has not yet been resolved.

The *control-based continuation* [17, 243] is a method that may be an interesting alternative to phase resonance testing. It allows to track the solutions and bifurcations of non-linear systems in a controlled manner by applying the theory of numerical continuation directly to a physical system. In particular, the method has been used to trace a backbone using the phase lag (a quadrature) between the force and response as a control indicator. Although the control-based continuation might potentially have widespread applications, it appears to be experimentally extremely complicated and it is so far limited to SDOF noise-free systems [16, 214].

Multi-modal non-linear identification through the direct decomposition of experimental measurements by the Hilbert-Huang transform into a set of oscillatory functions has also been presented in a number of papers [71, 118, 137, 181]. The strength of these approaches is that they require no a priori characterisation of the observed non-linearities and are generally applicable to non-stationary signals. Moreover, a free decay (a decay signal that consists of two or more modes of vibration) can be acquired using a basic impulse excitation and subsequently analysed. The experimental complexity of the phase resonance technique and control-based continuation is therefore replaced by a more sophisticated data processing. Although generally assumed, the connection between the non-linear modes and the Hilbert-Huang transform has never been shown. Chapter 4 presents an attempt to connect the HHT and complex non-linear modes through the reduced order model of slow-flow dynamics.

1.4 Limitations of the current methods

With the objectives of the thesis in mind, several limitations of the current methods have been identified in this literature review. The limitations of the current methods that are addressed in this thesis are repeated in this section.

- In section 1.3.1 it was concluded that the Hilbert transform in the frequency domain in conjunction with the non-linearity indexes appears to be the most suitable method for detection and characterisation of non-linearities from a single frequency response function. It seems to be suitable as a pre-step of modal analysis in an industrial framework where the time of measurement and processing must be usually minimised as much as possible. However, the main limitation associated with this method is the lack of an established methodology to determine if the distortion observed in an FRF is significant and what its character is. If the FRF is influenced by measured noise, detection and characterisation using visual inspection can be even more problematic. These limitations are overcome by the method proposed in chapter 2.

- In section 1.3.2 the Hilbert-Huang transform (HHT) has been identified as one of the most interesting methods for time-frequency analysis. It does not use a traditional concept of the frequency based on the Fourier transform, but rather utilises the instantaneous frequency (IF) and amplitude (IA). The IF and IA are traditionally estimated by the Hilbert transform. However, it is known that the Hilbert transform can suffer from a number of mathematical and numerical issues.

To avoid the use of the Hilbert transform several alternative methods, such as zero-crossing methods or direct quadrature, have been developed in other fields. However, they have been rarely used for the non-linear system identification in structural dynamics. Therefore, the comparison and assessment of the alternative methods are conducted in section 3.3 to evaluate their applicability for non-linear system identification.

- Although it is usually assumed that the Hilbert-Huang transform extracts vibration modes of the structure, the connection of the HHT and one of the concepts of non-linear modal analysis (section 1.3.3) has never been shown. This connection between the HHT and complex non-linear modes is investigated in chapter 4. Based on this investigation an approach to experimental non-linear modal analysis is proposed in chapter 5.

- It was found in section 1.3.2 that the Freevib algorithm cannot be applied to systems with asymmetric restoring forces. While the Hilbert vibration decomposition (HVD) is able to identify even such systems, its results are influenced by a number of signal processing issues. An alternative method for non-parametric identification of systems with asymmetric restoring forces is proposed in chapter 6.

Chapter 2

Characterisation of non-linearities in the frequency domain

Abstract

This chapter proposes a fast and noise robust means of detecting and characterising structural non-linearities from a single frequency response function using the Hilbert transform and artificial neural networks. In this method the difference between a frequency response function and its Hilbert transform is described using a set of scalar parameters, termed non-linearity indexes, which create training data of the artificial neural network. This network subsequently detects the presence of non-linearity and classifies its type. The usage of the method is demonstrated on a number of numerical test cases created by single-degree-of-freedom non-linear systems and a lumped parameter multi-degree-of-freedom system with a geometric non-linearity. The method is also applied to experimentally measured frequency response functions obtained from a cantilever beam with a clearance non-linearity, an under-platform damper experimental rig with a complex friction contact interface and the ECL benchmark.

2.1 Introduction

A number of methods for detection and characterisation from frequency response functions (FRFs) has been reviewed in section 1.3.1. It was found that the Hilbert transform in the frequency domain has the highest potential with regards to the first objective of the thesis, i.e. to enable robust and fast detection and characterisation of non-linearity of a single FRF. The main limitation associated with the Hilbert transform in the frequency domain (and all detection and characterisation methods that assess a distortion in measured FRFs) is the lack of an established methodology to determine whether the deviations observed in an FRF are significant. This limitation can be overcome by using artificial neural networks (ANNs) as suggested in [125, 126, 279].

The approach described in [125, 126] allows localisation and characterisation of the type of non-linearity, but it requires a full spatial model of the structure with all possible combinations of non-linearities. This makes the approach nearly impossible to use in practical applications due to enormous training data requirements. In contrast, the method proposed in [279] does not require the spatial model of the structure. It uses the gain (amplitude) of FRFs obtained in many spectral lines (frequencies) as training data for ANNs. Unfortunately, this leads to a large number of training cases as well. At the same time, however, the complex nature of FRFs is not fully taken into account due to missing phase information.

The method proposed in this chapter avoids the need for a vast set of training data by describing the difference between an FRF and its Hilbert transform using non-linearity indexes. These indexes transform the FRF measured in many frequency points into a set of several scalar parameters, thereby greatly reducing the training data requirements. In addition, principal component analysis (PCA) is applied to further reduce the dimensionality of the feature space created by the non-linearity indexes so that the structure of the network may eventually be very compact, whilst capturing the non-linear distortion of the FRF fully. In contrast to [125, 126], the method does not localise the non-linearity within the structure, it does not require any spatial model of the structure or any a priori knowledge of the type of non-linearity.

The chapter is organised as follows: section 2.2 gives an overview of the methods involved (the Hilbert transform in the frequency domain, principal component analysis and artificial neural networks) and, most importantly, proposes the non-linearity indexes. In section 2.3 the implementation of the method is described in detail. Then the noise robustness of the proposed method is numerically investigated in section 2.4. Following this investigation, the method is applied to a cantilever plate with a localised geometric non-linearity to demonstrate its application to a multi-degree-of-freedom (MDOF) system.

Section 2.5 shows the application of the proposed method to experimental FRFs obtained from three experimental test rigs - a cantilever beam with a clearance, an under-platform damper experimental rig and the ECL benchmark. Based on the observations from these test cases the advantages and disadvantages of the proposed method are discussed in section 2.6.

2.2 A method for detection and characterisation of structural non-linearities

The proposed method for detection and characterisation of structural non-linearities consists of several steps. Firstly, the Hilbert transform of a normalised frequency response function is computed. Then the difference between the FRF and its Hilbert transform is quantified using a set of non-linearity indexes. The feature space created by these indexes is reduced using principal component analysis and subsequently used as the input of an artificial neural network pattern recognition algorithm by which a decision about the type of non-linearity is made. A description of the steps that are required for successful detection and characterisation follows.

2.2.1 Normalisation of frequency response functions

Theoretically, the proposed method can be used with any type of frequency response functions - receptance $H(\omega)$, mobility $Y(\omega)$ or accelerance $A(\omega)$. However, the use of receptance is beneficial with regards to the numerical computation of the Hilbert transform [263, 289]. Any type of FRF can be converted to the receptance using [63]

$$A(\omega) = \mathrm{i}\omega Y(\omega) = -\omega^2 H(\omega). \tag{2.1}$$

Before computing the Hilbert transform it is proposed to normalise the receptance $H(\omega)$ to allow an effective comparison of different types of non-linearities and improve the overall performance of the proposed method. A frequency response function is transformed as

$$f \longrightarrow (0, 1)\,, \tag{2.2}$$

and

$$\|H(\omega)\| = 1, \tag{2.3}$$

where f is a measured frequency range, which is mapped to interval $(0, 1)$, and $H(\omega)$ is the receptance which is normalised so that its Euclidean norm $\|\bullet\|$ is equal to one. In the remainder of this chapter, all FRFs are assumed to be normalised. This normalisation does not remove any important information because the absolute values of amplitudes and frequencies are not important for detection and characterisation despite being crucial for quantification. The important factor is the shape of the FRF distortion, which remains unchanged by the normalisation.

To illustrate the effect of the normalisation an example of two non-linear frequency response functions is shown in Fig. 2.1. These FRFs were obtained numerically using

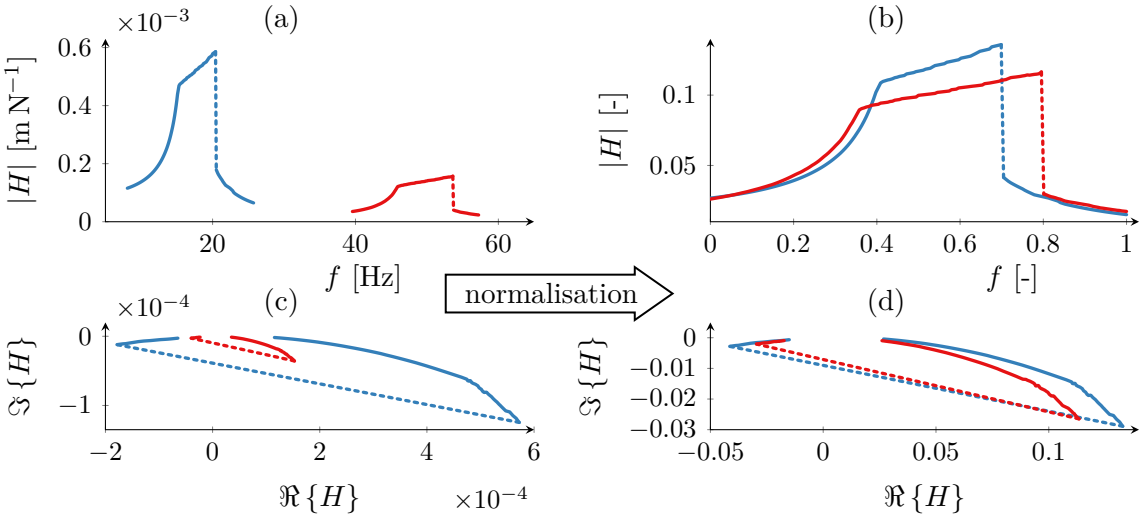

Figure 2.1 Normalisation of two frequency response functions obtained from SDOF systems with a clearance non-linearity: (a) amplitude of original FRFs, (b) amplitude of normalised FRFs, (c) Nyquist plot of original FRFs, and (d) Nyquist plot of normalised FRFs.

the time domain integration and frequency response analyser as detailed in section 2.3.1. It can be seen that the FRFs which were significantly different in the amplitudes and frequencies (Fig. 2.1(a)) are now much more comparable while retaining the original shape (Fig. 2.1(b)).

2.2.2 The Hilbert transform in the frequency domain

The Hilbert transform in the frequency domain can be used for detection and characterisation of non-linearities from frequency response functions [72, 289]. For a general

complex function in the frequency domain it is defined as

$$\mathscr{H}\{H(\omega)\} = \tilde{H}(\omega) = \frac{-1}{\mathrm{i}\pi}\mathrm{pv}\int_{-\infty}^{\infty}\frac{H(\Omega)}{\Omega-\omega}\mathrm{d}\Omega, \tag{2.4}$$

where $\mathscr{H}\{\bullet\}$ denotes the Hilbert transform operator, $\tilde{H}(\omega)$ stands for the Hilbert transformed receptance $H(\omega)$, and "pv" denotes the Cauchy principal value of the integral. In contrast to the Fourier transform, which transforms time domain data into the frequency domain and vice versa, the Hilbert transform maps functions from a domain into the same domain by shifting their phases by $-\pi/2$ [71, 72, 289]. Unfortunately, analytical methods for solving Eq. (2.4) are not generally applicable because $H(\omega)$ cannot be found as a closed-form expression. Hence, the Hilbert transform is computed numerically either by a direct method using the Kronig-Kramers [72, 263, 289] relations or by a means of the fast Fourier transform (FFT) using an analytic signal theory [147, 289]. It was found that the former over-performs the latter in the frequency domain in terms of the numerical accuracy and reduction of truncation errors. On the other hand, the computation using the FFT was found to be more suitable for the application in the time-domain. Therefore, the direct method is used in this chapter whereas the FFT approach is utilised for the computation of the Hilbert transform in other chapters where the time domain data are considered.

The direct method requires the evaluation of the Kronig-Kramers relations

$$\Re\{\tilde{H}(\omega)\} = -\frac{2}{\pi}\mathrm{pv}\int_{0}^{\infty}\frac{\Im\{H(\Omega)\}\Omega}{\Omega^2-\omega^2}\mathrm{d}\Omega, \qquad \Im\{\tilde{H}(\omega)\} = \frac{2\omega}{\pi}\mathrm{pv}\int_{0}^{\infty}\frac{\Re\{H(\Omega)\}\Omega}{\Omega^2-\omega^2}\mathrm{d}\Omega. \tag{2.5}$$

The integrals must be evaluated numerically (the trapezoidal integration rule was used) and the singularity at $\omega = \Omega$ avoided. The Hilbert transform computed by the direct method can suffer from truncation errors as explained in [263]. The truncation errors arise from the replacement of the lower and upper integration limits by non-zero and finite values, respectively. There are several correction schemes available in [289]. However, due to the introduced normalisation the truncation errors are minimised. The minimum frequency (i.e. the lower integration limit) is always equal to zero and it was found that the distortion caused by the upper integration limit is not significant. Moreover, the truncation errors are minimised by using the receptance rather than mobility or accelerance [289]. In addition, the non-linearity indexes that are proposed in section 2.2.3 to capture the distortion of an FRF and its Hilbert transform operate on a narrow frequency band close to the resonance. Therefore, as long as the FRF is not measured in

an extremely close proximity of the resonance frequency, the truncation errors are not a major problem since their effect is much more significant at the beginning and the end of the measured frequency band and the non-linearity indexes avoid these regions.

It was shown in [245] that the Hilbert transform of an FRF can be used to detect non-linearity using the following criterion

$$\mathscr{H}\{H(\omega)\} = H(\omega) \longrightarrow \text{linear system},$$

$$\mathscr{H}\{H(\omega)\} \neq H(\omega) \longrightarrow \text{non-linear system}.$$

This means that the FRF of a linear system is not affected by the Hilbert transform whereas the Hilbert transform of the non-linear FRF yields a distorted version of the original FRF. Strictly speaking, the Hilbert transform does not detect non-linearity, but non-causality. Non-causality does not refer to the fact that the system is non-causal in the sense that an effect precedes the cause. Instead, it refers to mathematical (artificial) non-causality, i.e. the fact that the inverse Fourier transform of an FRF should not be interpreted as the impulse response because it is non-zero for negative time. The non-zero values are not caused by numerical errors but are usually a consequence of non-linearities. A few examples of this mathematical non-causality can be found in [289]. It has not been proven that all non-linear FRFs are also non-causal [119]. Therefore, there might theoretically exist a class of non-linear systems whose non-linearity cannot be detected by the Hilbert transform. However, no such systems or failure of the Hilbert transform to detect a structural non-linearity have ever been reported in literature.

It was observed [263, 289] that the form of the FRF distortion can provide insight into the type of non-linearity, allowing its characterisation. Compared to the homogeneity method [119, 130, 289] the Hilbert transform can be applied to a single frequency response function which has been measured using a single excitation level [119]. Moreover, the Hilbert transform does not require a linear FRF or a spatial model of the structure. However, a subjective decision must be taken to detect and characterise non-linear behaviour. In order to simplify this decision, a set of scaler parameters, termed non-linearity indexes, which describe the difference between an FRF and its Hilbert transform is proposed in the next section.

2.2.3 Non-linearity indexes

Several definitions of a non-linearity index exist in literature as reviewed in section 1.2.1. In the scope of this thesis a non-linearity index (NLI) has been defined as a real scalar parameter that describes the difference between an FRF and its Hilbert transform.

Such an index is equal to zero if the system is linear and non-zero (either positive or negative) for a non-linear system. In total, fourteen non-linearity indexes are presented and discussed in this section. These indexes should ensure the comprehensive capture of a wide range of non-linearities.

Cross-correlation coefficient

Cross-correlation is commonly used as a measure of similarities between two data series as the function of a lag between these series. The application of cross-correlation in the frequency domain for detection of non-linearities was proposed in [130]. The cross-correlation computed in a close proximity of a single vibration mode $R_{H\tilde{H}}(\Delta\omega)$ between a receptance $H(\omega)$ and its Hilbert transform $\tilde{H}(\omega)$ is defined as

$$R_{H\tilde{H}}(\Delta\omega) = \int_{\omega_{\min}}^{\omega_{\max}} H(\omega)\tilde{H}(\omega + \Delta\omega)\mathrm{d}\omega, \tag{2.6}$$

where $\Delta\omega$ is a frequency shift (lag), and $\omega_{\min}$ and $\omega_{\max}$ are the lower and upper integral limits, respectively. These limits have to be chosen appropriately to capture the distortion of an FRF which is localised around the resonance frequency. As a convention [289], the half-power points that solve the equation

$$|H(\omega)| - \frac{\max|H(\omega)|}{\sqrt{2}} = 0 \tag{2.7}$$

are suitable. Alternatively, in a scheme of detection and characterisation, other limits could be chosen as long as they describe the distortion of an FRF. Equation (2.6) and all the following non-linearity indexes have to be evaluated numerically since the analytical expressions for $H(\omega)$ and $\tilde{H}(\omega)$ are not known.

The first non-linearity index (NLI_1) is defined based on the squared cross-correlation coefficient at the frequency shift $\Delta\omega = 0$ using the following expression

$$\mathrm{NLI}_1 = 1 - \|R_{H\tilde{H}}(0)\|^2. \tag{2.8}$$

Due to its definition this index is more sensitive to non-linearities that shift the resonance frequency, such as geometric non-linearities, and less sensitive to non-linearities that scale the amplitudes of FRFs, for instance non-linear damping or Coulomb friction.

Hilbert transform describers

It was proven in [263] that all spectral moments exist for an FRF and its Hilbert transform. These moments are defined as

$$M_H^{(n)} = \int_{\omega_{\min}}^{\omega_{\max}} \omega^n H(\omega) \mathrm{d}\omega, \tag{2.9}$$

where $M_H^{(n)}$ stands for the nth-order spectral moment of $H(\omega)$. In spite of the fact that these moments are complex, they can be considered as an analogy with statistical theory. The first- and second-order moments measure the mean and the standard deviation of a probability distribution. The third- and fourth-order moments then describe the skewness and kurtosis [289] and the zeroth-order moment can be considered as the area under the complex function. For the purpose of the non-linearity description, the relative differences between the spectral moments of a receptance $M_H^{(n)}$ and moments of its Hilbert transform $M_{\tilde{H}}^{(n)}$, termed Hilbert transform describers ($\mathrm{HTD}^{(n)}$) [289], were defined as

$$\mathrm{HTD}^{(n)} = \frac{M_{\tilde{H}}^{(n)} - M_H^{(n)}}{M_H^{(n)}}. \tag{2.10}$$

Although an arbitrary number of spectral moments can be computed, the first three (zeroth-, first- and second-order) are considered since the higher-orders do not seem to provide any additional information. The non-linearity indexes were defined as the real and imaginary parts of the Hilbert transform describers, i.e.

$$\mathrm{NLI}_2 = \Re\left\{\mathrm{HTD}^{(0)}\right\}, \qquad \mathrm{NLI}_3 = \Im\left\{\mathrm{HTD}^{(0)}\right\}. \tag{2.11}$$

In a similar manner $\mathrm{NLI}_{4,5}$ and $\mathrm{NLI}_{6,7}$ were defined, but $\mathrm{HTD}^{(1)}$ and $\mathrm{HTD}^{(2)}$ were used instead. The imaginary parts of the HTDs, which define NLI_3, NLI_5 and NLI_7, separate the stiffness hardening and softening very well. On the other hand, the real parts of the HTDs (NLI_2, NLI_4 and NLI_6) effectively distinguish between the quadratic damping and Coulomb friction.

Function describers

To describe relative changes between an FRF and its Hilbert transform, it is proposed to compute some parameters in an analogy with classic mechanics. First of which, the

centre of gravity of an FRF γ_1, can be calculated as

$$\gamma_1 = \frac{\int_{\omega_{\min}}^{\omega_{\max}} \rho(\omega) H(\omega) \mathrm{d}\omega}{\int_{\omega_{\min}}^{\omega_{\max}} \rho(\omega) \mathrm{d}\omega}, \tag{2.12}$$

where $\rho(\omega)$ would correspond to the length density in mechanics. Here it can be set to one or the coherence function can be used if available. If the coherence is employed, non-linear effects of the resonance frequencies would be theoretically emphasised. The non-linearity indexes NLI_8 and NLI_9 are assembled based on the relative difference between the centre of gravity of an FRF γ_1 and its Hilbert transform $\tilde{\gamma}_1$ by splitting its real and imaginary parts as

$$\mathrm{NLI}_8 = \Re\left\{\frac{\tilde{\gamma}_1 - \gamma_1}{\gamma_1}\right\}, \qquad \mathrm{NLI}_9 = \Im\left\{\frac{\tilde{\gamma}_1 - \gamma_1}{\gamma_1}\right\}. \tag{2.13}$$

These non-linearity indexes can distinguish particularly well between stiffness and damping non-linearities since the Hilbert transform of the FRFs with damping non-linearities usually scales the FRFs and therefore does not change the position of the centre of gravity significantly.

Two other parameters are proposed to describe complex function properties based on mechanical analogies, namely the moment of inertia about ω-axis γ_2 and with respect to origin γ_3 defined as

$$\gamma_2 = \int_{\omega_{\min}}^{\omega_{\max}} \rho(\omega) \left(\Re\{H(\omega)\}^2 + \Im\{H(\omega)\}^2\right) \mathrm{d}\omega, \tag{2.14}$$

and

$$\gamma_3 = \int_{\omega_{\min}}^{\omega_{\max}} \rho(\omega) \left((\omega - \bar{\omega})^2 + \Re\{H(\omega) - \gamma_1\}^2 + \Im\{H(\omega) - \gamma_1\}^2\right) \mathrm{d}\omega, \tag{2.15}$$

where $\bar{\omega}$ marks the mean of angular frequency. These moments can be interpreted as the torque needed for an unity angular acceleration about the ω-axis and the origin, respectively. These parameters are real so the next two non-linearity indexes can be defined as

$$\mathrm{NLI}_{10} = \frac{\tilde{\gamma}_2 - \gamma_2}{\gamma_2}, \qquad \mathrm{NLI}_{11} = \frac{\tilde{\gamma}_3 - \gamma_3}{\gamma_3}, \tag{2.16}$$

where $\tilde{\bullet}$ marks the quantities which have been computed from the Hilbert transform of an FRF. These non-linearity indexes are significantly higher for stiffness non-linearities

since the Hilbert transform shifts the frequencies of such non-linearities away from the resonance frequency and therefore changes the moments of inertia significantly.

Statistical description

The last group of non-linearity indexes can be assembled directly from the complex difference between an FRF and its Hilbert transform

$$G(\omega) = \tilde{H}(\omega) - H(\omega). \tag{2.17}$$

The difference $G(\omega)$ can then be described using describing statistics. The mean of the difference is defined as

$$\bar{G} = \frac{1}{\mathrm{N_{sl}}} \sum_{k=1}^{\mathrm{N_{sl}}} G(\omega_k), \tag{2.18}$$

where $\mathrm{N_{sl}}$ is a number of spectral lines (frequency points) between $\omega_{\min}$ and $\omega_{\max}$. Two non-linearity indexes $\mathrm{NLI}_{12,13}$ are then obtained by splitting $\bar{G}$ into the real and imaginary parts.

The last proposed non-linearity index is formed using the standard deviation of the difference $G(\omega)$

$$\mathrm{NLI}_{14} = \sqrt{\frac{1}{\mathrm{N_{sl}} - 1} \sum_{k=1}^{\mathrm{N_{sl}}} (G(\omega_k) - \bar{G})^2}. \tag{2.19}$$

It describes an amount of variation or dispersion of $G(\omega)$ about the mean $\bar{G}$.

Summary of non-linearity indexes

Most of the non-linearity indexes have an integral form so they are robust to measured noise and other errors which can occur in an FRF. All of them depend on the integration limits $\omega_{\min}$ and $\omega_{\max}$. Although the choice of these limits affects the absolute value of the non-linearity indexes, it is not a major issue as long as these limits are consistent for all computed non-linearity indexes. Generally, the half-power points given by Eq. (2.7) should be chosen. If they cannot be defined due to, for example, a jump in an FRF, the part of the FRF which covers the non-linear distortion should be taken. It should be also noted that for the indexes to be meaningful, and the method to work as intended, the modes should be well separated and no non-linear coupling should exist between them.

All non-linearity indexes can be used to detect non-linear behaviour. They are zero when the system is linear and non-zero (either positive or negative) for non-linear systems. In practical applications the NLIs are not exactly zero due to experimental and numerical

imperfections, but they are very close to zero compared to the NLIs of non-linear systems. Theoretically it is possible to assess the strength of non-linear behaviour using the NLIs as well. This would allow categorisation of weak, moderate and strong non-linear effects. However, although similar terms are often used in literature, there is no reliable means how to define them. All possible definitions must be bound to a specific application. Therefore, no attempt to quantify the strength of non-linear behaviour based on the NLIs has been made in this thesis.

It was observed [71, 72, 263, 289] that the distortion of an FRF and its Hilbert transform is unique for a given non-linearity type. Since the distortion is captured by the NLIs, the pattern created by them is also unique and suitable for classification. Classification (pattern recognition) is a subclass of machine learning methods which assigns the input data to given classes [57]. In this study the classes are created by the types of non-linearities and input data are given by the non-linearity indexes. Artificial neural networks (ANNs) [279, 300] are used as the classification algorithm.

2.2.4 Dimensionality reduction using principal component analysis

With regards to the feature of ANNs to grow exponentially with a number of the input parameters [91], a number of the non-linearity indexes is further reduced to not only decrease the complexity of the network, but also to eliminate a potential redundancy of these indexes.

Several methods for dimensionality reduction exist, for instance independent component analysis [57] and self-organizing maps [124]. However, one of the most established methods is the principal component analysis (PCA). The PCA, also known as Karhunem-Loève transform or proper orthogonal decomposition [98, 113], seeks a linear projection of high-dimensional data into lower dimensional space in a least-squares sense [57]. The principal component analysis projects the initial n-dimensional data vector of samples (observations) $\mathbf{x}_s = (x_1, \ldots, x_n)^T$ into a new n-dimensional vector $\mathbf{z} = (z_1, \ldots, z_n)^T$ called the principal component scores (PCS). The new coordinates have the following properties: z_1 is the linear combination of the original x_i with maximum possible variance, z_2 is the linear combination which explains most of the remaining variance and is orthogonal to z_1 and so on [286]. Dimensionality reduction is then achieved by selecting only those principal components which contribute significantly to the overall variance and therefore retain the important information of the data.

The principal component algorithm can be summarised as follows. For a set of observations $\{\mathbf{x}_1, \ldots, \mathbf{x}_N\}$ the scatter matrix $\mathbf{S}$ is assembled using

$$\mathbf{S} = \sum_{k=1}^{N} (\mathbf{x}_i - \bar{\mathbf{x}})(\mathbf{x}_i - \bar{\mathbf{x}})^T, \tag{2.20}$$

where $\bar{\mathbf{x}}$ is a vector of sample means. Then the scatter matrix $\mathbf{S}$ is decomposed (usually using singular value decomposition) as

$$\mathbf{S} = \mathbf{U}\mathbf{\Sigma}\mathbf{V}^T, \tag{2.21}$$

where $\mathbf{\Sigma}$ is a diagonal matrix interpreted as the relative contributions of the principal scores to the total variance and $\mathbf{U}$ is an orthonormal matrix which contains the principal directions. The principal component scores are subsequently obtained from

$$\mathbf{z}_i = \mathbf{U}^T(\mathbf{x}_i - \bar{\mathbf{x}}). \tag{2.22}$$

While the PCA is a linear transformation (PCS are straight and orthogonal), it cannot remove non-linear correlations within data sets. The linear PCA can also be extended to non-linear PCA using artificial neural networks [233]. However, it will be shown that the linear PCA is sufficient for the dimensionality reduction required in the proposed method. The linear PCA also allows a simple visualisation that can be directly used for detection and characterisation of non-linearity as shown in section 2.5.

The principal component scores do not have a physical unit and cannot be associated with the underlying dynamics of the system. However, they still capture most of the information while removing redundancy of the input data. The dimension of the problem can be significantly reduced using the PCA as shown section 2.3. In the next section they are used as the inputs of the neural network.

2.2.5 Artificial neural networks

Artificial neural networks (ANNs), which belong to a group of machine learning methods (also called soft or natural computation methods, or artificial intelligence), have been applied to many problems in recent years. In mechanical engineering they are usually used for classification, detection of abnormalities and input-output mapping [286]. Although many types of artificial neural networks can be found in literature, a multi-layer perception neural network is usually applied for classification tasks. Moreover, only a single hidden

layer is often used since it is known that such a network can solve almost any classification problem [57, 91].

The multi-layer perception network has nodes (neurons) arranged in layers that are passed by a signal from the input layer, through hidden layer(s), into the output layer. Each node i in layer k is connected to each node j in preceding layer $k-1$ through a weight $w_{ij}^{(k)}$ (see Fig. 2.2).

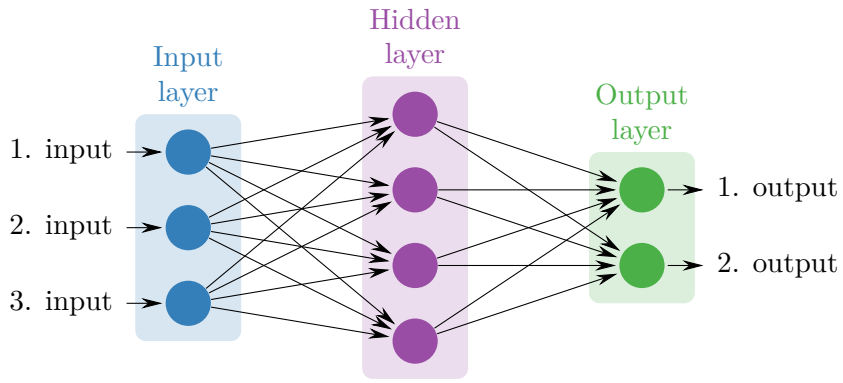

Figure 2.2 Illustrative architecture of a single hidden layer artificial neural network

A weighted sum $z_i^{(k)}$ of all signals $x_j^{(k-1)}$ at each node i in layer k is passed through an activation (also called transfer) function $f(z_i^{(k)})$ to obtain the signal $x_i^{(k)}$

$$x_i^{(k)} = f(z_i^{(k)}) = f\left(\sum_j w_{ij}^{(k)} x_j^{(k-1)}\right). \tag{2.23}$$

The choice of the activation function $f(z_i)$ depends on the application [91]. For classification the hyperbolic tangent function

$$f(z_i) = \tanh(z_i) = \frac{\mathrm{e}^{z_i} - \mathrm{e}^{-z_i}}{\mathrm{e}^{z_i} + \mathrm{e}^{-z_i}} \tag{2.24}$$

is usually used in the hidden layer and a non-linear activation function is used in the output layer. The so-called softmax activation,

$$f(z_i) = \frac{\mathrm{e}^{z_i}}{\sum_{i=1}^{N_\mathrm{H}} \mathrm{e}^{z_i}}, \tag{2.25}$$

where N_H is a number of neurons in the hidden layer, is very often used as the non-linear activation function because it forces the output of the network to sum to unity, thereby allowing the outputs to be interpreted as the probabilities of classes.

The first stage when applying the artificial neural network is to establish the appropriate values of the weights w_{ij}. This stage is referred to as the training phase in which the network is presented by a set of the input parameters and the corresponding outputs. At each training step the inputs are passed through the network yielding trial outputs that are compared to the desired outputs. If a significant error is found, the error is passed backwards through the network and the weights are adjusted. This training process is referred to as the backpropagation algorithm [91, 286].

The overall performance of a classification algorithm, such as the used ANNs, can be easily evaluated using so-called confusion matrix. A confusion matrix compares the output (identified) classes with the correct (target) classes. In an ideal case, 100 % of the systems are identified correctly. However, this case is purely theoretical and highly unlikely in reality due to a statistical nature of ANNs, uncertainty in measured FRFs and overlap of the input data.

One of the main problems of ANNs, and many soft computing methods, is generalisation of the network. The problem with generalisation occurs when the network is trained to fit one particular set of data, but does not represent any other case. The simplest solution to the problem is to adjust the number of neurons in the hidden layer N_{H} appropriately. If N_{H} is too high, the network is over-fitted so that it is fine tuned to a particular data set only. On the other hand, if there are too few neurons in the hidden layer, the network does not have enough parameters to fit the training data properly. Unfortunately, there is no versatile technique how to choose N_{H} (and therefore the number of weights w_{ij}) before training, but some guidelines have been established based on the practical experience in [57, 91, 286]. The number of hidden neurons should be chosen between the number of inputs and outputs, or it can be found in a systematic way using the so-called 1 to M training strategy. Using this strategy, an optimal N_{H} can be selected by a systematic evaluation of neural network errors for a varying number of hidden layer neurons [279, 286]. This training strategy has been used in this study.

Summary of the proposed method

The method is summarised in the flow chart in Fig. 2.3 in which two branches are distinguished. Although they look very similar, there is a major difference between them. The neural network must be trained only once and can be subsequently used multiple times to detect and characterise a structural non-linearity in different sets of experimental data. The preparation of the network is a time-consuming process, mainly because of the need for relevant training data. The training data can be either computed or experimentally measured which, however, would be extremely time-consuming. Once the

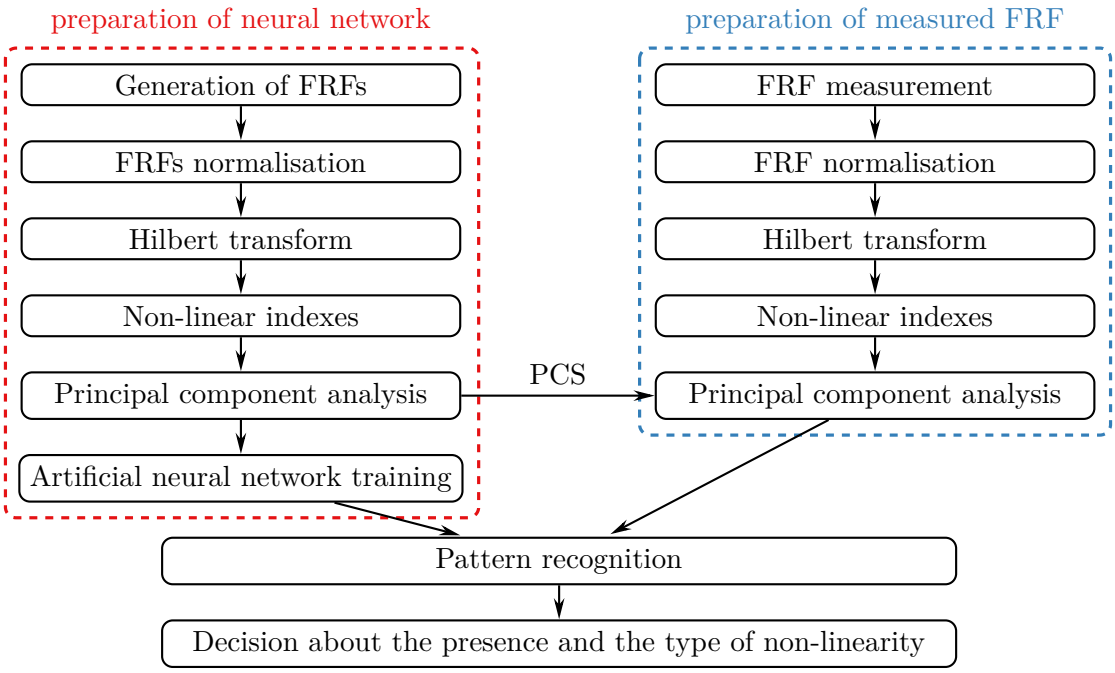

Figure 2.3 Summary of the proposed method for detection and characterisation of structural non-linearities

neural network has been trained, non-linear behaviour can be detected and characterised from a single frequency response function in a timely fashion.

The method operates on a single mode of vibration. Therefore, when applied to a MDOF system the modes must be treated separately as having been obtained from a SDOF system. It implies that for the method to work correctly the modes must be well-separated, with no significant linear or non-linear coupling. Unfortunately, there is no established methodology how to recognise well-separated modes. The well-separated modes must be recognised in individual cases based on experience.

In certain situations there might co-exist several non-linear elastic and dissipative mechanisms in the structure, for instance the Coulomb friction caused by joints and geometric non-linearities caused by large amplitudes. The proposed method does not provide any reliable information about how many or what combinations of non-linearities are present in the system. The combination of non-linearities is simply another non-linearity, and the separation of this non-linearity into two, or more, is not uniquely possible without a priori knowledge of the system. Still, if the neural network has been trained for certain types of non-linearities, some limited insight into the combination of the types involved can be provided due to the ability of ANNs to recognise unseen patterns. An example of such an ability is shown in section 2.5.2.

2.3 Implementation of the proposed method

Although the proposed method can be used for an arbitrary number of non-linearities, it is demonstrated using five common types. Each type is a class (marked by a capital letter) that is being classified by the ANN. Six classes were used in total: A - linear system, B - cubic hardening stiffness, C - cubic softening stiffness, D - clearance, E - Coulomb friction and F - quadratic damping. The proposed method was implemented according to Fig. 2.3 using the methods described in section 2.2.

2.3.1 Training data generation

The training data for ANNs were obtained numerically for a SDOF system with all listed types of non-linearities. This system is described using

$$m\ddot{x} + c\dot{x} + kx + f_{\mathrm{nl}}(x, \dot{x}) = F(t), \tag{2.26}$$

where m is a mass, c is a linear damping coefficient, k is a linear stiffness coefficient, $F(t)$ is an excitation force, and x, $\dot{x}$, $\ddot{x}$ are displacement, velocity and acceleration, respectively. The term $f_{\mathrm{nl}}(x, \dot{x})$ describes a non-linear restoring force. It is, therefore, zero for a linear system and varies with the type of the non-linearity involved (see Tab. 2.1).

Class - Non-linearity	$f_{\mathrm{nl}}(x, \dot{x})$	Parameter range
A - linear system	0	$m = 1$ kg
		$k \in (7 \times 10^3, 5 \times 10^5)$ N m^{-1}
		$c = \alpha m + \beta k$ N s m^{-1};
		$\alpha \in (2, 5)$; $\beta \in (10^{-8}, 10^{-6})$
B - cubic hardening stiffness	$k_{\mathrm{nl}}x^3$	$k_{\mathrm{nl}} \in (5 \times 10^3 k, 5 \times 10^4 k)$ N m^{-3}
C - cubic softening stiffness	$k_{\mathrm{nl}}x^3$	$k_{\mathrm{nl}} \in (-5 \times 10^3 k, -5 \times 10^4 k)$ N m^{-3}
D - clearance	$k_{\mathrm{nl}}x - k_{\mathrm{nl}}b, \quad x > b$	$k_{\mathrm{nl}} \in (1k, 10k)$ N m^{-1}
	$0, \quad \lvert x\rvert < b$	$b \in (0.1, 0.5)$ mm
	$k_{\mathrm{nl}}x + k_{\mathrm{nl}}b, \quad x < -b$	
E - Coulomb friction	$\mu N_{\mathrm{f}} \mathrm{sgn}(\dot{x})$	$\mu N_{\mathrm{f}} \in (0.05, 0.2)$ N
F - quadratic damping	$c_{\mathrm{nl}}\dot{x}\lvert\dot{x}\rvert$	$c_{\mathrm{nl}} \in (10c, 50c)$ N m^{-2} s^{-1}

Table 2.1 Non-linear restoring forces and parameter ranges of SDOF non-linear systems used for the generation of the training data

In order to obtain the frequency response functions of the non-linear systems, an experimental approach called the stepped sine excitation measurement was implemented

in a numerical simulation. The system was excited by a single-frequency sine wave, the time domain output was computed using the direct integration of Eq. (2.26) and a single point of an FRF was extracted using a frequency response analyser [63]. The process was repeated for all frequencies of interest.

There are other experimental and computation approaches to obtain FRFs. The example of the former would be the impact hammer or random excitation testing. However, none of these can obtain a non-linear FRF of a good quality [289]. The example of the latter is a harmonic balance method (HBM). It is not computationally so expensive as a simulated stepped sine experiment. However, the FRFs computed by the HBM usually includes unstable solutions that cannot be measured in reality. So there is no reason to include these unstable solutions into training data. Therefore, the simulated experiment is more suitable to generate the FRFs because it provides the data in an equivalent form to expected experimental measurements.

For each type of non-linearity the FRFs were generated with the coefficients of the system randomly chosen from the ranges shown in Tab. 2.1. The FRFs were calculated in 256 frequency lines distributed symmetrically around the undamped natural resonance $f_0 = \sqrt{k/m}/2\pi$ with the frequency resolution of 0.1 Hz. For all systems the stepped sine excitation with the increasing excitation frequency and constant excitation amplitude was used, with the exception of the system with the cubic softening stiffness where a decreasing rate was employed instead. The excitation amplitude was randomly selected from the interval $F = [0.1, 2]$ N. Eventually, 500 FRFs of each system were calculated (this number is justified in section 2.3.2).

The parameters of the system and excitation amplitude were chosen in such a manner that the distortion of the calculated FRFs was similar to the typical distortion observed during experimental measurements. The normalised FRFs and their Hilbert transform for weak, moderate and strong non-linear behaviour are displayed in Fig. 2.4 to illustrate the non-linear distortion.

Although the FRFs have been computed for different systems with different coefficients and excitation forces, they all can be well compared to each other after the normalisation. It can be seen for the linear system in Fig. 2.4(a) that the Hilbert transform yielded some small distortion of the original FRFs caused by truncation errors. However, this distortion is not significant because it is much lower than for non-linear cases.

It can be also noticed in Fig. 2.4 that the frequency resolution (0.1 Hz) is quite coarse in some cases. In a typical computational analysis a higher frequency resolution is usually required. On the other hand, while performing experimental studies, a trade-off between

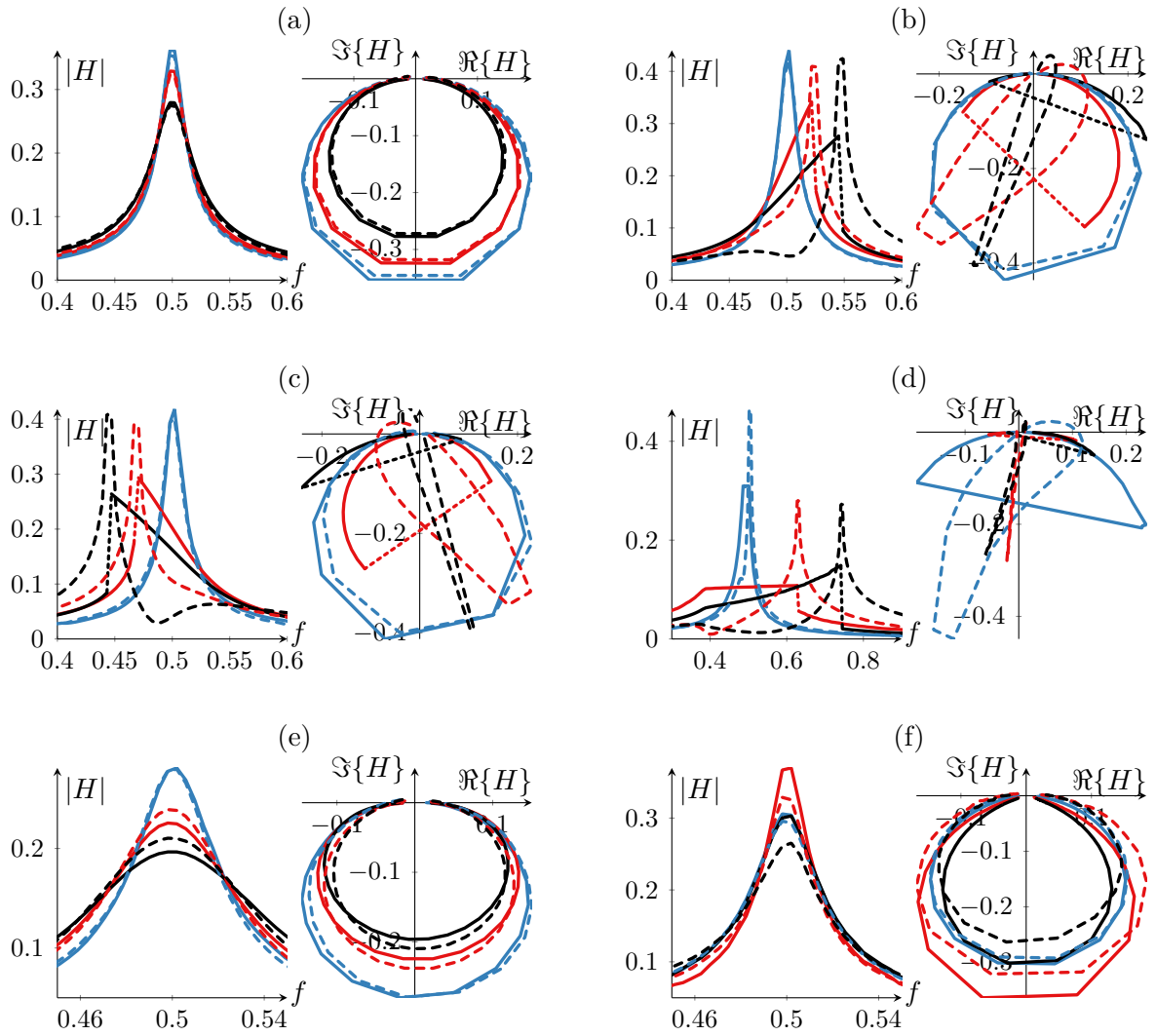

Figure 2.4 Frequency response functions (solid line) and their Hilbert transform (dashed line) with weak (blue), moderate (red) and strong (black) non-linear distortion: (a) linear system, (b) cubic hardening stiffness, (c) cubic softening stiffness, (d) clearance, (e) quadratic damping, and (f) Coulomb friction

the number of measured points and time of the measurements must be sought. Therefore, the frequency resolution was chosen to mimic a typical experimental measurement.

The difference between the FRFs of linear systems, which is barely influenced by the Hilbert transform, and the rest of the classes is evident. In particular, non-linearity in stiffness (hardening, softening and clearance) produces strong distortion of FRFs and their Hilbert transform. There are some similarities between the cubic hardening stiffness in Fig. 2.1(b) and clearance in Fig. 2.1(d). These systems produce similar FRFs, some of which contain a jump phenomenon. Their Hilbert transform is also similar, leading to a

narrower, longer versions of the original FRFs in the Nyquist plot. These similarities are not accidental since both non-linearities share a similar non-linear mechanics. Both of them are characterised by non-linear hardening when the stiffness is increasing with increasing amplitude. For the cubic hardening this increase is gradual whereas for the clearance, it is very rapid. Due to these similarities, the clearance and stiffness hardening FRFs can be sometimes confused and this confusion will be observed in the neural network too.

2.3.2 Non-linearity indexes calculation

For the non-linearity indexes calculation the half-power points were used and $\rho(\omega)$ in Eq. (2.12), Eq. (2.13) and Eq. (2.14) set to one. The non-linearity indexes were subsequently assessed using box plots. The purpose of this process was to observe if there is no strong overlap between the NLIs, or in other words, if linear and non-linear systems do not produce the same values. If this were the case, one of the NLIs would be discarded because it would not bring new information into the process and it could possibly decrease the quality of the pattern. This step is not essential since the redundancy will be eliminated by the PCA. However, it is included here to highlight the ability of the NLIs to distinguish between various non-linearity types.

An example of the box plots for 3 NLIs can be seen in Fig. 2.5. The non-linearity

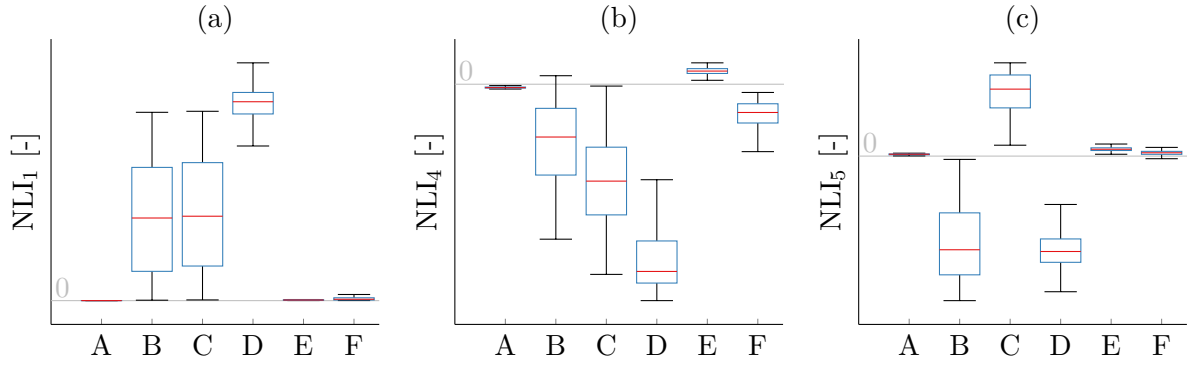

Figure 2.5 Assessment of the non-linearity indexes using box plots: (a) NLI_1 - correlation coefficient, (b) NLI_4 - real part of 1st-order HTD, (c) NLI_5 - imaginary part of 1st-order HTD; A - linear system, B - cubic hardening stiffness, C - cubic softening stiffness, D - clearance, E - quadratic damping, and F - Coulomb friction

index NLI_1 computed using Eq. (2.8) is shown in Fig. 2.5(a). It can be seen that NLI_1, which is based on the cross-correlation coefficient, distinguishes between stiffness and damping non-linearities very well. While cubic hardening, softening and clearance produce significantly higher values of this index, quadratic damping, Coulomb friction

and linear systems are very close to zero. This is in line with the definition of NLI_1 in Eq. (2.8) which is much more sensitive to non-linearities that shift the peak of the FRFs and almost insensitive to non-linearities that scale the amplitudes.

The non-linearity indexes NLI_4 and NLI_5 that have been calculated based on the 1st-order Hilbert transform describers are shown in Fig. 2.5(b) and Fig. 2.5(c), respectively. Unlike the NLI_1 these two indexes can be both positive or negative, but the values also differ for each type of non-linearity even if some overlap can be observed. The NLI_4 effectively distinguishes between Coulomb friction and quadratic damping and the NLI_5 between hardening and softening stiffness.

It is clear that the non-linear indexes significantly reduce the dimension of the pattern recognition problem. Starting from the complex frequency response functions, which have been evaluated in 265 frequency values, the problem has been reduced into 14 scalar parameters that represent the different types of non-linearities.

Reduction using principal component analysis

The principal component analysis was applied to further reduce the dimension of the feature space, i.e. to decrease the number of the input parameters for the ANN as much as possible and also to remove the redundancy of the NLIs. The contribution of the first five principal components (PCs) is captured in Fig. 2.6(a). It can be seen that

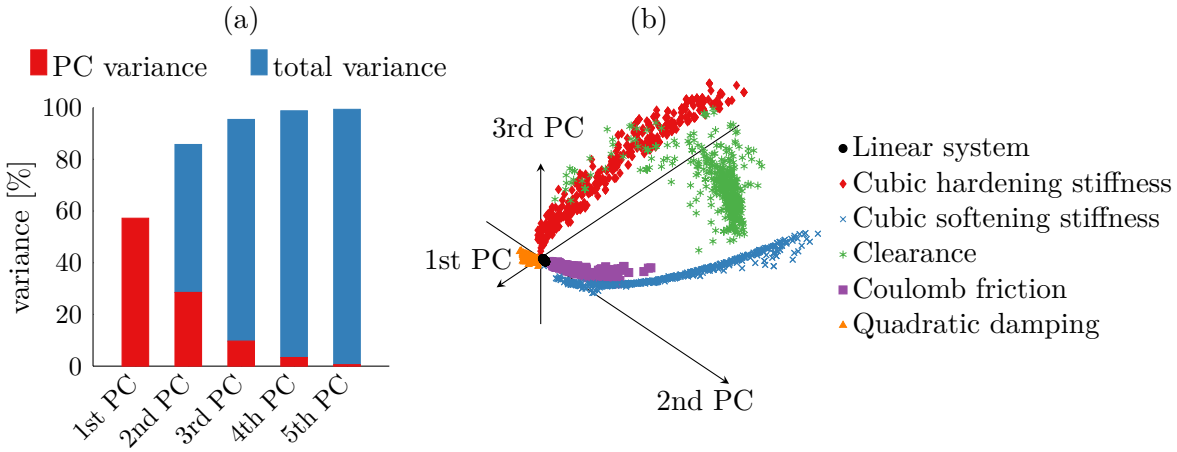

Figure 2.6 Principal component analysis: (a) variance captured by principal components and (b) principal component scores. With the exception of the cubic hardening stiffness and clearance which are mixed due to a similar physical mechanism of these non-linearities at high excitation amplitudes, the principal components score clearly separate the linear and non-linear systems from each other.

only 3 principal components are needed to retain just over 95 % of the total variance.

Therefore, only a set of the first three principal component scores is needed to classify the pattern almost completely. Moreover, these three components can be visualised using three dimensional space as shown in Fig. 2.6(b). It can be seen that the three principal components well separate the groups of the considered non-linear systems. In addition, such a plot allows direct classification of a new pattern by evaluating the position of the new principal component score in the graph. This technique will be demonstrated on experimentally obtained FRFs in section 2.5.

Artificial neural network training

The principal component scores were used as the input data of the artificial neural network and the output classes were defined by the types of non-linearities. The neural network therefore consists of 3 inputs nodes, 6 output nodes and a single hidden layer. A number of the nodes in the hidden layer was found using the 1 to M training strategy [286], leading to 4 nodes in this layer. The data were divided randomly into the data for training, validation and testing in ratio 0.70:0.15:0.15. The final network has the structure 3:4:6 hence possesses 46 weights. Therefore, 500 training FRFs for each non-linearity were required. This number is given with one of the rule of thumb which states that at least 10 times more data are required for good generalisation of unseen patterns [286].

Once the network was properly trained, it was presented again with the same set of 500 systems for each non-linearity to evaluate an overall performance of the trained network. The confusion matrix of the trained network can be seen in Tab. 2.2. Nearly

Identified class	Correct class					
	A	B	C	D	E	F
A	500 (100)	0	0	0	0	1 (0.2)
B	0	499 (99.8)	0	17 (3.4)	0	0
C	0	0	499 (99.8)	0	0	0
D	0	1 (0.2)	0	482 (96.4)	0	0
E	0	0	1 (0.2)	1 (0.2)	500 (100)	0
F	0	0	0	0	0	499 (99.8)

Table 2.2 Testing confusion matrix: A - linear system, B - cubic hardening stiffness, C - cubic softening stiffness, D - clearance, E - quadratic damping, and F - Coulomb friction (the parentheses contain the percentage out of 500)

all cases were identified correctly and only a low percentage (less than 5 %) of confusion can be seen for the systems with the clearance non-linearity. Some of these systems were

misclassified as the hardening stiffness. This, however, is understandable as the physical mechanism of these two non-linearities is similar and some overlap in the input data exists (see Fig. 2.6(b)).

2.4 Application to simulated data

In this section the proposed method is applied to several numerical cases. Firstly, the noise robustness is studied using SDOF systems with a clearance non-linearity. Then the application to a MDOF system is shown.

2.4.1 Noise robustness investigation

The robustness of automated characterisation methods against measured noise should be as high as possible to reduce the probability of errors. In order to investigate the robustness of the proposed method against measured noise, the method was applied to frequency response functions polluted by a varying amount of white noise.

Different levels of noise were introduced to all 500 FRFs for each non-linearity with the signal-to-noise ratio (SNR) of 25, 20 and 15 dB. Figure 2.7 depicts three examples of the noisy FRFs of a system with the clearance. It should be noted that such amount of noise is very unlikely in reality because the noise in the FRFs is highly reduced by processing of the measured time domain signals and their conversion to the frequency domain. During the testing of the robustness against measured noise, the class with

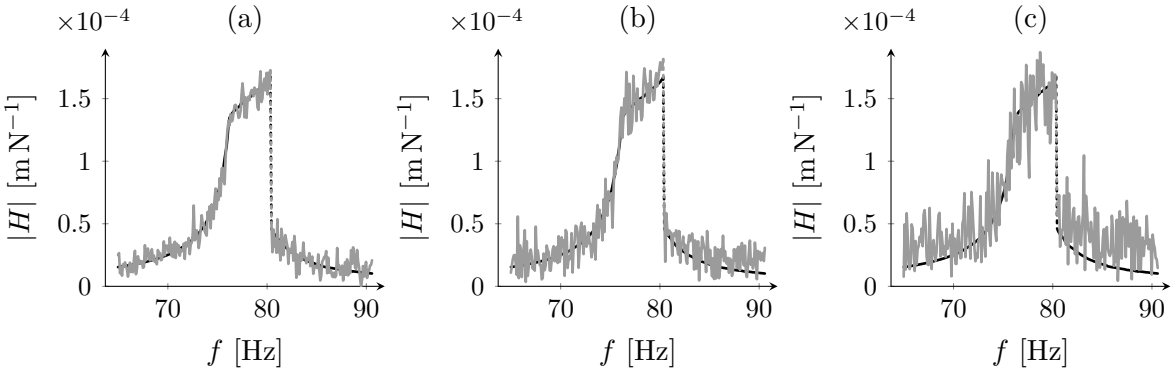

Figure 2.7 Frequency response functions of a system with a clearance non-linearity without noise (black) and polluted by noise (grey) with signal-to-noise ratio of: (a) 25 dB, (b) 20 dB, and (c) 15 dB

the highest network output (the highest probability) was taken as the identified class. No trade-off between probabilities of different classes was considered. The results of

the classification are summarised using confusions matrices in Tabs. 2.3, 2.4 and 2.5.

Identified class	Correct class					
	A	B	C	D	E	F
A	496 (99.2)	0	0	0	4 (0.8)	3 (0.6)
B	0	497 (99.4)	0	19 (3.8)	0	0
C	0	0	499 (99.8)	1 (0.2)	0	0
D	0	3 (0.6)	0	479 (95.8)	0	0
E	3 (0.6)	0	1 (0.2)	1 (0.2)	496 (99.2)	0
F	1 (0.2)	0	0	0	0	497 (99.4)

Table 2.3 Classification results for signal-to-noise ratio 25 dB: A - linear system, B - cubic hardening stiffness, C - cubic softening stiffness, D - clearance, E - quadratic damping, and F - Coulomb friction (the parentheses contain the percentage out of 500)

Identified class	Correct class					
	A	B	C	D	E	F
A	436 (87.2)	1 (0.2)	0	0	4 (0.8)	9 (1.8)
B	0	487 (97.4)	0	101 (20.2)	0	0
C	0	0	496 (99.2)	10 (2)	0	0
D	0	12 (2.4)	0	376 (75.2)	0	0
E	39 (7.8)	0	3 (0.6)	10 (2)	496 (99.2)	0
F	25 (5)	0	1 (0.2)	3 (0.6)	0	491 (98.2)

Table 2.4 Classification results for signal-to-noise ratio 20 dB: A - linear system, B - cubic hardening stiffness, C - cubic softening stiffness, D - clearance, E - quadratic damping, and F - Coulomb friction (the parentheses contain the percentage out of 500)

Comparing the results to Tab. 2.2 it is clear that the artificially introduced white noise influences the results of the classification. The influence is low for the highest SNR and becomes slightly more significant for the higher amount of noise. However, despite some misleading detection and characterisation, a majority of cases is classified correctly. The most significant problems were encountered for the clearance non-linearity under the strong influence of added noise (SNR 15 dB). Under this condition just under a half of the systems was characterised correctly while a significant portion of the systems was again misclassified as the cubic hardening stiffness. This is once more caused by a similar physical mechanics of these two non-linearities. Nevertheless, given the very high level of measured noise, the results can still be considered as satisfying.

Identified class	Correct class					
	A	B	C	D	E	F
A	342 (68.4)	1 (0.2)	0	0	16 (3.2)	18 (3.6)
B	12 (2.4)	472 (94.4)	0	215 (43)	2 (0.4)	1 (0.2)
C	2 (0.4)	0	491 (94.2)	32 (6.4)	2 (0.4)	2 (0.4)
D	0	27 (5.4)	0	213 (42.6)	0	0
E	75 (15)	0	7 (1.4)	37 (7.4)	479 (95.8)	2 (0.4)
F	69 (13.8)	0	2 (0.4)	3 (0.6)	1 (0.2)	477 (95.4)

Table 2.5 Classification results for signal-to-noise ratio 15 dB: A - linear system, B - cubic hardening stiffness, C - cubic softening stiffness, D - clearance, E - quadratic damping, and F - Coulomb friction (the parentheses contain the percentage out of 500)

A significant confusion can also be observed between linear systems and systems with quadratic damping and Coulomb friction for signal-to-noise ratios lower than 20 dB. Up to 30 % of systems have been classified as non-linear despite being linear, but due to the very large amount of noise (see Fig. 2.7(c)) this can still be considered as an acceptable result. As already noted, the considered amount of noise is very unlikely to be observed in measured FRFs due to the advanced signal processing required for their extraction. Nevertheless, the FRFs can be distorted due to other issues so the ability of the proposed method to characterise the non-linearity with high level of confidence from noisy FRFs is a valuable property.

2.4.2 Application to a multi-degree-of-freedom system

A simple model of a cantilever plate with a cubic hardening stiffness is used to demonstrate the performance of the proposed method on MDOF systems. The model shown in Fig. 2.8 consists of 15 discrete masses ($m = 1\,\mathrm{kg}$) which are connected by linear springs ($k = 1 \times 10^6\,\mathrm{N\,m^{-1}}$). The viscous damping is introduced using Rayleigh's proportional

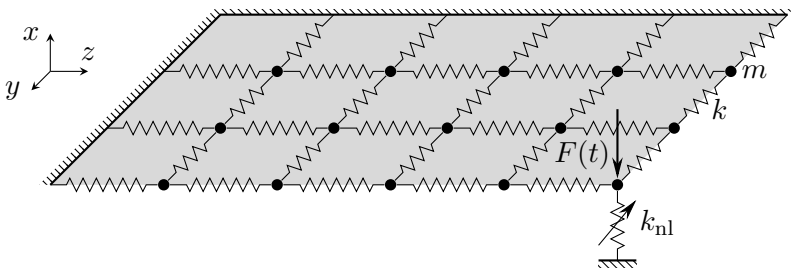

Figure 2.8 The model of the plate with a cubic hardening stiffness spring

damping model with $\alpha = 2$ and $\beta = 1 \times 10^{-8}$. The plate is clamped at two edges and free at the other two. The system is excited by a sinusoidal force $F(t)$ that is placed in the corner of the plate and pointed in vertical direction since the plate is allowed to vibrate only in this direction. Two amplitudes of the excitation force are chosen ($F = 10\,\mathrm{N}$ and $F = 20\,\mathrm{N}$) to emphasise the effect of the non-linearity. The non-linear spring with cubic hardening behaviour ($k_{\mathrm{nl}} = 1 \times 10^{10}\,\mathrm{N\,m^{-3}}$) is placed in the same position as the excitation force. The equations of motion, which were assembled based on the Lagrange equations of the second kind, are written in a matrix form as

$$\mathbf{M}\ddot{\mathbf{x}} + [\alpha\mathbf{M} + \beta\mathbf{K}]\,\dot{\mathbf{x}} + \mathbf{K}\mathbf{x} + \mathbf{f}_{\mathrm{nl}}(\mathbf{x}, \dot{\mathbf{x}}) = \mathbf{F}(t), \tag{2.27}$$

where $\mathbf{M}$, $\mathbf{K}$ are mass and stiffness matrices, $\mathbf{x}$, $\dot{\mathbf{x}}$, $\ddot{\mathbf{x}}$ marks displacement, velocity and acceleration vectors, respectively, and $\mathbf{F}(t)$ is the excitation force vector. The term $\mathbf{f}_{\mathrm{nl}}(\mathbf{x}, \dot{\mathbf{x}})$ describes the non-linear restoring forces, consisting of one non-zero element $k_{\mathrm{nl}}x^3$. The harmonic balance method (HBM) has been used to compute the FRFs and unstable parts have been removed to mimic the jump phenomenon of measured FRFs. The calculated receptance at the position of the non-linear spring can be seen in Fig. 2.9 where the frequency range covering the first 5 modes is shown. Generally, the FRF does

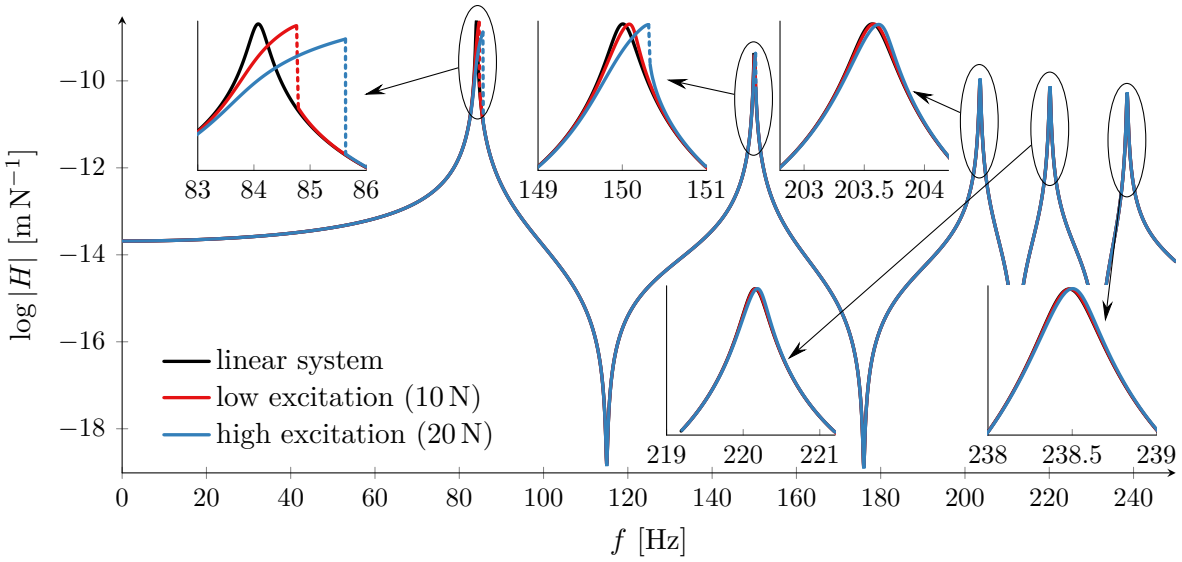

Figure 2.9 Frequency response functions of the plate with a cubic hardening stiffness spring

not have to be measured at the same position as the excitation and/or non-linearity and the method will still function as intended.

For detection and characterisation of non-linear behaviour the network was exactly the same as for the previous cases, i.e. no additional training data have been added and no

modification has been made to account for multi-mode FRFs. As discussed in section 2.2 the method has to be applied on a single mode of vibration. Therefore, the multi-mode FRF was divided at the anti-resonances and the modes were treated separately as if they were obtained from a SDOF system. The results of the classification are summarised in Tab. 2.6 in which the percentage in the brackets indicates the probability of the classified class.

mode	linear ($k_{\mathrm{nl}} = 0$)	low excitation (10 N)	high excitation (20 N)
1	linear (98.1)	hardening (98.8)	hardening (99.9)
2	linear (96.0)	hardening (99.6)	hardening (93.2)/clearance (6)
3	linear (97.9)	linear (83.3)/hardening (16.3)	hardening (98.3)
4	linear (95.7)	linear (92.6)	linear (78.9)/hardening (20.7)
5	linear (95.4)	linear (93.5)	linear (93.8)

Table 2.6 Classification results for the plate (the values in the parentheses stand for the probability of the output class)

All considered modes of the linear FRF have been classified correctly, but some confusion can be observed for non-linear FRFs. Some of the higher modes, especially mode 5, of the non-linear plate have been characterised as linear. This could be considered as an error of the proposed method. On the other hand, it can be seen from the insets of modes in Fig. 2.9 that the non-linear distortion is very weak in higher modes. This means that not only has the method been able to identify strong cubic hardening behaviour in several first modes, but it also provided an indication of the appearance of weaker non-linear effects by giving both linear and non-linear output classes. This behaviour can be seen in the 3rd mode under low excitation and in the 4th mode under high excitation. For these modes the network indicated about 20 % probability that the mode behaves non-linearly, which cannot be directly observed in Fig. 2.9. It can also be noticed in Tab. 2.6 that the probability of the hardening behaviour for the second mode is slightly lower for the higher excitation. This result is caused by the misclassification of the hardening behaviour as the clearance non-linearity. This misclassification may be again explained by similar physical mechanism of these two non-linearities. In a practical application of the proposed method this misclassification would not be probably even noticed since the class with 93 % would be most likely deemed as the only relevant output.

2.5 Application to experimental data

To evaluate the practical feasibility of the proposed method, it was applied to several experimentally measured frequency response functions. Three test rigs, namely a simple cantilever beam with a clearance non-linearity, an under-platform damper test rig and the ECL benchmark, are presented.

2.5.1 Cantilever beam with a clearance non-linearity

The experimental set-up can be seen in Fig. 2.10. A thin steel beam (300×36×3 mm) is

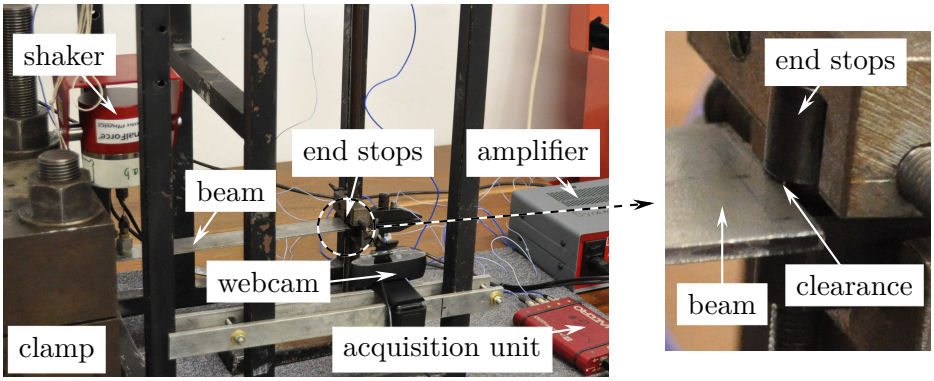

Figure 2.10 Cantilever beam: experimental configuration

held by a very stiff (considered rigid) clamp at one end and is unsupported at the other end. The system is excited by an attached shaker which is placed as close to the clamp as possible. Two end stops are placed close to the free end of the beam representing a backlash, which can be found in many engineering applications. The end stops are created by a smaller clamp, which is rigidly attached to the supporting bar. To ensure that the end stops are placed symmetrically to the beam, the webcam was used to capture a detailed image of the set-up and the gap between the end stops was digitally measured.

Since the strength of the non-linearity can be controlled through the size of the gap, the measurements were repeated for two different sizes (0.1 mm and 0.2 mm). The linear (without the end stops) and non-linear frequency response functions for the small and large clearance sizes measured around the first natural frequency can be seen in Fig. 2.11. It can be noticed that the FRFs were not measured with very high frequency resolution. The coarse frequency resolution of 0.1 Hz was intentionally chosen to observe the performance of the proposed method on non-ideal experimental FRFs. It can be seen that the FRFs for the beam with no end stops practically overlay each other whereas the end stops introduced significant non-linear behaviour, including the jump phenomena. It

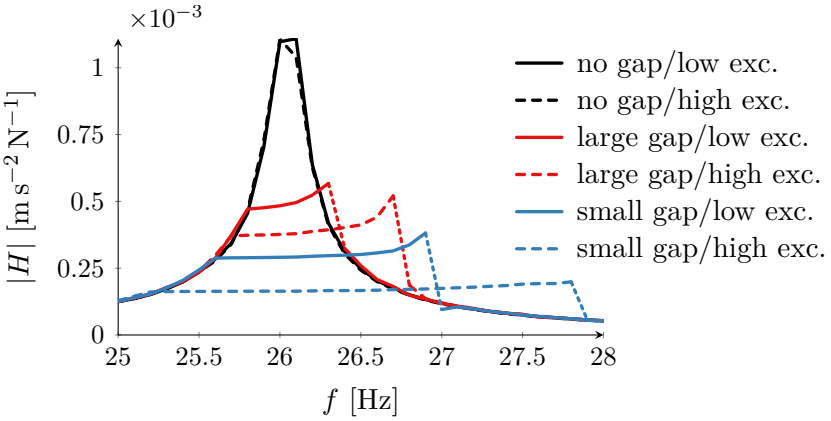

Figure 2.11 Cantilever beam: measured frequency response functions

is also clear that the smaller gap led to stronger non-linear behaviour (greater amplitude reduction and frequency shift) than the larger gap under the same excitation.

It is assumed that other modes do not significantly influence the response in a close proximity of the first bending mode. Therefore, the first mode may be treated as a response of a SDOF system and the proposed method may be applied. The measured FRFs were processed according to the flow chart in Fig. 2.3. The direct use of principal component scores obtained from the FRFs is illustrated in Fig. 2.12. It can be seen that

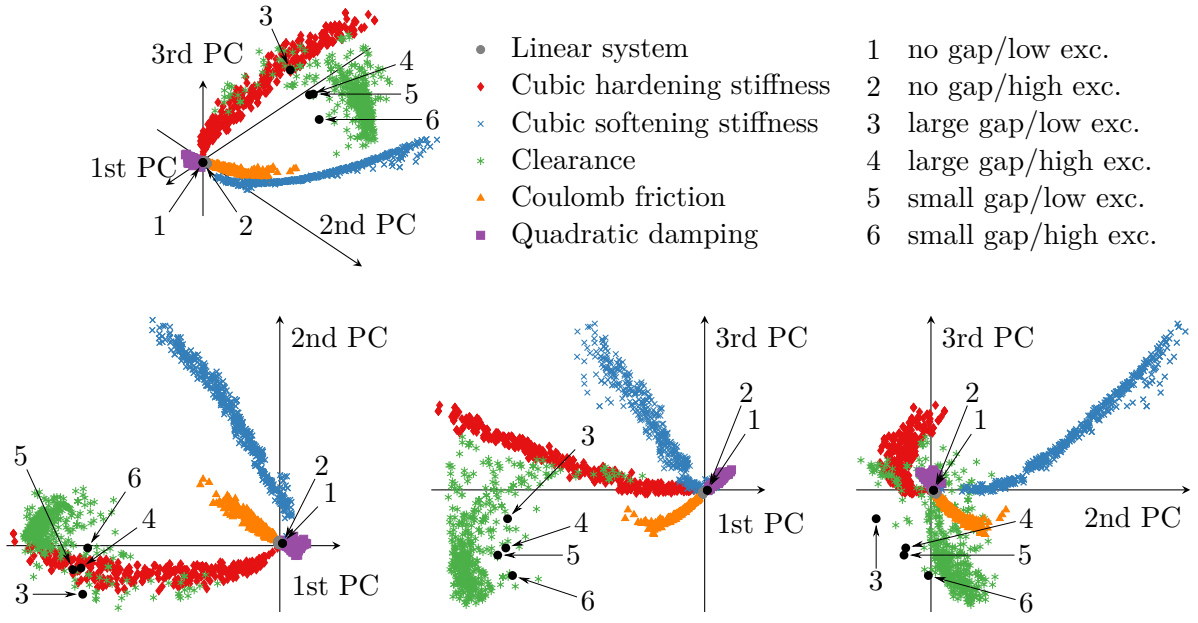

Figure 2.12 Principal component analysis of the cantilever beam: (top) perspective view and (bottom) side views. The coloured points represent the principal component scores of the training data while the labelled black points were obtained from the experimental frequency response functions.

the FRFs measured without the non-linearity are very close to the linear area of the graph despite some small overlap with the Coulomb friction. On the other hand, the PCS of the FRFs that are affected by the end stops lie clearly in the green area of the clearance non-linearity.

Although it is possible to observe the type of non-linearity directly from Fig. 2.12, a more accurate and fully automatic decision can be made using the ANN. The same network, which was trained using SDOF non-linear oscillators in section 2.3.2, was applied to these FRFs and the results of classification are summarised in Tab. 2.7. It is seen that

excitation	no gap	small gap	large gap
low	linear (70.4 %)/friction (29.1 %)	clearance (99.9 %)	clearance (99.9 %)
high	linear (73.9 %)/friction (25.2 %)	clearance (99.9 %)	clearance (99.9 %)

Table 2.7 Classification results for the beam with a clearance non-linearity

non-linear behaviour has been classified correctly with a high level of confidence. It is interesting to notice that the analysis of the FRFs measured without the end stops have revealed almost 30 % probability of friction in the structure. This seems to be reasonable since it can be explained by the presence of the clamp. This particular clamp had been extensively used for a variety of testing in the past, so its functional internal surfaces are not perfectly smooth. Therefore, despite the effort to ensure the linear behaviour, some micro-slip in the clamp can cause the observed friction. These results correspond to the observations made directly using principal component scores.

2.5.2 Under-platform damper

An under-platform damper is a metal device placed on the underside of the platform between adjacent blades. The under-platform dampers are commonly used in aircraft engines to dissipate energy on their friction interfaces, which leads to a frequency shift and significant decrease of vibration amplitude. The influence of the under-platform damper on dynamics of the blades has been extensively studied in [196–198] both experimentally and numerically. The experimental set-up seen in Fig. 2.13 was used to experimentally investigate the effects of an under-platform damper on the vibration behaviour of turbine blades. The FRFs measured in [196–198] were kindly provided for the demonstration of the proposed method.

Some of the FRFs measured around the first mode of vibration in which the blades simultaneously vibrate on the first bending mode can be seen in Fig. 2.14. A stepped

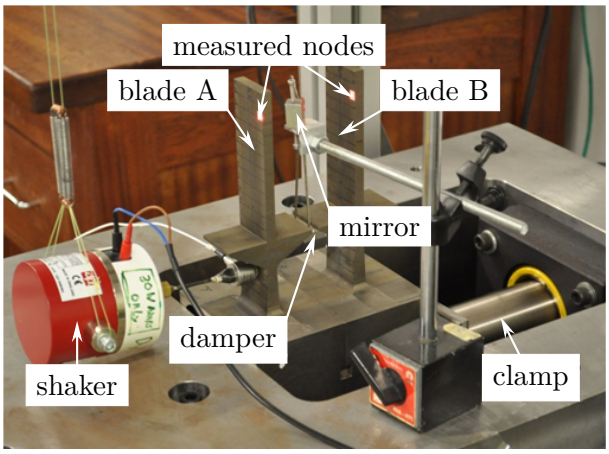

Figure 2.13 Under-platform damper: experimental configuration

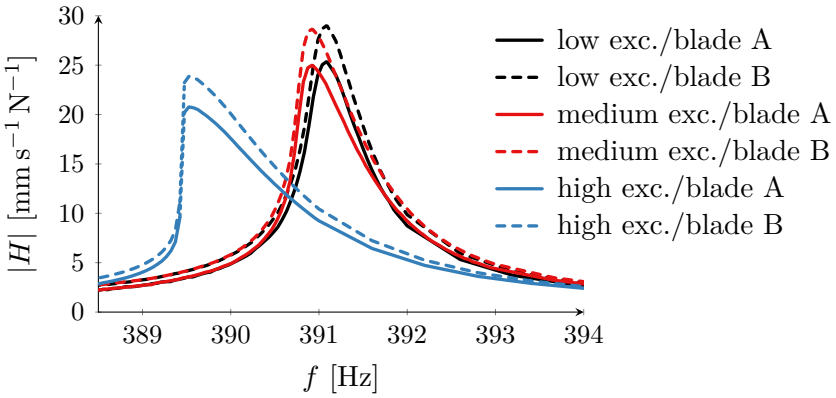

Figure 2.14 Under-platform damper: measured frequency response functions

sine excitation applied to the blade A with a decreasing frequency rate was used and the FRFs were measured using two non-contact laser Doppler vibrometers focused near the tip of each blade (see Fig. 2.13). It is assumed that the first mode is not significantly influenced by the higher modes and the proposed method can therefore be applied.

The measured mobility was converted to the receptance using Eq. (2.1) and processed according to the flow chart from Fig. 2.3. The principal component scores are shown in Fig. 2.15. It can be seen that no linear behaviour has been detected in the experimental test rig. Most of the measured PCS lie in the softening area although the PCS approach the linear and Coulomb friction area under the low level of excitation.

To obtain the quantitative values the same network was applied and the results are summarised in Tab. 2.8. In this case, no linear behaviour has been observed, not even at the lowest level of the excitation. The linear behaviour, however, was not expected since the damper is attached and introduces the non-linear effects, albeit weak, into

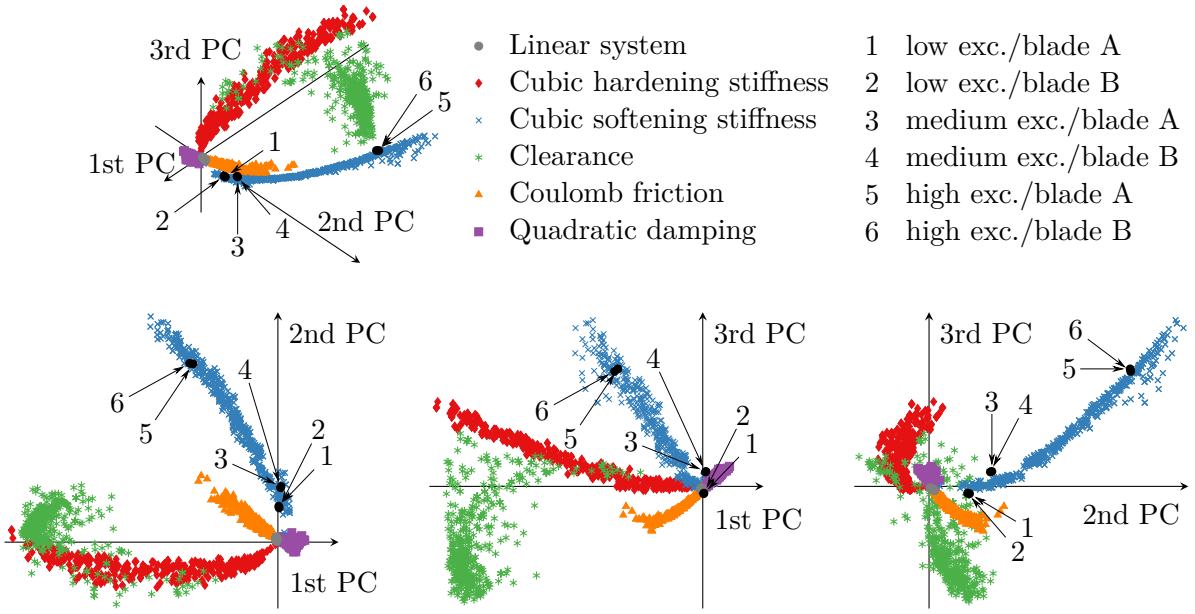

Figure 2.15 Principal component analysis of the under-platform damper: (top) perspective view and (bottom) side views. The coloured points represent the principal component scores of the training data while the labelled black points were obtained from the experimental frequency response functions.

excitation	blade A	blade B
low	softening (43.0 %)/friction (56.6 %)	softening (44.1 %)/friction (55.5 %)
medium	softening (69.9 %)/friction (30.0 %)	softening (70.8 %)/friction (29.2 %)
high	softening (99.6 %)	softening (99.7 %)

Table 2.8 Classification results for the under-platform damper (the values in the parentheses mark the probability of the output class)

the structure. Under the low level of excitation the classification yielded almost equal probabilities of softening stiffness and friction while only softening was observed at high amplitudes. The under-platform damper is usually modelled using sophisticated macro- and micro-slip models [196–198]. Although the results do not directly relate to these models, they reflect the effects observed in the FRFs. Under low excitation the amplitude is reduced with only a minor frequency shift, whereas at high excitation levels the resonance frequency is significantly shifted to the left and the jump in the response can be seen. The classification is consistent for the both blades although the FRFs that have been measured from blade A and B are slightly different.

2.5.3 The ECL benchmark

In this section the proposed method is applied to the ECL benchmark. The ECL benchmark was designed to compare non-linear system identification methods [261] and has been extensively used in the past 15 years for both numerical and experimental studies. Many non-linear system identification methods have been applied to this benchmark, including conditioned reverse path method [115], proper orthogonal decomposition [139], wavelet transform [10], normal non-linear modes [189, 191] and model updating [151].

The ECL benchmark consists of a main long cantilever beam with a thin short beam attached to its end. The thin beam is also clamped and introduces a strong geometric non-linearity. The nominal dimensions of the beams are the same as in [189, 191]. The main beam is 0.7 m long, 0.014 m wide and 0.014 m thick while the thin beam is only 0.04 m long, 0.014 m wide and 0.0005 m thick. Both beams are made of steel with nominal Young's modulus $E = 2.1 \times 10^{11}$ Pa and density $\rho = 7800\,\mathrm{kg\,m^{-3}}$.

The experimental set-up is shown in Fig. 2.16. The connection of the thin and main

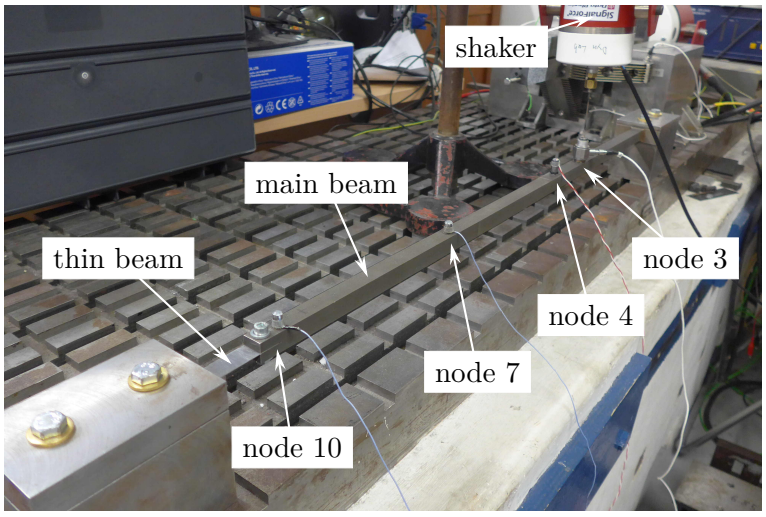

Figure 2.16 Experimental set-up of the ECL benchmark

beam is realised through a simple bolted joint. The care was taken to manufacture this connection as accurately as possible in order to minimise any friction effects. The dynamic response is measured by three accelerometers placed at node 4, 7 and 10. A sharer placed in node 3 is used for the measurements of frequency response functions used in this section.

The measured FRFs from nodes 4,7 and 10 in a close proximity of the first mode can be seen in Fig. 2.17. The influence of the higher modes on the FRFs measured around the first mode are assumed to be minimal so the proposed method can be applied. This

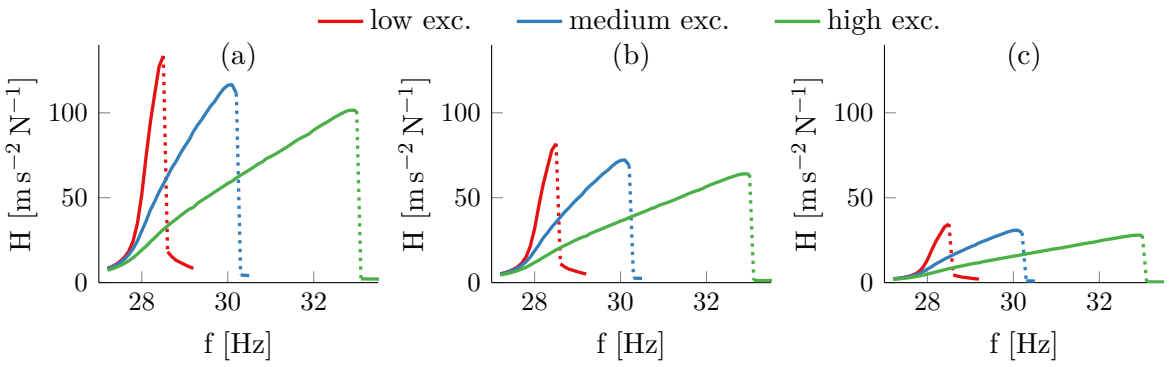

Figure 2.17 Measured frequency response functions of the ECL benchmark: (a) node 10, (b) node 7 and (c) node 4

assumption is justified because the second natural frequency is close to 150 Hz which over 100 Hz more than the first resonance frequency. It can be seen that the FRFs exhibit strong non-linear behaviour of a hardening type and are consistent for all measured nodes. It should be noted that it was attempted to measure an FRF with linear behaviour. However, this proved to be impossible due to the limitations of the acquisition hardware which was not able to provide such a low excitation level. The non-linearity can therefore be considered as inherent to the system.

The same neural network as in the previous cases was applied and the results are tabulated in Tab. 2.9. It can be seen that only non-linear behaviour has been detected.

excitation	node 10	node 7	node 4
low	hardening (98.1 %)	hardening (96.1 %)	hardening (94.1 %)
medium	hardening (97.8 %)	hardening (96.9 %)	hardening (99.3 %)
high	clearance (95.6 %)	clearance (99.7 %)	clearance (99.7 %)

Table 2.9 Classification results for the ECL benchmark (the values in the parentheses mark the probability of the output class)

This was expected because all FRFs exhibit a jump phenomenon which significantly influences the shape of the frequency response functions. All FRFs measured under low and medium excitation have been characterised correctly as cubic hardening stiffness. On the contrary, the FRFs measured under high excitation have been misclassified as clearance non-linearity. This type of misclassification has already occurred in this chapter. A large number of systems with cubic hardening stiffness were incorrectly classified as systems with clearance. This error is caused by similarities in the physical mechanisms of these two non-linearities.

In this section the proposed method was applied to the FRFs of the ECL benchmark and the hardening behaviour has been characterised. The ECL benchmark will be also used in section 5.4 to demonstrate the proposed approach to non-linear modal analysis.

2.6 Discussion

A method for detection and characterisation of non-linear behaviour from a single frequency response function (FRF) has been proposed in this chapter. The method uses a normalised single mode FRF together with their Hilbert transform to derive a set of non-linearity indexes for an accurate and effective description of non-linear behaviour. Dimensionality reduction of these indexes via principal component analysis allows the creation of a compact artificial neural network, which subsequently classifies the non-linearities. The performance of the method has been evaluated using a number of test cases - some of which were numerical while others were experimental.

It was found that the method is capable of detecting and characterising non-linearities accurately while being robust against measured noise. Moreover, provided that a suitable neural network has been trained, the method works in a timely-fashion and avoids a subjective decision which may require vast experience in the field. The proposed method can be therefore used as a pre-step of linear modal analysis to quickly verify the assumption of linear behaviour in routine industrial testing. The successful characterisation of three experimental cases, each with a different type of non-linearity, highlighted the applicability of the method to the experimentally measured FRFs.

In contrast to the similar method presented in [125, 126], the proposed method cannot localise the non-linearity within the structure. However, this is well balanced by the fact that it does not require any high or low fidelity model of the structure. The proposed method also dramatically minimises the number of data sets that are needed for the optimal training of the network.

The proposed method is very versatile - once the proper ANN has been trained for desired types of non-linearities, it can be applied to any kind of system as long as the modes are well separated. The need to train the ANN for certain types of non-linearities can be, however, also considered as a drawback. In order to detect and characterise a particular type of non-linearity, this non-linearity must be included in the training data. It is theoretically possible to obtain insight into the non-linear behaviour even if the non-linearity has not been included in the training data by carefully examining the output of the network. For instance, it was shown in section 2.5.2 that the network indicated almost equal presence of the cubic softening stiffness and Coulomb friction.

This was interpreted as an indication of a complex contact interface. This ability of the proposed method is sometimes referred to as identification of unseen patterns [91]. Although this ability can be sometimes useful the interpretation of such results require a good knowledge of the structure so it is likely that the detection and characterisation are not required.

As discussed in section 1.2.1 it may be sometimes useful to quantify whether the non-linearity is weak, moderate or strong, i.e. to estimate to what extent the non-linearity influences the linear behaviour of the structure. The quantification of non-linearity strength has not been attempted in this thesis because, as discussed in section 1.2.1, there is no universal way to define what weak, moderate or strong non-linearity mean. Such a classification must be bound to a specific application in which strong non-linearities would, for instance, cause structural damage, whereas weak non-linearities would only increase the amount of vibration-induced noise. For the specific application, the strength of non-linearity could be achieved by the proposed method if the neural network was appropriately trained. The present version of the proposed method can also provide a limited indication of the non-linearity strength. This was seen in section 2.4 where the transition between the linear and non-linear behaviour of the plate with cubic hardening stiffness was indicated by the probability of output classes.

2.7 Conclusion

This chapter proposed a new method for detection and characterisation of non-linearities based on the Hilbert transform in the frequency domain and artificial neural networks. It was shown that the method is robust against measured noise and can be applied to a single measured frequency response function. Due to the use of the artificial neural network, the method does not require expertise decision making and is therefore suitable as an automatised pre-step of the linear modal analysis in industrial context. The proposed method fulfils the requirements of the first objective of this thesis, i.e. it enables robust and fast detection and characterisation of non-linearity from a single frequency response in an industrial framework.

Chapter 3

The Hilbert-Huang transform in non-linear system identification

Abstract

This chapter creates a transition between the frequency domain detection and characterisation used in the previous chapter and the non-linear system identification using time-frequency methods used in the rest of the thesis. Firstly, it is discussed why the representation of a time series by the instantaneous frequency (IF) and amplitude (IA) can be potentially better than other time-frequency/time-scale methods. In particular, the Hilbert-Huang transform (HHT) is described in detail. The HHT consists of two steps - the empirical mode decomposition (EMD) and a method for instantaneous frequency and amplitude estimation. The EMD, which allows a multi-scale decomposition of a signal in terms of oscillatory functions, is reviewed and its problems and drawbacks discussed. Then, the methods for estimation of instantaneous frequency and amplitude are described and applied to the testing signal obtained from a Duffing oscillator to evaluate their performance and identify the properties that can be used for system identification. A new method which can identify intra-wave frequency modulation is proposed at the end of the chapter.

3.1 Introduction

In the previous chapter the new method for detection and characterisation from a frequency response function was proposed. The first objective of the thesis, i.e. to enable robust and fast detection and characterisation of non-linearity from a single frequency response function in an industrial framework, has been therefore achieved. This chapter starts addressing the second objective of the thesis, i.e. the investigation of time-frequency methods and their use in non-linear system identification. This chapter creates a transition between the frequency domain detection and characterisation and the non-linear system identification using time-frequency methods.

In section 1.3.2 it was found that the Hilbert-Huang transform (HHT) is potentially better than any other time-frequency analysis method because it does not use any fixed basis for decomposition. It is therefore fully adaptive, so it does not require any a priori knowledge of the system or non-linearity. Moreover, the HHT uses the concept of instantaneous frequency and amplitude which has more natural physical interpretation than the Fourier-based representation of time series. In the first step of the HHT a complicated (potentially) multi-component, non-linear and non-stationary signal is decomposed into oscillatory functions, termed intrinsic mode functions (IMFs). Subsequently, the instantaneous frequency and amplitude are estimated by the Hilbert transform or other methods.

The objective of the chapter is the introduce the Hilbert-Huang transform in detail. The empirical mode decomposition is described and its limitations and problems discussed. Then, a review of a number of methods for instantaneous frequency and amplitude estimation developed in other fields is conducted in order to identify methods that could potentially replace the Hilbert transform. This is needed because, despite the fact that the Hilbert transform is traditional used for the IF and IA estimation, it suffers from a number of numerical and mathematical issues which can cause problems when interpreting its results. Based on the comparison and assessment of the alternative methods, several suggestions about their usage is given and a new method which allows identification of intra-wave frequency modulation is proposed.

This chapter is organised as follows: section 3.1.1 justifies the selection of the Hilbert-Huang transform for non-linear system identification by showing the lack of physical interpretation of other time-frequency methods. Then, the Hilbert-Huang transform is described. Firstly, the empirical mode decomposition is introduced in section 3.2 where its problems, such as mode mixing, are discussed and some solutions suggested. Then, the review of methods for instantaneous frequency and amplitude estimation is conducted in section 3.3. Based on this review, a new method for detection and characterisation

of non-linearities using intra-wave frequency modulation is proposed in section 3.4 and its application shown on two numerical cases. The chapter concludes by the discussion (section 3.5) of problems and limitations of the Hilbert-Huang transform.

3.1.1 The physical interpretation of time-frequency methods

Three groups of time-frequency analysis methods have been described in section 1.3.2, namely time-frequency methods, time-scale methods, and methods based on the instantaneous frequency and amplitude. Many Fourier-based system identification methods (time-frequency and time-scale methods) have been developed as discussed in section 1.3.2. However, the Fourier representation of data lacks a meaningful physical interpretation for non-linear and non-stationary time series. This fact is discussed in this section to justify the use of the Hilbert-Huang transform for non-linear system identification in this thesis.

Any data can be expressed using the Fourier expansion as

$$x(t) = \sum_{j=1}^{n} a_j \mathrm{e}^{\mathrm{i}\omega_j t}, \tag{3.1}$$

where the amplitudes a_j and frequencies ω_j are constants. In contrast, the same data can be represented by the Hilbert-Huang transform [103] as

$$x(t) = \sum_{j=1}^{n} a_j(t) \mathrm{e}^{\mathrm{i}\int \omega_j(t)\mathrm{d}t}, \tag{3.2}$$

where the amplitudes and frequencies are functions of time. Therefore, they are called the instantaneous amplitude (IA) and instantaneous frequency (IF), respectively. The Hilbert representation of data is sometimes seen as a generalised Fourier expansion [101, 102] because it enables to accommodate non-stationary and non-linear data. It should be noted that Eq. (3.2) is very general, because both IF and IA are unspecified functions of time. This equation is only a formal representation of the Hilbert-Huang transform because it cannot be directly used to compute the transform.

The physical interpretation of the Fourier-based representation of measured time series is discussed using the data which are used in section 3.3 to evaluate the performance of IF and IA estimation methods. The system which has been used to compute the data is not important at the moment, but it is important to note that the data are both non-stationary and non-linear. The time series representing the displacement, velocity and acceleration of the testing system are shown in Fig. 3.1. The displacement is used to show why time-frequency and time-scale methods that are based on the Fourier

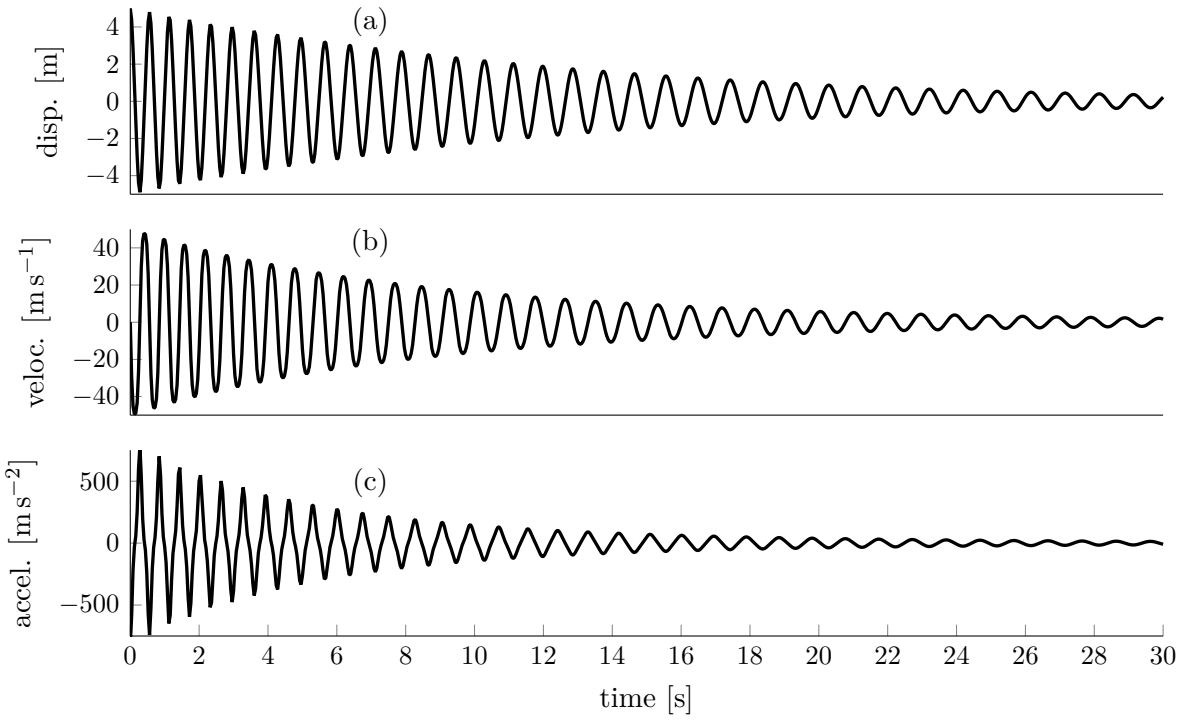

Figure 3.1 Response of the Duffing oscillator described in section 3.3.1: (a) displacement, (b) velocity and (c) acceleration

representation of the signals provide results which can be difficult to interpret [101–103] for non-linear and non-stationary signals.

The first issue is that the Fourier transform requires stationarity in the data. Therefore, it may not be clear how to interpret the spectrum of the displacement displayed in Fig. 3.2(a). It can be seen that the spectrum contains a region of high amplitudes centred about 1.5 Hz, which, however, does not look as a typical vibration mode with a sharp peak. Instead, the magnitude of the peak increases with the increasing frequency between 1 Hz and 2 Hz. There is no reliable way how to accurately define the natural frequency from this spectrum, or to known if the frequency is time-varying or if all frequency components appear in the response simultaneously. There is also no way of knowing whether the system approaches linear behaviour for high or low amplitudes. The use of the Fourier transform to non-stationary signals is therefore quite misleading, given very unclear information provided. However, if it is known that the peak corresponds to one mode whose frequency varies in time, the frequency and corresponding amplitude can be roughly estimated.

The requirement of stationarity can be removed by the application of the Fourier or wavelet transform to short blocks of data. Non-stationary data can be analysed

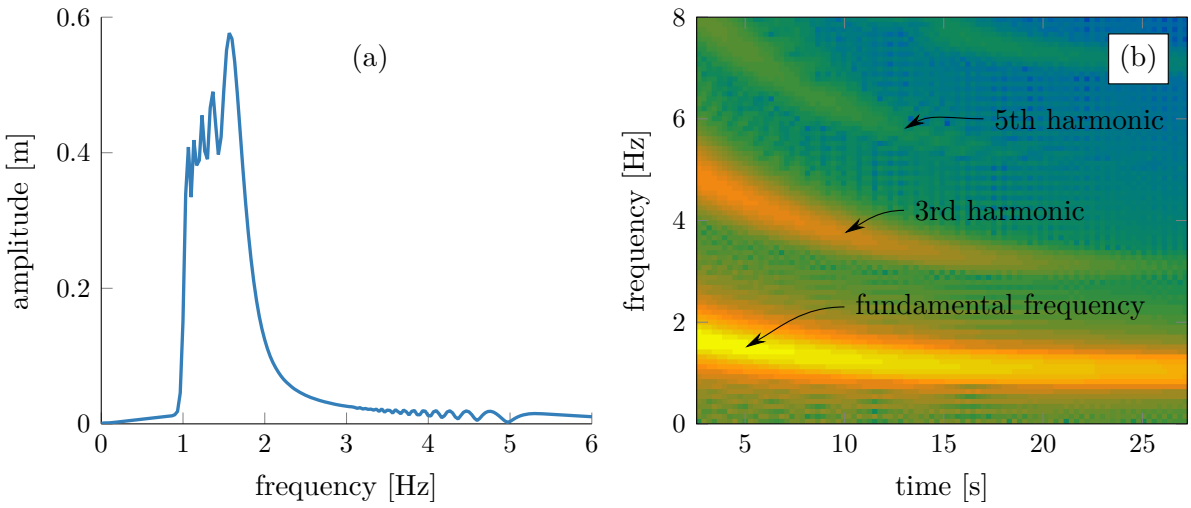

Figure 3.2 Application of the Fourier-based analysis to the testing signal: (a) spectrum and (b) spectrogram

because some stationary exists in a block, thereby allowing to interpret a set of spectra. However, a more serious issue remains - the Fourier transform does not have a meaningful physical interpretation for non-linear processes which would be suitable for non-linear system identification [103]. In order to describe non-linear signals, several harmonics are needed, but they are sometimes regarded as a mathematical artefact of the selected data processing [101, 102] as oppose to a reflection of a studied physical phenomenon. For example, the spectrogram of the displacement in Fig. 3.1 obtained by the short-time Fourier transform is shown in Fig. 3.2(b) where a logarithmic scale is used to emphasise the harmonics. The dominant frequency component and several higher harmonics can be seen. However, they cannot be directly observed in the time signals in Fig. 3.1 without the knowledge of the Fourier transform. Observing these signals, one cannot see several harmonic components with different decreasing amplitude and decreasing frequencies, but rather signals with one decreasing amplitude and frequency that is almost constant, fluctuating about a fix value. The fluctuating frequency is particularly visible in the acceleration in Fig. 3.1(c), where the slope of the signal changes significantly close to zero amplitudes. When Fourier based analysis methods are used for non-linear system identification, the harmonics are often ignored and only the amplitude and frequency of the dominant component are considered. That, however, means that the energy of the signal will not be correctly interpreted because some components are missing, and the amplitude of the dominant frequency does not correspondent correctly to the amplitude of the signal. Moreover, by looking at Fig. 3.2(b), there is no way of knowing how many structural modes should be estimated. One might correctly assume that the

higher components are a consequence of non-linearity or they can be misinterpreted as structural modes. Overall, the interpretation of the measured non-linear series based on the Fourier series is not very natural [71]. The methods for instantaneous frequency and amplitude estimation seem to offer more possibilities with regards to non-linear system identification [103].

However, it should be stressed that it does not mean that the Fourier transform is an invalid concept. Many extremely useful theories and methods (including the harmonic balance method and non-linear modal analysis used in this thesis) have been developed based on the Fourier transform and are widely used for computation studies in non-linear dynamics. The Hilbert-Huang transform simply presents an alternative concept which was observed to be better suited for the processing and interpretation of non-linear and non-stationary data. Unlike the Fourier transform, the HHT has very limited rigorous mathematical background, because Eq. (3.2) is only a formal representation of the transform, but cannot be used to perform the transform itself. Its two steps - the empirical mode decomposition and a method for instantaneous frequency and amplitude estimation - are described in the following.

3.2 Empirical mode decomposition

The empirical mode decomposition (EMD) is a key and unique concept of the Hilbert-Huang transform (HHT) which allows the decomposition of multi-component data into a set of mono-component signals called intrinsic mode functions. This section describes a basic algorithm of the EMD, the mode mixing problem and the methods that can remove or significantly reduce the mode mixing.

3.2.1 Basic algorithm of the empirical mode decomposition

The basic idea of the empirical mode decomposition (EMD) [103] is to decompose a multi-component, non-stationary and non-linear time series into a set of intrinsic mode functions (IMFs). The IMFs, each evolving at a different characteristic time scale, represent the oscillatory modes in the data. The decomposition is conducted in an adaptive manner, thereby requiring no a priori knowledge of the signal.

The EMD only assumes that the data have at least one maximum and one minimum and the characteristic physical time scale is defined by time span between the extrema. The former requirement is always satisfied while considering the identification of vibration systems, whereas the latter one is satisfied for the signals measured with a relatively

high sampling frequency. Typically, the sampling frequency should be between 20 and 80 times higher than the highest frequency of interest [72].

The basic algorithm of the EMD consists of several steps that are schematically summarised in the flowchart in Fig. 3.3 and explained in the following. Firstly, the

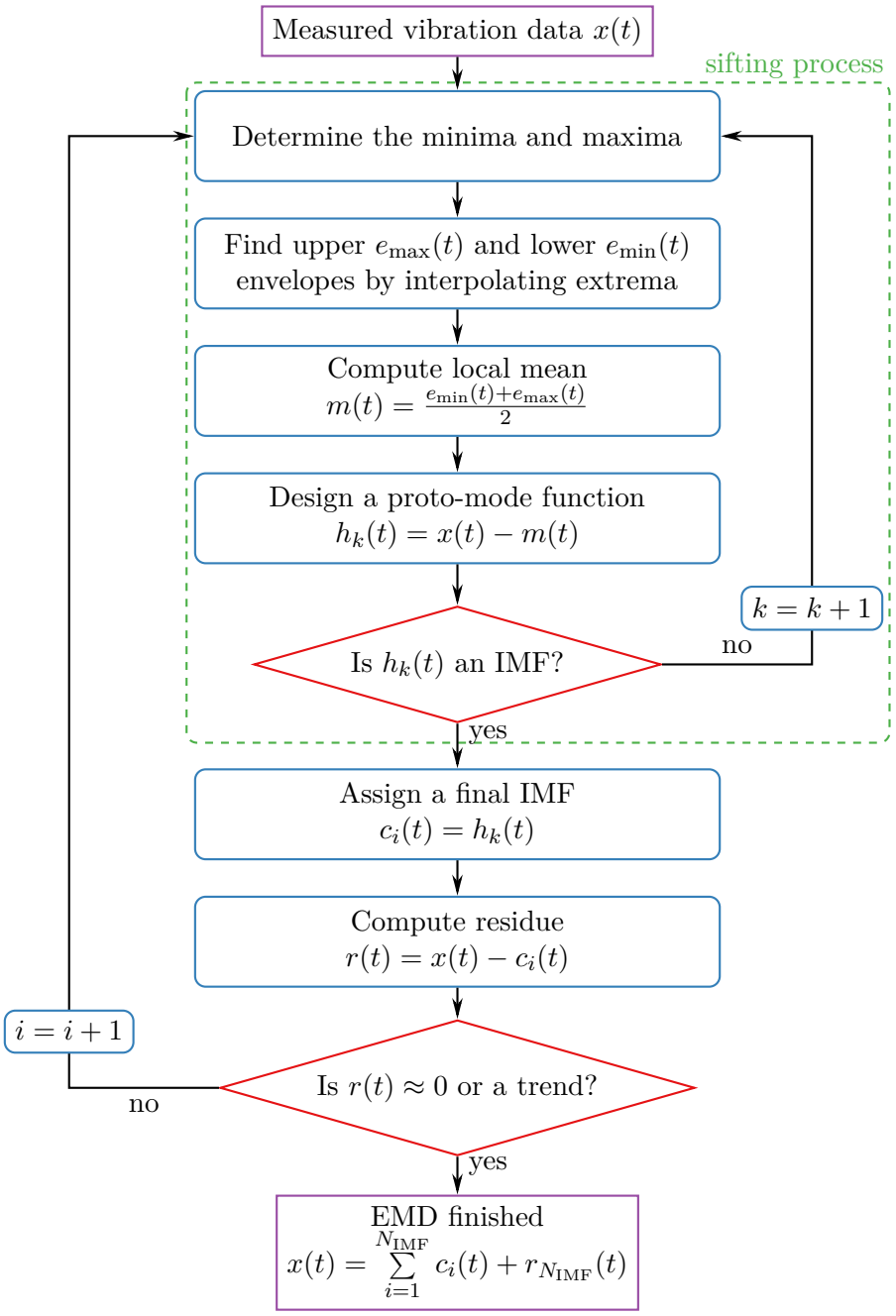

Figure 3.3 The basic algorithm of the empirical mode decomposition

maxima and minima of the multi-component signal $x(t)$ which has been measured in the

known spatial location of a structural system are identified by a peak finding algorithm. These extrema are then interpolated, usually using cubic splines, to create the upper $e_{\max}(t)$ and lower $e_{\min}(t)$ envelope. The difference of the envelopes defines the local mean of the signal

$$m_1(t) = \frac{e_{\min}(t) + e_{\max}(t)}{2}. \tag{3.3}$$

The first proto-mode function $h_1(t)$ is then estimated from the data as

$$h_1(t) = x(t) - m_1(t). \tag{3.4}$$

Ideally, the $h_1(t)$ would be the first final intrinsic mode function that satisfies two basic conditions: (i) the number of extrema and zero-crossing differs by no more than one and (ii) the mean defined by the upper and lower envelopes is zero at any point. However, due to the numerical problems and measured noise, these two conditions are not usually satisfied after a single interaction. Therefore, the so-called sifting process is repeated, i.e. the $h_1(t)$ is treated as the original data, the new mean $m_{11}(t)$ is found and the next proto-mode function is obtained as

$$h_{11}(t) = h_1(t) - m_{11}(t). \tag{3.5}$$

The process is referred to as the sifting because it separates the data with the finest characteristic time scale [102] of the rest of the signal. Generally, the sifting process must be repeated k-th times until the last proto-mode function, defined by

$$h_{1k} = h_{1(k-1)} - m_{1k}, \tag{3.6}$$

has become the first final IMF

$$c_1(t) = h_{1k}. \tag{3.7}$$

To guarantee that the final IMFs retain their physical interpretation, the sifting process must be appropriately terminated. The termination is typically achieved by limiting the size of the standard deviation computed from the two consecutive sifting results [103] or by a fix number of sifting iteration k [221]. Once the first final IMF $c_1(t)$ has been found, the following IMFs can be extracted from the residue

$$r_1(t) = x(t) - c_1(t) \tag{3.8}$$

by repeating the sifting process. The iterative process is repeated until all IMFs are extracted from the subsequent residue

$$\begin{aligned} r_2(t) &= r_1(t) - c_2(t), \\ &\vdots \\ r_{N_{\mathrm{IMF}}} &= r_{N_{\mathrm{IMF}}-1} - c_{N_{\mathrm{IMF}}}(t). \end{aligned} \tag{3.9}$$

The decomposition ends when the residue $r_{N_{\mathrm{IMF}}}(t)$ after the extraction of the last IMF $c_{N_{\mathrm{IMF}}}(t)$ becomes smaller than the predefined tolerance or when it is a monotonic trend with no dominant extrema. The original response $x(t)$ can be reconstructed by summarising all the IMFs and the last residue

$$x(t) = c_1(t) + c_2(t) + \cdots + c_{N_{\mathrm{IMF}}}(t) + r_{N_{\mathrm{IMF}}}(t). \tag{3.10}$$

The EMD explores sequentially the different time scales in the data and the IMFs are estimated from the highest-frequency to the lowest-frequency components. This may be quite inconvenient when using the EMD for non-linear system identification or non-linear modal analysis, because the last IMF $c_{N_{\mathrm{IMF}}}(t)$ corresponds to the first vibration mode which is often the dominant mode of interest. Therefore, all other modes, that might be potentially useless, must be firstly estimated before reaching the desired modes of interest. In addition, because the lowest-frequency components are estimated as the last ones, they may be influenced by numerical imperfections in the previous sifting processes.

The completeness of the decomposition is given by Eq. (3.10) and the orthogonality of the IMFs (although not theoretically guaranteed) can be numerically verified by orthogonality measures. The orthogonality of any two IMF $c_i(t)$ and $c_j(t)$ can be found as [103]

$$O_{ij} = \sum_t \frac{c_i(t)c_j(t)}{c_i(t)^2 + c_j(t)^2}. \tag{3.11}$$

This criterion is equal to 0.5 for $c_i(t) = c_j(t)$ and zero if $c_i(t)$ is orthogonal to $c_j(t)$. Working with this criterion can be sometimes difficult, because it can also be negative. Therefore, it is proposed here to replace Eq. (3.11) by

$$O_{ij} = \frac{(c_i(t) \cdot c_j(t))^2}{(c_j(t) \cdot c_j(t))(c_i(t) \cdot c_i(t))}, \tag{3.12}$$

where $(\cdot)$ marks the dot product. Equation (3.12) (which is formally the same as the widely-used modal assurance criterion (MAC) [63]) is also equal to zero when $c_i(t)$ and

$c_j(t)$ are orthogonal, but it is normalised to unity for $c_i(t) = c_j(t)$ and cannot be negative. Therefore, it might be easier to observe any imperfection in orthogonality using Eq. (3.12) than Eq. (3.11). The overall index of orthogonality $\overline{O}$ can be defined as the sum of all elements that are equal to zero if all IMFs are orthogonal with respect to each other

$$\overline{O} = \sum_{i \neq j} O_{ij}. \tag{3.13}$$

This index can be used to quantify the orthogonal properties of the IMFs by a single value which should be as low as possible.

The described EMD algorithm is simple, quite intuitive and applicable to almost all practical cases. Moreover, it was shown that its computation complexity is equivalent to the fast Fourier transform (FFT) [277]. However, in the every step of the procedure some signal processing related problems may occur [101, 211, 221].

- The task of finding maxima and minima of a signal does not have to be always straightforward. It requires very good control of the peak finding algorithm as shown in [211]. Any noise may introduce significant errors, which may lead to spurious IMFs being estimated. To eliminate measured noise, a range of standard smoothing techniques [242] can be used to pre-process the data.

- For fast-varying signals the cubic spline can over- or under-shoot the actually envelope, which leads to the incorrectly computed mean of the signal and therefore prevents a successful sifting process. Several enhanced approaches to create the envelope have been proposed, such as filtering of envelopes before mean estimation [40], replacement of cubic splines by rational splines [193] or Hermitian polynomials [42]. In addition, several optimisation schemes to avoid over- and under-shooting have been introduced [99, 209]. Nevertheless, despite a great number of available algorithms, their performance was found to be case sensitive. It was also observed in [101] that the standard cubic spline works reasonable well for most practical cases.

- Even in the cases where no over- or under-shooting occurred, the envelopes can be badly estimated at the beginning and the end of the signal. These problems are sometimes referred to as end-effects and, although the ends can be simply excluded from the following analyses, it is better to avoid the end-effects completely to maintain the full length of the data. To eliminate the end effects problem, mirroring of the signal ends [101] and the extension of the signal on both sides by neural networks [294] can be used.

- If the over- or under-shooting occurs, the estimate of the mean can be significantly influenced by the problems with the envelope, ultimately leading to estimation of spurious IMFs. In some cases, the estimation of the mean through the envelope can be completely avoided by finding the mean directly using the unconstrained optimisation [45].

- The stopping criteria are ambiguous from the signal processing point of view, e.g. even if the function appears as a trend, it still has several small maxima and minima due to the numerical representation of the signal. Therefore, more sophisticated stopping criteria are usually established based on a number of iteration in the shifting process, standard derivation of subsequent prospective IMFs or the mean value [221, 275]. These criteria may be combined and adjusted for a required performance of the EMD algorithm.

- The IMFs, which represent the characteristic time scales in the data, should have a physical meaning if the EMD algorithm has been executed properly. However, some spurious IMFs without the physical meaning can be sometimes estimated due to numerical problems in the shifting algorithm or measured noise. Fortunately, for non-linear system identification in structural dynamics, the premise (later discussed in chapter 4) is that the IMFs relate to the vibration modes of the investigated structure. These modes are often known beforehand, either from the previous testing or preliminary analysis of the structure. The knowledge of these modes can then be used to distinguish between proper and spurious IMFs.

The EMD is an adaptive data processing method and therefore its results must be carefully evaluated and verified. For certain cases of signals, one algorithm may perform well, whereas the same algorithm may not work at all for other sets of data. If the EMD algorithm fails, its modifications should be tried and the results compared to each other with the aim to establish which sets of results are correct and which include spurious intrinsic mode functions. The signal processing related issues described above can be overcome by a number of techniques, but it was found in [101] that a basic algorithm of the EMD is often sufficient in practical cases.

However, it was also found [101, 102] that so called intermittency is a major issue while using the EMD. Intermittency refers to the situations in which the IMFs of a particular time scale either suddenly appear in the signal or disappear entirely. Since the EMD locally estimates the highest-frequency component first, intermittency causes sudden jumps in the frequency of the extracted IMFs. The situation when an extracted IMF has components of different frequencies due to intermittency is called mode mixing.

The mode mixing is of particular concern in non-linear system identification, where it is usually attempted to separate all structural modes correctly. The mode mixing can sometimes limit the application of the EMD in structural dynamics and is therefore discussed in more detail in the next section.

3.2.2 The mode mixing problem of the empirical mode decomposition

The mode mixing refers to the fact that two or more mono-component functions with different time scales are combined or that a part of a mono-component function is estimated in a different IMF. This issue, also referred to as a frequency resolution of the EMD [220], can be a key limitation while using the HHT in structural dynamics where vibration structural modes are typically investigated. The separation of all modes is not always possible due to the lack of local extrema in the signal that could be used in the sifting process to separate the IMFs.

The frequency resolution of the EMD was numerically and analytically studied in [220]. The analysis is recalled here as it will be helpful in chapter 4 to investigate a range of validity of the relation between the HHT and non-linear modes. The investigated signal $x(t)$ combines two vibration modes given by pure sine waves

$$x(t) = a_1 \sin(2\pi f_1 t + \varphi_1) + a_2 \sin(2\pi f_2 t + \varphi_2), \tag{3.14}$$

where a_1, a_2 are the amplitudes of the modes ($a_2 \leq a_1$), f_1, f_2 their frequencies ($f_2 \geq f_1$), and φ_1, φ_2 are phases. When the discretisation of time series does not have any practical effects with regards to the EMD (the sampling frequency is sufficiently high), the problem can be reduced to [220]

$$x(t) = \sin(2\pi t) + a \sin(2\pi f t + \varphi), \quad a = \frac{a_2}{a_1}, \quad f = \frac{f_2}{f_1}, \quad \varphi = \varphi_2 - \varphi_1, \tag{3.15}$$

and only three parameters a, f, φ studied. The frequency resolution of the EMD can be investigated in a straightforward manner by performing the EMD for different combinations of the parameters and evaluating the quality of the resulting IMFs measured by

$$C = \frac{\|c_1(t) - a \sin(2\pi f t + \varphi)\|}{\|\sin(2\pi t)\|}. \tag{3.16}$$

If the first IMF $c_1(t)$ is fully separated from the original signal, then $C = 0$. On the contrary, if the EMD does not change the original signal, then $C = 1$. If the EMD does something else to the signal, then $C \in (0, 1)$.

The frequency resolution will be investigated for $f \in (1, 5]$, $a \in (0, 1]$ and $\varphi \in [0, 2\pi)$. It will be shown the results of the decomposition correspond to intuitive physical interpretation of the investigated signal. As an example, a set of signals for $\varphi = 0$ is shown in Fig. 3.4. In Fig. 3.4, the graphs under the line contain wave forms that

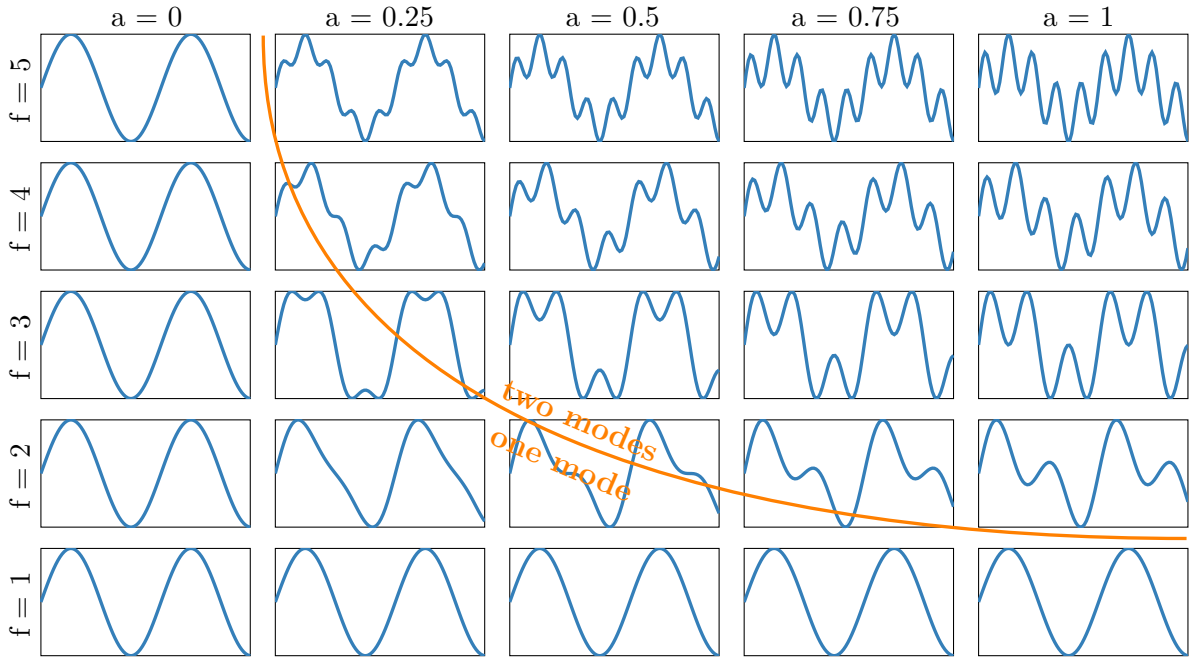

Figure 3.4 Two vibration modes with a different ratio of amplitudes and frequencies. The orange line passing through the centre of the figure indicates the mode separation ability of the empirical mode decomposition.

appear as one wave with modulated frequency and therefore it is not expected that the EMD should decompose two modes. It does not have to be always necessary to process such signals by the EMD because, despite being a combination of two modes, they can be interpreted using a single mode with a modulated frequency and amplitude. On the other hand, the signals above the line appear as two combined waves so it is natural to expect that two modes would be extracted by the EMD. In a close proximity of the dividing line, for example for $f = 2$ and $a = 0.5$, it is uncertain whether the signals should be interpreted using one or two modes

This intuitive physical interpretation also corresponds to the evaluation of the factor from Eq. (3.16) in Fig. 3.5. In order to display the results for all phases φ, the average over the phase $\overline{C}_\varphi$ and the standard deviation $\mathrm{std}(C)_\varphi$ are used. The black lines added

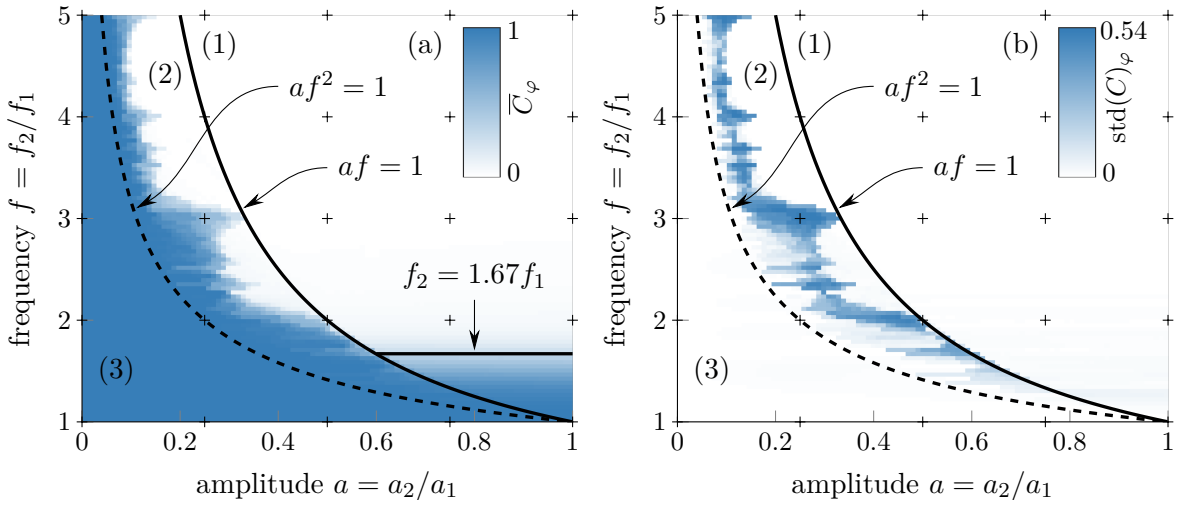

Figure 3.5 Frequency resolution of the EMD visualised using the quality factor from Eq. (3.16): (a) average of the factor over the phase angle, and (b) corresponding standard deviation. Three regions are numbered according to the ability of the EMD to separate the modes: (1) modes are always separated, (2) modes may or may not be separated depending on the phase angle, and (3) modes can never be separated.

in Fig. 3.5 are not only supported by the numerical results, but also theoretically derived [220].

Three well separated regions can be distinguished in Fig. 3.5:

- Modes are separable (region (1) located in upper right corner) if

$$af \geq 1 \quad \text{and} \quad f_2 > 1.67 f_1 \tag{3.17}$$

- Modes cannot be separated (region (3) located in the left bottom corner) if

$$af^2 \leq 1 \tag{3.18}$$

- The EMD does something else and, unlike in the previous cases, the result depends on the phase (region (2) located between the black lines) if

$$af < 1 \quad \text{and} \quad af^2 > 1 \tag{3.19}$$

What exactly happens in the last region (2) depends on the phase angle φ and the nature of the signal. Sometimes, new spurious IMFs can even be created so the application of the EMD in this region should be avoided or the results very well verified.

These criteria are valid for the basic algorithm of the EMD where the spline fitting is used to estimate the upper and lower envelopes. They can be used as a measure of closely spaced modes, i.e. if two modes do not satisfy Eq. (3.17), they can be classified as closely spaced. The relation between the HHT and complex non-linear modes in chapter 4 will be meaningful for well spaced modes only.

The criteria can be investigated before applying the EMD by performing the FFT and examining the frequency contents of the signal. Moreover, it is enough to investigate the relation of amplitudes and frequencies of the modes, because the phase information does not have to be considered as evidence by Fig. 3.5. Of course, the criteria cannot be exactly evaluated for non-linear systems due to energy split and a frequency shift of modes (see, for example, Fig. 3.2(a)). However, it can be assumed that the non-linear modes are continuation of the linear modes, and therefore, the fundamental frequency (the frequency corresponding to the highest amplitude of a mode) captured by the FFT is a good representative of the frequency captured by the instantaneous frequency and amplitude estimation methods.

Although the above analysis is performed for two pure linear tones, it is approximately valid for damped non-linear waves as well due to the local nature of the EMD. The same criteria can be applied when more than two modes are presented in the signal. As the EMD always attempts to separate the highest frequency mode from the rest, the criteria must be investigated for the two subsequent components.

To remove or reduce the frequency resolution issue, several alternatives of the EMD have been developed, for instance, the application of a masking signal [50, 138] or the ensemble empirical mode decomposition (EEMD) [292].

3.2.3 The application of masking signal

It was found in the previous section that the EMD cannot always separate all vibration modes. Although it was argued that in some fields the separation of all modes does not have to be a priority, in structural dynamics, it should be attempted to obtain as many structural modes as possible. In order to improve the frequency resolution of the EMD, the application of the masking signal was proposed in [50] and successfully used in [137, 138, 237].

The basic idea of the masking signal is to insert a new, artificially created signal into the original data. The signal must be chosen in such a way that it will prevent the lower-frequency components to be estimated in the higher-frequency component. Since the masking signal is known, it can be removed from the results.

In order to extract the first IMF, the masking signal is firstly constructed as

$$s_m(t) = a_m \sin(2\pi f_m t), \tag{3.20}$$

where its amplitude a_m and frequency f_m must be chosen appropriately (the phase is not included because it has little influence on mode mixing as seen in Fig. 3.5(b)). Both constants are empirical and non-unique. Therefore, they have to be tuned to obtain required IMFs with no mode mixing. Some guidelines for the selection, which, however, do not work well in all cases, were given in [50] and [237] based on the frequency contents of the original signal $x(t)$ which can be estimated by the FFT. In addition, an optimisation method for the selection of the masking signal has been recently proposed in [155]. Regardless of selected masking signal, the decomposition results must be well verified based on the knowledge of the identification problem.

Once the masking signal has been selected, two new signals are constructed as

$$x^-(t) = x(t) - s(t), \quad \text{and} \quad x^+(t) = x(t) + s(t) \tag{3.21}$$

and their first IMFs $c_1^-(t)$ and $c_1^+(t)$, respectively, are found. The first final IMF of the original signal $x(t)$ is found by averaging

$$c_1(t) = \frac{c_1^-(t) + c_1^+(t)}{2}. \tag{3.22}$$

After the extraction of the first IMF, the EMD can continue for other IMFs with different or without masking signal.

The masking signal has been used for non-linear system identification in [137, 138, 155] with a great success and will be used in chapter 5 with the experimental data measured from the ECL benchmark. The masking signal can be sometimes difficult to use because its selection is empirical. On the hand hand, this method is suitable for the application to vibration signals for which the extraction of structural modes should be a priority. When the mode mixing problem needs to be overcome without any a priori knowledge of the frequency contents or repeated selection of the masking signal, so-called ensemble empirical mode decomposition (EEMD) may be used instead.

3.2.4 Ensemble empirical mode decomposition

In order to dramatically reduce the mode mixing (intermittency), the algorithm called ensemble empirical mode decomposition (EEMD) was developed [292]. The core of the

method is the basic algorithm of the EMD presented in section 3.2.1. The measured data set is firstly polluted by the known amount of white Gaussian noise and then decomposed by the EMD in order to obtain the IMFs. The process is repeated up to a hundred times with different (randomly generated) noise and the IMFs are averaged so the ensemble means of the IMFs are obtained. This should lead to correct estimation of all IMFs and the mode mixing problem should be either completely avoided or massively reduced. At the same time, however, several artificial IMFs can be created due to the artificially added noise, so they must be removed from the final set of IMFs based on a priori knowledge of the problem. The EEMD has become a standard tool for performing the EMD in the fields where the changes in the signals (intermittency) are rapid and the masking signal cannot be property defined. A timely feasible application of the EEMD is allowed due to the optimised implementation of the EMD [277], which is equivalent to the FFT in terms of the number of operations.

To make the EEMD even more robust against any uncertainty in the data, the improved version was presented in [46, 299]. The complete ensemble empirical mode decomposition with adaptive noise (CEEMDAN) improves the generation of the random noise into the data and therefore may potentially decrease the number of runs needed for reliable estimation of all intrinsic mode function. On the other hand, it uses one additional signal created by random noise which serves as the reference and must be partly decomposed in each step. Therefore, this method is significantly slower than the standard EEMD, but the results can be superior in some cases, mainly because very few or no spurious IMFs should be estimated.

The EEMD and CEEMDAN are not very suitable for non-linear system identification in structural dynamics, because typical scales in the data change slowly and, in cases of free decay measurements that are of interest, all modes appear in the response simultaneously. Therefore, intermittency is not significant and the mode mixing problem can be removed using the masking signal in a more controlled manner. In addition, using a single EMD run is much faster than repeating hundreds of independent runs in the EEMD or CEEMDAN.

The EMD scheme used in this thesis is based on the code distributed alongside of [221][1]. In cases when many EMD runs must be executed, such as for the computation of Fig. 3.5 or parametric studies in chapter 4, a faster implementation of the EMD provided by [277][2] was used instead.

[1] Available at http://perso.ens-lyon.fr/patrick.flandrin/emd.html (cited in June 2017)
[2] Available at http://rcada.ncu.edu.tw/research1.htm (cited in June 2017)

3.3 Methods for instantaneous amplitude and frequency estimation

The intrinsic mode functions (IMFs) are narrow-band frequency components whose meaningful instantaneous frequency (IF) and amplitude (IA) can be estimated. Traditionally, the Hilbert transform was used to estimate the IF and IA. However, it is known that the HT can suffer from a number of numerical and mathematical issues [71]. Several alternative methods have been developed in different fields. The alternative method are compared in this section to evaluate their performance and identified their features that may be suitable for non-linear system identification. For each method, a brief description with relevant references is given, the application of the methods is demonstrated on the testing signal obtained from the Duffing oscillator in section 3.3.1 and the results are compared by means of backbone and damping curves.

The objective of this section is not only to show that all methods lead to very similar results after some additional processing, but also to emphasise that replacing the HT can help to recover additional information that can help to identify the system. Moreover, the combination of the methods allowed a new method for the estimation of the intra-wave frequency modulation (IFM) frequency to be proposed in section 3.4.

3.3.1 Testing signal and reference solutions

A well-known Duffing oscillator schematically shown in Fig. 3.6, which has extensively been studied [71, 103, 118, 127, 173, 181], is used to compute the testing signal. The Duffing oscillator is governed by

$$m\ddot{x}(t) + c\dot{x}(t) + kx(t) + k_{\mathrm{nl}}x^3(t) = 0, \tag{3.23}$$

where $m = 1\,\mathrm{kg}$, $c = 0.2\,\mathrm{N\,m^{-1}\,s^{-1}}$, $k = (2\pi)^2 \approx 39.5\,\mathrm{N\,m^{-1}}$, and $k_{\mathrm{nl}} = 5\,\mathrm{N\,m^{-3}}$. The initial conditions selected for the simulation were $x(0) = 5\,\mathrm{m}$ and $\dot{x}(0) = 0\,\mathrm{m\,s^{-1}}$, sampling frequency $f_{\mathrm{s}} = 50\,\mathrm{Hz}$ and time interval $t = 0 - 30\,\mathrm{s}$. The values of system parameters and initial conditions are not realistic, but they have been chosen to allow reliable demonstration of the presented methods. The validity of results is not corrupted by the choice of these values. The testing signal is used throughout this section to evaluate the performance of IF and IA estimation methods. It was also used in section 3.1.1 to show the difference between the Fourier and Hilbert representation of the signal.

In order to compare the performance of the different IF and IA estimation methods, the results are evaluated against two reference solutions. The first solution is obtained

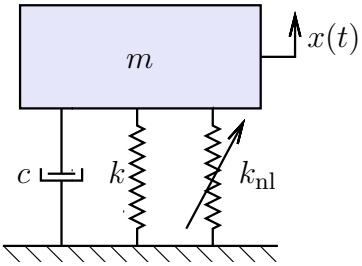

Figure 3.6 A single-degree-of-freedom system with a cubic hardening stiffness commonly known as a Duffing oscillator

analytically using perturbation methods [158]. The backbone and damping curves are given by

$$\omega(a) = \omega_0 + 3k_{\mathrm{nl}}a^2/(8\omega_0), \quad \delta(a) = c/2, \tag{3.24}$$

respectively, where ω_0 is the angular natural frequency of the underlying linear system and a is the amplitude of vibration. The second solution is obtained numerically using the complex non-linear modal analysis [127, 134] that is described in detail in section 4.2.1. Both solutions are shown in Fig. 3.7. It can be seen that the analytical and numerical

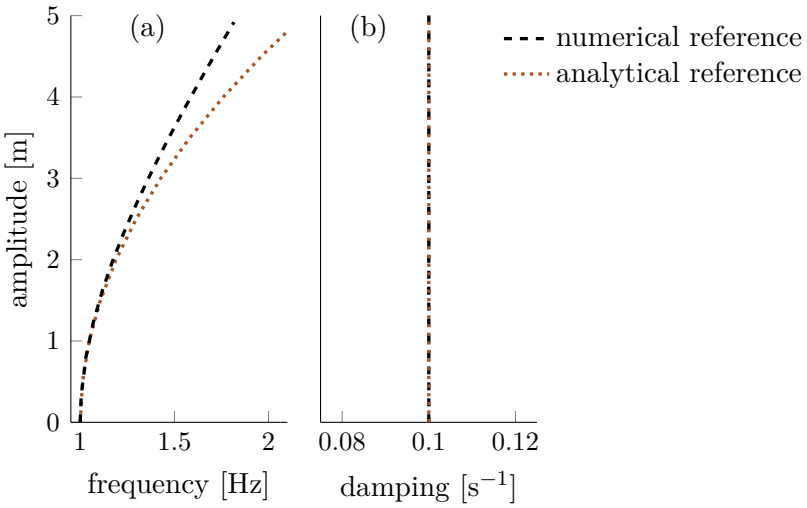

Figure 3.7 Analytical and numerical reference solutions: (a) backbone and (b) damping curve

solutions of the backbone are not the same. This difference is due to the assumption of weak non-linear behaviour in the analytical case, which is also the reason why both backbones match at low amplitudes. On the other hand, practically no difference can be observed in the damping curves in Fig. 3.7(b). It is anticipated that the numerical solution should match the estimated values more closely because it is not subjected to the assumption of weak non-linear behaviour.

Both solutions are based on the Fourier approach, i.e. the solution is approximated using a Fourier series in which a certain number of components (harmonics) is retained. This approach is often used for computation analyses of non-linear systems, but it does not offer a clear physical interpretation as discussed in section 3.1.1. The concept of instantaneous frequency and amplitude offers more natural framework for the interpretation of non-linear and non-stationary series by replacing the harmonics of constant frequencies by time-varying frequency. In the instantaneous frequency and amplitude concept, a new feature called intra-wave frequency modulation (IFM) can be found. The IFM represents the changes of frequency within the vibration cycle. No such changes can be seen in the Fourier concept because all frequencies are constant. This IFM concept is rarely used in non-linear system identification and often the intra-wave frequency modulation is incorrectly regarded as an unwanted distortion of results and consequently it is simply removed by smoothing or averaging. The IFM does not have to be necessary seen as unwanted high-frequency oscillations of the output and in fact, it can be used for detection and characterisation of non-linearities as explained in section 3.3.1 and shown in section 3.4. However, there are a few reasons for smoothing this frequency completely. Firstly, the raw (without smoothing) IF cannot lead to good results when using in the Freevib algorithm [67] to extract the backbone and damping curve, and secondly, the traditionally used Hilbert transform is not a reliable tool for the estimation of the IFM, thereby rendering its use impractical [71, 181]. Furthermore, the intra-wave frequency modulation does not have a very solid mathematical background, which might be the main reason why it is not so often used and well understood.

However, a basic mathematical principle of intra-wave frequency modulation was presented in [180]. The principle can be shown for the Duffing oscillator from Eq. (3.23) that is excited by a harmonic force, i.e.

$$m\ddot{x}(t) + c\dot{x}(t) + kx(t) + k_{\mathrm{nl}}x^3(t) = \cos(\Omega t + \varphi), \quad \text{with} \quad \Omega = \omega_0, \tag{3.25}$$

where φ is a phase angle and Ω is the excitation angular frequency which is equal to the angular natural frequency ω_0 of the underlying linear system. The solution of Eq. (3.25) can be approximated using a second-order asymptotic perturbation form [180] as

$$x(t) = A_1 \cos(\Omega t) + A_3 \cos(3\Omega t), \tag{3.26}$$

where $A_3 = \frac{\alpha A_1^3}{32\Omega^2} \ll A_1$. Equation (3.26) consists of the first and third harmonic, but it can also be rewritten into

$$x(t) = \underbrace{\sqrt{A_1^2 + A_3^2 + 2A_1A_3\cos(2\Omega t)}}_{\text{AM } (\approx A_1 \text{ since } A_3 \text{ is small})} \cos \underbrace{(\Omega t + \Theta(t))}_{\text{FM}}. \tag{3.27}$$

Equation (3.27) replaces the two harmonic components in Eq. (3.26) by a narrow-band frequency modulation (FM) with the intra-wave frequency modulation (IFM) $\Theta(t)$. The amplitude of $x(t)$ in Eq. (3.27) is almost constant since the amplitude modulation (AM) is very small. The IFM is approximately equal to [180]

$$\Theta(t) \approx \frac{A_3}{A_1}\sin(r\Omega t), \quad \text{with} \quad r = 2, \tag{3.28}$$

which means that the IFM frequency $\Omega_{\text{IFM}} = 2\pi f_{\text{IFM}} = r\Omega$ is modulated with the double of the excitation frequency Ω. Although Eq. (3.28) was found for a harmonic force excitation, the ratio of the IFM frequency and IF $r = \Omega_{\text{IFM}}/\Omega = f_{\text{IFM}}/f = 2$ also holds for a resonant decay response [181]. Provided that this ratio can be found, it can be used to gain insight into a type of non-linearity, because it is unique for odd and even non-linearities, being $r = 2$ and $r = 1$, respectively. However, it was concluded in [180] that it may be very difficult to find this ratio using the Hilbert transform due to its numerical problems. Therefore, a new method that allows accurate estimation of the IF, IFM and the ratio $r = f_{\text{IFM}}/f$ is proposed in section 3.4.

It can be seen that some basic mathematical relations exist between Fourier-based representation of signals and the concept of instantaneous frequency and amplitude with intra-wave frequency modulation. It was already discussed in section 3.1.1 that the physical interpretation of these approaches is ideologically different. In the following, the methods that can be used to estimate the instantaneous frequency and amplitudes are described.

3.3.2 The Hilbert transform

The Hilbert transform (HT) has traditionally been used for the estimation of the instantaneous frequency and amplitude [71, 103]. The HT $\tilde{c}(t)$ of a time domain signal $c(t)$, which is assumed to be an IMF, is defined as

$$\tilde{c}(t) = \frac{1}{\pi}\text{pv}\int_{-\infty}^{\infty}\frac{c(\tau)}{t-\tau}\text{d}\tau, \tag{3.29}$$

where "pv" demotes the Cauchy principal value of the integral. The Hilbert transform maps functions from a domain into the same domain by shifting their phases by $-\pi/2$. The resulting signal $\tilde{c}(t)$ is also called a quadrature of $c(t)$. Numerically, the HT is usually implemented via the fast Fourier transform (FFT) [147] which is fast, but might be sometimes affected by the Gibbs phenomenon [71]. The direct method based on Kronig-Kramers relations cannot be used in the time domain because it requires a complex function, such as the frequency response functions used in chapter 2.

Once the HT has been found, the analytic signal $z(t)$ can be derived as

$$z(t) = c(t) + \mathrm{i}\tilde{c}(t) = a(t)\mathrm{e}^{\mathrm{i}\theta(t)} \tag{3.30}$$

and the instantaneous amplitude $a(t)$ and instantaneous phase $\theta(t)$ can be calculated

$$a(t) = |z(t)| = \sqrt{c^2(t) + \tilde{c}^2(t)}, \qquad \theta(t) = \arg(z(t)) = \arctan\left(\frac{\tilde{c}(t)}{c(t)}\right). \tag{3.31}$$

The instantaneous frequency (IF) is then defined as the time derivative of the instantaneous phase

$$\omega(t) = \frac{\mathrm{d}\theta(t)}{\mathrm{d}t}. \tag{3.32}$$

There are several issues while evaluating the IF using the HT. It can sometimes lead to the estimation of a negative frequency and suffer from end effects [71, 184]. In addition, Eq. (3.31) involves the inverse tangent function which always produces sharp jumps between $-\pi$ and π and therefore an unwrapping algorithm is required. Moreover, the numerical derivative in Eq. (3.32) can produce incorrect and noisy results.

To avoid some of these issues alternative formulas were developed [67, 71]. First of them uses the initial signal $c(t)$, its Hilbert transform $\tilde{c}(t)$, and their time derivatives $\dot{c}(t)$ and $\dot{\tilde{c}}(t)$ to compute the IF $\omega(t)$ as

$$\omega(t) = \frac{c(t)\dot{\tilde{c}}(t) - \dot{c}(t)\tilde{c}(t)}{a^2(t)} = \Im\left[\frac{\dot{z}(t)}{z(t)}\right]. \tag{3.33}$$

The derivatives of the signal can be computed numerically or the velocity can be measured alongside the displacement. An unwrapping algorithm is not required when using Eq. (3.33).

Another algorithm that allows the calculation of the IF without the need for unwrapping or numerical derivative was proposed in [71]. Using this algorithm, the IF can be computed as

$$\omega(t) = \arctan\left(z_n z_{n+1}^*\right), \tag{3.34}$$

where z_n is a discrete analytic signal and * marks the complex conjugate. Therefore, only conjugate multiplication of adjacent complex samples and the inverse tangent must be evaluated. It should be noted, however, that for a noiseless signal the IFs estimated by Eq. (3.32), Eq. (3.33), and Eq. (3.34) are practically the same.

According to the Freevib algorithm [67], the estimated IF and IA are used to compute the natural frequency and viscous damping rate using

$$\omega_0^2 = \omega^2 - \frac{\ddot{a}}{a} + \frac{2\dot{a}^2}{a^2} + \frac{\dot{a}\dot{\omega}}{a\omega}, \qquad \delta = -\frac{\dot{a}}{a} - \frac{\dot{\omega}}{2\omega}, \tag{3.35}$$

respectively. It should be added that the non-linear elastic $\mathrm{F_{el}}$ and dissipative $\mathrm{F_d}$ restoring forces can be estimated using

$$\mathrm{F_{el}} = \begin{cases} \omega_0^2 a, & c(t) \geq 0 \\ -\omega_0^2 a, & c(t) < 0 \end{cases} \qquad \mathrm{F_d} = \begin{cases} 2\delta a_{\dot{c}}, & \dot{c}(t) \geq 0 \\ -2\delta a_{\dot{c}}, & \dot{c}(t) < 0, \end{cases} \tag{3.36}$$

respectively, where $a_{\dot{c}}$ is the instantaneous amplitude (envelope) estimated from the velocity signal. However, the estimation of the non-linear restoring force is not a focus of this chapter, so only the amplitude-dependent frequency (backbone) and damping curves are compared with the numerical and analytical references (described in section 3.3.1) to observe the features of the described methods.

The Hilbert transform was applied to the testing signal and the results are summarised in Fig. 3.8. It can be seen that the IA shown in Fig. 3.8(a) is originally not so smooth and suffers from the end effects. Such results are usually smoothed, thereby leading to the smooth envelope that encloses the signal very closely. The smoothing of the IF was also needed as seen in Fig. 3.8(b) due to strong end effects and estimated intra-wave frequency modulation (IFM). After the smoothing by low-pass filtering, the IF is smooth and decreases with decreasing amplitude. This decreasing trend relates to the hardening behaviour of the Duffing oscillator and can be used as a means of detecting and characterising the non-linearity.

The comparison between the estimated and reference backbones in Fig. 3.8(c) reveals some discrepancies, especially for higher amplitudes between the analytical solution and the estimated backbones. On the other hand, the estimated results correspond to the numerically obtained backbone very well. Even the results without smoothing capture the overall behaviour quite well and it can be seen that if the fitting of the numerical results to the initial (without smoothing) results were attempted, the result would not be far from the correct numerical reference.

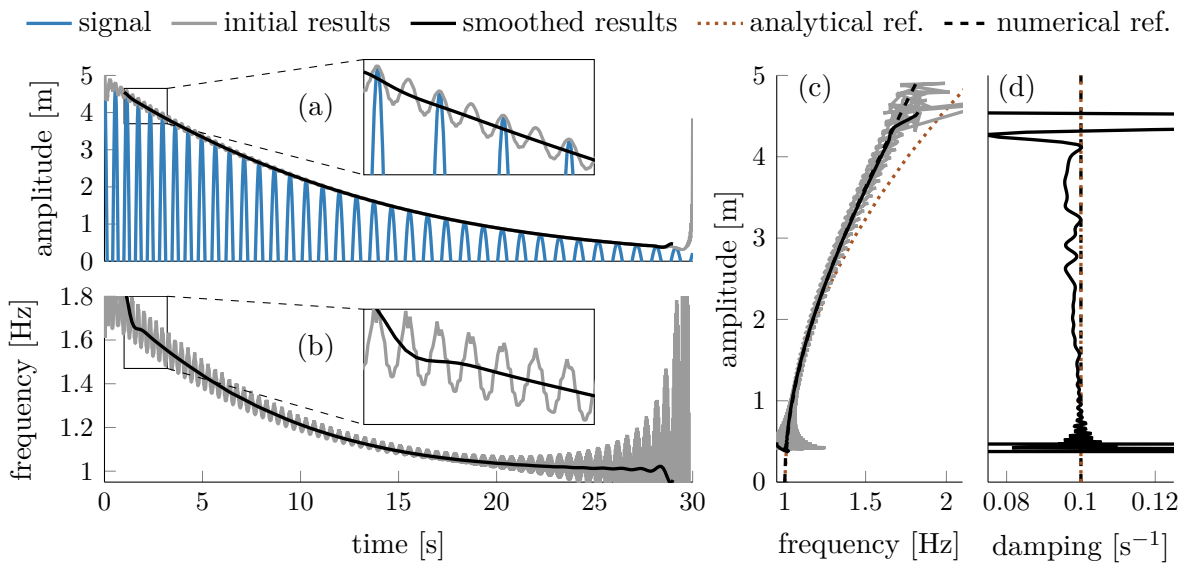

Figure 3.8 The Hilbert transform (HT) applied to the testing signal: (a) signal and instantaneous amplitude, (b) instantaneous frequency, (c) backbone, and (d) damping curve

The damping curve shown in Fig. 3.8(d) is very close to the reference ones, except large errors at low and high amplitudes that are caused by the derivatives in Eq. (3.35). However, in practical applications, low and high amplitudes may be removed from the results, which leave the damping curve close to the reference one with a slight include to the left. It is important to note that it is practically impossible to obtain the damping curve from the results that are not additionally smoothed. Sometimes, fitting of the envelope using the exponential function is preferred to obtain the damping. However, this fitting assumes that the damping is linear and the whole point of using adaptive processing methods is therefore lost.

The Hilbert transform (HT) has been used for the estimation of the natural frequency and viscous damping rate since the proposal of the well-known Freevib algorithm in [67]. As shown, the HT can deliver smooth results after the low-pass filtering. However, some signal processing issues exist and smoothing and/or averaging of the results must always be included. Having smoothed the results, the contribution of intra-wave frequency modulation is eliminated which, on one hand, allows the comparison of estimated and analytical backbones, but, on the other hand, it leads to the loss of some information about the underlying dynamics. The computation of the Hilbert transform can be subjected to a number of mathematical and numerical issues, such as the Gibbs phenomenon and end-effects, or negative frequency may be accidentally estimated [71, 72, 103, 104] as shown in Fig. 3.8(b) or Fig. 3.17(b).

3.3.3 Normalised Hilbert transform

Some of the problems of the HT, including negative frequency estimation [43], occur because the investigated data (even if they are IMFs) do not usually satisfy the Nuttall [171] and Bedrosian [18] theorems [104]. The Nuttall theorem gives the condition under which the HT yields the correct quadrature ($-\pi/2$ shifted signal) of a signal, while the Bedrosian theorem states that the data must be not only mono-component, but also narrow band signal. If these conditions are not satisfied, the amplitude modulated (AM) part of the signal contaminates the frequency modulated (FM) part, so the estimation of the IF becomes more difficult and its physical interpretation is then impossible [104]. The Bedrosian theorem is always satisfied if the EMD has been performed and the considered signal $c(t)$ is an IMF. To meet the Nuttall theorem as well, the empirical normalisation scheme was proposed in [104]. This normalisation separates the AM from the FM part of the signal. The HT can then be computed for the FM component which always fulfils the criteria set by the Nuttall and Bedrosian theorems since the AM part has been completely eliminated. The normalisation scheme can be summarised as follows:

1. Identify all the local maxima of the absolute values of the time domain data.
2. Connect all these maxima using, e.g. cubic splines to create an empirical envelope $a_i(t)$ in the ith step of the normalisation.
3. Normalise the time domain data by dividing them by the envelope $a_i(t)$.
4. Repeat the first three steps using the normalised data until all absolute maxima are lower than unity.
5. The FM part $\kappa(t)$ of the signal is represented by the resulting normalised data and the AM part $a(t)$ is designed as $a(t) = x(t)/\kappa(t)$.

The convergence of the normalisation is very fast - two or three iterations are usually sufficient [104]. The resulting FM part $\kappa(t)$ is a sinusoidal signal with a constant amplitude equalled to 1 and varying, narrow-band frequency. The FM part is sustainable for the computation of the IF using the standard Hilbert transform (Eq. (3.32)) because it satisfies all required conditions. The process of the normalisation followed by the HT is referred to as the normalised Hilbert transform (NHT).

It should be noted that other methods can be utilised to estimate the envelope of the time domain data instead of the cubic spline in step 2 of the normalisation. The envelope can be found using the HT (as in Eq. (3.31)), different types of spline fitting [101, 193], or using optimisation [297]. The choice of the algorithm is case-dependent,

but generally the cubic splines should be used, and if they fail, the alternatives should be tried and compared to each other to ensure the validity of the results.

The normalised Hilbert transform has been applied to the testing signal and the results are summarised in Fig. 3.9. The IA in Fig. 3.9(a) is smooth and encloses the

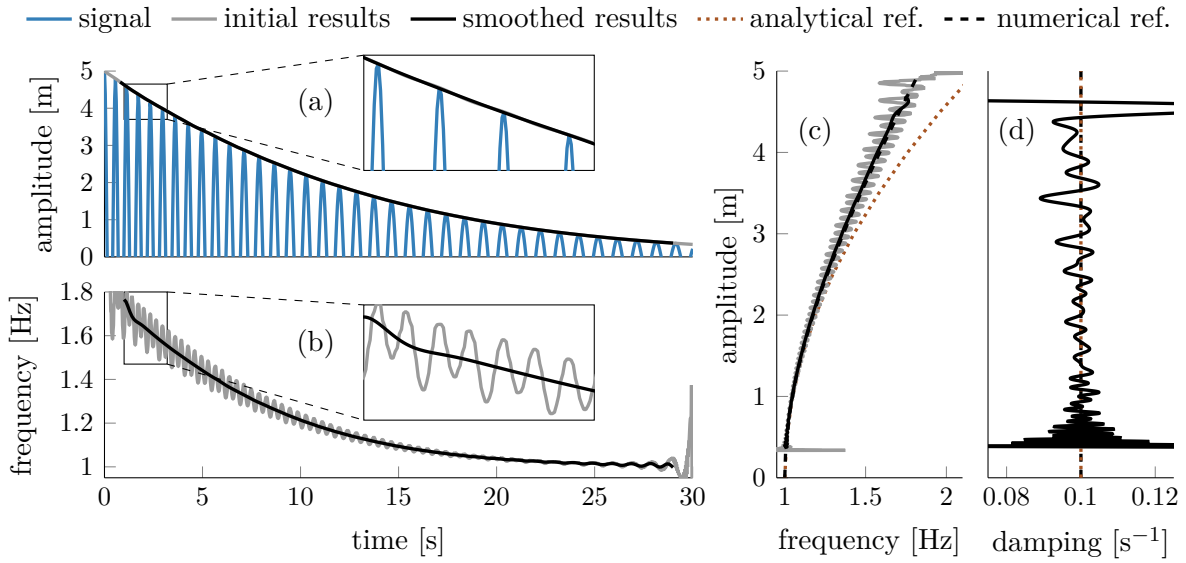

Figure 3.9 Normalised Hilbert transform (NHT) applied to the testing signal: (a) signal and instantaneous amplitude, (b) instantaneous frequency, (c) backbone, and (d) damping curve

signal perfectly. For noise-free signal, no smoothing is needed, but for noisy signal, some smoothing may be necessary. There are no observable end effects in the IA, which is not surprising, because both ends are smooth extensions of the cubic splines used in the normalisation process. The instantaneous frequency is shown in Fig. 3.9(b) where some minor end-effects can still be observed. However, compared to the Hilbert transform (Fig. 3.8(b)), they are not significant and the estimation of the negative frequency has not occurred. The intra-wave frequency modulation is present in the unsmoothed signal. As can be seen from the inset in Fig. 3.9(b), the IF and IFM are smoother than those estimated by the HT (see the inset in Fig. 3.8(b)). On the other hand, the NHT produced somewhat uneven IFM which probably caused by the numerical issues of the HT [104]. The smoothing is again required in order to evaluate the conventional backbone and damping curves.

After the smoothing, the estimated backbone shown in Fig. 3.9(c) corresponds quite closely to the numerical reference. There is a slightly higher difference than in the case of the Hilbert transform. The damping curve estimated in Fig. 3.9(d) fluctuates around the correct value which is again caused by the derivative in Eq. (3.35) combined with not so good smoothing of the IF.

Despite the fact that some of the problems of the HT have been removed by the normalised Hilbert transform. In particular, a negative frequency cannot be longer estimated, the Hilbert transform must still be used. Therefore, general numerical problems associated with the Hilbert transform remain and can influence the obtained results. The method that uses the normalised data as well, but bypasses the Hilbert transform completely is called the direct quadrature (DQ).

3.3.4 Direct quadrature

Having decomposed the signal into the AM and FM parts using the normalisation scheme in section 3.3.3, the FM part can be used for the direct computation of the quadrature. This approach avoids the HT completely and should provide an exact estimate of the IF [104].

Knowing that the FM signal obtained by the normalisation scheme is sinusoidal ($\kappa(t) = \sin(\theta(t))$), the IF can be determined using

$$\omega(t) = \frac{\mathrm{d}\theta(t)}{\mathrm{d}t} = \frac{\mathrm{d}}{\mathrm{d}t}\left[\arccos(\kappa(t))\right]. \tag{3.37}$$

Since Eq. (3.37) involves the evaluation of the inverse cosine, the numerical stability is not very good near the local extrema. Therefore, the outliers in the phase are sometimes fixed using a median filter [86] or a slightly different formulation can be used. Replacing the inverse cosine by the inverse tangent as per goniometric formulas [104] leads to

$$\omega(t) = \frac{\mathrm{d}}{\mathrm{d}t}\left[\arctan\left(\frac{\kappa(t)}{\sqrt{1-\kappa^2(t)}}\right)\right]. \tag{3.38}$$

Equation (3.38) implies that $\kappa(t)$ has to be perfectly normalised otherwise the quadrature becomes complex. The approach allows the four-quadrant inverse tangent to be used in order to uniquely determine the specific quadrant of the phase function. This leads to the correct unwrapping.

Another algorithm to remove the outliers was proposed in [99]. After the normalisation, Eq. (3.37) is evaluated only for values smaller than 0.9 and points with higher values are interpolated using a cubic spline. This process avoids the numerical instability in a proximity of the extrema. This procedure should provide a very good estimate of the IF, but the interpolation should not be performed over a long interval to avoid undesired distortion of results.

The methods based on the normalised data should yield very good results, but their main limitation is the normalisation process itself - it has to be perfect. If there are values which are not lower than 1, the estimation of the IF becomes impossible as Eq. (3.37) and Eq. (3.38) become complex. In general, the DQ appears to be particularly suitable for situations where high accuracy of the extracted IF and IA is required, such as detection of special events in the data or characterisation of non-linearities from noise-less data. Theoretically, the method yields exact estimates of the instantaneous frequency, but the noise level must be minimal.

The results obtained by the DQ using Eq. (3.38) are shown in Fig. 3.10. It can be

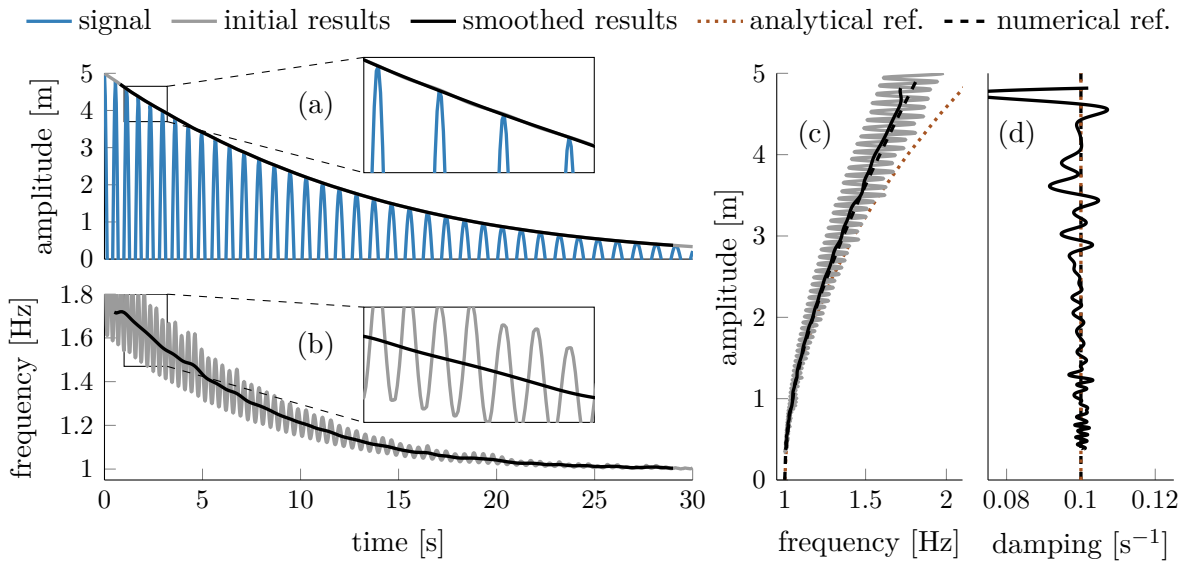

Figure 3.10 Direct quadrature (DQ) applied to the testing signal: (a) signal and instantaneous amplitude, (b) instantaneous frequency, (c) backbone, and (d) damping curve

seen that the IA shown in Fig. 3.10(a) is smooth and encloses the signal very closely. This IA is exactly the same as for the normalised Hilbert transform in Fig. 3.9(a). The IF in Fig. 3.10(b) does not exhibit any end effects and therefore provides information about the frequency over the whole time interval. While smoothed using the same low-pass filter as the Hilbert transform, the result is not so smooth as in Fig. 3.8(b). This is believed to be caused by the higher amount of intra-wave frequency modulation which has been estimated using the DQ and had to be smoothed out. The intra-wave frequency modulation is not noisy as seen in the inset in Fig. 3.10(b) as opposed to Fig. 3.8(b).

The comparison of the estimated and reference backbones in Fig. 3.10(c) shows some behaviour as in case of the NHT. The smoothed backbone is practically the same as the numerical reference solution. The damping curves shown in Fig. 3.10(d) is very close to the reference one and is much smoother than the one estimated by the NHT.

The DQ is not a standard tool used in non-linear system identification, but it offers the advantage of estimating the intra-wave frequency modulation very accurately. Unfortunately, the backbone estimated in the presence of intra-wave frequency modulation cannot be directly compared with that obtained analytically or numerically - some examples can also be found in [71, 181, 184]. If the IFM is ignored and smoothed, the results are very similar to those obtained by the Hilbert transform. This means that for noiseless signals, the DQ provides more information while allowing to carry out a well-established analysis.

3.3.5 Energy operators

The energy operators allow the computation of the IF and IA without an integral transform since they are solely based on differentiation. In practice, they might be of a limited use because they work properly for linear system only. On the other hand, this can be seen as an advantage since it allows detection of non-linearity.

A signal $c(t)$ of the form

$$c(t) = a(t)\sin(\omega t) \tag{3.39}$$

is assumed. For such a signal, kth-order operator is defined [49, 229] as

$$\psi_{p,q,m,l}[c(t)] = c^{(p)}(t)c^{(q)}(t) - c^{(m)}(t)c^{(l)}(t), \tag{3.40}$$

where the pth, qth, mth, and lth derivatives of the signal must satisfy the condition $k = p+q = m+l$, $p \neq m$ and $q \neq l$. The derivatives in Eq. (3.40) can be obtained either using numerical differentiation or measured directly.

The discrete form of the operators can be obtained using symmetric differentiation formulas as

$$\begin{aligned}\psi_{p,q,m,l}[c(n)] = \frac{1}{2}[&c(n+p)c(n+q) + c(n-p)c(n-q) \\ &- (c(n+m)c(n+l) + c(n-m)c(n-l))].\end{aligned} \tag{3.41}$$

The IF and IA can be computed using

$$\omega(n) = \sqrt{\frac{\psi_{p,q,m,l}[c(n) - c(n-1)]}{\psi_{p,q,m,l}[c(n)]}}, \tag{3.42}$$

$$a(n) = \sqrt{\frac{\psi_{p,q,m,l}[c(n)]}{\sin[(m-p)\Omega]\sin[(m+p-k)\Omega]}}, \tag{3.43}$$

where $\Omega = \omega(n)\mathrm{d}t$.

Several energy operators are available in literature, such as the 1st order Teager energy operator (TEO) [104] for $k = 1,\ p = 1,\ q = 0,\ m = 0,\ l = 1$, the 2nd order differential energy operator (DEO) [49] for $k = 2,\ p = 1,\ q = 1,\ m = 0,\ l = 2$, and the 4th-order higher energy operator (HEO) [229] for $k = 4,\ p = 4,\ q = 0,\ m = 3,\ l = 1$. When using higher-order operators, more sampling points are included, leading to lower sensitivity of the results against frequency fluctuations and measured noise, but less instantaneous results are estimated. For noise-free signal with a high sampling frequency, all operators should yield the same instantaneous frequency and amplitude.

Unfortunately, the operators are only valid for a linear signal since Eq. (3.39) is assumed. Therefore, they fail to extract any meaningful values a non-linear signal. It can be clearly seen in Fig. 3.11 that the estimates using TEO do not correspond to the correct IF or IA, especially for higher amplitudes of vibration. Although this makes a

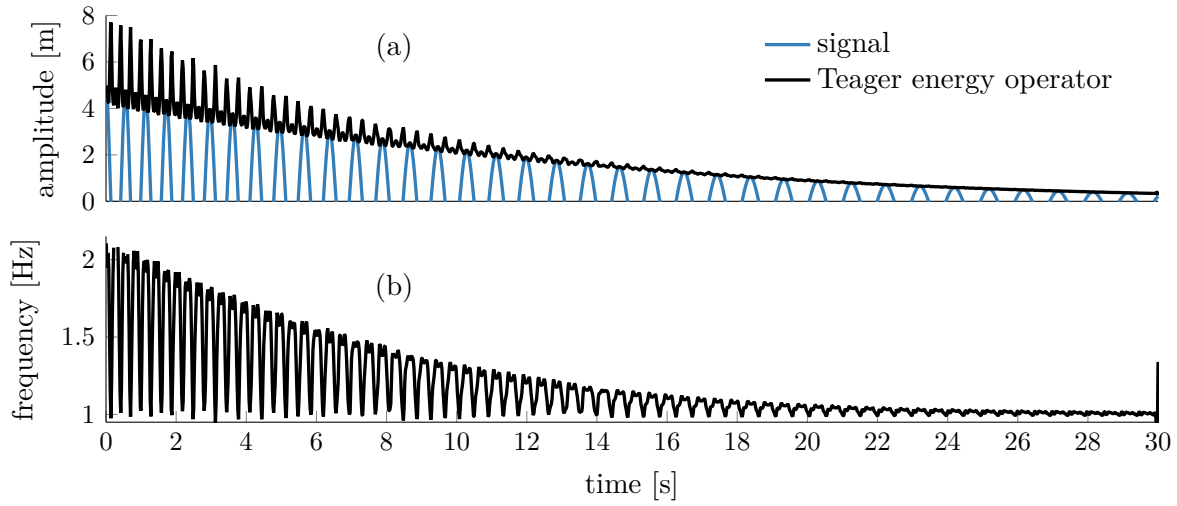

Figure 3.11 Teager energy operator (TEO) applied to the testing signal: (a) signal and instantaneous amplitude and (b) instantaneous frequency

meaningful interpretation impossible, this feature may be used as a conclusive detector of non-linearities [71, 104] in the initial step of non-linear system identification. The results approach the correct amplitude and frequency of the under-lying linear system for low amplitudes of motion. The behaviour indicates that the energy operators are able to recover correct characteristics for linear systems. As the numerical derivatives must be evaluated, the application to the signals polluted by measured noise can be complicated. In such case, the higher order operators should yield better results because they take into account a longer period of the signal and therefore they do not depend so strongly on local behaviour.

3.3.6 Zero-crossing methods

Several zero-crossing methods can be used to estimate the IF and IA [104, 142, 208] in a simple and intuitive matter. The basic zero-crossing method from [142] is illustrated in Fig. 3.12. The IF is determined from the inverse of the period over one complete

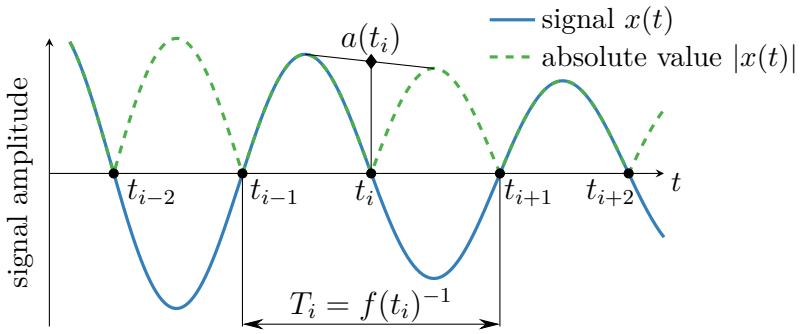

Figure 3.12 Zero-crossing method for systems with symmetric restoring forces

vibration cycle and is assigned to the crossing time at the centre of this cycle.

$$\omega(t_i) = 2\pi \left(t_{i+1} - t_{i-1}\right)^{-1} = 2\pi T_i^{-1}. \tag{3.44}$$

The IA is found using the first-order polynomial interpolation of the absolute extrema of the signal. The values of these polynomials are evaluated at the zero-crossing points t_i. Thus, a set of discrete values $(\omega(t_i), a(t_i))$ is obtained. This set does not characterise frequency and amplitude locally, but with one cycle accuracy. Despite this fact, the characteristics are commonly called instantaneous.

A slightly modified version of the ZC method has been recently presented in [207, 208]. In this modification a free decay response is divided into N intervals and the vibration period is estimated as

$$T_k = 2(t_{k,n_k} - t_{k,1})/(n_k - 1), \tag{3.45}$$

where $t_{k,i}$ is the ith zero-crossing point and n_k is the number of zero-crossing points within the kth interval. This method essentially averages the periods, assuming that the frequency does not change significantly within the interval. The instantaneous amplitude is found in a similar manner, i.e. absolute extrema of the signal are averaged over short intervals. Due to the averaging, this version of the zero-crossing method provides even less instantaneous results than the ZC, but it should be much less sensitive to measured noise.

The zero-crossing methods are intuitive, straightforward, and easy to implement. These methods do not capture any amplitude and frequency modulation within the

vibration cycle. Therefore, they provide a reliable means of estimating the backbones which correspond well with the backbones predicted using analytical and numerical approaches [142, 174, 208].

The basic ZC (with no averaging) has been applied to the testing signal and the results are visualised in Fig. 3.13. While most of the results are very similar to those

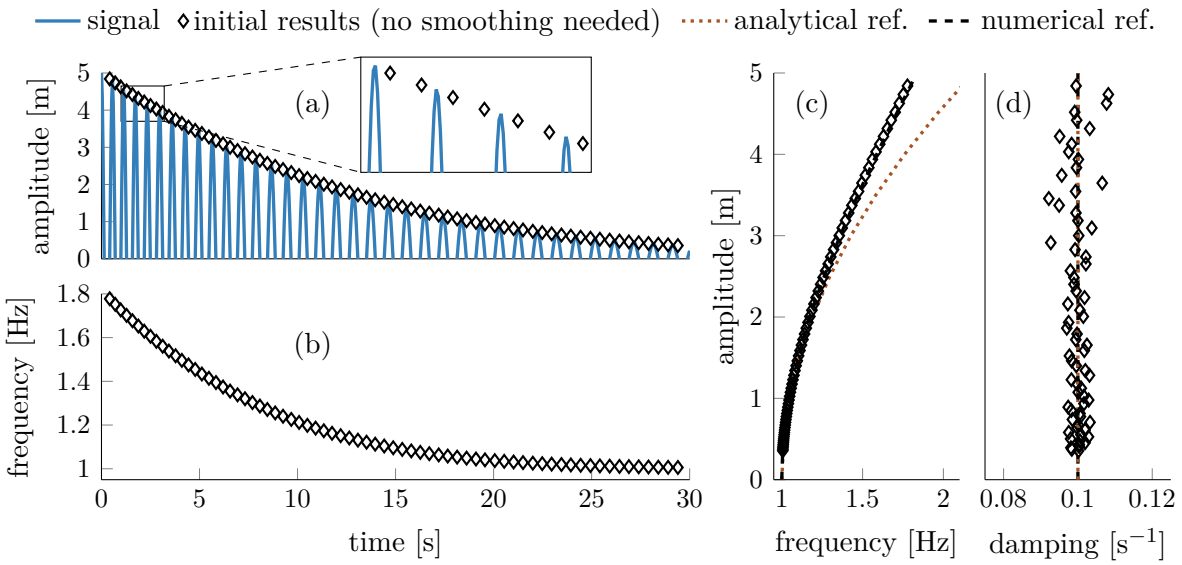

Figure 3.13 Zero-crossing (ZC) applied to the testing signal: (a) signal and instantaneous amplitude, (b) instantaneous frequency, (c) backbone, and (d) damping curve

obtained by the HT and DQ, no filtering, smoothing or averaging have been required. The IA in Fig. 3.13(a) is smooth, encloses the signal very well and no end effects occur. The IF in Fig. 3.13(b) is also very smooth and depicts the decreasing trend very well. The comparison of the backbones in Fig. 3.13(c) again reveals that the estimated backbone is practically identical to the numerical reference.

The damping curve shown in Fig. 3.13(d) seems a little more fluctuating than in the previous methods, but overall, it captures the correct value quite well. However, it should be noted that in order to obtain this damping curve, a careful evaluation of the derivative in Eq. (3.35) is crucial. In the previous cases, both IF and IA were continuous, so straightforward differentiation scheme could be used. In contrast, the IF and IA obtained by the ZC are not defined in equidistant steps. Therefore, a numerical differentiation rule that can incorporate an uneven time resolution must be utilised.

The zero-crossing method is able to estimate the trend in the IF, but fails to provide any information about the intra-wave frequency modulation. This method is very intuitive, straightforward, easy to implement, and its results can be easily verified. This, and the fact that no smoothing of intra-wave modulation is needed, makes the results suitable

for non-parametric identification of backbones of mechanical systems which was also demonstrated previously in [142, 208].

3.3.7 Generalised zero-crossing method

The generalised zero-crossing (GZC) method was proposed in [104]. The GZC still uses a few points to estimate the frequency and amplitudes, but provides better local properties and improves the time resolution to the quarter of the vibration cycle. For every point of interest the IF $\omega(t)$ is evaluated as

$$\omega(t) = \frac{2\pi}{12}\left(\frac{1}{T_1} + \sum_{j=1}^{2}\frac{1}{T_{2j}} + \sum_{j=1}^{4}\frac{1}{T_{4j}}\right), \tag{3.46}$$

where the meaning of the periods is explained in Fig. 3.14. By a similar principle the IA

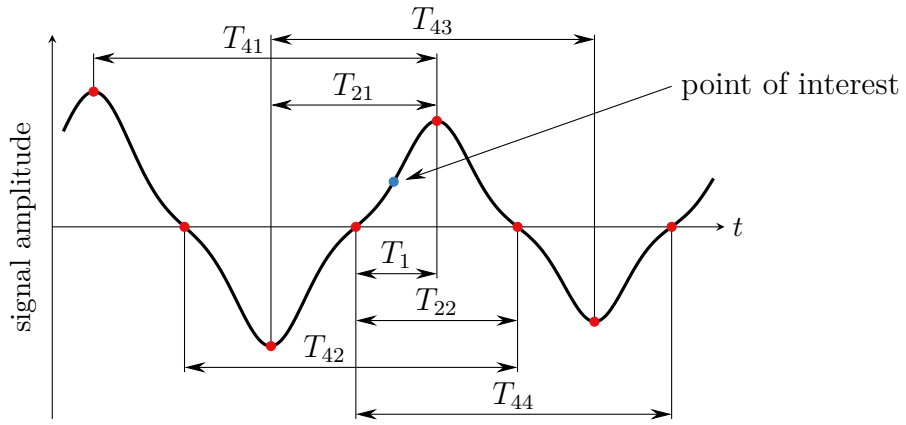

Figure 3.14 Generalised zero-crossing method

can be evaluated [104], i.e. seven different amplitudes are assigned to a point of interest and the averaged amplitude is computed in a similar way as the IF in Eq. (3.46). The resulting values are constant over the interval in which the point of interest lies. These estimates are the mean values of the instantaneous characteristics so they still retain a physical interpretation.

The generalised zero-crossing method has been applied to the testing scheme and the results are visualised in Fig. 3.15. The results need to be smoothed to obtain the conventional backbone and damping curve, but the smoothing does not have to be so strong as in the previous methods. The IA in Fig. 3.15(a) is constant on the quarter of a wave, but encloses the signal very well and no end effects occur. The IF in Fig. 3.15(b) appears to have some indication of intra-wave frequency modulation, but the true IF cannot be fully obtained due to the limited resolution.

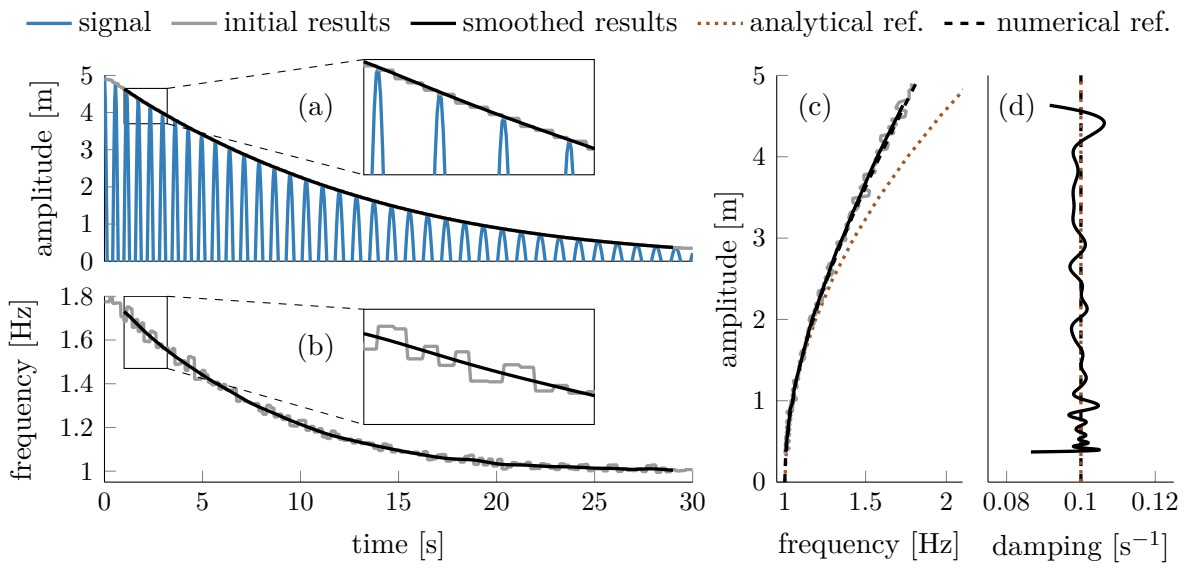

Figure 3.15 Generalised zero-crossing (GZC) applied to the testing signal: (a) signal and instantaneous amplitude, (b) instantaneous frequency, (c) backbone, and (d) damping curve

The comparison of the backbones in Fig. 3.15(c) again shows that the results are practically the same as the numerical reference. The damping curve shown in Fig. 3.15(d) seems to be quite accurate with a little fluctuation. However, it should be noted that in order to obtain this damping curve, a careful evaluation of the derivative in Eq. (3.35) is needed. The IF and IA are defined for all time, but they contain many jumps at the boundaries of the intervals that must be smoothed (see insets in Fig. 3.15). Otherwise, the numerical derivative would yield unrealistic results.

The GZC is a compromise between fully instantaneous results that follow the intra-wave frequency modulation (IFM) closely and zero-crossing methods that estimate several points. The method is still able to estimate some IFM with the resolution to a quarter of vibration period. The GZC can be used to verify the results of other methods, because the obtain IF and IA should be a mean of true characteristics [104]. This method is also easy to implement and since it uses the zero-crossing points and maxima only, it may be more robust against measured noise than the HT, NHT and DQ.

3.3.8 Summary of the IA and IF estimation methods

Several methods have been reviewed in this section. It should be, however, noted that other methods, such as generalised pencil of function method [84], exist, but they are not of interest here, because they do not bring such appealing features as the presented methods. The Hilbert transform has been used for the estimation of the IF and IA for

a long time. However, it can be replaced by other methods that not only provide very similar results after low-pass smoothing, but also each method has unique properties which can be utilised for the investigation of vibration signals.

- Hilbert transform (HT) - this method has been used for a long time and provided good results (usually after additional low-pass smoothing) in many studies. However, it suffers from a number of numerical and mathematical issues.
- Normalised Hilbert transform (NHT) - due to the normalisation scheme used, the signal theoretically satisfies all conditions necessary to remove some problems of the Hilbert transform. However, since the HT must still be used, some numerical problems can occur.
- Direct quadrature (DQ) - this method theoretically provides absolutely accurate instantaneous frequency, but it is sensitive to measured noise. Therefore, it is suitable for applications where noise-free signals can be measured and where the frequency must be tracked very accurately. It will be shown in the next section that the DQ can be utilised for characterisation of non-linearities as well.
- Energy operators - this group of methods works correctly on linear time series only. For non-linear data, it fails to provide any meaningful results. This feature can be theoretically used for detection of non-linearities.
- Zero-crossing method - Unlike the previous methods, the ZC does not provide instantaneous estimates of the IF and IA. The values are provided in zero-crossing points only and do not capture any intra-wave frequency modulation (IFM). The frequency estimated by this method is a mean of true IF. Due to a complete lack of IFM, the results do not have to be smoothed for the identification of backbones and damping curves.
- Generalised zero-crossing method - This method uses a similar principle as the zero-crossing method, but it estimates the frequency and amplitude with the resolution of a quarter the vibration period. This estimated frequency is a mean of IF which, unlike the ZC, captures some information about the intra-wave frequency modulation. Since this method is easy to implement and noise robust, it can be used to verify other methods.

A new method, which is a combination of the described methods and which allows the estimation of the intra-wave frequency modulation (IFM) frequency is described in the next section. This method can be used for the characterisation of non-linearity

using Eq. (3.28). It should be also noted that all described methods can estimate the symmetric restoring forces using Eq. (3.36). A new method for the estimation of asymmetric restoring forces in proposed in chapter 6.

3.4 A method for the estimation of the intra-wave frequency modulation

Equation (3.28) can be used to decide whether a structural non-linearity is of a hardening or softening type. However, in order to do that not only the IF must be identified accurately, but also the intra-wave frequency modulation (IFM) must be found. Therefore, it was concluded in [180] that this principle is of little practical value as neither the IF, nor the IFM can be correctly estimated by the Hilbert transform.

Since the Hilbert transform can be replaced by other methods, in particular by direct quadrature (DQ), the IF including the IFM part can be estimated properly. In addition, a method which estimates the IFM frequency f_{IMF} with the accuracy which is required in Eq. (3.28) for characterisation of non-linear behaviour is proposed hereafter. The method is suitable for mono-component functions and combines the direct quadrature and zero-crossing method. The proposed method can be described in the following steps:

1. The IF is separately found using the DQ and ZC methods, yielding $f_{\mathrm{DQ}}(t)$ and $f_{\mathrm{ZC}}(t_i)$, respectively.

2. Because $f_{\mathrm{ZC}}(t_i)$ is estimated in the zero-crossing times t_i, a cubic spline is used to interpolate $f_{\mathrm{ZC}}(t_i)$ to obtain $f_{\mathrm{ZC}}(t)$.

3. The signal which represents only the IFM is obtained by the subtraction $f_{\mathrm{DQ}}(t) - f_{\mathrm{ZC}}(t)$. Because the $f_{\mathrm{ZC}}(t)$ is a mean of IF, the resulting signal should have zero mean.

4. The ZC is again applied to the new signal in order to obtain the IFM frequency $f_{\mathrm{IFM}}(t_j)$, which is again interpolated to $f_{\mathrm{IFM}}(t)$.

5. The ratio $r(t) = f_{\mathrm{IFM}}(t)/f_{\mathrm{ZC}}(t)$ is obtained and used for characterisation of non-linear behaviour based on Eq. (3.28), i.e. there is an odd non-linearity for $r = 2$ and even non-linearity for $r = 1$.

It is worth mentioning that the ZC method does not have to be necessary used in 1st and 4th steps. Other methods could be used too as long as their results are smoothed

to estimate the IF without any intra-wave modulation. However, when applying the ZC it is guaranteed by the nature of Eq. (3.44) that the estimated IF is free of any intra-wave modulation, but still represents the mean of IF. Similarly, the normalised Hilbert transform could be used instead of the DQ. However, the DQ is preferable because it theoretically leads to absolutely correct IF, whereas the NHT is still influenced by numerical issues of the HT.

The DQ and ZC used in the proposed method are non-parametric, thereby requiring no a priori knowledge of the system. However, in order to characterise non-linearity, the characteristic ratio must be known beforehand. It was shown [184] that for odd non-linearities this ratio is equal to 2, whereas for even non-linearities, this ratio is 1. Therefore, this method can only distinguish between odd and even stiffness non-linearities and it does not give any indications of their order. This, and the fact that the DQ can be sensitive to measured noise, limits the practical applicability of the proposed method. Nonetheless, it can still be used as an additional indicator of a non-linearity type.

In the following the method is applied to two simulated cases, first of which is the testing signal used through this chapter and another one is a SDOF system with a quadratic stiffness non-linearity.

3.4.1 Application to a system with cubic hardening stiffness

The same Duffing oscillator which was presented in section 3.3.1 and used as the testing signal in this chapter is also used to demonstrate the proposed methodology. The IF

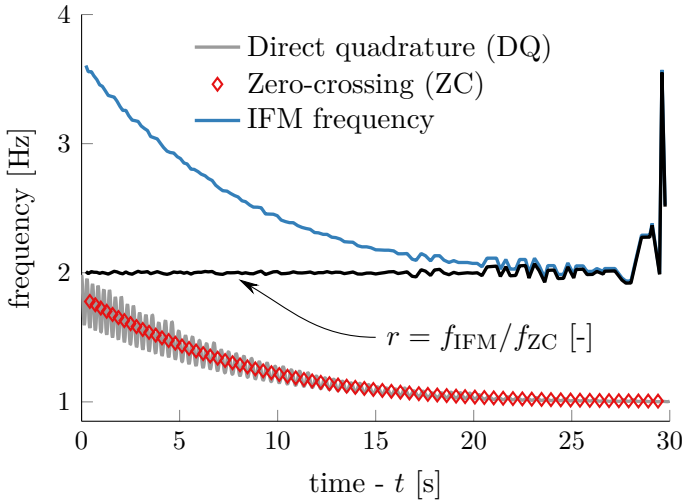

Figure 3.16 Estimation of the intra-wave frequency modulation frequency for the system with cubic hardening stiffness

estimated by the DQ (from Fig. 3.10(b)) and ZC (from Fig. 3.13(b)) is again displayed in Fig. 3.16 together with the IFM frequency $f_{\mathrm{IFM}}(t)$ estimated by the proposed method.

It can be clearly seen that $f_{\mathrm{IFM}}(t)$ is twice as high as $f_{\mathrm{ZC}}(t)$ over the most of the time interval. The values of the IFM are distorted at the end ($t \gtrapprox 25$ s) of the time interval because the intra-wave frequency modulation is very low and therefore significantly influenced by numerical errors.

The ratio r is also displayed in Fig. 3.16. This ratio is dimensionless, so its display in the same figure is for convenience only. This ratio is almost entirely equal to 2 over almost whole time interval which correctly indicates the hardening non-linearity ($r = 2$ in Eq. (3.28)).

3.4.2 Application to a system with quadratic stiffness

The second system that is used to demonstrate the proposed method is the system with quadratic stiffness governed by

$$m\ddot{x}(t) + c\dot{x}(t) + kx(t) + k_{\mathrm{nl}}x^2(t) = 0, \tag{3.47}$$

where $m = 1\,\mathrm{kg}$, $c = 0.1\,\mathrm{N\,s^{-1}\,m^{-1}}$, and $k = (2\pi)^2 \approx 39.5\,\mathrm{N\,m^{-1}}$ and $k_{\mathrm{nl}} = 3\,\mathrm{N\,m^{-2}}$. The initial conditions were $x(0) = 5\,\mathrm{m}$ and $\dot{x}(0) = 0\,\mathrm{m\,s^{-1}}$, sampling frequency $f_{\mathrm{s}} = 50\,\mathrm{Hz}$ and the response was simulated for time $t = 0 - 30\,\mathrm{s}$.

The obtained signal is asymmetric due to the presence of asymmetric restoring force so it cannot be studied by the Freevib algorithm. The same system is studied in section 6.4.3 to illustrate a new method for processing of asymmetric signals that is introduced in chapter 6.

Although the restoring force cannot be correctly estimated by the Hilbert transform, the IF and IA can still be found. The upper part ($x(t) \geq 0$) of the signal with the estimated IA are shown in Fig. 3.17(a). The Hilbert transform would not be necessary in the proposed method, but it is included here to provide another example where the HT estimates the negative frequency. It can be seen that the IA obtained using the HT and DQ oscillates, i.e. it does not enclose the signal closely. These oscillations are caused by the asymmetry of the signal. The HT and DQ yield instantaneous characteristics which are defined for all times. In contract, the IA obtained using the ZC is defined only at discrete time as emphasized by the markers in Fig. 3.17. The IA estimated by the ZC does not enclose the signal either, because it is estimated via the interpolation of the absolute values of minima and maxima (see Fig. 3.12). Regardless of the used method,

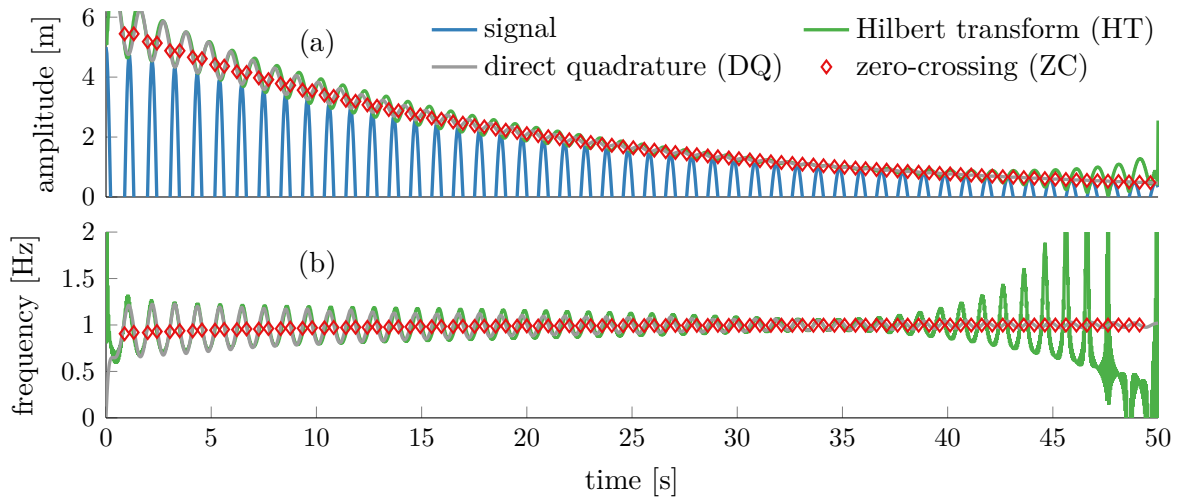

Figure 3.17 The Hilbert transform, direct quadrature and zero-crossing method applied to the system with quadratic stiffness: (a) signal and instantaneous amplitude and (b) instantaneous frequency

the IA of the asymmetric signal estimated using any method is not very useful because it does not enclose the signal closely.

The obtained IF is shown in Fig. 3.17(b). The HT estimated noisy IF despite the noiseless input signal. Moreover, the end effect is easily observed and also the negative frequencies were estimated at the end of the signal. The DQ produced smooth and instantaneous estimate of the IF, whereas the ZC produced smooth, but only discrete IF values without intra-wave frequency modulation. The IF obtained using the DQ and ZC

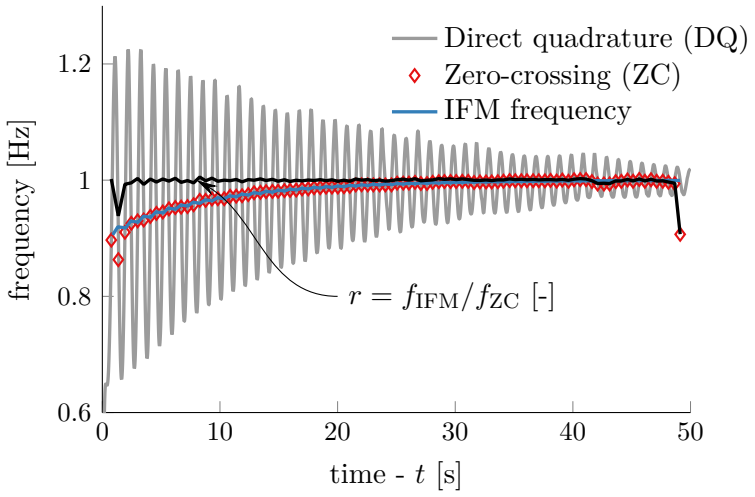

Figure 3.18 Estimation of the intra-wave frequency modulation frequency for the system with quadratic stiffness

approaches the linear natural frequency of the system at the end of the time interval, where the system behaves linearly.

The IF is again displayed in Fig. 3.18 together with the IFM frequency $f_{\mathrm{IFM}}(t)$ that was estimated by the proposed method. It can be seen that $f_{\mathrm{IFM}}(t)$ is the same as the mean value of $f_{\mathrm{ZC}}(t)$ over the most of the time interval. The ratio $r(t)$ was also estimated and is displayed in Fig. 3.18 as well. This ratio is almost entirely equal to 1 over almost whole time interval, which correctly indicates even stiffness non-linearities [184].

3.5 Discussion

The Hilbert-Huang transform introduced in this chapter is a versatile tool which has attracted a widespread interest in many fields, including structural dynamics where it has been used for the experimental and operational modal analysis [210, 295, 296], structural health monitoring [38], and parametric and non-parametric identification of non-linear systems [25, 72, 182–184, 265]. Despite not having a rigorous mathematical background, the method has a solid logical justification as evidenced by a number of successful studies. In addition, physics-based foundations of the EMD were derived in [118, 138]. Specifically, it was shown how IMFs relate to the slow-flow dynamics of mechanical systems derived by the complexification-averaging technique (CxA). However, no connection to non-linear modal analysis has so far been demonstrated in literature. An attempt to connect the HHT and non-linear modal analysis is made in chapter 4. The found approximative relation will serve as a theoretical base for non-linear system identification method proposed in chapter 5.

The basic algorithm of the EMD was discussed in section 3.2 and some of the signal processing issues reviewed. Then, a considerable focus was on the mode mixing problem in section 3.2.2 where it was found that the EMD can, depending on the ratio of their frequencies and amplitude, either (i) correctly separate two subsequent modes, (ii) leave the signal unchanged or (iii) do something else, possibly even creating spurious IMFs. It was argued that although the mode mixing does not have to be a significant problem in the fields where the correct separation of the modes is not important, it is crucial for non-linear modal analysis in this thesis. Fortunately, some techniques to remove or significantly reduce the mode mixing exist, one of which, the masking signal (see section 3.2.3) was found to be appropriate for the applications in structural dynamics.

The thorough comparison of methods for the instantaneous frequency and amplitude estimation developed in other field was conducted in section 3.3 in order to evaluate their potential for non-linear system identification. The summary of these methods and their

features is given in section 3.3.8. It was found that not only all methods lead to very similar results after low-pass filtering, but also that each method can provide unique features that can be utilised for non-linear system identification. The combination of the methods then led to the proposal of a new method for IFM frequency estimation in section 3.4. The proposed method was applied to two numerical cases which highlighted its functionality for noise-free signal. Unfortunately, a range of applicability of the proposed method is quite narrow due to its sensitivity to measured noise and its ability to distinguish solely between odd and even stiffness non-linearities. Nevertheless, the method can still be used as an indicator of non-linearity type.

3.6 Conclusion

The Hilbert-Huang transform (HHT) was discussed in this chapter. In particular, the mode mixing problem of the empirical mode decomposition was described and it was shown how it can be investigated before applying the EMD. A significant part of the chapter was devoted to the comparison and evaluation of the methods for instantaneous frequency and amplitude estimation, namely normalised Hilbert transform, direct quadrature, energy operators and zero-crossing methods. The comparison led to the conclusion that while all methods provide equivalent results after low-pass filtering or other smoothing, each method has unique features that can be used to detect and characterise the non-linearity. In addition, this evaluation motivated the development of the new method for the estimation the intra-wave frequency modulation (IFM). The method also provides the ratio of the fundamental frequency and IFM frequency which is subsequently used to determine the type of stiffness non-linearity. Although the proposed method can be used as an additional indicator of the non-linearity type, its practical applicability is very limited due to its sensitivity to measured noise. The Hilbert-Huang transform is used in the following chapters for non-linear system identification.

Chapter 4

The relation between non-linear modes and the Hilbert-Huang transform

Abstract

In structural dynamics, the assertion that the Hilbert-Huang transform (HHT) relates to non-linear vibration modes seems to be widely accepted. However, this relation has never been systematically investigated. The objective of this chapter is therefore to study this relation by examining the match between IMFs and non-linear modes responses. The concept of complex non-linear modes (CNMs) is used because, unlike the normal non-linear modes (NNMs), it can be applied to non-conservative systems. Since it has been previously shown that the HHT relates to the slow-flow dynamics of the system derived using a complexification-averaging (CxA) method, the relation between the HHT and CNMs is also sought through the reduced order model (ROM) of slow-flow dynamics. It is shown that the relation is supported by a number of similarities between the methods and it is also highlighted by a range of numerical studies. However, it cannot be concluded that the CNMs provide a solid theoretical framework for the HHT since the relation is only approximative.

4.1 Introduction

The Hilbert-Huang transform (HHT) has been identified as one of the most appealing methods for time-frequency analysis in section 1.3.2. It does not use a traditional interpretation of the frequency based on the Fourier transform, but utilises the instantaneous frequency (IF) and amplitude (IA) instead. As such, it can supposedly estimate the backbones, damping curves or intra-wave frequency modulation (IFM) as described in chapter 3. Unfortunately, the HHT, especially the EMD, does not have a rigorous mathematical background. The physics-based foundation of the HHT was however already established [118, 138] by showing the correspondence of the IMFs and slow-flow dynamics derived by the complexification-averaging (CxA).

However, the relation between the HHT and non-linear modes has never been shown. Yet, a number of studies [155, 168, 181] utilised the HHT for non-linear system identification in a normal non-linear mode (NNM) framework. In these studies, it was intuitively assumed that the IMFs should compose some approximation of the total response of individual NNMs and therefore the estimated IF and IA correspond to the system's backbones. However, the relation of the IMFs and one of the concept of the non-linear modal analysis has never been investigated in detail.

The objective of this chapter is to investigate if IMFs relate to the response of non-linear modes of mechanical systems. By doing so, the premise that the HHT leads to the estimation of correct backbones should be further strengthened. The often used concept of non-linear normal modes (NNMs) is replaced by complex non-linear modes (CNMs) to accommodate the potential non-linear dissipative effects in the system. The relation between the HHT and CNMs is supported by showing the correspondence of intrinsic mode functions (IMFs) and the reduced order model (ROM) of slow-flow dynamics derived from CNMs on several MDOF non-linear systems. Unfortunately, it is found that the relation is only approximative - qualitatively the ROM responses do correspond to IMFs whereas some quantitative discrepancies can be observed. As a consequence, it must be concluded that the CNMs cannot be accurately estimated by the HHT.

The chapter is organised as follows: Firstly, the theoretical background of the CNMs, ROM and CxA is described in section 4.2. This is required in order to present the argumentation supporting the relation between the HHT and CNMs in section 4.3. Then, several numerical studies are used to demonstrate this relation in section 4.4. Three non-linear systems are studied, namely a system with a cubic hardening spring, a system with a quadratic damping and a cantilever beam with a geometric non-linearity. Free decay responses are dominantly considered because they allow several vibration modes to be measured simultaneously, thereby being suitable for the application of the EMD,

but a few examples of resonant decay response and slow-sweep harmonic excitation are also given. Section 4.5 then discusses a range of validity of the described relation, its possible implications and limitations.

4.2 Theoretical background

The Hilbert-Huang transform has been introduced in detail in chapter 3. This section introduces the background theory of complex non-linear modes (CNMs), reduced order model (ROM) and complexification-averaging (CxA) that is necessary to discuss the relation among them.

4.2.1 Complex non-linear modes of mechanical systems

A complex non-linear mode (CNM) of motion is defined in [135] as an oscillation of an autonomous system with a (potentially) phase difference between its degrees of freedom. The concept of complex non-linear mode has been chosen instead of widely-used non-linear modes (NNM) or invariant manifold approach because, by definition, it is more suitable for a free decay description. In addition, unlike NNMs, it can be applied to non-conservative systems.

Consider an autonomous general dynamic system governed by

$$\mathbf{M}\ddot{\mathbf{x}}(t) + \mathbf{C}\dot{\mathbf{x}}(t) + \mathbf{K}\mathbf{x}(t) + \mathbf{f}(\mathbf{x}(t), \dot{\mathbf{x}}(t)) = \mathbf{0}, \qquad \mathbf{x}(0) = \mathbf{x}_0, \quad \dot{\mathbf{x}}(0) = \dot{\mathbf{x}}_0 \tag{4.1}$$

where $\mathbf{M}$ is a mass matrix, $\mathbf{C}$ is a linear damping matrix, $\mathbf{K}$ is a linear stiffness matrix, and $\mathbf{x}(t)$ is a vector of generalised coordinates. The operator $\mathbf{f}(\mathbf{x}, \dot{\mathbf{x}})$ comprises all non-linear effects, which depend on the displacement and velocity. In line with the definition of the complex non-linear mode, the motion is sought in the form

$$\mathbf{x}(t) = q\Re\left\{\sum_{n=0}^{N_\mathrm{h}} \mathbf{\Psi}_n \mathrm{e}^{n\lambda t}\right\}, \tag{4.2}$$

where q is a modal amplitude, λ is a complex fundamental eigenfrequency, n is the index of harmonics, and $\mathbf{\Psi}_n$ is a multi-harmonic complex eigenvector. Unlike in the linear modal analysis, the complex eigenvector is approximated by a truncated Fourier series, thereby having N_h components. The complex fundamental eigenfrequency λ relates to an undamped natural angular frequency ω_0 and a damping ratio ζ as

$$\lambda = -\zeta\omega_0 + \mathrm{i}\omega_0\sqrt{1-\zeta^2}. \tag{4.3}$$

A set of unknown parameters λ, $\boldsymbol{\Psi}_0$, $\boldsymbol{\Psi}_1$, $\ldots$, $\boldsymbol{\Psi}_{N_\mathrm{h}}$ can be then regarded as amplitude-dependent modal properties.

Equation (4.2) is submitted to Eq. (4.1) and subsequent Fourier-Galerkin projection yields the following non-linear system of algebraic equations [128, 135]

$$\left[(n\lambda)^2\mathbf{M} + n\lambda\mathbf{C} + \mathbf{K}\right]\boldsymbol{\Psi}_n q + \langle \mathbf{f}(\mathbf{x}_\mathrm{p}, \dot{\mathbf{x}}_\mathrm{p}), \mathrm{e}^{\mathrm{i}n\omega_0 t}\rangle = \mathbf{0}, \quad \text{for} \quad n = 0, \ldots, N_\mathrm{h}. \tag{4.4}$$

For the computation of the generalised Fourier coefficients $\langle \mathbf{f}(\mathbf{x}_\mathrm{p}, \dot{\mathbf{x}}_\mathrm{p}), \mathrm{e}^{\mathrm{i}n\omega_0 t}\rangle$ of non-linear effects, a periodic formulation of displacement $\mathbf{x}_\mathrm{p}(t)$ and velocity $\dot{\mathbf{x}}_\mathrm{p}(t)$ are used (instead of the pseudo-periodic formulation defined by Eq. (4.2)), i.e.

$$\mathbf{x}_\mathrm{p}(t) = q\Re\left\{\sum_{n=0}^{N_\mathrm{h}} \boldsymbol{\Psi}_n \mathrm{e}^{\mathrm{i}n\omega_0 t}\right\}, \quad \dot{\mathbf{x}}_\mathrm{p}(t) = q\Re\left\{\sum_{n=0}^{N_\mathrm{h}} \mathrm{i}n\omega_0 \boldsymbol{\Psi}_n \mathrm{e}^{\mathrm{i}n\omega_0 t}\right\}. \tag{4.5}$$

Although this periodic formulation is an approximation, it is justified [134, 135] by realising that the decrease of amplitude due to damping is relatively small within one period of motion. The periodic definition allows an effective numerical evaluation (analytical is rarely possible) of the generalised Fourier coefficients $\langle \mathbf{f}(\mathbf{x}_\mathrm{p}, \dot{\mathbf{x}}_\mathrm{p}), \mathrm{e}^{\mathrm{i}n\omega_0 t}\rangle$. The same Fourier coefficients are used in a conventional harmonic balance method so all the approaches developed therein can be used here too, including the alternating frequency/time-domain (AFT) procedure [29, 54, 134, 135] and condensation of the problem into the non-linear degrees of freedom [127].

Equation (4.4) cannot be solved directly because the number of unknowns is greater than the number of equations. Therefore, similarly to the linear modal analysis, normalisation conditions must be added. Several normalisation schemes have been proposed, for instance using the modal amplitude [134, 135] or kinetic energy [127]. However, the normalisation with respect to the mass matrix [128] is the most beneficial for the computation of the ROM and is also consistent with the normalisation in the linear modal analysis. Two normalisation conditions must be enforced

$$\boldsymbol{\Psi}_1^H \mathbf{M} \boldsymbol{\Psi}_1 = 1, \quad \Re\{\mathbf{t}^\mathrm{H}\boldsymbol{\Psi}_1\} = 0, \tag{4.6}$$

where $\mathbf{t}$ is a complex vector. The first condition represents an amplitude constrain while the second serves as a phase normalisation.

The frequency-domain solution of the non-linear eigenproblem given by Eq. (4.4) subjected to normalisation conditions given by Eq. (4.6) can be found using a Newton-Raphson method in conjunction with numerical continuation on modal amplitude such

that $q \in (q_{\min}, q_{\max})$. The linear modal properties may be used as a suitable starting guess. The numerical implementation of the complex non-linear modal analysis is described in more detail in appendix B.

4.2.2 Reduced order model of slow-flow dynamics

Having obtained the amplitude-dependent modal properties, the reduced order model of slow-flow dynamics can be derived. The slow-flow dynamics relies on the partition of the dynamics to fast (the frequency of oscillation) and slow dynamics (slowly varying amplitudes and phases). The ROM of slow-flow dynamics represents the system by slowly-varying variables and it is restricted to a regime where no modal interaction occurs.

The ROM can be derived by a modified complexification-averaging (CxA) technique [128]. The displacement and velocity are firstly transformed using complex variables as

$$\mathbf{x}(t) = q\frac{\boldsymbol{\nu}(q,\vartheta) + \boldsymbol{\nu}(q,\vartheta)^*}{2}, \quad \dot{\mathbf{x}}(t) = \mathrm{i}\Omega q\frac{\boldsymbol{\nu}(q,\vartheta) - \boldsymbol{\nu}(q,\vartheta)^*}{2}, \tag{4.7}$$

where the asterisk marks a complex conjugate, the manifold $\boldsymbol{\nu}(q,\vartheta)$ is generally equal to

$$\boldsymbol{\nu}(q,\vartheta) = \sum_{n=0}^{N_\mathrm{h}} \boldsymbol{\Psi}_n \mathrm{e}^{\mathrm{i}n\vartheta}, \quad \vartheta = \vartheta(t) = \phi(t) + \Theta(t), \quad q = q(t), \tag{4.8}$$

and the angular frequency Ω is the time derivation of the fast phase $\phi(t)$. The angular frequency relates to the excitation force (the right-hand side of Eq. (4.1)). For an autonomous system, no excitation is present, so $\Omega = \omega_0$. For a non-autonomous system, the right-hand size of Eq. (4.1) may generally be expressed as

$$\mathbf{F}(t) = \mathbf{F}_\mathrm{e}\frac{\mathrm{e}^{\mathrm{i}\phi_\mathrm{e}(t)} + \mathrm{e}^{-\mathrm{i}\phi_\mathrm{e}(t)}}{2}, \tag{4.9}$$

where $\mathbf{F}(t)$ is a vector of excitation forces, $\mathbf{F}_\mathrm{e}$ is a vector of the amplitudes of excitation forces and $\phi_\mathrm{e}(t)$ is an excitation phase. In this case, $\Omega = \frac{\mathrm{d}\phi_\mathrm{e}}{\mathrm{d}t}$.

An important aspect of the formulation in Eq. (4.8) is that the total phase $\vartheta(t)$ combines fast $\phi(t)$ and slowly $\Theta(t)$ varying components. The fast varying phase can be removed by an averaging process (detailed in [128]), and the amplitude $q(t)$ and slow

phase $\Theta(t)$ can be computed from an averaged system

$$\begin{aligned} 2\Omega\dot{q} &= -2\zeta\omega_0\Omega q - \boldsymbol{\Psi}_1^{\mathrm{H}}\mathbf{F}_{\mathrm{e}}\sin\Theta, \\ 2\Omega\dot{\Theta} &= \omega_0^2 - \Omega^2 - \frac{1}{q}\boldsymbol{\Psi}_1^{\mathrm{H}}\mathbf{F}_{\mathrm{e}}\cos\Theta. \end{aligned} \tag{4.10}$$

This system of non-linear differential equations can be numerically solved, provided that the initial conditions q_0, Θ_0 are given. Unfortunately, the initial conditions are not directly accessible because the initial state of the system is usually described by $\mathbf{x}_0, \dot{\mathbf{x}}_0$. To estimate the initial conditions, an optimisation scheme was proposed in [128]

$$q_0, \Theta_0 = \underset{q,\Theta}{\operatorname{argmin}} \|\mathbf{x}_0 + \frac{1}{\mathrm{i}\Omega}\dot{\mathbf{x}}_0 - q\boldsymbol{\nu}(q, \vartheta(\Theta))\|. \tag{4.11}$$

Using this optimisation, it is possible to find the closest projection of the initial states $\mathbf{x}_0, \dot{\mathbf{x}}_0$ on the manifold of a vibration mode. In case that the initial states do not lie on the manifold directly, the exact agreement with the original dynamics cannot be guaranteed. However, it will be shown in section 4.4 that the total response can still be well approximated even if the initial states are not directly on the manifold.

The system in Eq. (4.10) avoids the evaluation of the numerically expensive non-linear effects $\mathbf{f}(\mathbf{x}, \dot{\mathbf{x}})$ completely and has much lower dimension than the original system in Eq. (4.1). In addition, Eq. (4.10) can be further reduced for an autonomous system [128] to

$$\dot{q} = -2\zeta\omega_0 q \quad \text{and} \quad \Theta = \Theta_0. \tag{4.12}$$

and under the steady-state conditions ($\dot{q} = \dot{\Theta} = 0$) to an algebraic system [127]

$$0 = -2\zeta\omega_0\Omega q - \boldsymbol{\Psi}_1^{\mathrm{H}}\mathbf{F}_{\mathrm{e}}\sin\Theta, \quad \text{and} \quad 0 = \omega_0^2 - \Omega^2 - \frac{1}{q}\boldsymbol{\Psi}_1^{\mathrm{H}}\mathbf{F}_{\mathrm{e}}\cos\Theta. \tag{4.13}$$

After solving Eq. (4.10), Eq. (4.12) or Eq. (4.13) for $q(t)$ and $\Theta(t)$, the displacement and the velocity can be evaluated from Eq. (4.7).

Summary of the reduced order model computation

The following steps are required to obtain the ROM of slow-flow dynamics:

1. Compute λ, $\boldsymbol{\Psi}_0$, $\boldsymbol{\Psi}_1$, $\ldots$, $\boldsymbol{\Psi}_{N_{\mathrm{h}}}$ from Eq. (4.4) subjected to Eq. (4.6) using a continuation on the modal amplitude for $q \in [q_{\min}, q_{\max}]$ (see appendix B).

2. Project initial conditions $\mathbf{x}_0, \dot{\mathbf{x}}_0$ on the manifold using Eq. (4.11) to obtain q_0 and Θ_0.

3. To find slowly-varying variables $q(t)$ and $\Theta(t)$, solve Eq. (4.10) for general excitation, Eq. (4.12) for an autonomous system or Eq. (4.13) for steady-state excitation.

4. Construct the manifold $\boldsymbol{\nu}(q, \vartheta)$ in Eq. (4.8) while considering the type of excitation.

5. Evaluate the displacement and velocity from Eq. (4.7).

4.2.3 Complexification-averaging technique

The complexification-averaging (CxA) is an analytical technique that derives a slow-flow model of a system by partitioning its response into slow and fast components [118, 137, 138]. Such decomposition is possible when the response is composed by a number of well-separated dominant fast-frequency $(\omega_1, \omega_2, \ldots, \omega_N)$ components, so the response $x(t)$ can be expressed as the sum of these components

$$x(t) = y_1(t) + y_2(t) + \cdots + y_N(t). \tag{4.14}$$

For each component, a new complex variable is introduced

$$\psi_m(t) = \dot{y}_m(t) + \mathrm{i}\omega y_m(t) = \varphi_m \mathrm{e}^{\mathrm{i}\omega_m t}, \quad m = 1, 2, \ldots, N \tag{4.15}$$

where $\mathrm{e}^{\mathrm{i}\omega_m t}$ represents the fast component and φ_m is the slow complex component. The latter can be expressed in the polar coordinates as

$$\varphi_m = a(t)\mathrm{e}^{\mathrm{i}\Theta(t)}, \tag{4.16}$$

where $a(t)$ is the amplitude and $\Theta(t)$ is the slowly varying phase. By submitting Eq. (4.15) into the equation of motion (Eq. (4.1)) and applying the method of multiphase averaging, the fast-frequency components can be removed, and an averaged system governing the slow-flow dynamics obtained

$$\dot{\boldsymbol{\Phi}} = \mathbf{F}(\Phi), \quad \Phi = [\varphi_1, \varphi_2, \ldots, \varphi_N]^{\mathrm{T}}. \tag{4.17}$$

The operator $\mathbf{F}$ can become quite cumbersome even for small systems, for example, for a two-degree-of-freedom system studied in section 4.4.1 the operator, an 8 by 8 matrix, can be found in [118]. The slowly varying amplitude and phase are then obtained by solving this averaged system. In some cases, the system can be even solved analytically and this is often the reason why the CxA is used to study non-linear systems. Unfortunately,

the application of the method is limited to the small academic systems with simple polynomial non-linearities.

4.3 The relation between the Hilbert-Huang transform and non-linear modes

It has been shown in [118] that the slow-flow dynamics derived by the CxA relates to the IMFs. The relation was not proven mathematically, but rather supported by a number of similarities in the formal definitions of equations governing the CxA and HHT. The relation was further studied in [138] by deriving approximative mathematical expressions for the empirical slow-flow and showing the correspondence with the analytical expressions derived by the CxA.

The reduced order model of slow-flow dynamics can therefore be seen the link between the HHT and CxA, but also between the HHT and CNMs. The hypothesis of this relation is supported by the following arguments:

- The representation of the total response is consistent in all three methods. The HHT and CxA assume that the total response can be expressed as the sum of well separated mono-components (Eq. (3.10) and Eq. (4.14), respectively). Although the ROM is only exact in a close proximity of the mode, it has been already suggested in [128] that by superimposing the responses of different modes (which are always mono-component functions), the approximation of the total response can be obtained. Moreover, [200] presented that the concept of invariant manifold also leads approximately to the total response. Since CNMs trace trajectories on this manifold, their superposition should also lead to the approximation of the total response.

- All the methods share a common representation of dynamics. The methods partition the dynamics into slow and fast components. Although this partition is not a priori enforced in the HHT, the HHT always leads to it as evidenced by analytic signal analysis [138]. The slow-fast partition is also a key concept of the CxA and ROM given by Eq. (4.15) and Eq. (4.8), respectively.

- All three methods represent the signal in the complex domain, and these representations are comparable. Each method transfers a real-valued response into the complex domain. This complexification is carried out by the Hilbert transform (see Eq. (3.30)) in the Hilbert-Huang transform and by Eq. (4.15) in the CxA. It might

be argued that the complexification is merely a cosmetic choice, but it was shown that these two complexifications are closely related [138]. The complexification used in the ROM given by Eq. (4.7) is essentially the same as the one used in the CxA. The difference is that the scalar complex variable in the CxA is replaced by the multi-component complex manifold in the ROM.

- The approximative relation is supported by numerical studies. The relation between the HHT and CxA was numerically demonstrated in [118, 137, 138] and the numerical investigation is also carried out in section 4.4 to highlight the relation.

Based on these similarities, it can be hypothesised that the response of the ROM of slow-flow dynamics derived from CNMs corresponds approximately to the IMFs obtained by the EMD. By extension, this would mean that there is a relation between the HHT and the CNMs of mechanical systems. If the hypothesis is proved to be true, the HHT can be used as a means of non-linear modal analysis, i.e. to extract the CNMs from experimental data. It is not possible to mathematically prove this hypothesis due to the empirical and numerical nature of involved methods. Therefore, it is investigated using a range of numerical examples and parametric studies.

4.4 Numerical investigation of the relation using simulated data

In order to highlight the relation between the HHT and CNMs, three non-linear systems are studied - a system with a cubic hardening spring, a system with a quadratic damper, and a cantilever beam with geometric non-linearity. In each case, the equation of motion is given and results of the complex non-linear modal analysis briefly presented. Then, the time series is simulated using the direct time integration, processed by the empirical mode decomposition and compared with the ROM. The focus is mainly on free decay responses because they generally contain multiple vibration modes and are therefore suitable for the application of the EMD.

4.4.1 A system with cubic hardening stiffness

A simple two-degree of freedom system with a cubic hardening stiffness is considered. A similar system, sometimes with the same parameters, has been studied in many publications, including [96, 117, 118, 127, 128, 191]. Since it is so often used, it is studied here in more detail than other systems. The system consists of two masses connected by

three linear springs as depicted in Fig. 4.1. The non-linear (cubic hardening) stiffness is

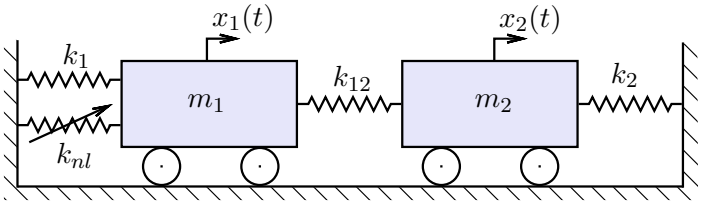

Figure 4.1 A two-degree-of-freedom system with a cubic hardening stiffness

located between the left mass and the ground and the system is allowed to vibrate only in the horizontal direction.

This system can be described by Eq. (4.1), in which

$$\mathbf{M} = \begin{bmatrix} m_1 & 0 \\ 0 & m_2 \end{bmatrix}, \quad \mathbf{K} = \begin{bmatrix} k_1 + k_{12} & -k_{12} \\ -k_{12} & k_2 + k_{12} \end{bmatrix}, \quad \mathbf{f}(\mathbf{x}, \dot{\mathbf{x}}) = \begin{bmatrix} k_{\mathrm{nl}} x_1^3 \\ 0 \end{bmatrix}, \tag{4.18}$$

where the parameters chosen in this study are the same as in [117, 128], i.e. $m_1 = m_2 = 1\,\mathrm{kg}$, $k_1 = k_2 = k_{12} = 1\,\mathrm{N\,m^{-1}}$, $k_{\mathrm{nl}} = 0.5\,\mathrm{N\,m^{-3}}$ and modal damping ratio of 1% is also introduced.

The computed backbones, normalised mode shapes and a set of frequency response functions (computed using the harmonic balance method) can be seen in Fig. 4.2. It can

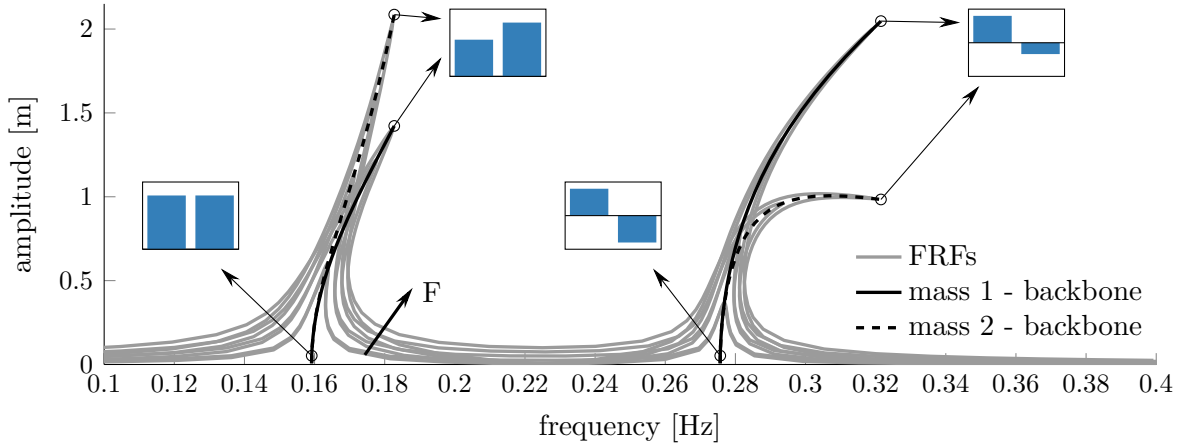

Figure 4.2 The computed backbones (black) and normalised mode shapes (blue) of the system with cubic hardening stiffness. The frequency response functions (grey) from both masses were added to highlight their relation to the non-linear modes.

be seen that both modes are non-linear, exhibiting the hardening behaviour. The relation between the non-linear modes and FRFs is also seen, i.e. all backbones pass the maximum

amplitudes of the FRFs. The computed damping (not shown) is not amplitude-depended and it is equal to the selected modal damping. The small insets in Fig. 4.2 depict the normalised mode shapes to emphasise the difference between the dynamics for the first and second mode. At the first mode, where both masses vibrate in phase, the amplitude of mass 1 is lower than the amplitude of the mass 1 at high amplitudes. Whereas at the second mode, the response of the first mass becomes dominant at high amplitudes. These results are consistent with the NNMs presented, for example, in [117, 128].

The backbones will be used in the rest of this section to compute the ROM of slow-flow dynamics which is then compared with the extracted IMFs. It should be noted that the ratio of the natural frequencies of the system, $f_1 = 0.1591\,\text{Hz}$ and $f_2 = 0.2757\,\text{Hz}$, is equal to 1.73. It is therefore very close to the mode mixing limit set by Eq. (3.17) so it is possible that some mode mixing may occur.

Three loading cases are considered - a resonant decay response of the first mode, slow-sweep harmonic excitation response around the first mode, and a number of free decays for general initial conditions. The first two cases are not so interesting from the perspective of this study, because the EMD does not have to be used at all. In addition, it was already shown in [128] that for these two cases, the ROM is exact. They are included here to show that the performed evaluation is numerically correct.

A free decay computed for general initial conditions is studied more extensively, because it cannot be directly compared to the ROM so the EMD must be performed. Firstly, a detailed comparison (including the comparison with the CxA from [118, 138]) is made for the parameters of the nominal system listed above and one case of the initial conditions. Then, the parameter space is greatly extended and it is studied how the relation of the HHT and CNMs behaves for a wider range of non-linear stiffness coefficients, modal damping ratios, and initial conditions.

A resonant decay response

Experimentally, the resonant decay response can be measured using phase resonance testing (see section 1.3.3), whereas numerically, it can be found by setting the initial conditions in such a way that the motion starts exactly on the invariant manifold and stays on the manifold. Hence, it decays as a single-mode response. Here, the first mode, which is excited for the initial displacement $\mathbf{x}_0 = [1.1192\,\text{m}, 1.4128\,\text{m}]^T$ and zero initial velocity, is considered. These initial conditions have been chosen to allow a potential comparison with [128].

The computed resonant decay responses of both masses can be seen in Fig. 4.3. The signals do not consists of several frequency components and they can therefore be

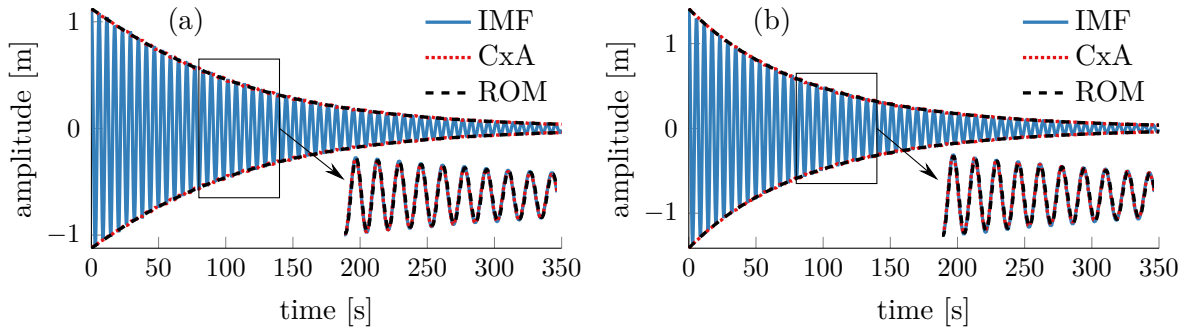

Figure 4.3 Resonant decay response of the first mode: (a) displacement of mass 1 and (b) mass 2

considered as the IMFs without using the EMD.

For the same initial conditions, the ROM of slow-flow dynamics was computed using the CNMs and CxA, and both sets of results are shown in Fig. 4.3 as well. As expected, the match between the IMFs, ROM and CxA is extremely good. Since the time-domain results are practically identical, the estimated IF and IA would also correspond very closely (depending on the IF and IA estimation method selected as discussed in section 3.3).

Figure 4.3 evidences that the HHT relates to the CNMs through the ROM of slow-flow dynamics in case of the excitation which is very close to a single non-linear mode. More examples of resonant decay responses for this system, the influence of initial conditions, and modal damping ratio can be found in [128].

A slow-sweep harmonic response

The response around the first mode to the excitation force given by Eq. (4.9) with $\mathbf{F}_\mathrm{e} = [\mathrm{N}, 0]^T$, $\phi_\mathrm{e}(t) = 0.0001t^2$ and zero initial displacements and velocities is shown in Fig. 4.4. As the slow-sweep excitation was used, there is minimal influence of the

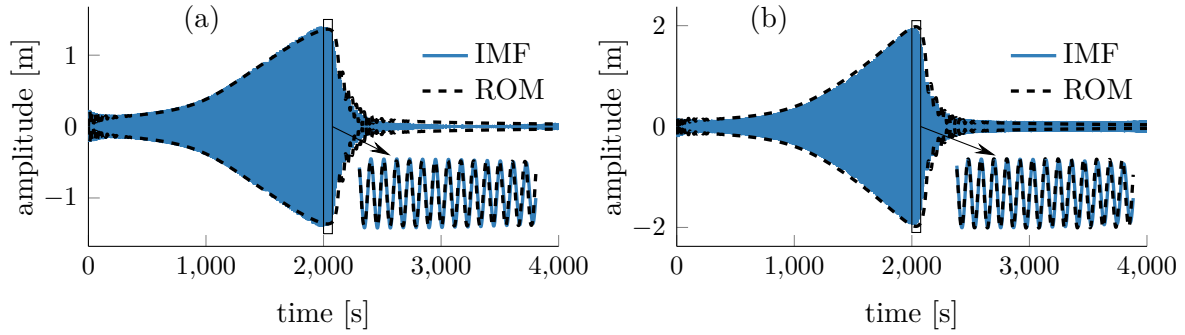

Figure 4.4 Comparison of the IMFs and ROM for sweep excitation: (a) mass 1 and (b) mass 2

second mode in the response of the first mode. Therefore, this is a trivial case from the point of view of the presented topic as the EMD does not have to be used, i.e. the response already corresponds to an IMF. The IMF has the shape that is typical for cubic hardening stiffness. Unlike for a linear system, the peak is not symmetric due to the hardening behaviour and sudden decrease in the amplitude can be observed.

For the same loading conditions, the ROM of slow-flow dynamics was computed and is shown in Fig. 4.4 as well. It can be seen that the match between the two models is very good, especially in a close vicinity of the first mode where the ROM is supposed to be exact. Understandably, the differences are observable at the beginning of the time interval, because the signal computed by the time-domain integration also includes a transition zone where both natural frequencies are present at the same time. Likewise, away from the resonance, the ROM is not exact, because it does not take into account any influence of the second mode. These results are in line with [128], in which more examples of sweep responses for this system and the study of influence of the sweep rate can be found.

A free decay for general initial conditions

This case, in which a free decay response for general initial conditions is considered, is the most interesting with regards to the presented topic. Free decays can be easily experimentally obtained from the hammer impact test [63] which excites several modes over a large frequency range simultaneously. Because the impulse is still finite, only the first few modes are usually excited. Numerically, similar free decays can be obtained by the numerical integration of an autonomous system subjected to the general initial conditions. The difference between the measured and computed free decay is that the computed one consists of all modes of the structure.

In this section, the initial displacement $\mathbf{x}_0 = [1\,\mathrm{m}, 0]^T$ and zero velocity are used. The computed data are shown in Fig. 4.5. It can be seen that both responses consist of two modes of different frequencies, so the EMD is necessary to separate the modes from each other. The basic algorithm of the EMD described in section 3.2.1 was used and the resulting IMFs (there were no spurious IMFs extracted) are shown in Fig. 4.6. Unlike the original signal, the IMFs are single frequency components. Therefore, they look very similar to resonant decay responses. Despite the use of the basic algorithm of the EMD, no numerical problems can be observed, i.e. there are no end effects and modes are clearly separated.

For the same initial conditions, the ROM of slow-flow dynamics derived from the CNMs and by the CxA are also shown in Fig. 4.6. Overall, all three responses match

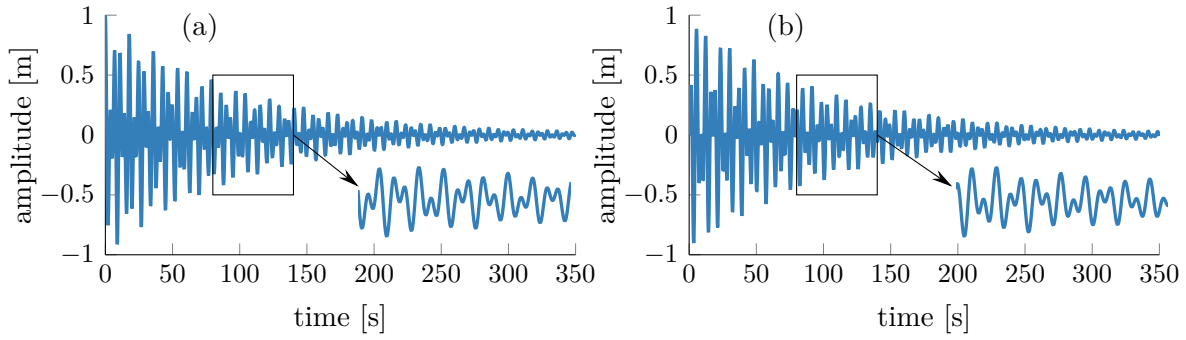

Figure 4.5 Computed free decay response of the system with cubic hardening stiffness: (a) mass 1 and (b) mass 2

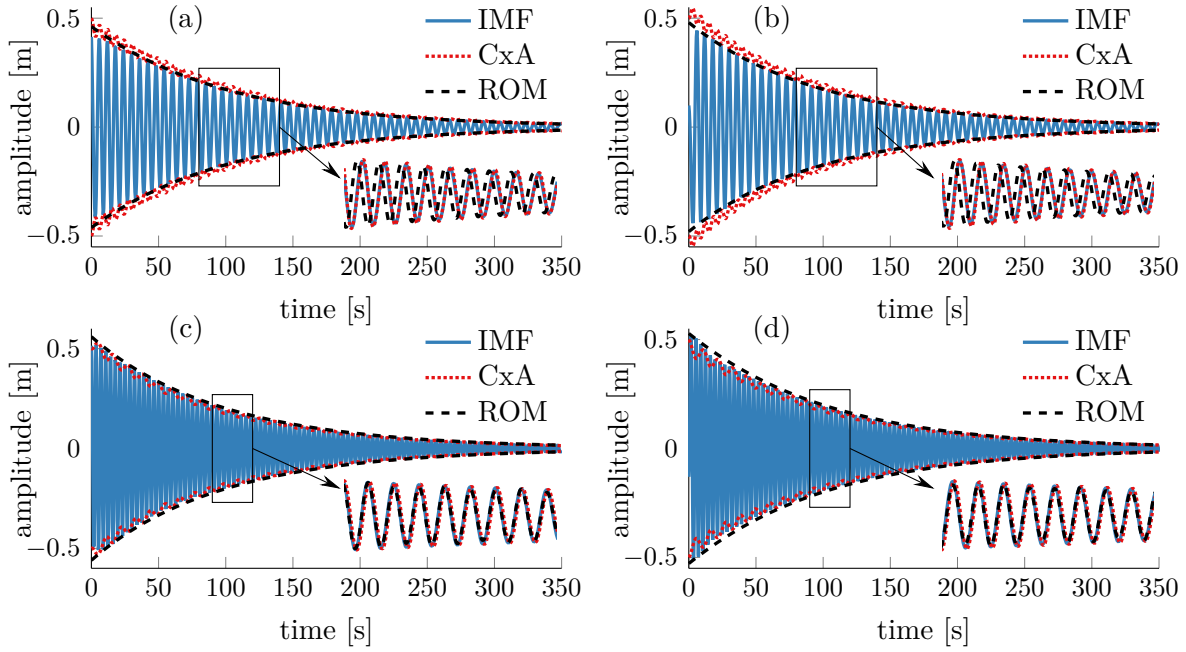

Figure 4.6 Comparison of the IMFs and ROM for the system with cubic hardening stiffness: (a) first mode, mass 1, (b) first mode, mass 2, (c) second mode, mass 1, and (d) second mode, mass 2

for both masses and both modes. However, there are a few small differences that are worth noting. Firstly, the first mode response of the ROM is slightly different than the response of the CxA and the IMFs. The amplitude (envelope) is captured correctly, but the frequency appears to be slightly lower at the beginning which cumulatively causes an apparent shift of the ROM response (see the inset in Fig. 4.6(a) and Fig. 4.6(b)). Secondly, despite the fact that the amplitude of the CxA responses corresponds well to the maxima of the IMFs, the amplitude appears to fluctuate in between extrema. Similar, but not so severe, fluctuation of the amplitude can also be seen in [118]. Nevertheless,

the final CxA response, seen in the insets in Fig. 4.6, appears to match the IMFs very well, with no shift in the frequency or mismatch in the amplitude.

The Hilbert spectrum of the IMFs together with the ROM frequency is shown in Fig. 4.7. It can be seen that the ROM indeed predicted the frequency lower than the

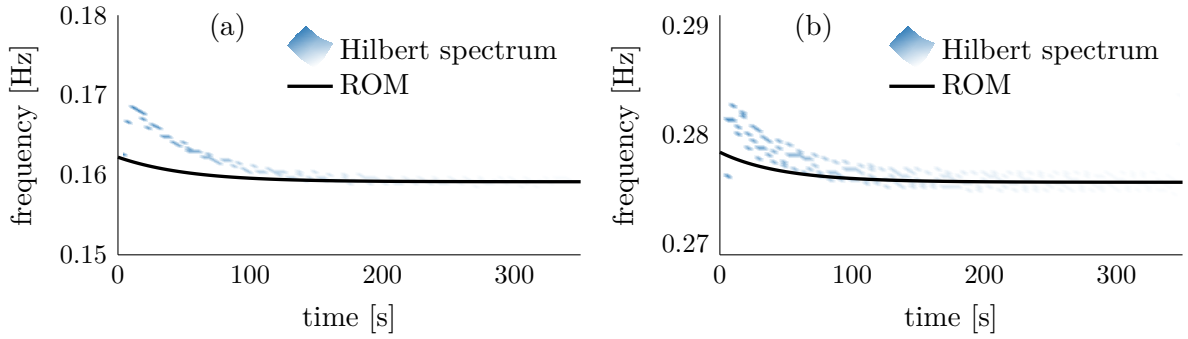

Figure 4.7 The Hilbert spectrum of the two-degree-of-freedom system with the cubic hardening non-linearity: (a) the first mode and (b) the second mode

frequency which is estimated by the HHT. The differences in frequency are less than 5 % for both modes.

Based on the presented cases, it appears that some approximative relation may indeed exist between the HHT and CNMs. However, it is also obvious that the match is not exact. It appears that the match of the IMFs and ROM is less accurate for the first mode due to the slightly lower frequency of the ROM response. This is unfortunate, because the first mode is usually the most non-linear one, thereby being of the highest interest.

So far, only a single set of parameters and very few loading conditions have been studied to support the assertion that the HHT relates to CNMs. In order to further highlight the relation and improve the understanding of the difference observed between the IMFs and ROM, two parametric studies are conducted.

Parametric study 1 - The influence of non-linear stiffness and modal damping ratio

To further highlight the relation between the HHT and CNMs, a wider range of system parameters is studied. It would be ideal to vary all parameters of the system and observe how the relation holds. However, it would be practically impossible to visualise and evaluate the results in a systematic manner. Therefore, the focus in this section is on the influence of the modal damping ratio in a range $\zeta \in [0,\, 3]$ % and non-linear stiffness coefficient $k_{\mathrm{nl}} \in [0,\, 2]$ N m^{-3}. These two parameters have been previously observed to have a significant influence on the ROM of a single mode of vibration [128]. The

parameters of the under-lying conservative system and the initial conditions have not been changed. The parametric study is conducted in an automatic manner so the performance of the EMD is not explicitly verified for each case. However, the correspondence of the ROM and IMFs is evaluated in such a way that possible end effects will not influence the results.

In order to evaluate the correspondence of the ROM and IMFs, the following matching factor has been used

$$C_m^{(k)} = \left\| \left(c_m^{(k)}\right)^2 - \left(x_m^{(k)}\right)^2 \right\|, \tag{4.19}$$

where $c_m^{(k)}$ and $x_m^{(k)}$ are the IMF and the response of the ROM of the k-th mass and m-th vibration mode, respectively. The factor $C_m^{(k)}$ is equal to zero if there is no difference between the IMFs and ROM and increases with the increasing mismatch. It would be also zero if $c_m^{(k)}$ and $x_m^{(k)}$ were the same, but out of phase signals (which has not happened in either of the parametric studies presented herein). However, it should be noted that if the only difference between the $c_m^{(k)}$ and $x_m^{(k)}$ is a phase angle, they can be considered as identical with regards to the HHT, because their IF and IA would be the same. The reason for this is the definition of the instantaneous frequency, which is a derivative of phase (see, for example, Eq. (3.32)) so the constant off-set is not important. The Eq. (4.19) takes into account the whole response so it captures the information about the amplitude and frequency at the same time.

It should be mentioned that it would be probably better to use a factor which is normalised in such a way that the worst possible case is equal to 1. In that case, it would be easier to interpret the relative errors for different parameters. Unfortunately, it is impossible to find a sensible normalisation which could be used in both parametric studies for all investigated cases. In order to make up for this deficit of the performance factor, the direct comparisons of the ROM and IMFs are included in the results. Therefore, it is possible to see how the size of the factor relate to the amount of correspondence between the IMFs and ROM.

Comparing whole responses would not be practical, due to significant changes in the frequency and decay rate caused by the different stiffness and damping. Moreover, the end effects of the EMD could influence the resulting factor too. Therefore, in order to perform a meaningful comparison, first two periods of the response were removed and the next five periods were used for the computation of $C_m^{(k)}$.

In total, 77 systems for different values of non-linear stiffness coefficient and damping ratio have been investigated. In each case, four factors, corresponding to two modes and two masses, were obtained. To evaluate an overall relation between the HHT and CNMs,

these four factors were averaged. The results of the first parametric study are shown in Fig. 4.8. This surface covers a number of systems, ranging from linear to strongly

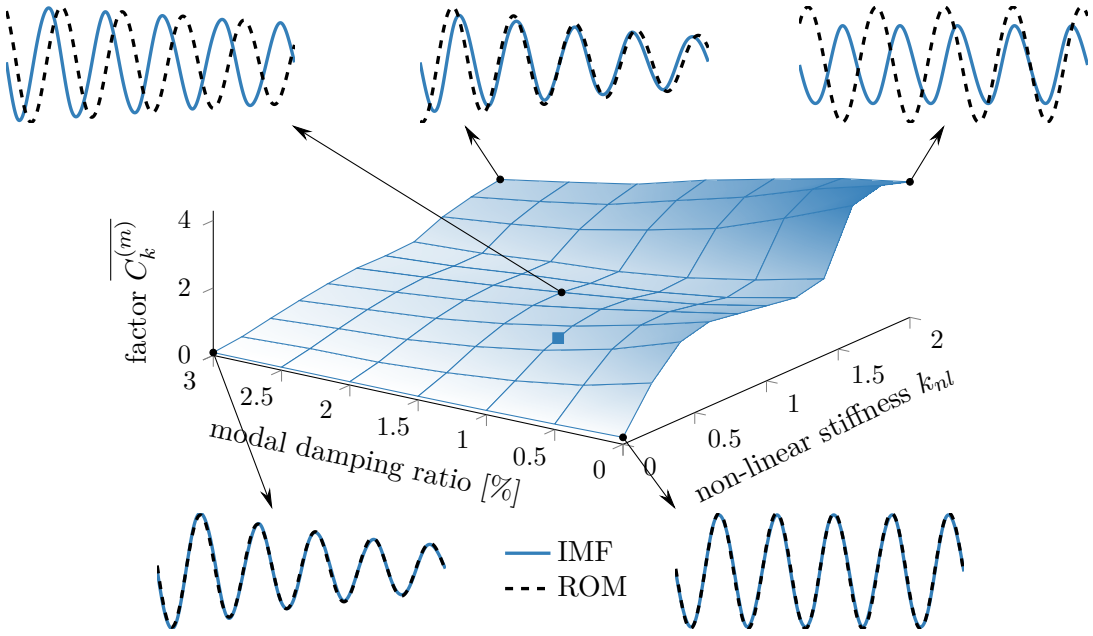

Figure 4.8 Parametric study 1: the influence of the non-linear stiffness and modal damping ratio on the relation between the HHT and CNMs visualised using the quality factor from Eq. (4.19). The insets contain the comparison between the intrinsic mode functions (blue) obtained by the empirical mode decomposition and the reduced order model (black) computed from the complex non-linear modes.

non-linear ($k_{nl} \in [0, 2]$ N m^{-3}) with no to strong modal damping ($\zeta \in [0, 3]$ %). The insets contain the direct comparison of the IMFs and ROM of the first mode and first mass (similarly to Fig. 4.6(a)) and make up for the missing normalisation in Eq. (4.19). This comparison in the insets is made for the five periods that have been used to evaluate the matching factor. It should be noted that the insets represent the worst observed cases since the match for the second mode is usually much better (similarly to Fig. 4.6).

It is clear from Fig. 4.8 that for linear systems the match between the IMFs and ROM is perfect and independent of the damping. On the other hand, for non-linear systems, the factor is not equal to zero and the damping, albeit linear, also influences its value. A trend can be observed - the factor increases with the increasing stiffness and decreasing damping. This means that the overall correspondence between the HHT and CNMs is not so good for lightly damped, strongly non-linear systems. The insets in Fig. 4.8 show that in a majority of cases, the discrepancies between the HHT and CNMs originate in the difference between the frequencies, whereas the amplitudes match reasonably well. This is not true for the largest values of non-linear stiffness and lowest damping. In that

case, even the amplitudes do not match very well as visualised for $k_{nl} = 2\,\mathrm{N\,m^{-3}}$ and $\zeta = 0\,\%$ (the upper right inset in Fig. 4.8).

The blue square in Fig. 4.8 at $k_{nl} = 0.5\,\mathrm{N\,m^{-3}}$ and $\zeta = 1\,\%$ indicates the system which was investigated in detail in Fig. 4.6. Similar conclusions as for this system can be made for a large number of systems investigated in this parametric study too. Mainly, the frequency obtained by the ROM seems to be slightly lower at the beginning of the time interval, which then causes the shift of the ROM response. The CxA response has not been shown in this parametric study, but similarly to Fig. 4.6 the CxA produces very good approximation of the IMFs. Unlike the ROM, the CxA is able to describe the frequency more accurately, but the fluctuating amplitude is obtained. It should be also noted that the correspondence for the first mode and the first mass is not so good as for other IMFs (again, similarly to Fig. 4.6). Therefore, the responses in the insets in Fig. 4.8 represent one of the worst scenarios.

The ROM can fail to predict the phase of the signal correctly if the optimisation in Eq. (4.11) fails. The unique solution of such optimisation is not guaranteed in a general case so it is possible that some shift of the ROM can be caused by inappropriate initial conditions for the solutions of Eq. (4.10). These shifts are visible in the considered time domain signals but since they are almost constant, they have a little impact on the estimated frequency and amplitude, especially toward the end of the signal.

To summarise the first parametric study, it can be stated that the relation between the HHT and CNMs approximately holds for a wide range of damping and non-linear stiffness parameters. The relation is not exact - despite the fact that the IMFs and ROM exhibit always the same qualitative features, the quantitative error may be significant in some cases. However, with regards to strong non-linearities considered and that fact that a widely-studied configuration of the system shows satisfactory results, it can be concluded that the assertion of the approximative relation between the HHT and CNMs is justified.

Parametric study 2 - The influence of initial conditions

The free decay response of a system is significantly influenced by not only the system parameters, but also by the initial conditions. For this reason, the influence of the initial displacements on the relation between the HHT and CNMs is investigated in a range $x_1(0) \in [0, 1.5]$ m and $x_2(0) \in [0, 1.5]$ m. The other parameters of the system were the same as in the original configuration and the initial velocity was set to zero. The analysis has been conducted in the same manner to the previous parametric study, i.e. the time

response was calculated, the EMD applied and compared to the ROM by means of the matching factor from Eq. (4.19).

Because both initial conditions varied, it was not always possible to decompose the response into two IMFs for each mass. Sometimes, only a resonant decay response is excited whereas in some cases, the contribution of one of the modes is so weak that the EMD cannot extract both modes property. Therefore, for the evaluation using Eq. (4.19), only the first mode from the first mass is considered, i.e. only the factor $C_1^{(1)}$ is determined. Furthermore, before attempting the EMD, it was verified whether it can obtain the proper IMFs. This was achieved by applying the process described in section 3.2.2. The FFT was applied, the fundamental frequency and corresponding amplitude of both modes investigated, and the criteria given by Eqs. (3.17)-(3.19) evaluated. When it was found that the EMD can separate the modes clearly (region (1) in Fig. 3.5), the ROM of the first mass was compared with the last IMF, which corresponds to the first mode. On the other hand, when it was determined that the EMD cannot separate the modes (region (3) in Fig. 3.5), the response of the system, which is very close to a resonant decay response, was directly compared with the ROM of the first mode. The cases where the EMD cannot clearly separate the modes, but changes the original signal (region (2) in Fig. 3.5), were not considered.

In total, 10200 systems for different values of the initial displacements have been investigated. The parametric study yielded the surface shown in Fig. 4.9 which covers the area around the first mode. Three well separated regions can be recognised, specifically, in region (1) the EMD returns 2 correct modes, in region (2) the EMD changes the signal, but cannot give correct modes, and in region (3) the EMD cannot decompose the signal at all without using the masking signal, EEMD or CEEMAN as discussed in section 3.2. The theoretical lines corresponding to the criteria from Eqs. (3.17)-(3.19) are also shown. In addition, the dashed line, passing roughly through the center of the graph in region (3), indicates the initial conditions which lead to the excitation of a resonant decay response of the first mode only. The shown factor $C_1^{(1)}$ is not normalised, so the insets in Fig. 4.9 contains the direct comparison of the ROM with either the IMFs (region (1)) or the response of the system (in regions (2) and (3)).

In region (1), the factor monotonically increases with increasing initial conditions, indicating that the match between the IMFs and ROM is not so good for high initial displacements. This is in line with the previous observation, since the increase of initial conditions essentially leads to stronger non-linear behaviour for higher amplitude at the beginning of the signal. It therefore indicates that the relation of the HHT and CNMs is less accurate for strong non-linearity. Most of the discrepancies between the

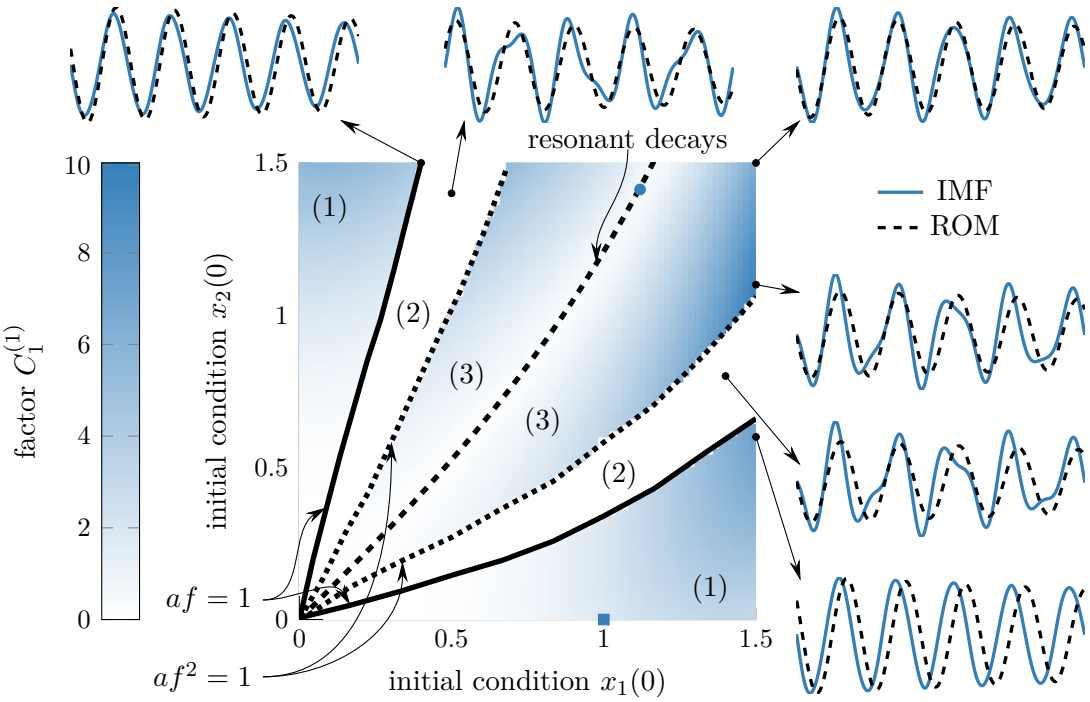

Figure 4.9 Parametric study 2: the influence of the initial displacement on the relation between the HHT and CNMs visualised using the quality factor from Eq. (4.19). The thick black lines represent the criteria for the frequency resolution of the EMD developed in section 3.2.2 and divide the graph into three regions: (1) the EMD separated the vibration modes, (2) the EMD was not applied since its effect to the signal is uncertain, and (3) the EMD cannot separate the modes so the simulated signals were directly compared to the ROM computed from the complex non-linear modes.

IMFs and ROM originate in the frequency, whereas the amplitude appears to match well. This can be nicely observed in the insets in Fig. 4.9 for $\mathbf{x}_0 = [0.4,\ 1.5]$m (upper left) and $\mathbf{x}_0 = [1.5,\ 0.6]$m (bottom right). In both cases, the amplitude match very well while the frequency causes an apparent shift of the ROM response. As expected, the factor approaches zero for very low initial conditions. This is due to the fact, that for such a low initial displacement, the system basically behaves as a linear one. The blue square in Fig. 4.9 marks the configuration of the system studied previously in Fig. 4.6. Similar conclusions can be drawn for a number of systems in this parametric study too. It can be again argued that the insets represent the worst possible cases of the correspondence between the IMFs and ROM. This means that the relation between the HHT and CNMs appears satisfactory for a wide range of initial conditions, provided that the EMD has extracted correct structural modes. However, the relation is not exact, but rather approximative, due to the quantitative errors that exist between the IMFs and ROM responses.

In region (3), in which the EMD neither separates the modes, nor changes the original signal, the first observation is that for the low initial displacements ($< 0.5\,\mathrm{m}$), the match of the response of the system and the ROM is very good, despite the fact that no EMD was needed. For higher initial conditions, the match is extremely good when the system is released with the initial conditions corresponding to the first mode (dashed line in Fig. 4.9), or in a close proximity of these conditions. The example of an exact match for the initial conditions that are indicated by the blue dot in Fig. 4.9 was previously given in Fig. 4.3. The region (3) suggests that even if the initial conditions are not adjusted perfectly for resonant decay measurements in an experimental setting, it may still be possible to capture a resonant decay response of a considered mode exactly. However, it must be noted that for the higher initial conditions, the ROM ceases to exist due to modal interactions [128] so the comparison with the HHT is no longer possible. In the rest of region (3), the factor $C_1^{(1)}$ increases with the distance from the resonant decay response. This is in line with the under-lying assumption that the accuracy of the relation between the HHT and CNMs is violated when the IMF is not extracted or measured appropriately as well as the fact the ROM can capture only non-linear modal responses accurately. Most of the discrepancies seen between the HHT and ROM are caused by mismatch in the frequency, whereas the total amplitude seems to be captured correctly. For example, the insets in Fig. 4.9 for $\mathbf{x}_0 = [1.5,\ 1.5]$m (upper right corner) and $\mathbf{x}_0 = [1.5,\ 1.1]$m (under the legend) show that the overall amplitude is correctly captured, whereas the frequency seems to have a significant modulated component that causes the mismatch of the responses. Based on these findings, it can be concluded that the response of the first mode can still be approximated by the ROM of slow-flow dynamics, even if it has not been measured with the exact initial conditions of a considered mode.

In region (2), no factor has been evaluated, because the EMD may lead to spurious IMFs and directly measured responses are far from the resonant decay response. It can be seen in the insets for $\mathbf{x}_0 = [0.4,\ 1.4]$m (right) and $\mathbf{x}_0 = [1.4,\ 0.8]$m (above) that the time domain signal is composed of two modes, but these cannot be separated by the EMD due to a lack of local extrema. When showing the ROM in the same inserts, it is revealed that the qualitative difference between two signals is quite significant, thereby rendering any comparison meaningless.

To summarise the second parametric study that explored the influence of the initial conditions on the relation between the HHT and CNMs. Provided that the EMD has led to the correct structural modes, they match with the ROM quantitatively very well. However, for general initial conditions, some quantitative differences exist which renders the relation between the HHT and CNMs approximative. On the other hand, in the

case that the initial conditions are such that a specific mode is excited, the response of the system corresponds to the ROM accurately. In the region where the EMD does not produce correct modes, the HHT cannot be related to the CNMs at all. It should be noted that it does not mean that the practical application of the EMD is significantly limited. As described in section 3.2, a number of methods can be used to resolve a mode mixing problem, usually extending the feasibility of the EMD to all practical cases.

4.4.2 A system with quadratic damping

A simple two-degree of freedom system with non-linear quadratic damping is considered in this section. The system has the same spatial layout as the system in Fig. 4.1, but the cubic spring has been replaced by a non-linear dashpot. Such system can be therefore described by Eq. (4.1) with mass and stiffness matrix given by Eq. (4.18), but the non-linear restoring force now reads

$$\mathbf{f}(\mathbf{x}, \dot{\mathbf{x}}) = \begin{bmatrix} c_{\mathrm{nl}} \dot{x}_1 |\dot{x}_1| \\ 0 \end{bmatrix}, \tag{4.20}$$

where c_{nl} is the coefficient of the quadratic damping. The parameters of the system chosen in this study were $m_1 = m_2 = 1\,\mathrm{kg}$, $k_1 = 0.1\,\mathrm{N\,m^{-1}}$, $k_2 = k_{12} = 1\,\mathrm{N\,m^{-1}}$, $c_{\mathrm{nl}} = 0.5\,\mathrm{N\,s\,m^{-1}}$ and linear modal damping of 1 % was introduced as well. Due to the presence of the non-linear damping, this case cannot be studied by the classical definition of the NNMs.

The computed backbones, damping curves, normalised mode shapes and a set of frequency response functions can be seen in Fig. 4.10. Despite the fact that no stiffness non-linearity has been added to the system, the backbones lean slightly to the left. This amplitude-dependent nature of the resonance frequency due to the quadratic damping has also been observed in [82]. Unlike in Fig. 4.2, the backbones do not pass through the peak of the FRFs exactly. The validity of the FRFs and backbones have been verified by convergence studies for different number of harmonics, but the results remained unchanged. The difference between the peaks of FRFs and backbones is less than 8 % in all cases and it is most likely caused by the used periodic formulation in Eq. (4.4). This formulation assumes that the decrease in the amplitude due to damping is relatively small. However, it will be seen in this section that this assumption is not well satisfied for this system, thereby probably causing a slight mismatch between the FRFs and the backbones.

Unlike in the previous system with cubic hardening non-linearity, the damping curves are strongly dependent on the amplitude as seen in Fig. 4.10(b). The damping increases

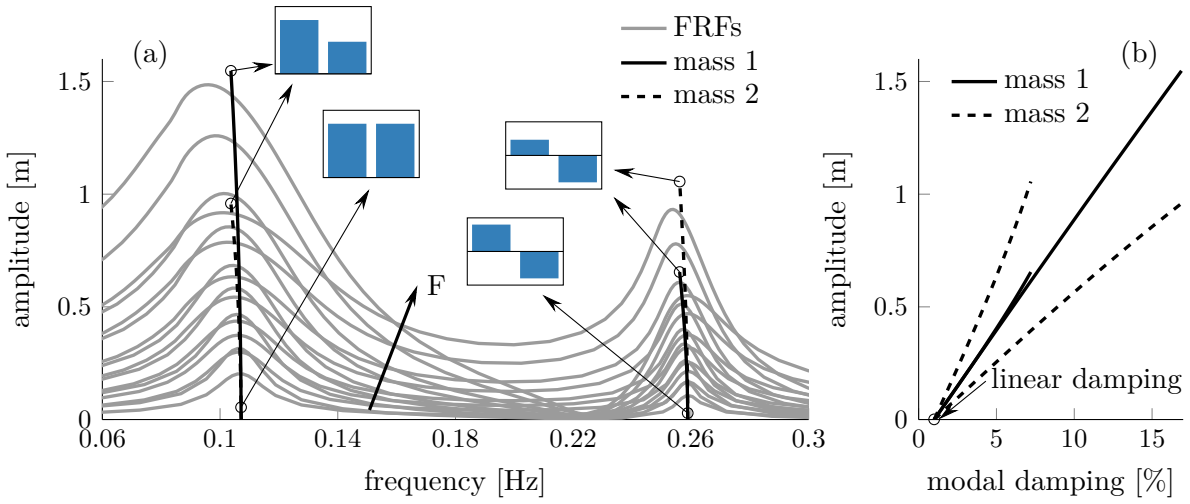

Figure 4.10 The system with quadratic damping: (a) backbones, normalised mode shapes and frequency response functions, and (b) the modal damping

non-proportionally with the increasing amplitude, which is in line with [82] in which a similar linearity plot of a SDOF with quadratic damping was presented. The non-linear behaviour of the frequency and damping can be also observed from the FRFs in Fig. 4.10(a). The FRFs are flat due to damping just like the FRFs in Fig. 2.4(e) for a SDOF with the same non-linearity, and their peaks are slightly shifted to the left. As can be seen in the insets in Fig. 4.2, the non-linear mode shapes exhibit the same behaviour as for the previous system, i.e. at the first mode, the motion of mass 1 becomes prominent at high amplitudes, whereas at the second mode, mass 2 has larger displacements.

The results of non-linear modal analysis will be used to compute the ROM that is compared to either the resonant decay response, sweep response or estimated IMFs.

A resonant decay response

As for the system with the cubic hardening spring, the resonant decay response has been obtained by setting the initial conditions which correspond directly to the first mode, i.e. $\mathbf{x}_0 = [1, 0.6466]^{\mathrm{T}}$ and zero velocity. The resonant decay responses of both masses are displayed in Fig. 4.11. It can be seen that although computed for the MDOF system, the responses again consist of a single mode of vibration. Therefore, they do not require the EMD to be used and can be directly considered as the IMFs. Compared with the cubic system in Fig. 4.3 the effect of damping is clearly seen. The amplitude is reduced by 50 % in the first vibration period, but then the rate of amplitude decrease is much lower.

The ROM has been computed for the same initial conditions. Despite the rapid decrease of the amplitude at the beginning of the signal, which seems to violate the

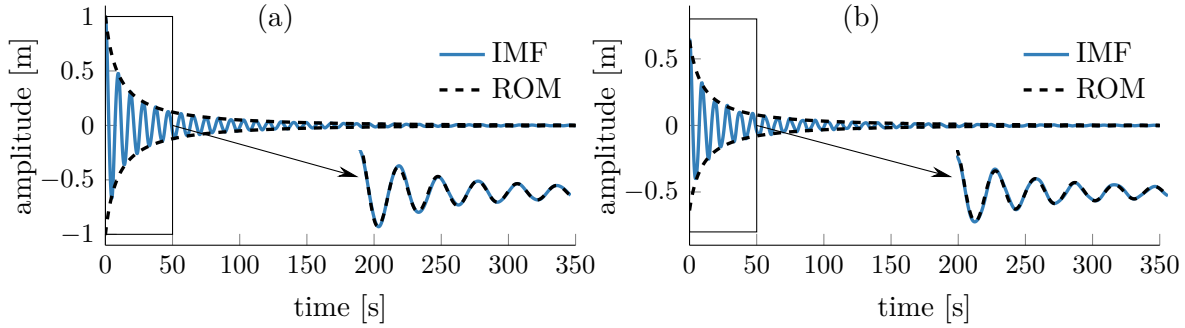

Figure 4.11 Resonant decay response of the first mode: (a) mass 1 and (b) mass 2

assumption of the periodic formulation in Eq. (4.4), the ROM matches the resonant decay responses exactly for both masses of the system. This match once again demonstrates that the ROM is able to capture the behaviour of a non-linear system exactly in a close proximity of the resonance.

A slow-sweep harmonic response

The response around the first mode to the excitation force given by Eq. (4.9) with $\mathbf{F}_\mathrm{e} = [0.1,\, 0]^\mathrm{T}$, $\phi_\mathrm{e}(t) = 0.0002t^2$ and zero initial displacements and velocities is shown in Fig. 4.12. Due to the slow-sweep excitation used, the response has a single-mode

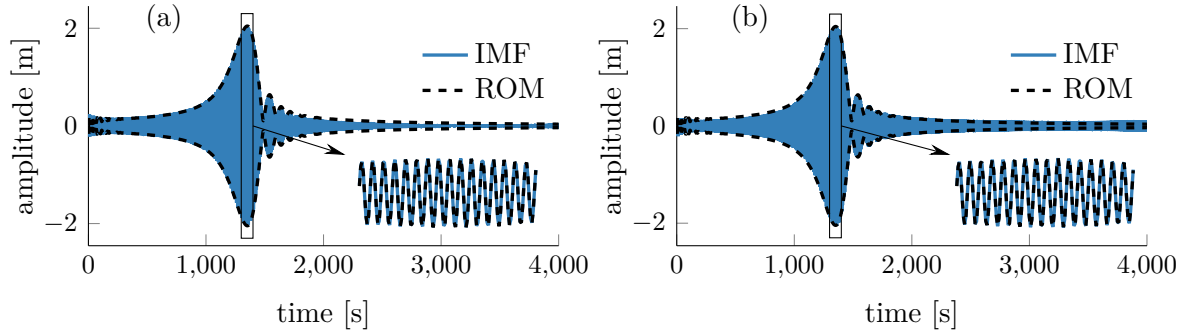

Figure 4.12 Comparison of the IMFs and ROM for sweep excitation: (a) mass 1, and (b) mass 2

characters with no influence of the second mode. Therefore, the EMD does not have to be used and the response can be considered as an IMF. The response has a very different shape than for the cubic hardening non-linearity in Fig. 4.4. There is no sudden decrease in the amplitude due to the stiffness, but rather a gradual transition over the resonance.

For the same loading conditions, the ROM of slow-flow dynamics is shown in Fig. 4.12 as well. It can be seen that the match is very good, especially in a close proximity of the

resonance crossing. Again, some differences occur at the beginning and the end of the signal, but this was expected because the ROM is not valid when there is a contribution of multiple modes in the response.

A free decay for general initial conditions

The free decays shown in Fig. 4.13 were computed for the initial displacement $\mathbf{x}_0 = [1, 0]^T$ and zero initial velocities. It can be seen that both responses consist of both modes.

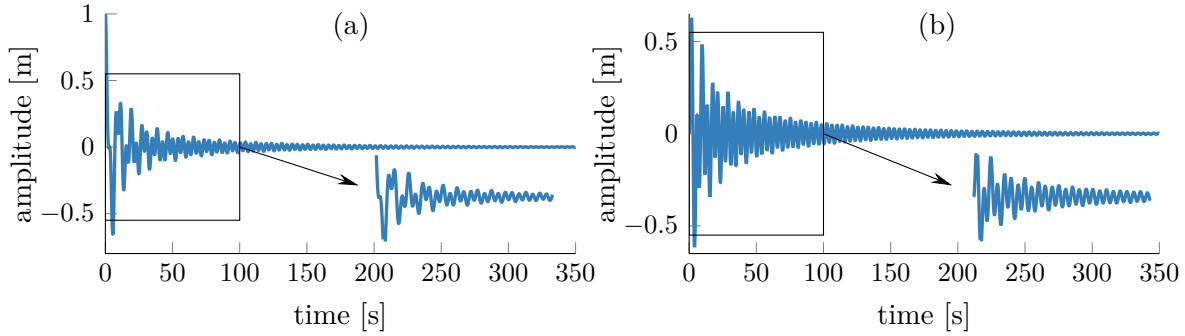

Figure 4.13 Computed free decay response of the system with quadratic damping: (a) mass 1 and (b) mass 2

The overall character of the response is significantly different compared to Fig. 4.13 for the system with cubic hardening stiffness. The presence of strong damping effects is prominent at the beginning of the signal where a dramatic decrease in the amplitude can be clearly seen. Despite the fact that mass 1 was released from 1 m, its amplitude was less than 0.4 m in the second period of vibration. The damping is much stronger at the beginning, but becomes weaker toward the end of the signal as can be seen from the gradual decay rate after first 20 s.

Because the signals consist of both vibration modes, they must be decomposed into the IMFs by the EMD. The IMFs are shown in Fig. 4.14. Unlike the original signal, the IMFs seemingly look as responses of a SDOF system or resonant decay responses. There are several numerical imperfections which originated in the EMD that can be observed in the IMFs. Most importantly, the end-effects at the beginning of the signal can be seen in Fig. 4.14(c). There is no physical reason for a short increase in the amplitude at the beginning of the signal, so this is regarded as the unwanted end-effect. In addition, the correct initial value of 1 m is not obtained by summarising the amplitudes of the IMFs corresponding to mass 1 (Fig. 4.14(a) and Fig. 4.14(c)). The total amplitude would be approximately 20 % lower that the original one.

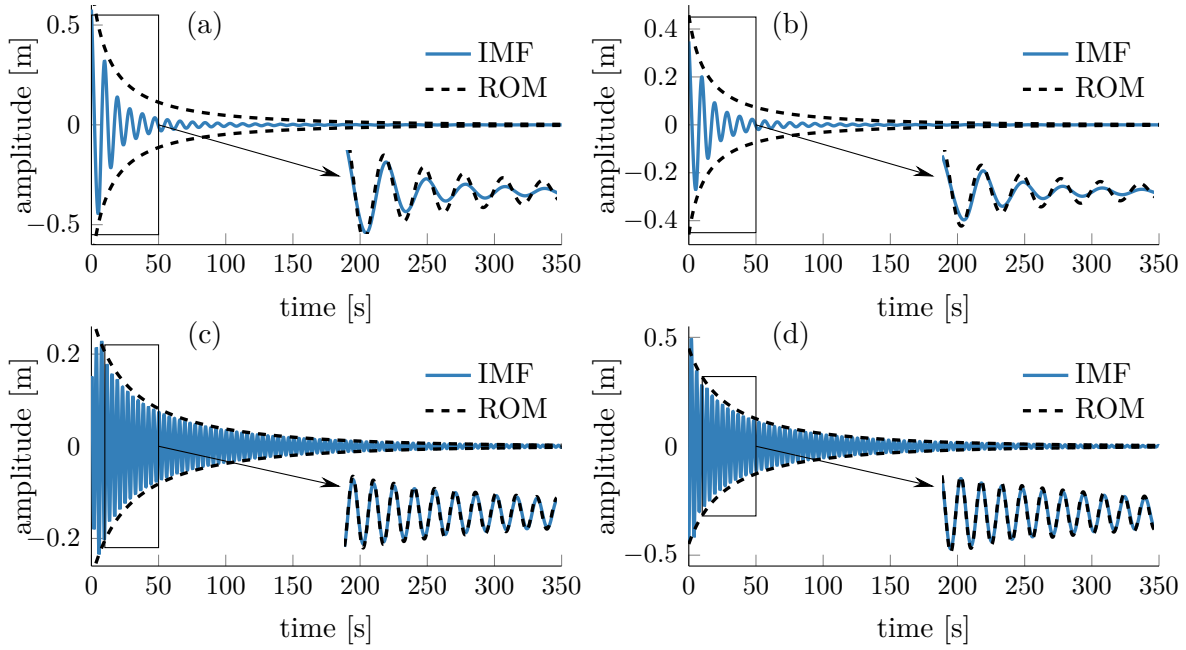

Figure 4.14 Comparison of the IMFs and ROM for the system with quadratic damping: (a) first mode, mass 1, (b) first mode, mass 2, (c) second mode, mass 1, and (d) second mode, mass 2

For the same initial conditions, the ROM has been computed and the results are shown in Fig. 4.14 as well. As can be seen, the match of the ROM and IMFs is very good, apart from the beginning, for the second mode (Fig. 4.14(c) and Fig. 4.14(d)) where both amplitude and frequency match to each other. On the other hand, the match of amplitudes is not so good for the first mode (Fig. 4.14(a) and Fig. 4.14(b)) where the amplitude of the IMFs seems to be decreasing more rapidly at the beginning of the time interval. This is probably caused by the numerical problems in the EMD which has not been able to recover the beginning of the original signal correctly. This is particularly visible in Fig. 4.14(c) where the end-effects of the EMD caused the amplitude of the first period to be lower than the second one. In spite of the difference in the amplitude, the frequency of the ROM matches the IMF very well. Although the match of the IMFs and ROM is not exact for the first mode, this system again demonstrates that the relation between the HHT and CNM approximately holds even for non-linear damping.

4.4.3 A cantilever beam with geometric non-linearity

For the last demonstration, a numerical model of a cantilever beam is used. This model is based on the ECL benchmark, which was originally designed for the comparison of

non-linear system identification methods [119, 261] and has been intensively used ever since, e.g. for numerical [190] and experimental demonstration of NNMs [191]. The ECL benchmark consists of a long cantilever beam with a geometric non-linearity introduced by a much thinner beam at one end (see chapter 5 for details).

The finite element (FE) model of the beam is graphically represented in Fig. 4.15. The main beam was discretised by 10 Euler-Bernoulli beam elements and the effect of

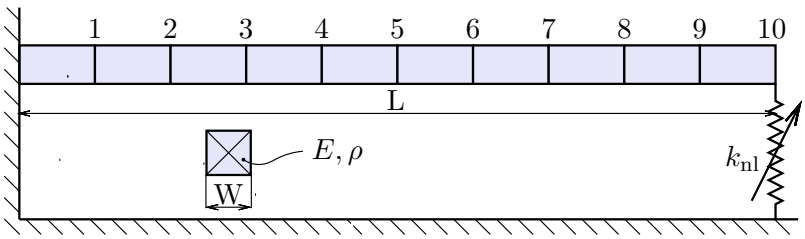

Figure 4.15 A model of the cantilever beam with geometric non-linearity

the thin beam was introduced by the cubic hardening spring at the tip of the main beam. The geometrical and mechanical properties of the beam were $L = 0.7\,\mathrm{m}$, $W = 0.014\,\mathrm{m}$, $E = 2.1 \times 10^{11}\,\mathrm{Pa}$, $\rho = 7800\,\mathrm{kg\,m^{-3}}$ and the system is allowed to vibration in the vertical direction.

The system can be modelled based on the FE model using Eq. (4.1), in which the mass $\mathbf{M}$ and stiffness $\mathbf{K}$ were assembled by a standard FE procedure using beam elements (the vector $\mathbf{x}$ consists of displacements and rotations). Unlike in the previous cases, the linear viscous damping was introduced using Rayleigh's proportional damping model, i.e. $\mathbf{C} = \alpha\mathbf{M} + \beta\mathbf{K}$, with $\alpha = 2$ and $\beta = 1 \times 10^{-8}$. The vector of non-linear restoring forces consists of a single non-zero element corresponding to the displacement DOF of node 10 with the chosen cubic hardening stiffness coefficient $k_{\mathrm{nl}} = 1 \times 10^{8}\,\mathrm{N\,m^{-3}}$.

The computed backbones, normalised mode shapes and a set of frequency response functions can be seen in Fig. 4.16. Three harmonics were again used in both non-linear modal analysis and harmonic balance method since the convergence analysis indicated that this number was sufficient. It can be seen that both displayed modes are non-linear, exhibiting the hardening behaviour. The backbones pass correctly the peaks of the FRFs and the computed damping (not shown) is not amplitude-dependent. The first and second mode shapes, which are normalised so that the amplitude of node 10 is equal to 1 or -1, respectively, are depicted in Fig. 4.16(c) and Fig. 4.16(d), respectively. It can be seen that both mode shape change with the increasing amplitude. However, the change is not so dramatic as in the simpler systems that were previously studied. These results

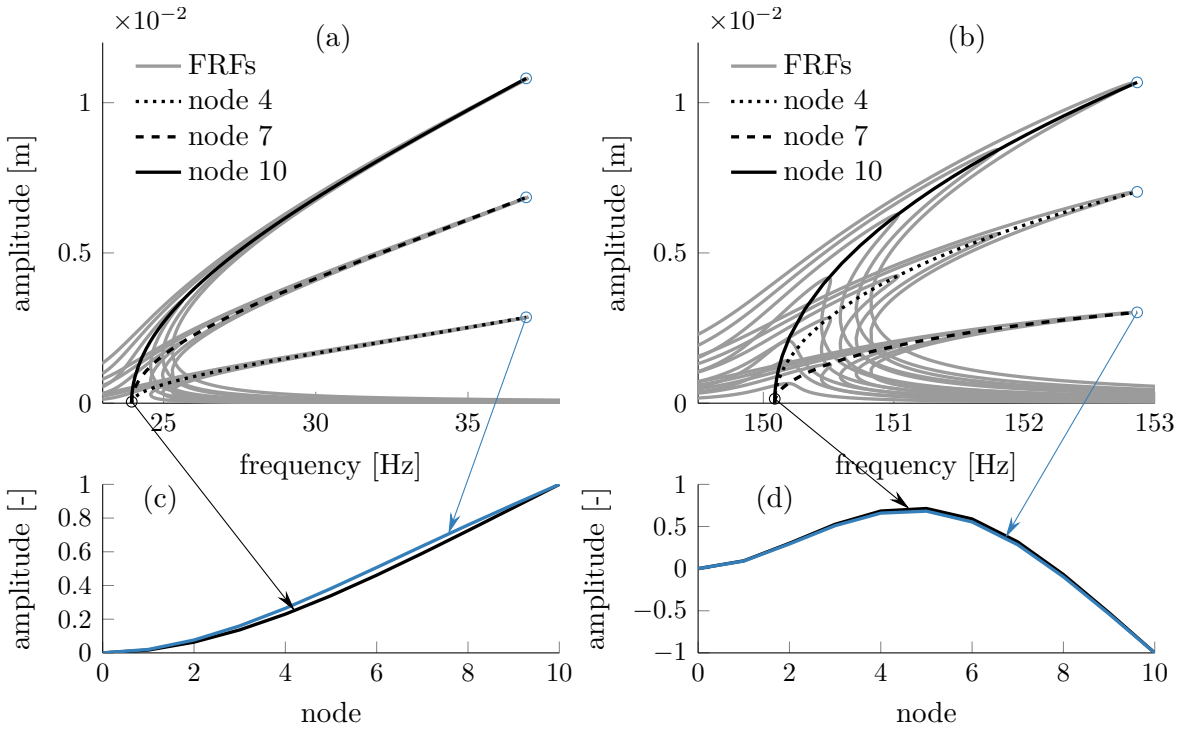

Figure 4.16 The cantilever beam with geometric non-linearity: (a) computed backbones and frequency response functions of the first mode, (b) computed backbones and frequency response functions of the second mode, (c) the first mode shape, and (d) the second mode shape

are consistent with the computational studies of the ECL benchmark using NNMs in [189, 190, 192] and will be also obtained experimentally in chapter 5.4.

Resonant decay response

The computed resonant decay responses can be seen in Fig. 4.17. The initial conditions

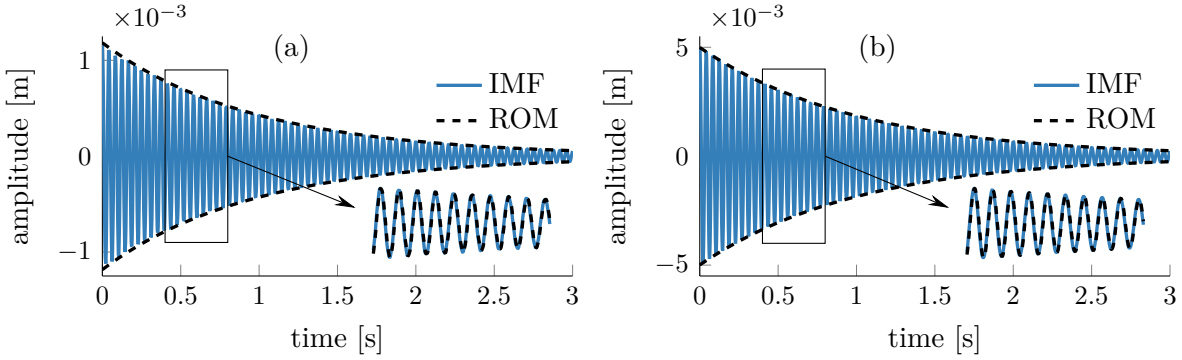

Figure 4.17 Resonant decay response of the first mode: (a) displacement of node 4 and (b) displacement of node 10

have been set in such a way that the beam was released from the first bending mode with the displacement of node 10 equal to $x_{10}(0) = 0.005\,\mathrm{m}$. The responses do not consists of several frequency components and they can therefore be considered as the IMFs without using the EMD.

For the same initial conditions, the ROM of slow-flow dynamics had been computed using the CNMs and added to Fig. 4.17. As expected, the match between the IMFs and ROM response is extremely good. Since the time-domain results are practically identical, the estimated IF and IA would also correspond very closely.

Figure 4.17 again evidences that the HHT relates to the CNMs through the ROM of slow-flow dynamics in case of the excitation which is very close to a single non-linear mode.

Free decay response for general initial conditions

The response of the system was simulated for the initial displacement of the tip of the beam $x_{10}(0) = 0.1\,\mathrm{m}$ and the free decays obtained can be seen in Fig. 4.18. The results

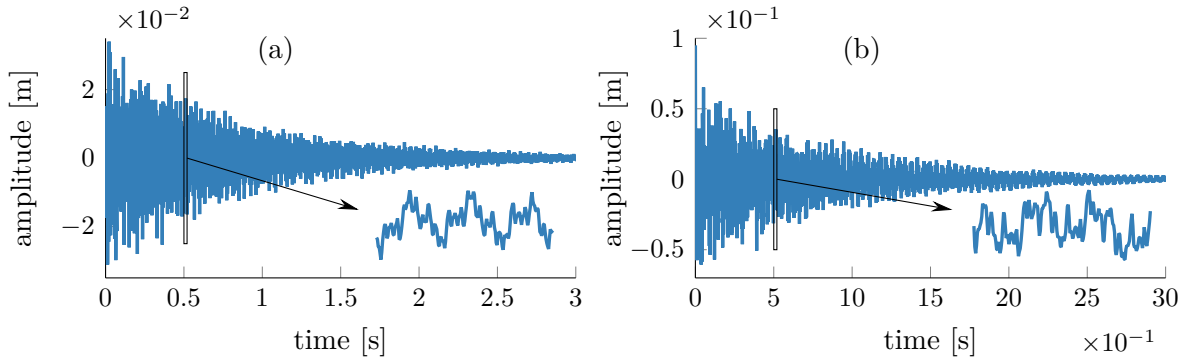

Figure 4.18 Free decay responses of the cantilever beam with geometric non-linearity: (a) node 4, (b) node 10

are herein presented for the vertical displacements of two nodes - node no. 4, which is close to the middle of the beam, and node no. 10, which is at the tip of the beam and to which the non-linear spring is attached. As can be seen, both responses exhibit multiple modes, thereby preventing direct estimation of the IF and IA.

After the application of the EMD, several IMFs have been obtained. In Fig. 4.19, only the last two IMFs, which correspond to the first and second mode, are shown. Because these two IMFs are the last ones that were extracted using the EMD (excluding the final trend), the quality of them is not so high as in the previous cases. A noisy appearance is caused by the imperfections in the shifting process. It will be observed in chapter 5 that the EMD performs much better for experimental data. The reason is that when

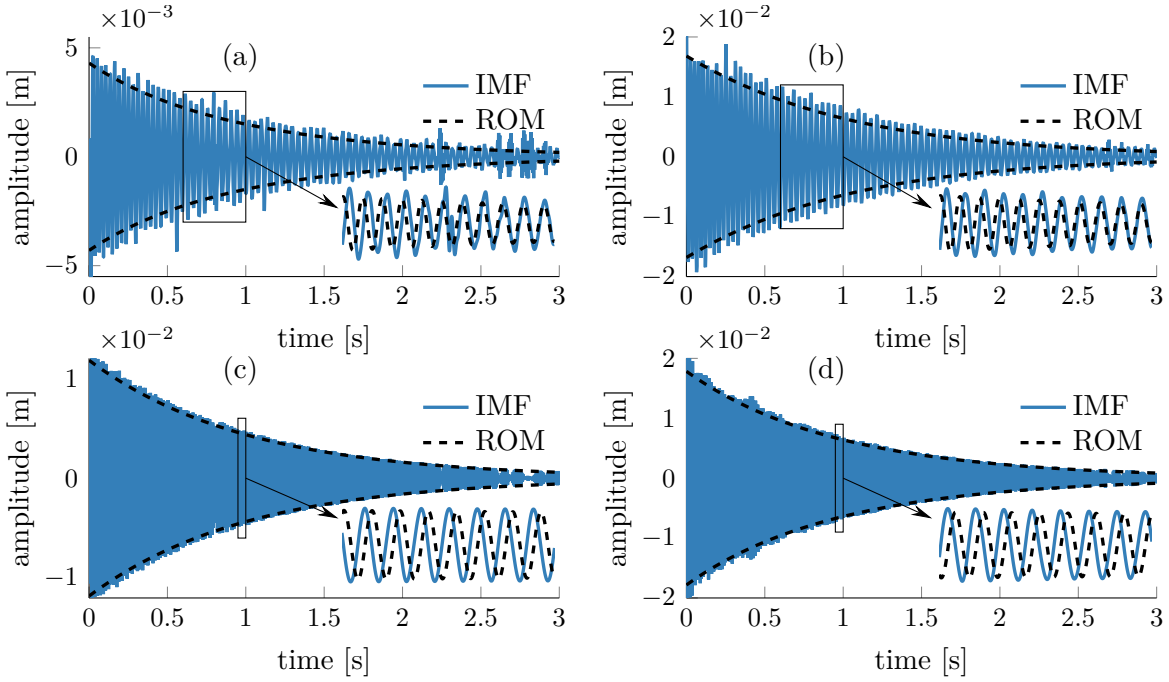

Figure 4.19 Comparison of the IMFs and ROM for the cantilever beam with geometric non-linearity: (a) first mode, node 4, (b) first mode, node 10, (c) second mode, node 4, and (d) second mode, node 10

computing free decay by setting initial conditions instead of applying a short time impact, all structural modes are excited and must therefore be separated from the data. On the other hand, if real impulse excitation is applied, only a first few modes are excited, allowing the EMD to perform better. Nevertheless, it is clear that the IMFs in Fig. 4.19 are not multi-component signals any more and that they vibrate with different time scales.

For the same initial conditions, the ROM has been computed and is shown in Fig. 4.19 as well. Although the match of IMFs and ROM is not so good as in the previous cases, the amplitudes seem to match quite well. The local discrepancies in the amplitudes are believed to be mainly caused by the imperfections of the EMD. The match in terms of frequency is acceptable as well. However, some small differences can still be observed, indicating slightly higher frequency of the IMFs.

To further investigate the difference between the ROM and IMFs in this case, the IF and IA are estimated using the ZC method. The results are plotted in the Hilbert spectrum (time-frequency-amplitude maps [102]) in Fig. 4.20. The Hilbert spectrum of the first mode (Fig. 4.20(a)) shows that the estimated IF is indeed higher than the frequency predicted by the ROM at the beginning of the signal. The difference is

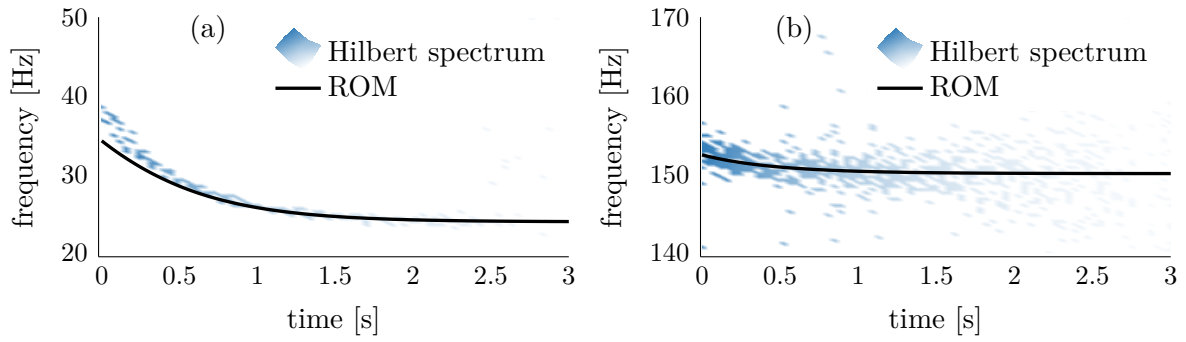

Figure 4.20 The Hilbert spectrum of the cantilever beam with geometric non-linearity: (a) the first mode (b) the second mode

approximately 10 %, which is quite significant. On the other hand, the frequency of the second mode predicted by the ROM fits the IF very well. It can be seen that the second mode does not display such a strong non-linear behaviour. The Hilbert spectrum is not so clear, especially for the lower amplitudes. This is believed to be caused by the numerical imperfections in the EMD.

A reasonably good match between the response of the ROM and IMFs in Fig. 4.19 and the frequency predicted by the ROM and the estimated IF in Fig. 4.20 further supports the assertion that the HHT relates to the CNMs at least approximately. Using this case, it was possible to show that the relation holds even in case when many modes must be extracted from the data before reaching the modes of interest.

4.5 Discussion

The objective of the chapter was to support the assertion that the relation between the Hilbert-Huang transform (HHT) and complex non-linear modes (CNMs) exists. The investigation was conducted in preparation for the use of the HHT and CNMs for non-linear system identification. It was suggested that this relation should approximately hold based on the similarities of the methods involved. The link among the methods has been established by the reduced order model (ROM) of slow-flow dynamics and supported by a variety of numerical cases and parametric studies in section 4.4. Unfortunately, it was found that this link holds only approximately, which will limit the capability of the identification method introduced in chapter 5.

A similar relation was already utilised in a number of papers [155, 164, 181] where the HHT was used for non-linear system identification in a non-linear normal mode (NNM) framework. However, no validation that the HHT relates to the NNMs was given. It

was only intuitively assumed that the IMFs should compose some approximation of the responses of individual NNMs. Subsequently, the estimated IF and IA should correspond to the computed backbones. However, the NNMs are not defined for the conservative system, so their use for non-linear system identification of dissipative systems might be sometimes complicated, at least ideologically. For these reasons, the use of CNMs appears to be preferable - not only the relation between the HHT and CNMs has been shown in this chapter in terms of IMFs and ROM, but the applicability to non-conservative systems can be guaranteed.

The HHT does not have a rigid mathematical background, but the physics-based foundation was already established [118, 138]. This was achieved by showing the correspondence of the IMFs and slow-flow dynamics derived by the CxA. This relation has been used throughout this study to further support the assertion of the HHT-CNM relation. Unfortunately, the CxA is an analytical method and its applicability is therefore limited to small academic systems with simple non-linearities. In contrast, the CNMs can be numerically computed for large industrial structures with complex non-linearities [127, 129, 134, 135]. Therefore, effectively replacing the CxA with the CNMs may extend the applicability to a broader range of non-linear systems with complex non-linearities. This means that the gap between the academic studies and industrial application has been slightly reduced.

In full accordance with the fundamental restriction of the ROM, i.e. it does not take into account more than one mode which automatically excludes any modal interactions, the response is predicted accurately in the close proximity of a non-linear mode. This accuracy was shown for the resonant decay responses in [128] and in section 4.2. In addition, the accuracy was demonstrated for near resonance forcing, provided by a slow sweep excitation, in [128] and in section 4.2 as well. These cases are trivial from the point of view of the presented topic, because the EMD, a key and unique concept of the HHT, does not have to be applied.

In [118, 137, 138], it was concluded that the CxA led to the satisfactory approximation of the response. A similar degree of approximation has been observed for the ROM derived by the CNMs in this chapter. The approximation of the total response was already theorised in [128] where it was stated that by simply superimposing the ROM responses of several modes, the total response could be obtained. However, this theoretical claim was not further investigated in [128]. Although this chapter did not target this in particular detail, it partly addressed this issue too. It has been found that the response of the ROM approximates the IMFs and since the superposition of the IMFs always gives the total response (guaranteed by Eq. (3.10)), it follows that also the superposition of the ROM

responses leads to the total response. Therefore, the theoretical claim from [128] is partly validated. The total response, however, is not obtained exactly, but only approximately. This is also in line with [200] which showed that the concept of invariant manifold also approximatively leads to the total response. Since CNMs trace trajectories on the manifolds, their superposition should also lead to a good approximation of the total response.

Strictly speaking, the relation between the HHT and CNMs must be considered as an approximation. It was shown that even for noise-free decay, the match of the ROM response and IMFs is not exact. Furthermore, since the HHT is used for the processing of experimental data, the errors originating in experimental setting imperfections, measured noise, and data processing uncertainty might further increase the margin of this approximation. Therefore, it cannot be concluded that the CNMs provides mathematical framework for the empirical HHT.

The range of validity and applicability of the relation between the HHT and CNMs is given by the limitations of the methods involved. Several important limitations are introduced by the HHT, especially by the EMD. The most concerning one is the mode mixing problem described in section 3.2.2. However, it was shown in section 3.2.3 that by applying a simple procedure, the frequency splitting capabilities can be investigated before applying the EMD. This has been demonstrated in the second parametric study where the region in which the EMD can accidentally extract spurious IMFs was not identified. The mode mixing may also be overcome by increasing the number of shifting iterations [103] or by applying some of the advanced EMD schemes [45, 50, 137, 292] as described in chapter 3.

One more problem associated with the HHT can be troublesome in practical situations. The EMD yields, by definition, symmetric IMFs so when applied to systems with asymmetric restoring forces it can lead to physically incorrect conclusions. Moreover, even if the resonant decay response of a system with asymmetric non-linearity is measured, the Hilbert transform or any of its alternatives from section 3.3 cannot estimate the forces correctly (the Freevib algorithm cannot be used in a presence of asymmetric restoring forces [67]). The analysis of the systems with asymmetric non-linearities, including gaps, pre-stress effects and piece-wise linear stiffness, has just recently been allowed by the Hilbert vibration decomposition (HVD) [73]. However, the HVD is difficult to used due to a number of sophisticated signal processing techniques needed. A new method which is based on the zero-crossing, is proposed in chapter 6. The developed method as well as the HVD provide equivalent results which characterise the non-linear behaviour in terms of congruent functions, also called pseudo-backbones and pseudo-damping in chapter 6.

Whether or not the congruent functions relate to the CNMs is not clear because the congruent functions, which are a direct consequence of the selected signal processing [72], cannot be analytically or numerically computed.

A key limitation given by the ROM derived from the CNMs is its incapability to deal with internal resonances. Therefore, internal resonances have been excluded from the consideration in this thesis. It can be, however, stated that the relation of the HHT and CNMs is not guaranteed in the presence of internal resonances, because the key link cannot be found. It is quite possible, that this limitation of the ROM will be removed in the future. The concepts of the CNMs and associated ROM have just recently been developed and are still establishing their place in the field of non-linear dynamics. It has been already suggested that the future development of the ROM should address the cases where modal interactions do exist [128]. When and if such extended ROM is developed, it is possible that the accuracy and a range of applicability of the argued relation between the HHT and CNMs will extend too. It can be only hypothesised that the ROM which includes several non-linear modes would lead to the IMFs exactly.

However, even if the ROM could describe the internal resonances, it is unclear how the HHT should be used to study them. Due to its definition, the HHT cannot extract dependencies between the IMFs (the IMFs are practically orthogonal to each other). Therefore, it is likely that the internal resonances cannot be studied by the traditional HHT at all. However, an extension of the HHT, called the Holo-Hilbert spectral analysis (HHSA) method [100], has been recently proposed. Theoretically, it should allow to recover cross-scale coupling between the IMFs so it may perhaps be possible to study internal resonances using this method. It has never been applied in structural dynamics so its practical feasibility is yet to be determined.

In spite of the described limitations, the established relation theoretically means that the ROM could be directly computed from the measured mass-normalised non-linear modes of the system. Although this possibility has not been further investigated in this thesis, it means that the non-linearity would not have to be quantified or even characterised because it is not explicitly used in the ROM. On the other hand, it would require to estimate the mass normalised non-linear modes (see Eq. (4.6)). However, the mass normalisation is not generally possible to achieve from the experimental data as discussed in chapter 5.

It should be also noted that the relation between the HHT and vibration modes is exact for linear systems so the HHT can be also used for linear modal analysis as in [295, 296]. However, since the system is linear, it is better to use other techniques for linear modal analysis, thereby avoiding potential numerical imperfections of the HHT.

For non-linear systems, the relation between the HHT and CNMs provides a theoretical base for non-linear experimental modal analysis proposed in chapter 5. However, the proposed method would work well for the cases where the relation of the HHT and CNMs is exact, i.e. for resonant free decays and nearly resonant forcing. The accuracy of the proposed method will be limited for general initial conditions, because the relation found in this chapter is only approximative.

4.6 Conclusion

The objective of this chapter has been to demonstrate that the Hilbert-Huang transform (HHT) relates to complex non-linear modes (CNMs) of mechanical systems. This has been achieved by studying a relation between the intrinsic mode functions (IMFs) and reduced order model (ROM). It was discussed that the relation is supported by a number of similarities between the methods and it has been highlighted using a range of numerical studies. This relation paves the way for using the HHT for non-linear system identification in a non-linear modal analysis framework. Such non-linear system identification method would be based on a direct decomposition of measured data, thereby requiring no a priori detection or characterisation of non-linearity. In addition, it would be very similar to the well-established experimental modal analysis for linear systems in terms of excitation and expected results. This non-linear system identification method is proposed in the next chapter.

Chapter 5

Non-linear system identification using the Hilbert-Huang transform and non-linear modes

Abstract

In this chapter an approach to experimental non-linear modal analysis is introduced. It builds on the approximative relation between the Hilbert-Huang transform (HHT) and complex non-linear modes (CNMs). Firstly, the non-linearity in the system is detected and characterised using the HHT and then the quantification is performed via the optimisation in terms of CNMs. The accuracy of the quantification is limited by the approximative relation between the HHT and CNMs. The introduced method is applied to several numerical test cases and demonstrated on the experimental data obtained from the ECL benchmark. The limitations and applicability of the method are discussed at the end of the chapter.

5.1 Introduction

In non-linear system identification, the Hilbert-Huang transform usually serves as a means of detecting and characterising a structural non-linearity. The quantification of non-linearity can be performed as well, but it was not entirely clear how to use the instantaneous frequency (IF) and instantaneous amplitude (IA) to obtain the parameters of a selected structural model or what the model should be. Several ways of quantifying non-linear behaviour using the HHT can be found in literature.

Firstly, the quantification can be performed by fitting the analytical expression [181, 184, 185] which has been previously found for the given system using the perturbation analysis [158]. This is limited to SDOF systems with polynomial non-linearities and works well under the assumption of weak non-linearities. The analytical solution is not accurate for stronger non-linear behaviour as already evidenced in section 3.3 where the analytical solution obtained using Eq. (3.24) did not match to the estimated backbones of the Duffing oscillator or numerically computed non-linear modes. In order to find the analytical expression for MDOF systems, it must be assumed that an IMF represents a single vibrational system which can be represented by an independent SDOF equation of motion whose analytical solution can be found. This independent equation of motion does not have a relation to the original equations of motion, which describes a MDOF system, so it does not enable the quantification of non-linear coefficients in the physical space.

A similar assumption, i.e. an IMF corresponds to a single mode of vibration, has also been utilised in [39, 62, 137] where a method, called a time domain non-linear system identification based on multi-scale dynamic partitions, was proposed. Instead of quantifying the non-linearities, the dynamics of the system is represented through reduced order modes, termed intrinsic modal oscillators (IMOs). The IMOs are defined as the equivalent linear oscillators that can reproduce a given time series over different time scales and whose forcing terms are derived directly from the experimental measurements. The forcing terms of the IMOs can also include information about other vibration modes so it is possible to use IMOs for the computation of internal resonances.

The two previous approaches to the quantification (analytical expression and IMOs) cannot quantify the physical coefficients of non-linearity for MDOF systems. Instead, they attempt to create equivalent models that can reproduce the motion for a given time scale and measured location. The physical coefficients of non-linearities, which can be found in the original equations of motion, can be identified through the complexification-averaging (CxA) as presented in [118] by direct fitting of the operator $\mathbf{F}$ from Eq. (4.17). However, as pointed out in section 4.2.3 the operator is cumbersome even for small

systems so it is not applicable for more complex structures and non-linearities. In [189, 191], it was shown that the IF and IA estimated from a resonant decay response by the wavelet transform correspond to the non-linear normal mode. Therefore, it is theoretically possible to identify the parameters of the system by matching the estimated IF and IA with the NNMs. A similar idea, which can be used to identify the coefficients of non-linearities of the original equations of motion, also motivated this chapter.

It should be noted that the contents of this chapter had been developed before the detailed analysis of the relation between the HHT and CNMs studied in chapter 4. Since the relation had not been investigated and its approximative nature had been unknown, the original idea that led to this chapter was to use the Hilbert-Huang transform in conjunction with the complex non-linear modes to detect, characterise and quantify the non-linearity. The quantification would be performed by matching the CNMs and the estimated backbones and damping curves. Unfortunately, since it was later found in chapter 4 that the complex non-linear modes do not correspond to the IMFs exactly, the accuracy of the quantification is very pure for transient data. Therefore, the proposed method can, for general data, only detect and characterise non-linearities. However, it allows accurate quantification only for resonant decay responses. Despite the fact that the attempt to develop a general approach to the experimental non-linear modal analysis has not been successful, the method offers the possibility to quantify the coefficients of the original equation of motion with potentially damping non-linearities.

This chapter is organised as follows: the proposed non-linear system identification method using the Hilbert-Huang transform is described. Then, it is applied to some of the numerical cases used in chapter 4 where it is shown that the accuracy of the quantified parameters is not high for general free decays, but very high for the resonant decay responses. In section 5.4 the described method is applied to the experimental data obtained from the ECL benchmark where three non-linear modes are recovered for a free decay response. At the end of the chapter, the advantages of limitations of the suggested approach to experimental non-linear modal analysis using the HHT and CNM are discussed.

5.2 Towards experimental non-linear modal analysis

The method described in this chapter combines the Hilbert-Huang transform (HHT) and the complex non-linear modes (CNMs). A structural non-linearity is firstly detected and characterised using the HHT and subsequently the coefficients of the selected model are

quantified by the optimisation in terms of the CNMs. The proposed method can be summarised in the following steps:

1. Measured (or simulated) data of a particular form (section 5.2.1)
2. The Hilbert-Huang transform (chapter 3)
   (a) Empirical mode decomposition (section 3.2)
   (b) Instantaneous amplitude and frequency estimation (section 3.3)
3. Extraction of non-linear modes (section 5.2.2)
4. Detection (section 5.2.3) and characterisation (section 5.2.4) of non-linearity
5. Model selection (section 5.2.5)
6. Optimisation of the selected model based on the CNMs by a weighted global criterion method (section 5.2.6)

The outlined method works for the systems with localised or geometrical non-linearities with symmetric restoring forces. The method works only in presence of no mode interaction and for well separated modes since it is subjected to the frequency resolution capabilities of the EMD. It must be emphasised that the accuracy of the quantification is significantly limited by the relation between the HHT and CNMs described in chapter 4.

5.2.1 Experimental data requirements

A specific and well controlled experimental measurements must be usually used for dynamic testing based on non-linear modes. Each type of excitation leads to a different data type. The data types suitable for the presented methods are:

- Resonant decay response - since this response consists of a single mode of vibration, it is expected that the proposed non-linear system identification method will work very well for this type of data. The excitation force history or initial conditions do not have to be explicitly recorded. Experimentally, the resonant decay response can be obtained using the sophisticated phase resonance testing [59, 190, 191, 291] described in section 1.3.3. The requirements for the experimental set-up, acquisition hardware and control software are high.
- Free decay - unlike the resonant decay response, a free decay consists of several vibration modes. Therefore, the EMD must be used to decompose it into intrinsic

mode functions before the IF and IA can be estimated. It was shown in chapter 4 that the obtained IMFs correspond only approximately to the response of the ROM derived from the CNMs. Hence, the IF and IA estimated from the IMFs only approximately match to the CNMs. Since it was observed that the match is not exact, it is expected that, although the described method would be able to detect and characterise non-linear behaviour correctly, it would fail to quantify it accurately. Experimentally, acquisition of free decays is very quick compared to any other excitation types. A simple hammer impact excitation [63] can be used so no sophisticated experimental set-up is needed. On the other hand, it might be difficult to excite the non-linearity adequately [289] by this excitation. The excitation force history or initial conditions do not have to be explicitly recorded.

- Slow-sweep harmonic response - in this case, the EMD does not have to be applied since the slow-sweep excitation produces mono-component responses. However, some additional data processing is needed to estimate the modal characteristics property. The Forcevib [68, 71], which takes into account the excitation force, must be performed. Therefore, the excitation force history must be recorded. This type of data is not considered in this chapter any further.

It should be noted, that the steady-state excitation, often used for the testing of non-linear systems using frequency response functions (FRFs), is not suitable. Similarly, the random excitation does not provide vibration data appropriate for the introduced method.

Regardless of the excitation type, care should be taken to minimise the amount of measured noise as much as possible. In addition, the sampling frequency must be relatively high since the HHT is used. It is recommended in [71] to use the sampling frequency 20 to 80 times higher than the highest frequency of interest.

5.2.2 Non-linear modes extraction

The instantaneous frequency (IF) and amplitude (IA) are extracted by means of the Hilbert-Huang transform as described in chapter 3. The extraction of vibration characteristics, which approximately relate to complex non-linear modes as shown in chapter 4, is similar to [10] in which the wavelet transform was used instead of the HHT and to [295, 296] where the HHT was utilised for the linear modal analysis. To comply with the CNMs definition, the IF and IA should be as smooth as possible so the ZC method described in section 3.3.6 is preferable and additional smoothing, either by a conventional low-pass filter or Whittaker smoother (see appendix C), can be also recommended. It is also necessary to note that the IF and IA should be known for all sampled time points

of the original signal. Therefore, if the ZC method, which estimates the IF and IA in the discrete zero-crossing points, has been used, the IF and IA must be fitted either by polynomials or splines.

The instantaneous frequency $\omega(t) = \omega_m^k(t) = 2\pi f_m^k(t)$ and amplitude $a(t) = a_m^k(t)$ of the m-th vibrational mode measured in k-th location, are used to compute the natural frequency using the Freevib algorithm [67, 68] as

$$\omega_0(t)^2 = \omega(t)^2 - \frac{\ddot{a}(t)}{a(t)} + \frac{2\dot{a}(t)^2}{a(t)^2} + \frac{\dot{a}(t)\dot{\omega}(t)}{a(t)\omega(t)}. \tag{5.1}$$

Often, it is possible to neglect the second-order terms and higher derivatives [71], so the natural frequency is well approximated by the measured IF, i.e. $\omega_0(t) \approx \omega(t)$.

The viscous damping rate $\delta(t) = \delta_m^k(t)$ of the m-th mode measured in k-th location can be also evaluated based on the Freevib algorithm as

$$\delta(t) = -\frac{\dot{a}(t)}{a(t)} - \frac{\dot{\omega}(t)}{2\omega(t)}. \tag{5.2}$$

However, it was seen in chapter 3 that the damping estimation in this way can be sometimes quite inaccurate even for the Duffing oscillator due to the need to evaluate the derivatives of the amplitude and frequency. Therefore, it can be sometimes better to assess the linear viscous damping by examining the logarithmic value of the amplitude

$$d_m^k(t) = \log(a_m^k(t)). \tag{5.3}$$

It is well known that $d_m^k(t)$ is a straight line when the system is linear so the factor $d_m^k(t)$ indicates the deviation from the linear damping.

The fundamental amplitude of the m-th mode shape $|\phi_m^k(t)|$ measured in k-th location can be determined from the instantaneous amplitude as

$$|\phi_m^k(t)| = \frac{a_m^k(t)}{a_m^{k_0}(t)} \tag{5.4}$$

where k_0 is the index of the selected location. The difference between the phase angle of two modal elements $\phi_m^k(t)$ and $\phi_m^{k+1}(t)$ can be determined from

$$\angle\phi_m^k(t) = \theta_m^k(t) - \theta_m^{k+1}(t), \tag{5.5}$$

where $\theta(t)$ is the instantaneous phase defined by Eq. (3.31). The investigation of the phase does not always have to be conducted since the non-linear modes are the continuation of the linear modes so the approximate phases can be taken from the linear modal analysis.

Both absolute values and phase angles of all modal elements relative to the selected element can be determined and the mode shapes vector $\boldsymbol{\phi}_m = [\phi_m^1, \phi_m^2, \ldots, \phi_m^k]^{\mathrm{T}}$ assembled. It must be emphasised that the estimated modes shapes $\boldsymbol{\phi}_m$ are not entirely the same as the modes shapes defined by Eq. (4.2). Firstly, the difference is that only the fundamental amplitude of the mode shape is captured in $\boldsymbol{\phi}_m$ and secondly, the estimated modes are normalised with respect to the selected coordinate k_0 instead of the mass matrix. Unfortunately, it is not possible to correctly enforce the mass normalisation according to Eq. (4.6) because the mass matrix is generally unknown. Even if it was known, not only the values of the modes shapes in Eq. (4.6) but also the modal amplitude q in Eq. (4.2) would need to be adjusted to obtain a correct set of mass normalised non-linear modes.

Eventually, for m-th mode and k-th measured location, the frequency ω_m^k, damping δ_m^k and mode shape $\boldsymbol{\phi}_m$ are identified. This set of modal properties is then used for detection, characterisation and quantification of non-linearities.

It would be also possible to compute the non-linear elastic $\mathrm{F}_{\mathrm{el},m}^k = \mathrm{F}_{\mathrm{el}}$ and dissipative $\mathrm{F}_{\mathrm{d},m}^k = \mathrm{F}_{\mathrm{d}}$ restoring forces using the Freevib algorithm as

$$\mathrm{F}_{\mathrm{el}} = \begin{cases} \omega_0^2 a, & x(t) \geq 0 \\ -\omega_0^2 a, & x(t) < 0 \end{cases} \qquad \mathrm{F}_{\mathrm{d}} = \begin{cases} 2\delta a_{\dot{x}}, & \dot{x}(t) \geq 0 \\ -2\delta a_{\dot{x}}, & \dot{x}(t) < 0, \end{cases} \tag{5.6}$$

respectively, where $a_{\dot{x}}$ is the instantaneous amplitude estimated from the velocity signal. However, these restoring forces are not directly related to the original restoring force in the equation of motion. Therefore, they cannot serve for the quantification, although they can still be used for the detection and characterisation.

5.2.3 Detection

At this stage, the Hilbert-Huang transform has been applied to the measured data as described in chapter 3 and the non-linear modes extracted. It is assumed that all processing problems, such as mode mixing and end-effects, have been effectively avoided or reduced so the extracted non-linear modes are not significantly influenced.

Several simple visual ways to detect non-linearity can be used.

- The basic feature of the linear modal analysis is that the modal properties are amplitude independent. Therefore, any significant amplitude dependency of the

backbones or damping curves is a consequence of non-linearity. The visualisation of modal properties as a function of the vibration amplitude is sometimes called a linearity plot [82].

- The presence of the intra-wave modulation frequency, which must be smoothed to obtained required form of the non-linear modes, is a direct consequence of non-linearity as discussed in section 3.4. Therefore, it can be used to detect non-linearity prior to the extraction of the mode shapes.

- Alternatively, the non-linear restoring forces may be examined. If the force characteristics are not linearly dependent on the vibration amplitude, the system is non-linear.

- When the energy operators [229] described in section 3.3.5 are used, the extracted IF does not make any sense when the system is non-linear [104]. However, the application of this detection method can be somewhat complicated, because it is unclear how different the estimated IF and IA should be.

- The damping estimation using Eq. (5.2) can be often inaccurate as shown in chapter 3. Therefore, it is often better to assess the damping using the logarithmic value in Eq. (5.3). The factor d_m^k is linearly dependent on the amplitude if the system is linear whist it deviates from the straight line for systems with non-linear dissipative effects.

As discussed in section 1.2.1 it may be sometimes beneficial to estimate to what extent the non-linearity influences the linear behaviour of the structure, i.e. to quantify whether the non-linearity is weak, moderate or strong. This can be achieved by the described detection approaches as well, simply by quantifying the difference between the measured characteristics and their linear counter-pairs. However, this is not further investigated in this thesis, because, as discussed in section 1.2.1, there is no universal way to quantify what weak, moderate or strong non-linearity mean. Such classification would need to be bound to a specific application in which strong non-linearities would, for example, lead to performance loss, whereas weak non-linearities would only shift the frequency of the maximum vibration amplitude.

5.2.4 Characterisation

Characterisation of the non-linearity which has been previously detected in the structure can be performed based on the extracted non-linear modes as well.

- Similarly to a typical shape of frequency response functions, the estimated backbones and damping curves have also their typical shapes determined by the type of non-linearity. The backbones and damping curves can be visually compared to typical shape or a decision making algorithm, similar to the one presented in chapter 2, could be designed. The backbones and damping curves for the same types of non-linearities whose FRFs are shown in Fig. 2.4 are shown in Fig. 5.1. This figure can

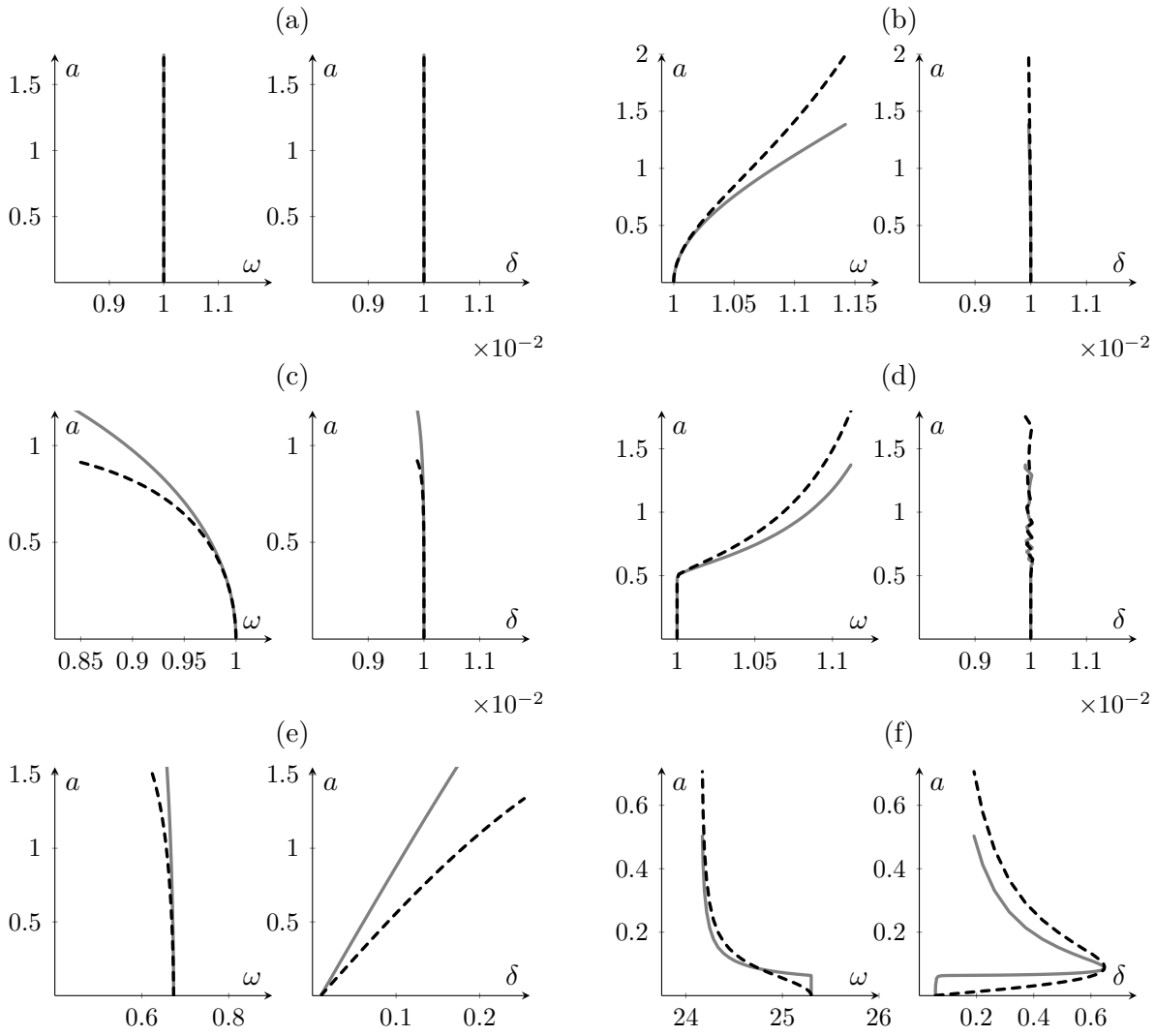

Figure 5.1 Backbones and damping curves for the first mode and mass 1 (gray) and mass 2 (black) of a two-degree-of-freedom system with: (a) no non-linearity, (b) cubic hardening stiffness, (c) cubic softening stiffness, (d) clearance, (e) quadratic damping, and (f) Coulomb friction

serve as a reference (sometimes called a footprint library [83]) for characterisation. The non-linear systems used to produce the figure were:

(a) the two-degree of freedom system described in section 4.4.1, but without non-linear stiffness or damping

(b) the two-degree of freedom system with cubic hardening stiffness described in section 4.4.1

(c) the two-degree of freedom system described in section 4.4.1, but the non-linear stiffness was negative $k_{\mathrm{nl}} = -0.5\,\mathrm{N\,m^{-3}}$ leading to the softening behaviour

(d) the two-degree of freedom system described in section 4.4.1, but the cubic stiffness was replaced by the clearance non-linearity defined by

$$f_{\mathrm{nl}} = \begin{cases} k_{\mathrm{nl}}x - k_{\mathrm{nl}}b, & x > b \\ 0, & |x| < b \\ k_{\mathrm{nl}}x + k_{\mathrm{nl}}b, & x < -b \end{cases}$$

where the coefficients were chosen as $b = 0.5\,\mathrm{m}$ and $k_{\mathrm{nl}} = 1\,\mathrm{N\,m^{-1}}$.

(e) the two-degree of freedom system with the quadratic damping described in section 4.4.2

(f) the two-degree of freedom system with Coulomb friction presented in appendix B

- An interesting way to characterise geometrical non-linearities was presented in [184], where, a unique ratio of fundamental and intra-wave frequency modulation was established based on the perturbation analysis. Subsequently, this ratio was used to determine whether the geometrical non-linearity is even or odd. The method for the estimation of this ratio was proposed in section 3.4 and its application demonstrated on two simulated examples.

- The shape of elastic or dissipative restoring forces can be used to characterise the non-linearity as well.

The characterisation of non-linearity is arguably the most difficult step in non-linear system identification since a wide range of structural non-linearities exists [119]. Despite the fact that the HHT does not require any a priori information about the type of non-linearity to obtain the backbones and damping curves, considerable experience is needed to characterise the non-linear behaviour correctly. Although no additional information about the structure is theoretically needed, having the engineering knowledge of the problem can significantly increase the likelihood of characterising the mechanism of non-linearity correctly. The care should be also taken to correctly determine if the deviation

of the backbones and damping curves from their linear counter-pairs are statistically significant. Sometimes, the non-linear appearance may be a consequence of experimental and processing errors, such as measured noise or end effects.

5.2.5 Model selection

At this stage, it is already known that a structural non-linearity is present in the system and its type has also been characterised. So far, the used methods could have been regarded as non-parametric, i.e. no model of the structure has been needed. However, for the quantification of non-linearity using non-linear modes the model must now be selected. There are several possible choices. The complexity of the selected model depends on its required application, the amount of information known about the structure, and the computational and software resources available for the quantification.

- A single-degree-of-freedom model can be used to describe one specific measured location and mode of interest. This is the simplest approach, which has been previous used in conjunction with the HHT in [10, 71]. Since the analytical expressions for the backbone and damping curve can be found for a SDOF with polynomial non-linearity, they can be fitted to the estimated backbones and damping curves and the model can be therefore quantified. However, this process does not consider the multi-degree of freedom nature of structures and it does not directly use any non-linear modes. On the other hand, the model obtained in this way is relatively simple, but should still be able to describe the vibration in the selected spatial location in a close proximity of the mode of interest. The range of applicability of this model would be similar to the IMOs used in [39, 62, 137], i.e. it should accurately represent the dynamics for each location and the mode of interest. On one hand, this is not very practical since the description of the structure as a whole is not available and the physical mechanism of non-linearity is not quantified. On the other hand, all computational studies on a set of such SDOF models are bound to be quick or even analytical.

- A simple multi-degree-of-freedom model which masses correspond to the measured locations. Such a model should be already able to capture the multi-mode nature of the vibration structure including the non-linear structural effects. No analytical expressions that would describe the backbones and damping curves can be found for such a model, thereby allowing no direct fitting of measured results. For this type of model, the quantification described in section 5.2.6 must be used. If successfully quantified, the model is able to provide much more information about the structure

than a simple SDOF model. This type of model can still be considered as a low-fidelity one because it is unlikely that it would be able to describe any local behaviour. The advantage of this model is that the important information about the dynamics can be obtained while the computational effort can be kept minimal. The size of the model is given by a number of measured locations.

- A full finite element (FE) model can be used as a means of high-fidelity modelling of the investigated structure. Clearly, this model is the most complex, thereby potentially requiring significant computational effort during the quantification and in subsequent analyses. Theoretically, the size of the model is only limited by the computational resources and the required application of the quantified model.

Regardless of the selected model type, the location and mathematical form of non-linearity must be specified. The presented method does not offer any possibility of locating the non-linearity within the structure. Therefore, the location must be determined based on the knowledge of the problem, its geometry and modelling possibilities. The selection of the mathematical form of non-linearity can be complicated as well. The mathematical form of non-linearity is often determined by its type. However, any closer indication as to what mathematical expression(s) should be used to model the characterised type is not readily available in the proposed method.

5.2.6 Quantification

This part of the proposed method is essentially a model updating technique. It is no longer non-parametric because the model of the structure with unknown parameters has to be selected. These parameters are now quantified using the complex non-linear modes. The non-linear modes can be estimated for all measured locations and (possibly) several vibration modes. It was found in chapter 4 that the backbones and damping curves approximately correspond to these modes. Therefore, in order to quantify the non-linear behaviour, these two sets of results must be matched by adjusting the linear and non-linear parameters of the selected model. The quantification can be done either manually by adjusting the parameters of the model until the required match is achieved, or the following optimisation procedure may be used instead.

If the estimated frequency and damping rate of the m-th mode measured in the location k are marked $\hat{\omega}_m^k$ and $\hat{\delta}_m^k$, respectively, and the corresponding computed modal properties as ω_m^k and δ_m^k, then a single objective function can be formulated as

$$G_m^k(\mathbf{u}) = \|\hat{\omega}_m^k - \omega_m^k(\mathbf{u})\| + \|\hat{\delta}_m^k - \delta_m^k(\mathbf{u})\|, \tag{5.7}$$

where $\|\cdot\|$ is the Euclidean norm, i.e. the distance between the two characteristics, and the vector $\mathbf{u}$ contains all structural parameters that are being sought. It may be beneficial to normalise the parameters in $\mathbf{u}$ by their nominal values (if known) in such a way that the rate of change of the objective function with respect to all parameters is approximately the same. Although the normalisation is not necessary, it may sometimes improve the performance of the optimisation algorithms. The suggested objective function cannot be negative and is (i) equal to zero if the measured and computed non-linear modes are exactly the same or (ii) positive for non-matching results. The progress and results of the optimisation can be graphically visualised by comparing the measured and optimised backbones, damping curves and potentially mode shapes.

Alternatively, the objective function could be assembled based on the reduced order model (ROM) and the IMFs as

$$G_m^k(\mathbf{u}) = \|c_m^k - x_m^k(\mathbf{u})\| \tag{5.8}$$

where $x_m^k(\mathbf{u})$ is the response of the ROM presented in section 4.2.2 which depends on the model parameters $\mathbf{u}$, and c_m^k is the corresponding IMF obtained by the EMD. A possible advantage of this objective function would be that it would remove the need to use the IF and IA methods. However, the computation of the ROM brings additional numerical difficulties and increases the computational burden. For these reasons, this objective function has not further been investigated in this thesis. Only the objective function given by Eq. (5.7) is used in the following.

A set of single objective functions

$$\mathbf{G}(\mathbf{u}) = \left[G_1^1(\mathbf{u}), G_2^1(\mathbf{u}), \ldots, G_m^1(\mathbf{u}), G_1^2(\mathbf{u}), \ldots, G_m^k(\mathbf{u})\right] \tag{5.9}$$

can be simultaneously minimised by a multi-objective optimisation method [11]. In the case of the proposed method, the optimisation is typically subjected to several linear and non-linear constrains. The range of parameters $\mathbf{u} \in [\mathbf{u}_{\min}, \mathbf{u}_{\max}]$ should be typically provided based on the physical understanding of the problem. It is important to note that this is not the multi-objective problem since one vector of unknowns $\mathbf{u}$ should optimise all objective functions to the level of numerical and experimental error. Theoretically, there should not be any conflict between the objective functions, so the parameters $\mathbf{u}$ that minimise one of the objective functions should also minimise the other individual objective functions. This is expected to hold quite well for the structural systems. However, it is still better to consider this problem as a multi-objective optimisation because it allows

one to take into account several modes and measured locations simultaneously. Therefore, the model that can adequately describe a full set of measured data can be obtained.

There are many methods for optimisation available in literature [11]. Since the objective functions are non-linear, it might be difficult to select one method which would work universally. In order to evaluate the objective function, the CNMs must be computed by the process described in appendix B which can be relatively time-consuming process. Therefore, it is ideal to use such optimisation methods which require a low number of evaluations of the objective function. The global weighted criterion method described in the following section offers extensive possibilities that can help to establish a good model of the structure while minimising the number of evaluations of the objective functions.

It should be also noted, that the manual adjustment of the coefficients might sometimes be better than any optimisation method due to several reasons. Firstly, the optimisation problem is non-linear so its solution cannot be guaranteed and optimisation procedure can diverge. Secondly, the shape of the objective function is not generally known so the optimisation can take a long time to reach or even approach the minimum. Lastly, due to the nature of the problem, several acceptable local minima can co-exist so the results must be always carefully assessed even if the optimisation converged.

Weighted global criterion method (WGC)

It is suggested to use the weighted global criterion method (WGC) [11] for the quantification of non-linearities. The WGC can optimise the functions in Eq. (5.7) separately as well as all at once with preferences. The WGC is a scalarisation method that combines all normalised objective functions to form a single objective function which is then minimised. The minimisation problem can be written as

$$\min_{\mathbf{u}} \left\{ \sum_m \sum_k \left[w_m^k \left(G_m^k(\mathbf{u}) - G_m^{ko} \right) \right]^p \right\}^{1/p}, \tag{5.10}$$

where the weights w_m^k reflect the preferences, p governs the physical interpretation of the optimisation problem, and G_m^{ko} are the minima of the single objective functions (also called utopia points [11]).

The WGC is very flexible in terms of user preferences and any optimisation engine can be used (local, global or genetic). If the utopia points G_m^{ko} are the same for each function (or lie in the range of required accuracy), the multi-objective optimisation does not have to be performed. Although it is not necessary, a full set of Pareto front points can be theoretically obtained by systemically varying the weights. Generally, the WGC

requires fewer objective function evaluations compared to genetic algorithms to obtain the Pareto front [11]. The global minimum may or may not be found depending on the used optimisation engine and starting point. In any case, the performance of optimisation should be carefully monitored by a direct comparison of the backbones and damping curves, and by assessing the quality of the final parameters. Sometimes, even parameters corresponding to local minima can be satisfactory.

The proposed quantification of non-linearities using the optimisation can be summarised in the following steps:

1. Minimise single-objective functions in Eq. (5.7) for all m and k to obtain the utopia points G_m^{ko} and the corresponding parameters $\mathbf{u}_m^{ko}$.

2. Check whether $\mathbf{u}_m^{ko}$ are the same for all objective functions considering predefined range of accuracy

   - if so, all single objective functions have been optimised by $\mathbf{u}_m^{ko}$ so the parameters of the system are quantified. This should be verified by the visual comparison of the estimated non-linear modes with the optimisation results.
   - if not, the system might be badly defined, i.e. a wrong type of non-linearity might have been selected or multi-objective optimisation must be carried out due to the presence of the trade-off in the objective functions. The trade-off should not relate to the physical structure, but rather to random errors originating in experimental set-up, data acquisition and processing.

3. For multi-objective optimisation using the WGC, select p (typically $p = 1$) and preferable weights w_m^k. If the weights are the same for all modes and measured location, no preferences are considered

4. Solve Eq. (5.10) and then decide whether the results are plausible. If not, change the model or optimisation preferences.

The main advantage of the proposed procedure is that if there are no trade-offs, it is theoretically enough to evaluate one utopia point and check how well other objective functions satisfy that solution. This can dramatically reduce the number of evaluations of the objective function(s). The evaluation of the objective function can take a long time, so the reduction of the evaluation count is desired. The starting point needs to be selected only once and after the first utopia point has been found, it can be used as the next starting point. This should also reduce the number of evaluations of the objective functions.

In terms of the optimisation engine, it is proposed to use classical optimisation algorithms, such as a Newton's iterative method and its derivatives, which generate a single point at each iteration by deterministic computation and use the sequence of points to approach an optimal solution. Compared to the heuristic algorithms, for instance genetic algorithms, which generate a population of points at each iteration and select the next population by the computation involving random number generators, the classical algorithms do not usually guarantee that the global minimum is found. If needed, this disadvantage can be overcome by running the optimisation from a number of different starting points and evaluating the results. In addition, the classical algorithm cannot be used for non-smooth problem so the smoothness of the problem must be ensured by the selection of the suitable range of optimised parameters. The classical algorithms are preferred over the heuristic approaches to reduce the number of evaluation of the objective function.

It should be noted that the described optimisation is quite general since it takes into account multiple modes and multiple locations. However, in chapter 4 it was found that the accuracy of the obtained parameters will be high only for the resonant decay responses whereas the free decay response will be subjected to the error caused by the discrepancies between the HHT, ROM and CNM.

5.3 Application to simulated data

In this section, the described quantification of non-linearity is demonstrated on the simulated data from the numerical examples used in chapter 4. The two-degree of freedom system with cubic stiffness and quadratic damping as well as the beam with a geometric non-linearity are considered.

5.3.1 A system with cubic hardening stiffness

The same system with a cubic hardening spring that was used throughout section 4.4.1 is presented hereafter. Firstly, the resonant decay response is considered for which it is shown that the quantification is very accurate. Subsequently, the case of the free decay response is described to show that the quantification struggles due to the error in the relation between the IMFs and ROM presented in chapter 4.

Resonant decay response

The simulated resonant decay response, which has been compared to the ROM in Fig. 4.3, is used. The IF and IA have been estimated by the ZC method from the simulated signals in Fig. 4.3 and the non-linear modes extracted. The extracted backbones for both masses can be seen in Fig. 5.2(a) and the logarithm of the amplitude in Fig. 5.2(b).

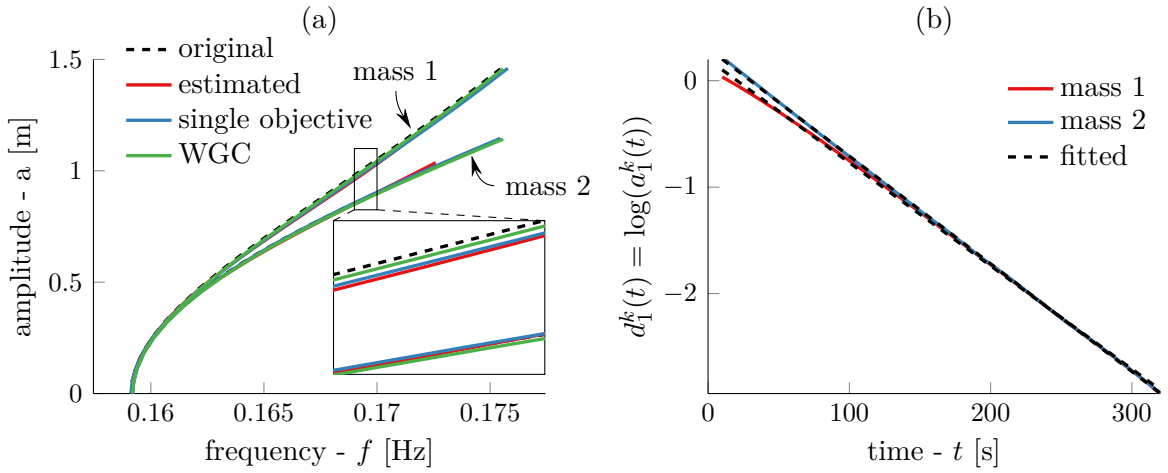

Figure 5.2 Vibration characteristics of the system with cubic hardening stiffness estimated from resonant decay responses: (a) backbones and (b) logarithm of the amplitude

Detection and characterisation can be performed using these characteristics. It can be seen that the frequency is dependent on the amplitude, whereas damping is not. This means that the non-linearity is present in the stiffness, but the damping behaves linearly. The cubic non-linear stiffness could be also characterised by comparing the backbones in Fig. 5.2(a) to the footprint library in Fig. 5.1.

Since the damping is linear, its numerical values can be estimated by the line fitting approach [63]. The obtained damping is tabulated in Tab. 5.1. All estimated damping values are very close to the original ones, with the maximum error being 3 %.

The cubic hardening spring coefficient cannot be quantified directly by fitting the backbones in Fig. 5.2(a) since, as discussed in section 5.2.5, the analytical expressions for MDOF system backbones are not readily obtainable. The analytical expression found for the SDOF system with a cubic stiffness spring in Eq. (3.7) could be used instead to fit the backbones curves separately. However, such process would obviously lead to a different non-linear coefficient for each mass. Moreover, it would not consider the MDOF nature of the system, thereby limiting the applicability of the obtained model(s).

In contrast, the described quantification procedure is able to identify the coefficient of the cubic spring for the MDOF system. The structural model selected for the

Method	k [N m^{-1}]	k_{nl} [N m^{-3}]	ζ [%]
Original	1	0.5	1
Estimated from mass 1	1.0008 (0.08 %)	0.4864 (−2.72 %)	0.97 (−3 %)
Estimated from mass 2	0.9998 (−0.02 %)	0.5167 (3.34 %)	1.01 (1 %)
WGC	1.0006 (0.06 %)	0.4940 (−1.20 %)	-

Table 5.1 The quantification results for a two-degree-of-freedom system with cubic hardening stiffness from resonant decay responses (values in parentheses indicate the relative error of estimated parameters)

quantification was the same as in Eq. (4.18). It was assumed that the mass is known and since the damping has been already identified, the unknown coefficients were $k = k_1 = k_{12} = k_2$ and k_{nl}. Therefore, the vector of unknowns to be quantified is $\mathbf{u} = [k, k_{\mathrm{nl}}]^T$.

The quantification procedure described in section 5.2.6 was conducted and the results are summarised in Tab. 5.1. Even when the objective functions were optimised separately (which led to the utopia points) the results were quite accurate. The errors in the linear stiffness were practically zero, whereas the errors in non-linear stiffness coefficients did not exceed 3.5 per cent for either mass. For the application of the weighted global criterion method (WGC) the equal weights for both masses were used which led to the lower error in the estimated cubic stiffness coefficient while the linear stiffness has not changed. The equal weight are justified in this case because there is no reason or indication to prefer one backbone over the other.

This example demonstrates that the quantification is very accurate for the resonant decay response of the system with an elastic structural non-linearity.

Free decay

The free decay data which were compared to the ROM in Fig. 4.6 are now considered. The IF and IA, which are also shown in the Hilbert spectrum in Fig. 4.7, were estimated by the ZC method and the non-linear modes extracted. Since the damping is linear, it is not shown again. The extracted backbones for both masses and both modes can be seen in Fig. 5.3. Clearly, the estimated backbones and computed original non-linear modes do not match. This was also seen in Fig. 4.7 in which the ROM was superposed onto the Hilbert spectrum and the same discrepancy revealed. This mismatch is not caused by the error in the estimation of the IF and IA, but it is a consequence of the fundamental inability of the HHT to recover the IMFs which would match the ROM as shown in chapter 4. Although it is anticipated that the quantification of non-linearity will yield

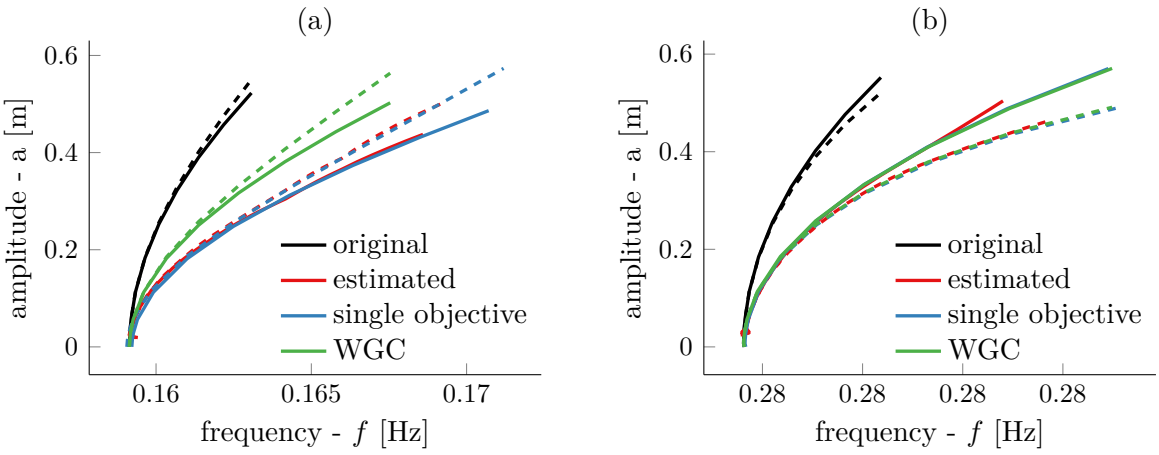

Figure 5.3 Backbones of the two-degree-of-freedom system with cubic hardening stiffness estimated from free decays of mass 1 (solid lines) and mass 2 (dashed lines): (a) 1st mode and (b) 2nd mode

incorrect results, it is shown in this example to highlight the amount of the error in the obtained linear and non-linear parameters.

As for the resonant decay response, the vector of unknowns to be determined was $\mathbf{u} = [k, k_{\mathrm{nl}}]^T$. The results of the quantification are summarised in Tab. 5.2. It can be

Method	k [N m^{-1}]	k_{nl} [N m^{-3}]
Original	1	0.5
Mass 1 mode 1	1.0010 (0.10 %)	1.8000 (260 %)
Mass 2 mode 1	0.9990 (−0.1 %)	1.9800 (296 %)
Mass 1 mode 2	1.0002 (0.02 %)	1.1980 (139.6 %)
Mass 2 mode 2	1.0000 (0 %)	1.2300 (146.0 %)
WGC	1.0000 (0 %)	1.2125 (142.5 %)

Table 5.2 The quantification results for a two-degree-of-freedom system with cubic hardening stiffness from a free decay (values in parentheses indicate the relative error of estimated parameters)

seen that only the linear stiffness has been quantified correctly with practically zero errors. On the contrary, truly significant errors were obtained for the non-linear stiffness coefficients. When the objective functions were optimised separately (the utopia points found), the results for k_{nl} also varied significantly. In particular, the difference between the first and second mode is distinct. The values estimated from the first mode are nearly three times as high as the original value whereas the cubic stiffness coefficients estimated from the second mode are much closer to the original values, but still over twice as high.

This incorrect quantification is in line with chapter 4 where it was observed that the mismatch of the IMF and ROM for the first mode is typically greater than for higher modes. Reflecting on this knowledge, the weights in the WGC (in Eq. (5.10)) were chosen in such a way that the first mode was considered by 20 per cent and the second by 80 per cent, i.e. $w_1^1 = w_1^2 = 0.1$ and $w_2^1 = w_2^2 = 0.4$. Setting the weights in this way yielded the non-linear stiffness coefficient with the error of nearly 150 %. As can be seen in Fig. 5.3 the backbones after the WGC match for the second mode and are closer to the estimate backbone for the first mode. However, since the estimated backbones do not match the original ones, the quantification has not been successful.

This again confirms the unfortunate findings of chapter 4 that the IMFs compose only the approximation of the CNMs. This means that the described quantification cannot be used with the free decays to identify coefficients of MDOF non-linear systems as originally intended. The amount of error in the estimated coefficients varies with the changes in the accuracy of the relation between the IMF and ROM. In spite of the fact that the quantification fails for free decays, it was shown that it is accurate for resonant decay responses. Moreover, in contrast to the NNMs, the systems with non-linear damping can be also correctly quantified (from resonant decay responses) as evidenced in the following section.

5.3.2 A system with quadratic damping

Only the resonant decay response data which are seen in Fig. 4.11 are considered since it has been already concluded that there is no point trying to quantify the system accurately from free decays. The IF and IA have been estimated by the ZC method and the non-linear modes extracted according to section 5.2.2. The extracted damping rate for both masses can be seen in Fig. 5.4. It is clear that the damping rate increases rapidly with the vibration amplitude. This behaviour clearly indicates that the damping, and by extension the system, is non-linear. Despite of the damping fluctuation at higher amplitudes the non-linearity can be characterised as quadratic damping by visually comparing Fig. 5.4 to the footprint library in Fig. 5.1.

For the quantification of the system, the model used in section 4.4.2 was again utilised. The selected optimisation parameters were the stiffness coefficient k_1 of the linear spring parallel to the non-linear damper described by c_{nl}. The vector of unknowns was therefore $\mathbf{u} = [k_1, c_{\mathrm{nl}}]^T$. The quantification results are tabulated in Tab. 5.3. The errors were slightly higher than for the resonant decay response of the system with the cubic hardening stiffness. The lower errors are obtained for the linear stiffness coefficient k_1 and larger for the non-linear damping. When the optimisation of the single objective

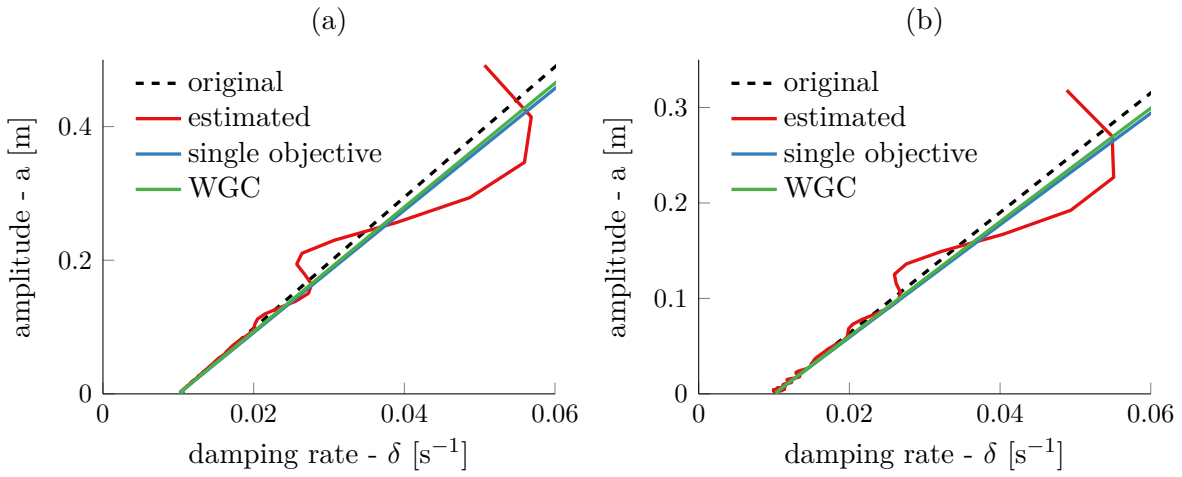

Figure 5.4 Damping curves of the two-degree-of-freedom system with quadratic damping estimated from resonant decay responses of the first mode: (a) mass 1 and (b) mass 2

Method	k_1 [N m^{-1}]	c_{nl} [N s m^{-1}]
Original	0.1	0.5
Estimated from mass 1	0.0977 (−2.3 %)	0.5361 (7.22 %)
Estimated from mass 2	0.1015 (1.5 %)	0.5171 (3.42 %)
WGC	0.0991 (−0.9 %)	0.5265 (5.3 %)

Table 5.3 The quantification results for a two-degree-of-freedom system with quadratic damping from resonant decay responses (values in parentheses indicate the relative error of estimated parameters)

function is carried out, the results are more accurate for mass 2 than mass 1. It is possible that the results are influenced by the fluctuation of the damping around the original values. Since there is no reason to prefer one damping curve over the other, the weights for the WGC were equal. The obtained results, also in Tab. 5.3, are essentially a compromise between the mass 1 and 2. The stiffness was quantified with the error less than 1 % whereas the non-linear damping coefficient with over 5 %. These errors are not considered to be significant because they do not lead to the significant discrepancies between quantified and original damping curves in Fig. 5.4.

This example demonstrates that the quantification can be carried out accurately for a MDOF system with the non-linear damping from the resonant decay response. Similar quantification cannot be achieved by other quantification approaches, usually due to their inability to cope with non-conservative systems.

5.3.3 A cantilever beam with geometric non-linearity

The final simulated example is the beam studied in section 4.4.3. Specifically, the resonant decay responses compared to the ROM in Fig. 4.17 are considered. The IF and IA have been again estimated by the ZC method and the non-linear modes extracted. The backbones are shown in Fig. 5.5 (the damping is linear so it is not considered). Unlike

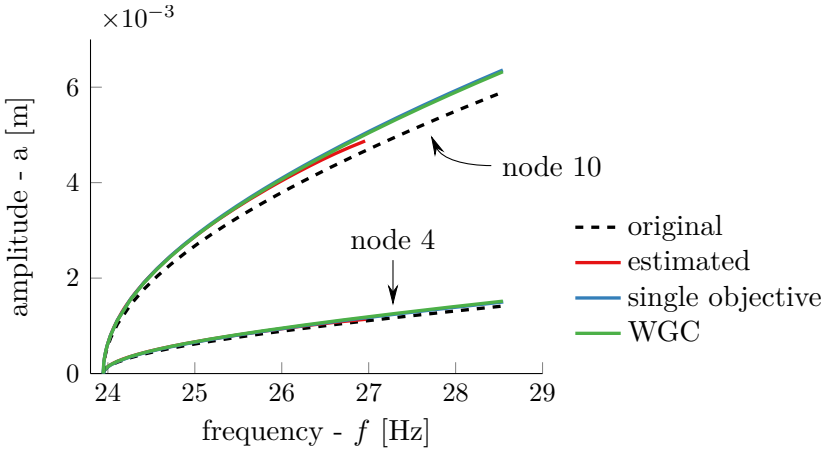

Figure 5.5 Backbones of the cantilever beam with geometric non-linearity estimated from resonant decay responses

in the previous cases, it can be noticed that the estimated backbones are not exactly the same as the original one. A larger difference can be observed for the node 10. The discrepancies are caused by the smoothing which had to be applied to estimate the backbones in order to comply with the definition of the CNMs.

Detection and characterisation could be again carried out using these backbones. For the quantification, the full FE model used from section 4.4.3 was used and the Young's modulus E and non-linear stiffness k_{nl} were considered as unknowns. The results of the quantification are summarised in Tab. 5.4. The non-linear stiffness has been estimated

Method	k_{nl} [N m^{-3}]	E [Pa]
Original	1e8	2.1e11
Estimated from node 4	8.9775e7 (−10.22 %)	2.1005e11 (0.02 %)
Estimated from node 10	8.6547e7 (−13.45 %)	2.0998e11 (−0.01 %)
WGC	8.7987e7 (−12.01 %)	2.0998e11 (−0.01 %)

Table 5.4 The quantification results for the cantilever beam with geometric non-linearity from resonant decay responses (values in parentheses indicate the relative error of estimated parameters)

with higher errors, exceeding 10 %, but Young's modulus was estimated very accurately. The errors in the non-linear stiffness seem to originate in the error of the ZC method for the estimation of the backbones. However, as it can be seen in Fig. 5.4 the error might seem to be significant, but the visual difference in the re-contracted and original backbones are not dramatic.

5.4 Application to experimental data

The proposed method is now demonstrated on the experimental data acquired from the ECL benchmark described in section 2.5.3. The experimental set-up is the same as in Fig. 2.16. In this section, the linear modal analysis and the demonstration of the proposed method will be described.

Linear modal analysis

The linear modal analysis was performed on the main beam only, i.e. without the thin beam attached. The accelerometer on the tip of the beam (in node 10) was used and the impact hammer excitation was applied to measure the frequency response functions (FRFs). The FRFs were processed using a least-squares frequency domain method [172] which estimated natural frequencies and damping ratios summarised in Tab. 5.5 and corresponding modes shapes depicted in Fig. 5.6. It can be seen that four

Mode no.	natural frequency [Hz]	damping ratio ζ [%]
Mode 1	23.8	0.33
Mode 2	148.1	0.052
Mode 3	414.4	0.024
Mode 4	806.9	0.015

Table 5.5 Linear natural frequencies and damping ratios of the ECL benchmark without the thin beam

natural frequencies have been identified in the frequency band $0 - 1000$ Hz. The natural frequencies are not close to each other so no significant mode mixing in the EMD should occur unless there is a prominent difference in amplitudes as discussed in section 3.2.2. The damping ratios are relatively weak, being less than 0.1 % for higher modes. This fact justified the use of the ECL benchmark in the studies about NNMs [189, 191] in which the damping is not considered but the conservative system can be still adequately studied.

The modes shapes shown in Fig. 5.6 are normalised so that the amplitude is equal to one or minus one in node 10. It can be seen that the estimated mode shapes are well

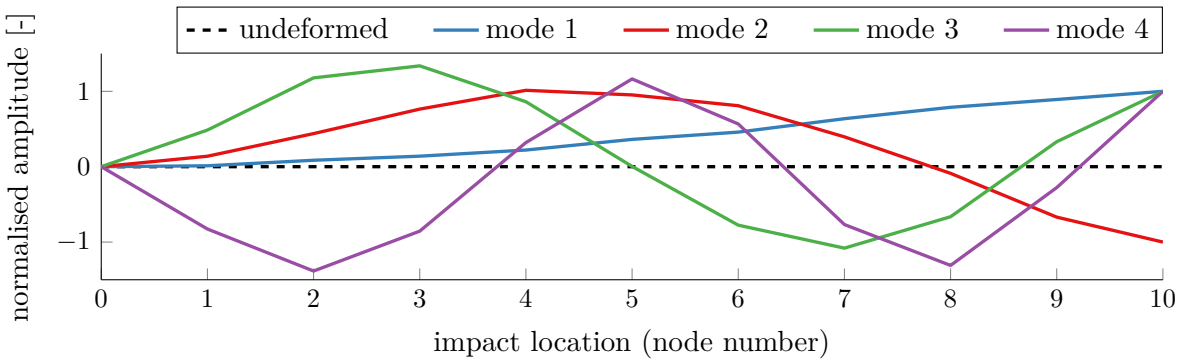

Figure 5.6 The (linear) modes shapes of the ECL benchmark without the thin beam

known shapes of a cantilever beam. In the following, the frequency range $0 - 500\,\text{Hz}$ will be studied so only the first three non-linear modes will be considered.

The demonstration of the proposed method

As seen from the application to simulated data, the method leads to accurate results only when a resonant decay response is used. Unfortunately, due to the problems with the control of the excitation and the fact that it was not possible to disconnect the shaker without significantly influencing the dynamics of the system, the acquisition of resonant decay responses has not been successful.

Therefore, the method is demonstrated on the free decay responses which were measured by applying a short impact to node 9. All three accelerometers simultaneously acquired the response in nodes 4,7 and 10. The processing will be shown in detail for the responses of node 4 and 10 shown in Fig. 5.7. These responses have a multi-component character so the IF and IA cannot be directly estimated. Therefore, the EMD must be applied to obtain the IMFs. The acceleration has been measured, but the method is intended to be used with the displacement signals. Therefore, the responses have been integrated twice to obtain the required form of data. It should be noted that a trend in the data usually appears after the integration. This trend can be removed by standard de-trending algorithms or it can be left in the data, because the EMD will remove it automatically as well.

The EMD was not initially able to estimate clear modes that would be close to nominal linear modes due to mode mixing problems. However, by applying the masking signal approach repeatedly (for each IMFs a different masking signal was used), it was

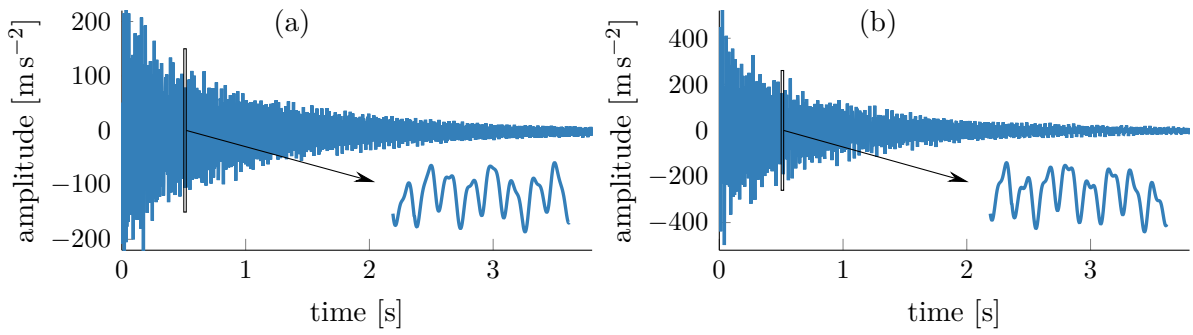

Figure 5.7 The measured free decay acceleration of the ECL benchmark: (a) node 4 and (b) node 10

possible to separate the three intrinsic mode functions shown in Fig. 5.8. These IMFs correspond to the first three non-linear modes of the structure. It can be seen that the IMFs look like individual resonant decay responses. Unlike the IMFs of a cantilever beam in Fig. 4.19 they are not so noisy. This is caused by the fact that not so many modes were excited in this experiment. In fact, there were only a few spurious IMFs which did not seem to have any relation to the non-linear modes and which had an order of magnitude lower amplitude. Most of them seemed to be a consequence of the data processing so they were not shown here. Although the IMFs appear to be sufficiently smooth, some end-effects can be seen at the beginning and the end of the signals. These regions are therefore excluded from the subsequent analyses.

Because a sequence of the masking signals had to be used, the orthogonality of IMFs might have been violated. Therefore, the orthogonality is verified using the index of orthogonality proposed in Eq. (3.12). The orthogonality of the three IMFs and the residuum, which was obtained by subtracting the sum of IMFs from the signal, can be seen in Fig. 5.9. Since the index of orthogonality is equal to one for the same IMFs and zero otherwise, the IMFs are orthogonal to each other. They are also orthogonal to the residuum which implies that the contribution of the individual modes has been completely estimated in the respective IMFs. The overall index of orthogonality defined by Eq. (3.13) is only 2.2534×10^{-4}. The orthogonality analysis confirms that the IMFs are correct.

Prior to the IF and IA estimation, it is attempted to detect the non-linearity using the Teager energy operator (TEO) as described in section 3.3.5. The frequency and amplitude have been estimated using Eq. (3.42) and Eq. (3.43), respectively, and the results are shown in Fig. 5.10. It can be seen that the TEO did not produce a smooth envelope or frequency. However, it did not produce characteristics that do not make any sense either (it is stated in [104] that if the system is non-linear, the TEO results

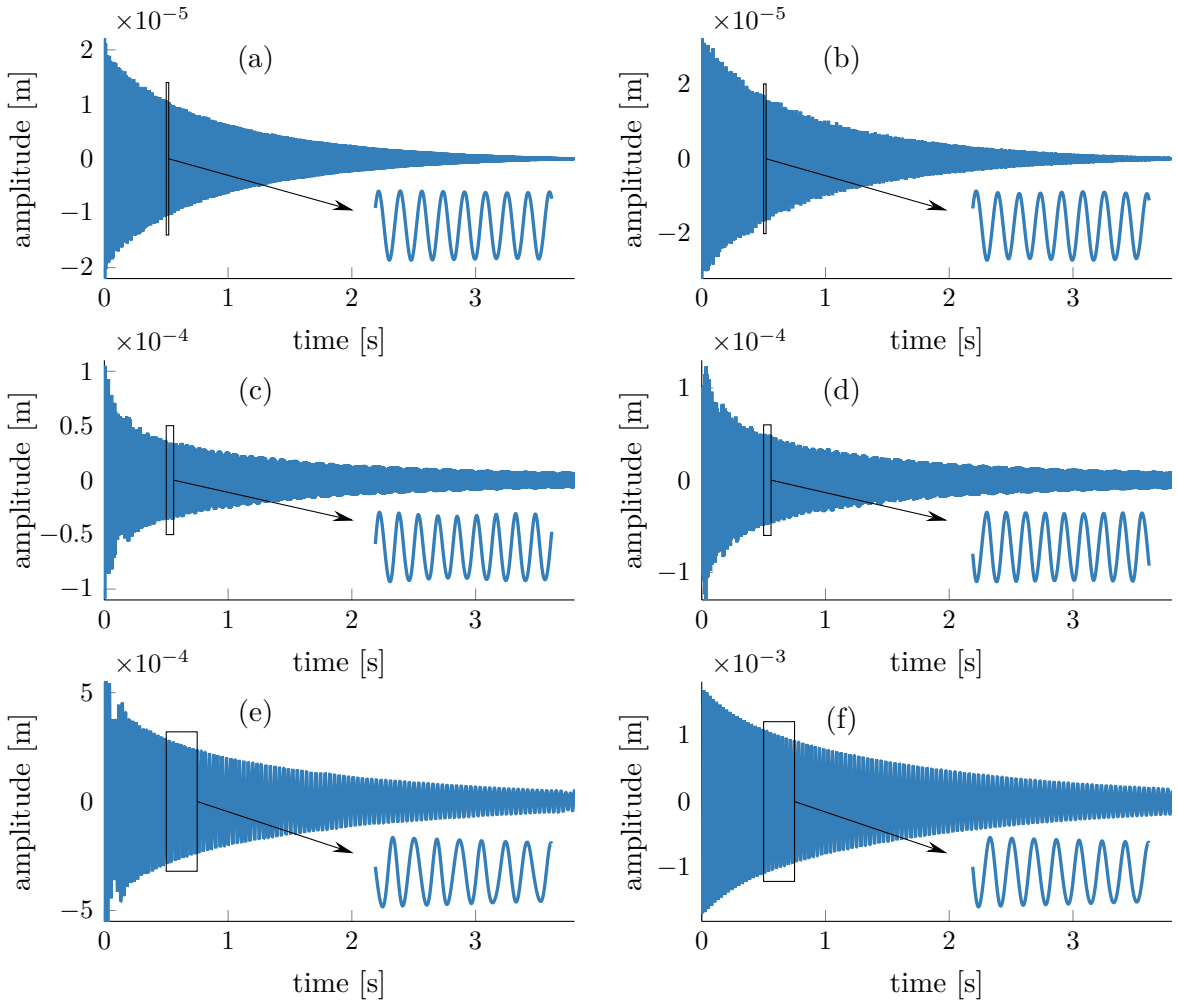

Figure 5.8 Intrinsic mode functions extracted from free decays of the ECL benchmark: (a) 3rd mode, node 4, (b) 3rd mode, node 10, (c) 2nd mode, node 4, (d) 2nd mode, node 4, (e) 1st mode, node 4, and (f) 1st mode, node 10

should not make any sense, i.e. it should be impossible to interpret the results). This seems to be a serious problem of this detection approach because it is not clear what can be considered as the indication of non-linearity and what can be a consequence of the measured noise. It can be seen in Fig. 5.10(a) and Fig. 5.10(c) that the distortion of the amplitude increases with the increasing amplitude. This could be interpreted in such a way that the TEO actually indicates non-linear behaviour at the high amplitude and rather linear behaviour at the low amplitude. The frequency estimated using the TEO is spread around the frequencies which will be also estimated by the zero-crossing method. The estimated frequency can be either interpreted as the consequence of non-linearity or

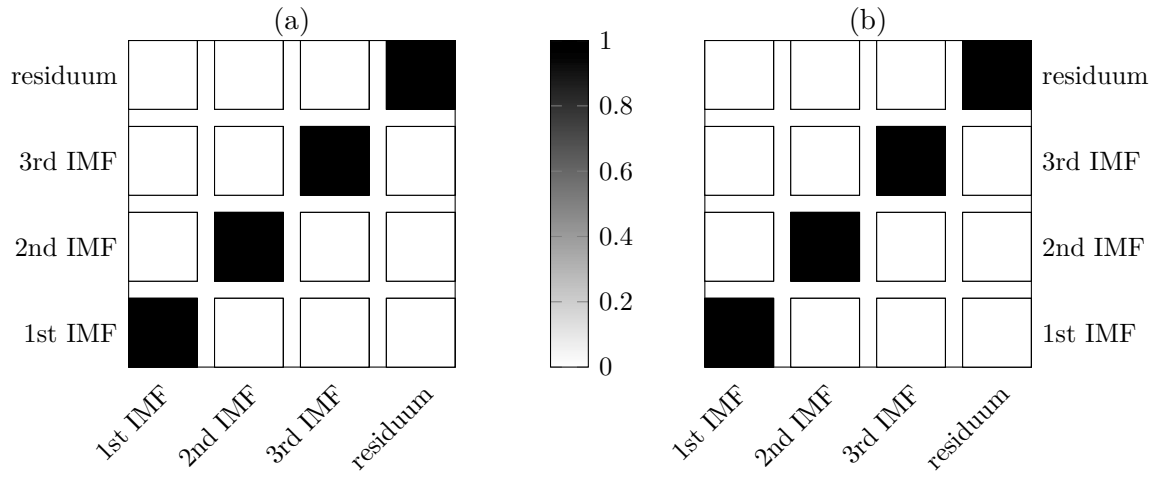

Figure 5.9 Index of orthogonally for the first three modes and the residuum related to (a) node 4 and (b) node 10

the correct, albeit noisy, frequency. Therefore, the Teagor energy operator does not seem to be a reliable means of detecting the non-linearity in this case.

The final IF and IA have been estimated by the ZC method. Consequently, the backbones were calculated and the damping assessed by the logarithm of the amplitude. The results are shown in Fig. 5.11. From the backbones, it is immediately obvious that the system is non-linear and that it exhibits the hardening type of non-linearity. The hardening behaviour can be observed in all three investigated modes. The frequency shift is dominant for the first mode (over 10 Hz) and smaller for the second and third modes. It can be also noticed that the frequencies for very low amplitudes (presumably linear natural frequencies) are not identical to the frequency of the main beam without the non-linearity summarised in Tab. 5.5. The first frequency is slightly higher whereas the other two are slightly lower. It was found that this phenomenon is caused by the thin beam which, besides introducing the non-linearity, adds the linear stiffness that causes the shift of the frequencies. It was also observed that the pre-stress of the thin beam influences this stiffness as well. Unfortunately, a means of controlling the pre-stress of the thin beam was not available so a more detailed, systematic study of its effects have not been conducted. A similar shift in the linear natural frequency due to the presence of the thin beam has been also observed in other studies [119, 189, 191]. To account for this effect in computational models, the rotational stiffness that captures the presence of the beam and its pre-stress was often added. It can be also noted that the amplitude-dependent frequency of the first mode in Fig. 5.11(a) is roughly 2 Hz lower

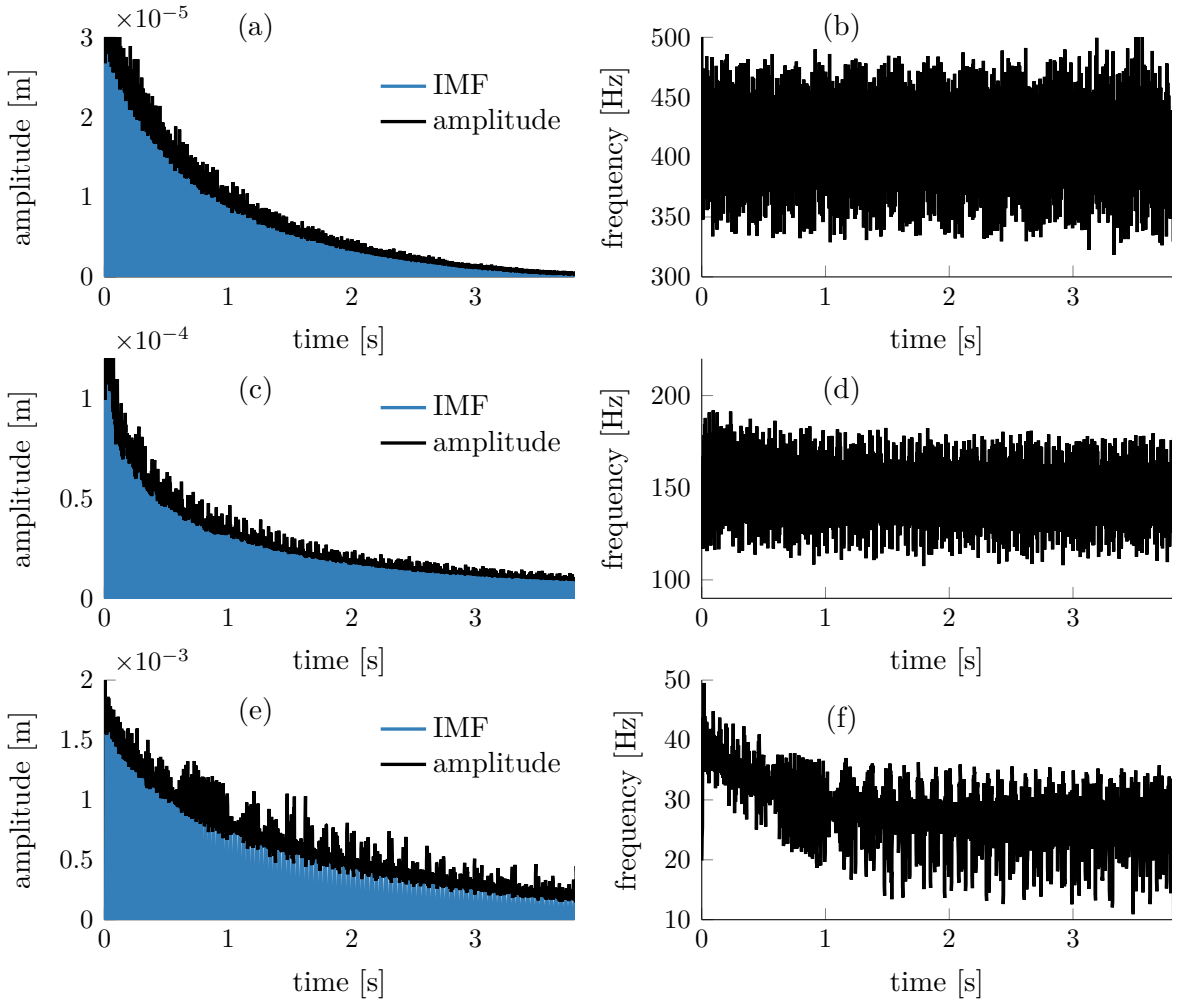

Figure 5.10 Application of the Teager energy operator (TEO) to the ECL benchmark at node 10: (a) frequency of the 3rd mode, (b) amplitude of the 3rd mode, (c) frequency of the 2nd mode, (d) amplitude of the 2nd mode, (e) frequency of the 1st mode, and (f) amplitude of the 1st mode

than the frequency of the FRFs shown in Fig. 2.17. This difference is believed to be caused by the presence of the shaker that was used to measure the FRFs in chapter 2.

No significant non-linearity in damping can be observed from the logarithm of the amplitude in Fig. 5.11. Therefore, the linear damping ratios can be estimated by the line fitting which yields $\zeta_1 = 0.3415\,\%$ for mode 1, $\zeta_2 = 0.0539\,\%$ and $\zeta_3 = 0.0396\,\%$ for mode 3. The estimated values are slightly higher than the values obtained by the linear modal analysis. The small discrepancies do not have to be solely caused by the presence of the thin beam. They can also be a consequence of different estimation methods.

It should be also mentioned that the backbone in Fig. 5.11(b) for node 7 is not estimated for the frequency higher than 150 Hz. Likewise, the factor $d_2^7(t)$ in Fig. 5.11(e)

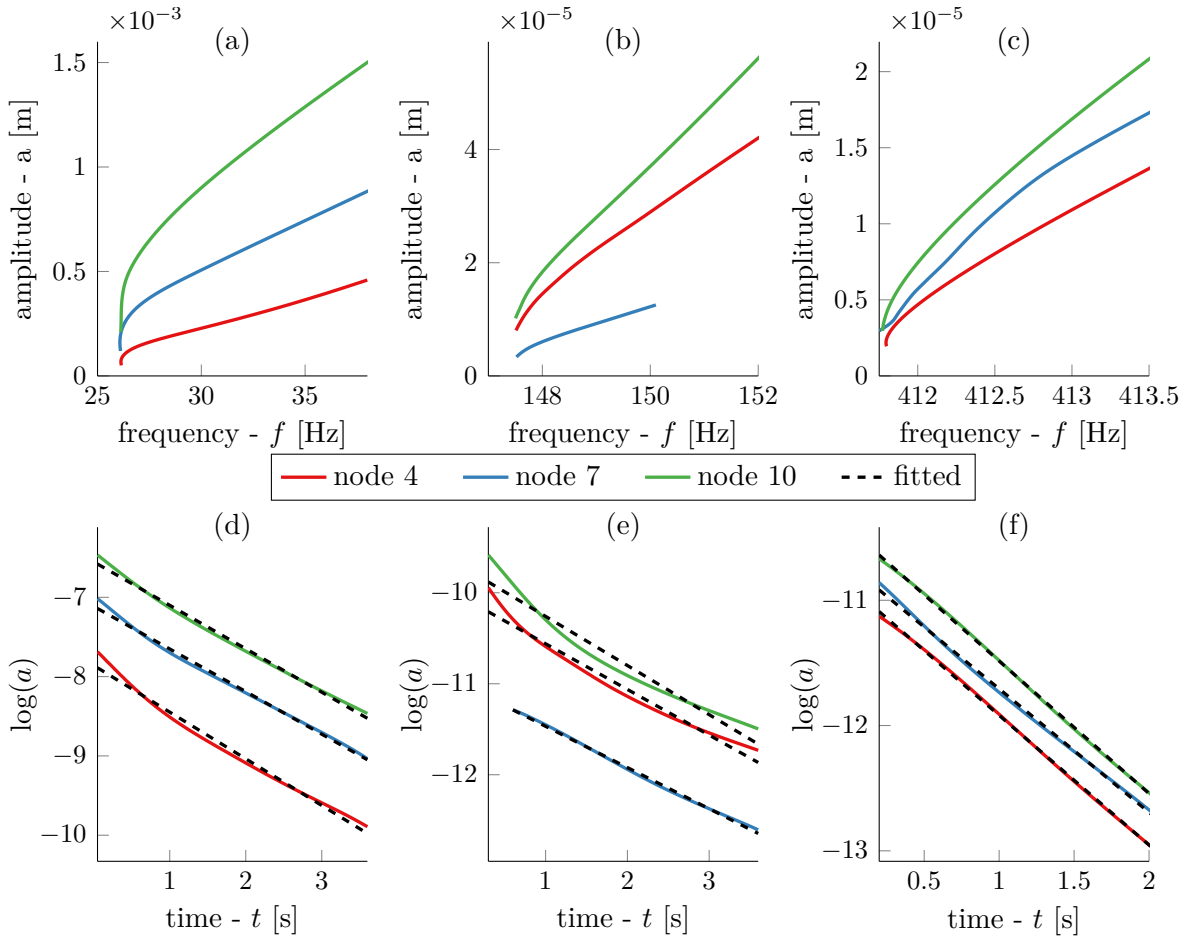

Figure 5.11 Estimated non-linear modes of the ECL benchmark: (a)-(c) the backbones of the first three modes and (d)-(f) the logarithms of the vibration amplitude of the first three modes

is not available for the time lower than 0.7 s. These missing parts of the results are a consequence of the end effects that occurred in the EMD. It is possible that the second mode in node 7 is influenced by the end-effects more than the other results, because node 7 lies close to the node of vibration (zero value of mode shape) of the second mode. Therefore, the data acquired are more likely to be corrupted by measured noise and processing errors.

The mode shapes estimated according to section 5.2.2 as a function of time are shown in Fig. 5.12. By comparing the mode shapes with Fig. 5.6 it is clear that the character of the mode shapes estimated for the non-linear system is the same as the linear mode shapes. This was expected because the estimated non-linear modes are the continuation of their linear companions.

In order to illustrate the change of the mode shapes due to the non-linearity, the first two modes shapes are shown in Fig. 5.13 again. The third mode is not included because

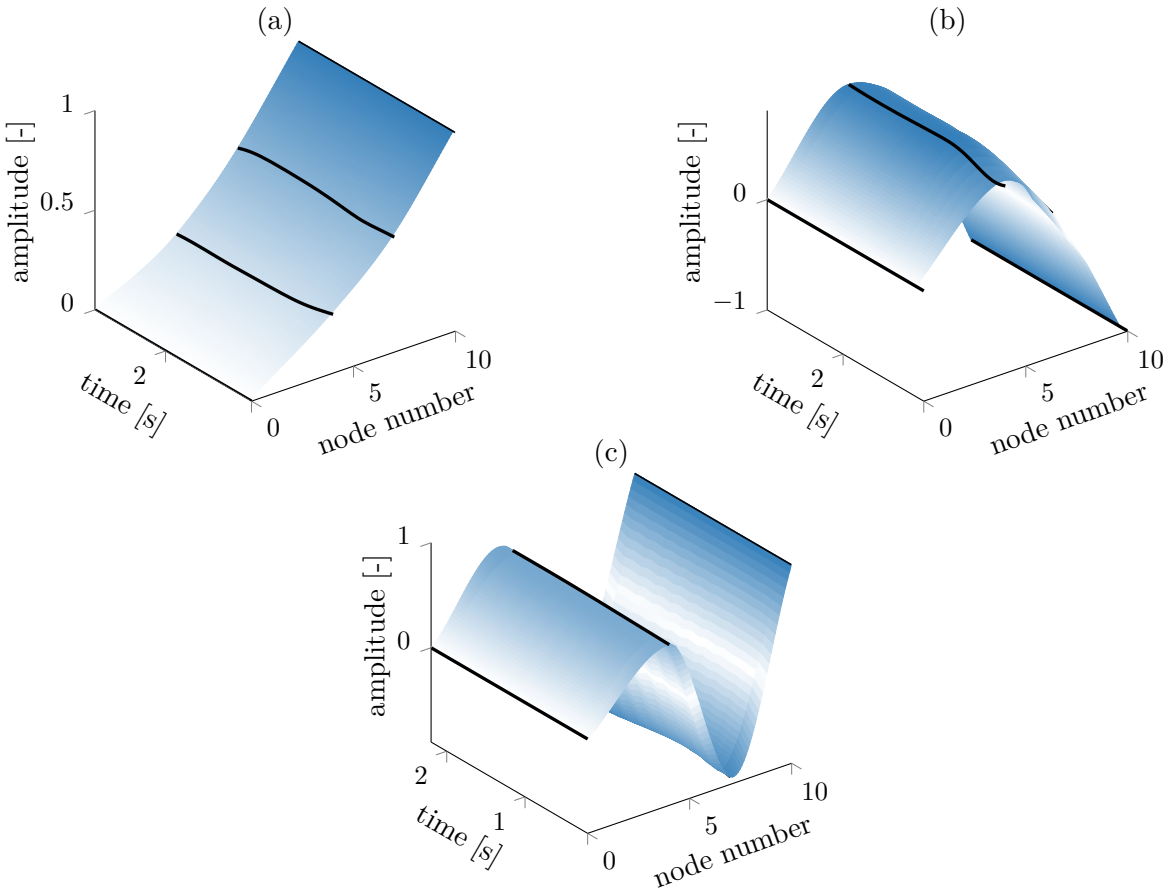

Figure 5.12 The estimated mode shapes of the ECL benchmark as a function of time: (a) 1st mode, (b) 2nd mode, and (c) 3rd mode

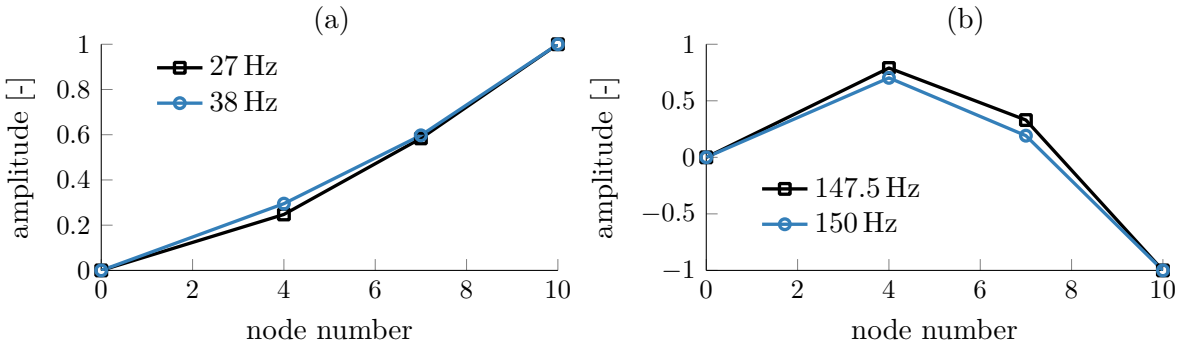

Figure 5.13 Estimated modes shapes of the ECL benchmark: (a) 1st mode and (b) 2nd mode. These estimated mode shapes are very similar to the mode shapes of the simulated cantilever beam shown in Fig. 4.16.

it does not display any significant change. It can be seen that the mode shapes change with the frequency (and therefore amplitude) of vibration. The normalised values of the

first mode increase for the higher frequency whereas the normalised amplitude of the second mode decreases. This is consistent with the simulated CNMs of the beam with a geometric non-linearity seen in Fig. 4.16(c) and Fig. 4.16(d). The estimated modes shown not only confirm the presence of the cubic hardening but also demonstrate the ability of the HHT to obtain multiple non-linear modes from a single measurement. However, it should be noted that the level of measured noise was minimal and no uncertainty has been considered.

The detection and characterisation of non-linearity as well as the quantification of damping have now been shown. For the quantification of the non-linearity, the model similar to Fig. 4.15 with the rotational linear stiffness in node 10 could be selected. Unfortunately, it has been concluded that the quantification without measured resonant decay responses does not lead to the satisfactory results. Since the experimental measurement of resonant decay responses using phase resonant testing has not been successful, the quantification has not been performed.

Summary of the application to experimental data

The proposed method has been applied to a free decay response of the ECL benchmark. It has been able to determine the presence and the character of non-linear behaviour. The non-linear behaviour in stiffness has been detected by the amplitude dependence of the backbones and characterised by visual inspection. The damping was determined as being linear by examining the logarithm of the vibration amplitude. Unfortunately, the method is not able to quantify the non-linear behaviour since the resonant decay response has not been measured. Although the method cannot be used for the quantification, it brought a lot of information about the structural behaviour in a non-linear modal analysis framework from a single, very quick measurement.

5.5 Discussion

The original idea of this chapter was to use the Hilbert-Huang transform (HHT) in conjunction with the complex non-linear modal analysis to perform non-linear system identification. The identification would be conducted in modal analysis framework, i.e. the amplitude-dependent frequency, damping and mode shapes would be directly used to detect, characterise and quantify non-linear behaviour of structure. The described method enables non-parametric detection and characterisation of structural non-linearities for free decays as well as quantification of full FE structural models of non-linear conservative and

non-conservative systems if resonant decay responses have been measured. Unfortunately, the accurate quantification from free decays is not possible due to the findings in chapter 4 that the non-linear modes cannot be correctly reproduced by the HHT.

The detection of structural non-linearities is performed by one or more concepts described in section 5.2.3. Most of them are based on the violation of basic properties of linear systems. The characterisation is then carried out by a careful visual inspection of the estimated non-linear modes as described in section 5.2.4. The idea of a footprint library (Fig. 5.1) can be used to simplify the decision. The main issues with both detection and characterisation is how to establish when the deviation of the non-linear modes from their linear counter-pairs is statistically significant and when it is merely caused by experimental and processing errors. As many visual inspection techniques as possible should be used or it may perhaps be possible to design a decision making algorithm based on artificial neural networks similar to the method described in chapter 2 which would remove the need to visually inspect each result separately.

The quantification of the non-linear behaviour described in section 5.2.6 is based on the optimisation of the selected model in terms of the complex non-linear modes (CNMs). The weighted global criterion method (WGC) was suggested for this application. The method is often used for the multi-objective optimisation, but here, it is used only as a means of combining several objective functions with preferences. The full set of Pareto front points is therefore not computed. The WGC is mainly used to minimise the time of the optimisation and include the preferences. However, even if the WGC is applied the optimisation still leads to the satisfactory results only for the resonant decay responses. It was shown that the optimisation (or even manual adjustments of the parameters) fails for free decays, which was expected due to the findings in chapter 4.

The method is mainly designed to work with free decays and resonant decay responses. However, it would be also able to process the slow-sweep data if the Forcevib algorithm [68] was added to the extraction of non-linear modes in section 5.2.2. The slow-sweep harmonic excitation is able to excite the non-linearity very well, but the experimental hardware and software need to be sophisticated. On the contrary, the free decay response can be measured very quickly with a minimum requirements on the experimental set-up, hardware and software. It is known that it has a distinct disadvantage of being unable to excite the non-linearity fully [289]. The resonant decay response is potentially the most suitable type of data for the proposed method as evidenced by the simulated cases and supported by a number of studies which use the NNMs [142, 168, 189, 215]. However, in order to measure the resonant decay response using the phase resonance testing [59, 190, 191, 291] a very sophisticated experimental set-up, acquisition hardware

and control software need to be adopted. Especially, a reliable control must be used and a means of removing the excitation suddenly designed.

Unlike other methods, such as the complexification-averaging [118] or time-domain non-linear system identification based on multi-scale dynamic partitions leading to the intrinsic modal oscillators [39, 62, 137], the proposed approach offers the opportunity to quantify the linear and non-linear coefficients of a full FE model instead of representing the dynamics using a SDOF approximation or the need to know analytical expressions. Moreover, the use of complex non-linear modes enables applications to systems with dissipative non-linear effects.

The limitations of the proposed method are given by the techniques involved (EMD, IF and IA estimation and numerical computation of the CNMs) and were discussed in section 4.5. Despite the fact that the described quantification is able to work accurately for resonant decay responses, it will not provide accurate results for free decays since it has been found in chapter 4 that the ROM derived from the CNMs does not correspond to the IMFs obtained by the EMD. This means that the CNMs cannot be correctly recovered using the HHT as also shown in Fig. 5.3.

The experimental non-linear modal analysis is not older than 10 years as evidenced by a lack of publications in [119] on this topic and a number of publications in [168]. All the methods from this category are not yet ready for an industrial usage, but are elements of basic research. The proposed method is the same - unfortunately, it is not possible to apply it to industrial cases, but it is believed it contributes to the developing field of non-linear modal analysis.

5.6 Conclusion

In this chapter, the method for detection, characterisation and quantification of structural non-linearities has been described. The detection and characterisation are conducted in non-parametric matter since the Hilbert-Huang transform is used. A full FE model or low-fidelity models can be quantified through the optimisation in terms of CNMs, but the accuracy of this optimisation is only guaranteed for the resonant decay responses. The method was applied to three simulated cases, namely to a two-degree of freedom system with cubic hardening stiffness, a two-degree of freedom system with quadratic non-linearity, and a cantilever beam with a geometric non-linearity. It was found that the accuracy of the quantification vary even in case of resonant decay response, but the error in the quantified parameters was rarely greater than 10 per cent. The linear coefficients were quantified with higher accuracy than the non-linear ones. The method

was also applied to free decay responses of the ECL benchmark where it has been shown that multiple modes can be simultaneously recovered from a single, simple and quick measurement. Despite the fact that the applicability of the quantification is limited to the cases where the resonant decay response has been measured, it is believed that the described method presents the step forward in the fundamental research of experimental non-linear modal analysis because of its use of complex non-linear modes which can be applied to non-conservative system.

Chapter 6

Identification of systems with asymmetric restoring forces

Abstract

In the chapter a method for non-parametric identification of systems with asymmetric non-linear restoring forces is proposed. The method, named the zero-crossing method for systems with asymmetric restoring forces (ZCA), is an extension of zero-crossing methods and allows identification of vibration characteristics from a resonant decay response. The validity of the proposed method is firstly demonstrated on three simulated resonant decay responses of the systems with off-centre clearance, bilinear and quadratic stiffness. Then, the method is applied to experimental data from a micro-electro-mechanical resonator in order to quantify its non-linear damping and stiffness effects. Throughout the chapter the proposed method is also compared with the Hilbert vibration decomposition to demonstrate that the ZCA yields more accurate results with much less effort.

6.1 Introduction

A number of non-linear system identification methods, including those proposed in the previous chapters of this thesis, is limited to systems with symmetric restoring forces. The measured signals may however exhibit asymmetry with respect to the time axis caused by different stiffness or dissipative restoring forces for the positive and negative part of the motion. Such signals can originate from systems with bilinear, piecewise or off-set stiffness, which are not uncommon in engineering structures. For instance, gaps, end stops and pre-stress effects can exhibit asymmetric restoring forces. These signals cannot be readily analysed to obtain asymmetric restoring forces by the methods described in section 3.3. An example of this could be seen in section 3.4.2 where a SDOF system with quadratic (asymmetric) stiffness was analysed by the Hilbert transform, zero-crossing method and direct quadrature. Although these methods can be applied, their results cannot be interpreted correctly, because as seen in Fig. 3.17(a) the instantaneous amplitude does not represent the amplitude of the signal. The only method based on the IF and IA capable of such identification is the Hilbert vibration decomposition (HVD) [71–73]. The HVD will be used throughout this chapter for comparison purposes.

The chapter is organised as follows: the Hilbert vibration decomposition is firstly briefly introduced in section 6.2. Then, the zero-crossing method for asymmetric systems (ZCA) is described in section 6.3. In section 6.4 the ZCA is applied to three simulated cases, namely to the systems with bilinear stiffness, off-centre clearance (backlash) and quadratic stiffness. Section 6.5 then shows the application of the ZCA to the data obtained experimentally from a micro-electro-mechanical beam ring-down measurements. Section 6.6 discusses the limitations and a range of applicability of the proposed method.

6.2 The Hilbert vibration decomposition

The Hilbert vibration decomposition (HVD) [25, 69–73] is a method dedicated to the analysis of quasi-periodic or almost periodic oscillating signals, such as free decays of non-linear systems. It is an extension of the Hilbert transform that allows to estimate the instantaneous frequency (IF) and amplitude (IA) of a multi-component non-stationary and non-linear vibration signal. It is similar to the Hilbert-Huang transform (HHT) described in chapter 3, but it does not use the empirical sifting process based on the cubic splines but rather it separates the different time scales based on the time domain analysis of the IF of the original signal. The HVD assumes that (i) the signal is a superposition of

quasi-harmonic components, (ii) the envelopes of each component differ, and (iii) several longest periods of the corresponding slowest components are included in the signal.

The HVD decomposes a multi-component signal $x(t)$ into a sum of components $x_i(t)$ with slowly varying IF and IA as

$$x(t) = \sum_{i=1}^{N_{\mathrm{HVD}}} x_i(t) = \sum_{i=1}^{N_{\mathrm{HVD}}} a_i(t) \cos\left(\int \omega_i(t) \mathrm{d}t\right), \tag{6.1}$$

where $a_i(t)$ is the IA and $\omega_i(t)$ is the IF of the i-th component. The decomposition is performed by iterating the following steps [69]: (1) the IF $\omega_i(t)$ of the largest energy component is extracted by low-pass filtering of the IF of the original signal (which is not physical meaningful) obtained by the Hilbert transform, (2) the synchronous detection, which is also based on the Hilbert transform and low-pass filtering, then extracts the amplitude $a_i(t)$ of the vibration component with the previously estimated frequency, (3) having estimated the IF and IA of the largest energy component, it can be subtracted from the original signal and the process repeated until all N_{HVD} components are extracted. The decomposition ends when the standard deviation of two subsequent components is smaller than a defined tolerance or the selected total number of components N_{HVD} has been reached. The obtained components are not generally equal to intrinsic mode functions obtained by the empirical mode decomposition (EMD) described in section 3.2 because the means of decomposition is different. The HVD does not use the shifting process so the potentially problematic cubic spline fitting is avoided and the frequency resolution of the HVD can be better [71]. On the other hand, the low-pass filtering and the Hilbert transform are extensively used, both of which are influenced by numerical problems. The properties of the low-pass filter, especially the cut-off frequency, must be carefully selected because the results of the decomposition can vary significantly due to the setting of the filter.

The Hilbert vibration decomposition for asymmetric systems is based on the idea that each signal branch (the lower and upper part of the signal with respect to time axis) is defined on its half-plane only. Therefore, in order to recover the initial restoring forces, these parts must be analysed separately. The applicability of the HVD for asymmetric systems is limited to resonant decay responses for which the extracted components x_i represent the primary and higher harmonics.

In order to identify asymmetric restoring forces, a congruent amplitude and frequency must be defied as [73]

$$a_c(t) = \sum_{i=1}^{N_{\mathrm{HVD}}} a_i(t) \cos\left(\phi_i(t)\right), \tag{6.2}$$

and

$$\omega_c(t) = \sum_{i=1}^{N_{\mathrm{HVD}}} \omega_i(t) \cos\left(\phi_{\omega i}(t)\right), \tag{6.3}$$

where $\phi_i(t)$ and $\phi_{\omega i}(t)$ are phase angles between the amplitude and frequency of the primary and i-th harmonic, respectively. The congruent amplitude represents is an envelope of the amplitude (also called the envelope of the envelope in [73]). For instance, it could be seen in Fig. 3.17(a) that the amplitude estimated by the Hilbert transform oscillates. Its values vary between the envelope of the upper and lower part of the signal. Therefore, by defining the congruent amplitude as the envelope of the envelope (and similarly the congruent frequency as the envelope of the frequency), the correct instantaneous characteristics for the positive a_{cp} (ω_{cp}) and negative a_{cn} (ω_{cn}) part of the original signal can be obtained as

$$a_c(t) = \begin{cases} a_{cp}(t), & x_i(t) \geq 0 \\ a_{cn}(t), & x_i(t) < 0 \end{cases} \qquad \omega_c = \begin{cases} \omega_{cp}(t), & x_i(t) \geq 0 \\ \omega_{cn}(t), & x_i(t) < 0 \end{cases}. \tag{6.4}$$

The congruent functions allow to estimate the static restoring forces separately for the positive and negative parts of a signal as

$$\mathrm{F_{el}} = \begin{cases} \omega_{\mathrm{cp}}^2 a_{\mathrm{cp}}, & x(t) \geq 0 \\ \omega_{cn}^2 a_{cn}, & x(t) < 0, \end{cases} \qquad \mathrm{F_d} = \begin{cases} 2\delta_{cp} a_{\dot{x}cp}, & x(t) \geq 0 \\ 2\delta_{cn} a_{\dot{x}cn}, & x(t) < 0, \end{cases} \tag{6.5}$$

where δ_{cp} and δ_{cn} are congruent damping rates estimated using Eq. (5.2) from the positive and negative part, respectively, and $a_{\dot{x}cn}$ and $a_{\dot{x}cn}$ are congruent amplitude of the positive and negative parts of the velocity, respectively. Although the damping was not considered in [73] it will be shown that it can be estimated using the HVD as well. It should be noted that for asymmetric resonant decay responses, the trend (aperiodic slowly varying component) should be excluded.

The modal frequency and damping obtained by the HVD are called congruent modal properties. The word "congruent" refers to the fact that these characteristics are obtained in line with the concept of phase congruency as the envelope of (signal) envelope or envelope of frequency [72, 73]. The term "congruent modal properties" would not be appropriate for the results of the ZCA as the concept of phase congruency is not directly applied. However, in order to distinguish the modal properties defined by the complex non-linear modes in section 4.2.1 from the modal properties obtained from the upper and lower part of the signal, the latter will be referred to as *pseudo-modal properties*. For the same reason, the terms "pseudo-backbones" and "pseudo-damping curves" will also be

used. Although the HVD and ZCA estimate pseudo-modal properties, both methods recover the initial non-linear restoring forces.

The Hilbert vibration decomposition determines the congruent backbones, damping curves, elastic and dissipative asymmetric non-linear restoring forces. However, it involves extensive signal processing which may be sensitive to measured noise and suffer from numerical issues of the Hilbert transform. The HVD used throughout this chapter as a reference method was computed by the code distributed alongside of [71][1]. It will be shown that the proposed method based on the zero-crossing method can estimate the vibration characteristics with higher accuracy while being less demanding in terms of signal processing.

6.3 A zero-crossing method for systems with asymmetric restoring forces

A straightforward, intuitive and easy to implement method, hereafter referred to as zero-crossing method for systems with asymmetric restoring forces (ZCA), is described in this section. The ZCA allows non-parametric identification of non-linear vibration systems with asymmetric non-linearities from a resonant decay response. The proposed method is an extension of the ZC methods described in section 3.3.6 and follows the same principal idea as the Hilbert vibration decomposition, i.e. by identifying the instantaneous frequency and amplitude of the upper and lower part of the signal individually, the vibration characterisations of the system can be obtained.

In line with the principal idea, the upper (in the following marked by subscript u) and lower (subscript l) parts of the signal are treated separately as indicated in Fig. 6.1 where t_u and t_l stand for the times of maxima and minima of the upper and lower part, respectively, and t_i marks the zero-crossing points. The IF of the upper and lower part are estimated as inverse values of the periods T_u and T_l from Fig. 6.1. The values of the IF are then assigned to the time of maxima or minima and marked as $f_\mathrm{u}(t_\mathrm{u})$ and $f_\mathrm{l}(t_\mathrm{l})$, respectively. The IA of the upper $a_\mathrm{u}(t_\mathrm{u})$ and lower $a_\mathrm{l}(t_\mathrm{l})$ part are given by the maxima and minima as indicated in Fig. 6.1. The procedure does not yield fully instantaneous results, i.e. $f_\mathrm{u}(t_\mathrm{u})$, $f_\mathrm{l}(t_\mathrm{l})$, $a_\mathrm{u}(t_\mathrm{u})$ and $a_\mathrm{l}(t_\mathrm{l})$ are not estimated for all time, but only at the times of maxima and minima. This resolution is, however, sufficient for reliable identification as demonstrated in section 6.4 and section 6.5.

[1] Available at http://ht.net.technion.ac.il/ (cited on 5 July 2017)

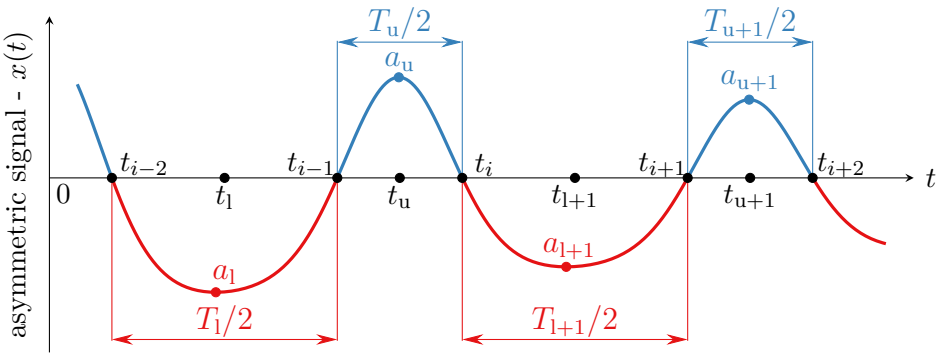

Figure 6.1 Zero-crossing method for non-linear vibration systems with asymmetric restoring forces

Two sets of values $[f_u, a_u]$ and $[f_l, a_l]$ (the time-dependency is dropped for brevity) can be recast into pseudo-modal properties. Similarly to the evaluation of modal properties in the Freevib algorithm [67] in section 5.2.2, it is assumed that the mode of interest can be described by the following general model with viscous damping

$$\ddot{x} + \underbrace{2\delta(\dot{x})\dot{x}}_{\mathrm{F_d}} + \underbrace{\omega_0(x)^2 x}_{\mathrm{F_{el}}} = 0, \tag{6.6}$$

where $\mathrm{F_{el}}$ is an elastic restoring force, $\mathrm{F_d}$ is a dissipative restoring force, δ is a damping rate and ω_0 is a modal angular frequency. Then, the angular pseudo-modal frequency can be evaluated separately for the upper and lower part as

$$\omega_{0u}^2(t) = \omega_u^2 - \frac{\ddot{a}_u}{a_u} + \frac{2\dot{a}_u^2}{a_u^2} + \frac{\dot{a}_u\dot{\omega}_u}{a\omega_u}, \qquad \omega_{0l}^2(t) = \omega_l^2 - \frac{\ddot{a}_l}{a_l} + \frac{2\dot{a}_l^2}{a_l^2} + \frac{\dot{a}_l\dot{\omega}_l}{a_l\omega_l} \tag{6.7}$$

with $\omega_u = 2\pi f_u$ and $\omega_l = 2\pi f_l$. If it is further assumed that the variation in the IF and IA is not significant, it is possible to neglect the second-order derivatives. This assumption is well justified while estimating the IF and IA using Fig. 6.1, because no intra-wave modulation can be captured. The angular pseudo-modal frequency of the upper and lower parts is then reduced to

$$\omega_{0u} \approx 2\pi f_u, \qquad \omega_{0l} \approx 2\pi f_l. \tag{6.8}$$

In the following, the subscript 0 is dropped and all frequencies are assumed to be pseudo-modal. The pseudo-modal damping rate of the upper and lower parts is given by

$$\delta_u(t_u) = -\frac{\dot{a}_u}{a_u} - \frac{\dot{\omega}_u}{2\omega_u}, \qquad \delta_l(t_l) = -\frac{\dot{a}_l}{a_l} - \frac{\dot{\omega}_l}{2\omega_l}, \tag{6.9}$$

where the first-order numerical derivatives must be evaluated numerically. Unfortunately, the numerical differentiation is often problematic and it can yield distorted results. This can be partly prevented by the use of sophisticated differentiation formulas, for instance, the central difference approximation of the fourth order was used in this thesis. However, in cases where linear behaviour in the damping can be assumed, the use of the logarithm of the amplitude from Eq. (5.3) should be preferred as it is often more robust against the measured noise [142, 208].

Having estimated pseudo-modal frequency and pseudo-modal damping, the elastic $\mathrm{F_{el}}$ and dissipative $\mathrm{F_d}$ restoring forces can be calculated using

$$\mathrm{F_{el}} = \begin{cases} 4\pi^2 f_\mathrm{u}^2 a_\mathrm{u}, & x(t) \geq 0 \\ 4\pi^2 f_\mathrm{l}^2 a_\mathrm{l}, & x(t) < 0, \end{cases} \qquad \mathrm{F_d} = \begin{cases} 2\delta_\mathrm{u} a_{\dot{x}\mathrm{u}}, & x(t) \geq 0 \\ 2\delta_\mathrm{l} a_{\dot{x}\mathrm{l}}, & x(t) < 0, \end{cases} \tag{6.10}$$

where $a_{\dot{x}u}$ and $a_{\dot{x}l}$ are the maxima and minima of velocity. Equation (6.10) is generally valid for all common types of non-linearities and its apparent simplicity neither prevents, nor limits the identification of the original restoring forces.

All results obtained by the proposed method closely correspond to those obtained by the HVD, because the HVD and ZCA share the same underlying idea. In addition, the identification of damping and restoring forces is governed by the same equations. The key difference is that the IF and IA from the upper and lower part used in Eq. (6.10) are replaced by positive and negative congruent characteristics in Eq. (6.5).

Although the two methods can theoretically reach the same accuracy, the results of the ZCA are obtained with much less effort in contrast to the HVD. There is no complicated decomposition or filtering required so the method is straightforward to implement. Moreover, the ZCA should be less sensitive to measured noise due to the use of maxima, minima and zero-crossing points only. As long as these points are well estimated, the noise in the rest of the signal does not have any effect on the estimated results. In order to estimate zero-crossing points of a noisy signal, a local smoothing [142] or interpolation [207] around zero-crossing points may be used. Furthermore, similarly to the zero-crossing method proposed in [208] and described in section 3.3.6, a sensitivity of the ZCA to measured noise may be improved by averaging of the frequencies and amplitudes over the intervals in which neglectful changes of the IF and IA are assumed. Although some information may be lost due to the averaging, the results are much smoother, allowing better visualisation and interpretation. This averaging capability is shown in section 6.5 for the experimental data. In general, a range of standard tools for de-noising of the signal may be used, one of which, the Whittaker smoother described in

appendix C, has also been used in this thesis. The use of the Whittaker smoother was mainly required to allow a reliable comparison between the ZCA and HVD.

The pseudo-modal frequency, pseudo-modal damping and restoring forces are obtained in a non-parametric manner, i.e. no specific model of the structure is needed and only a general governing equation (Eq. (6.6)) is assumed. If the proposed method is applied to a system with symmetric restoring forces, the identified characteristics for the upper and lower parts will be the same and they will correspond to the results obtained by zero-crossing methods [173]. The shape of the pseudo-backbones, pseudo-damping curves and restoring forces can be used for detection and characterisation of non-linearities as well. If these backbones and damping curves are straight lines and the same for the upper and lower parts of the signal, the system is linear. If there is any significant deviation from the constant values and/or the characteristics are not the same for the upper and lower part, the system is non-linear. Furthermore, the shape of pseudo-backbones, pseudo-damping curves and restoring forces is unique for common types of non-linearities as evidenced in section 6.4. Therefore, the shape can help to deduce the type and the mathematical expression of the non-linearity. This expression can then be fitted to restoring forces to obtain the coefficients of non-linearities.

The ZCA can be applied to any resonant decay response which may be described by Eq. (6.6). Such resonant decay response can be either measured from a SDOF system or using a phase resonance method (also known as force appropriation) [59, 191, 291].

6.4 Application to simulated data

To demonstrate the validity of the ZCA, it is applied to three numerical examples in this section, namely to the systems with bilinear stiffness, off-centre clearance (backlash), and quadratic stiffness. The corresponding non-linear restoring forces are drawn in Fig. 6.2. These three cases are described here to show the capabilities of the ZCA and allow its detailed comparison with the HVD.

In each case, the resonant decay response was simulated by the numerical integration. For the piece-wise characteristics, i.e. bilinear stiffness and off-centre clearance, a special integration scheme had to be implemented [290]. A sampling frequency was fifty times higher than the expected natural frequency. This value of sampling frequency is in line with the recommendations given in [71, 72] for the HVD which requires the sampling frequency to be twenty to eighty times higher than the highest frequency of interest. By using this high sampling frequency, some of the possible signal processing problems in the HVD were prevented and a reliable comparison with the ZCA therefore allowed.

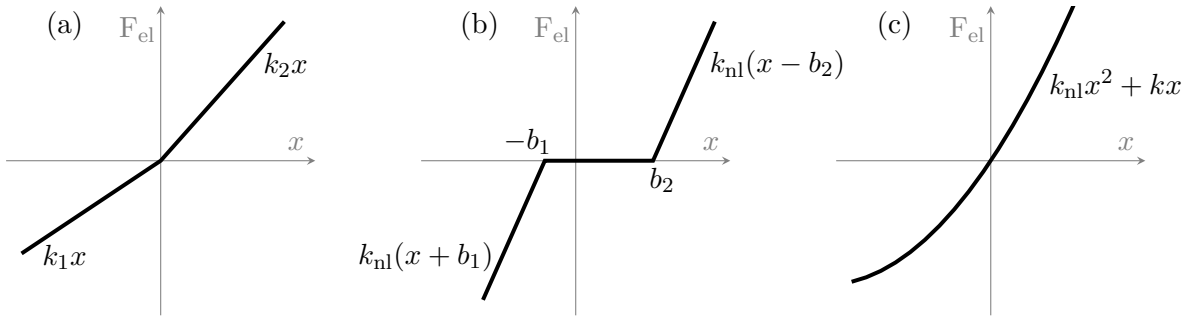

Figure 6.2 Asymmetric non-linear restoring forces of simulated systems: (a) bilinear stiffness, (b) off-centre clearance, and (c) quadratic stiffness

Before applying the ZCA and HVD, the response was polluted by white Gaussian noise with signal-to-noise ratio 25 dB to make the data more realistic. Although some amount of noise in the data does not prevent either of the methods to estimate the IF and IA, it was decided to apply to the Whittaker smoother before applying the methods. Without this initial smoothing, the results obtained by the HVD and pseudo-modal damping obtained by the ZCA according to Eq. (6.9) were very distorted. As a consequence, no reliable comparison of the methods was possible in that case.

6.4.1 A system with bilinear stiffness

The system is governed by

$$m\ddot{x}(t) + c\dot{x}(t) + f_{\mathrm{nl}}(x) = 0, \quad f_{\mathrm{nl}}(x) = \begin{cases} k_1, & x(t) \leq 0 \\ k_2, & x(t) > 0, \end{cases} \tag{6.11}$$

where $m = 1\,\mathrm{kg}$ and $c = 0.2\,\mathrm{N\,s\,m^{-1}}$. The non-linear elastic restoring force $f_{\mathrm{nl}}(x)$ is shown in Fig. 6.2(a) and its coefficients are $k_1 = (2\pi 2)^2 \approx 157.9\,\mathrm{N\,m^{-1}}$ and $k_2 = (2\pi 4)^2 \approx 631.7\,\mathrm{N\,m^{-1}}$. These stiffness values were chosen so that the pseudo-modal frequencies of the upper and lower parts are 2 Hz and 4 Hz, respectively. The initial conditions were $x(0) = 5\,\mathrm{m}$ and $\dot{x}(0) = 0\,\mathrm{m\,s^{-1}}$, sampling frequency $f_{\mathrm{s}} = 200\,\mathrm{Hz}$, and the response was simulated for time $t = 0 - 25\,\mathrm{s}$. The large initial displacement was selected to emphasise the effect of the non-linearity. The displacement of 5 m is not common, but the validity of the results is not corrupted by this choice. These parameters and the initial conditions were chosen to allow reliable demonstration of the proposed method and its comparison with the HVD.

The noisy resonant decay response was processed using the Whittaker smoother. The smoothing parameter was automatically determined by a leave-one-out strategy (see

appendix C). The original and smoothed signals are shown in Fig. 6.3(a). It can be seen

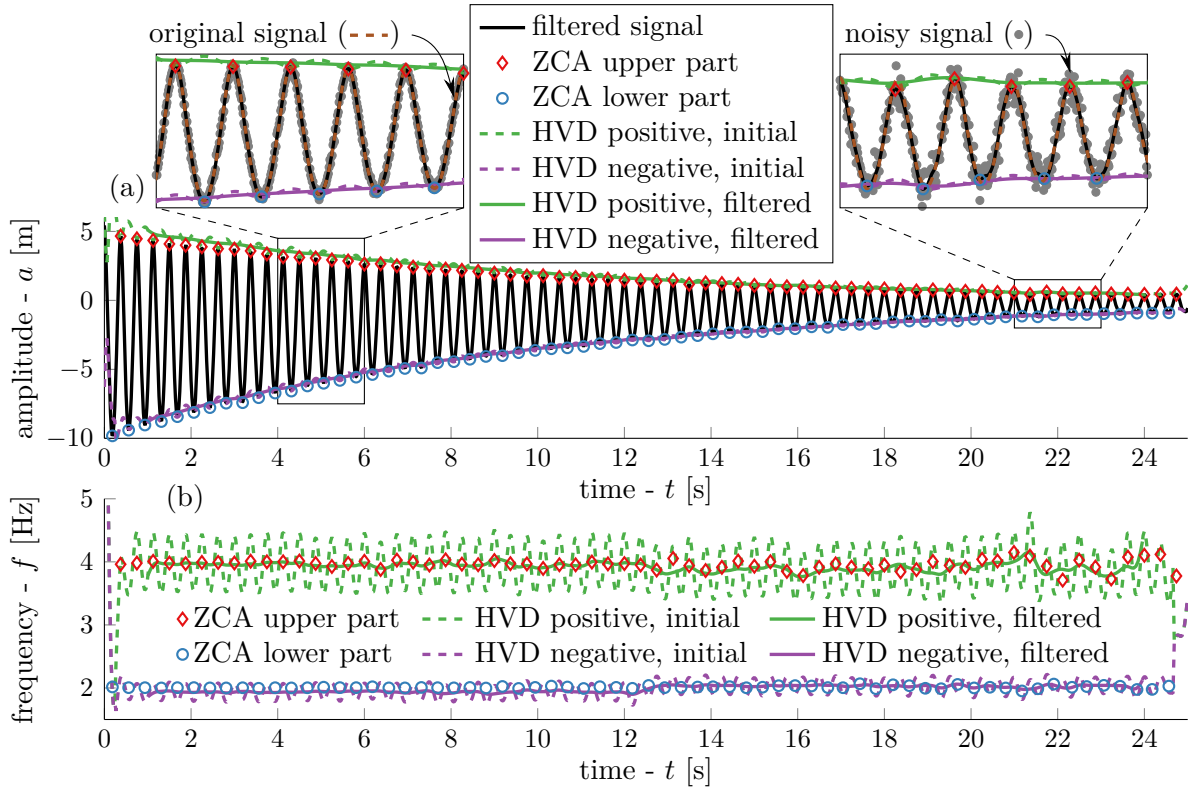

Figure 6.3 Bilinear stiffness: (a) resonant decay response with instantaneous amplitude and (b) instantaneous frequency

that despite a significant level of noise, especially in a region of lower amplitudes, the Whittaker smoother was able to achieve reasonably smooth and accurate approximation of the original signal. However, some inaccuracies in extreme amplitudes can still be observed in the region of lower amplitudes as seen in the right inset in Fig. 6.3(a).

The resonant decay response is not symmetric with respect to the time axis. Although the initial displacement was $x(0) = 5\,\mathrm{m}$, the minimum value of displacement is almost 10 m. This increase in the absolute amplitude is given by the significantly lower stiffness k_1 for $x \leq 0$.

The ZCA and HVD were applied to the smoothed signal. The resulting IA is displayed in Fig. 6.3(a). The IA estimated using the ZCA corresponds by definition to the maxima (minima) of the signal. The HVD did not initially produce the smooth estimate of the IA. However, after additional low-pass filtering the IA was also obtained with good accuracy. This IA is relatively smooth and encloses the signal closely.

The IF estimated using the ZCA and HVD is shown in Fig. 6.3(b). These frequencies are the pseudo-modal frequencies defined by Eq. (6.4) and Eq. (6.8). The two estimated

frequencies are in line with Eq. (6.11) which, if treated piece-wise, describes two linear systems with different natural frequencies of 2 Hz and 4 Hz. The ZCA was able to estimate both of these frequencies correctly. Some small discrepancies can be observed close to the end of the signal ($t > 20$ s) where the smoothing of the original noisy signal is not as good as at the beginning (see the insets in Fig. 6.3(a)). The HVD produced two fluctuating IF so they had to be again smoothed using a low-pass filter and the ends excluded to obtain the desired estimates.

The estimated pseudo-backbones of the system are shown in Fig. 6.4(a). For the sake

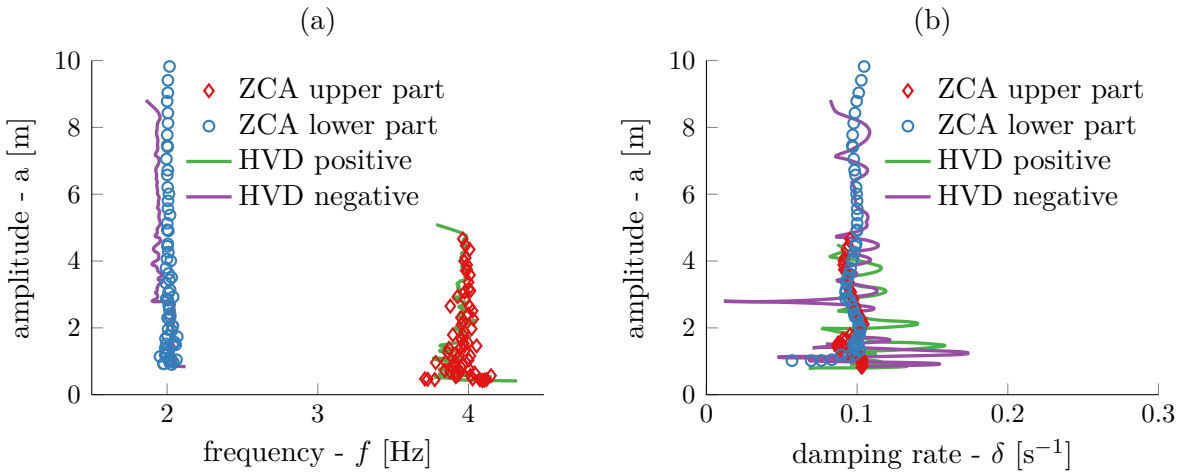

Figure 6.4 Bilinear stiffness: (a) pseudo-backbone and (b) pseudo-damping curve

of clarity, the raw (without smoothing) results of the HVD are not shown. The two clearly separated pseudo-backbones centred around 2 Hz and 4 Hz can be seen. The difference between the ZCA and the smoothed HVD results is minimal. Both pseudo-backbones are only slightly influenced by residual noise. On the other hand, the distortion of the estimated pseudo-damping curves in Fig. 6.4(b) is more significant despite the additional smoothing. This highlights the problems with the numerical differentiation in Eq. (6.8). Due to residual noise, the estimated amplitudes are not perfectly smooth decreasing functions so the numerical derivative cannot be estimated accurately. The ZCA is less influenced because it uses fewer amplitude points. Nevertheless, despite this distortion the values of the estimated damping rate are centred around the correct value of $0.1\,\mathrm{s}^{-1}$.

The estimated elastic restoring forces are shown in Fig. 6.5(a). Similarly to the pseudo-backbones, the qualitative difference between the two methods is minimal. Both of them led to visually smooth elastic restoring forces that correspond to the original restoring force given by Eq. (6.11). The estimated dissipative restoring forces shown in Fig. 6.5(b)

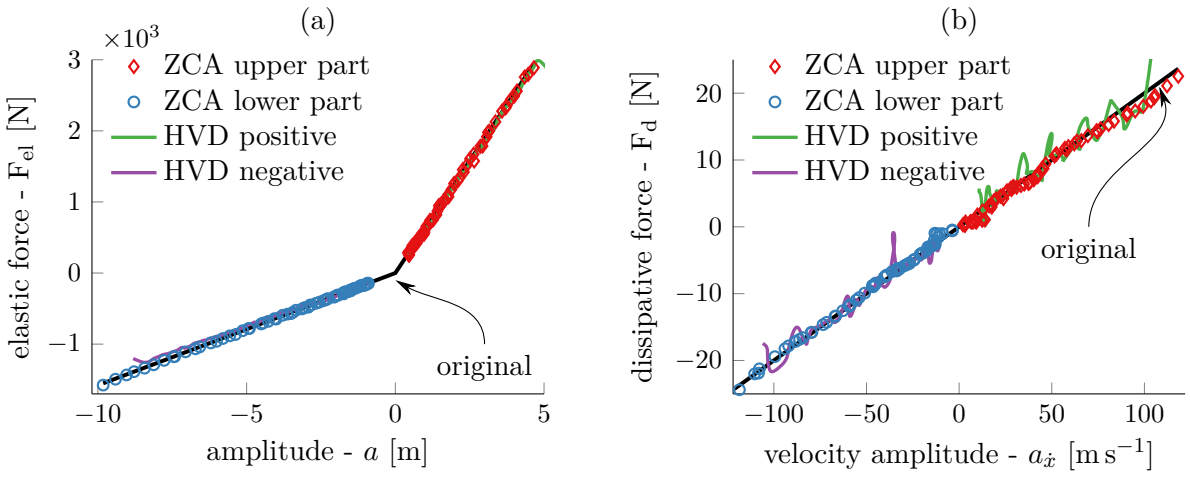

Figure 6.5 Bilinear stiffness: (a) elastic and (b) dissipative restoring forces

correspond to the original one as well. However, similarly to the pseudo-damping curves, they are influenced by residual noise.

The detection and characterisation of non-linearity are possible using the pseudo-backbones and pseudo-damping curves as well as the restoring forces. The two pseudo-backbone curves in Fig. 6.4(a) are straight lines, but on different frequencies. This is a clear indication that the dynamics of the system is different for the upper and lower part of the signal. Based on this finding the bilinear stiffness model can be deduced. In contrast, the pseudo-damping curves in Fig. 6.4(b) are straight, but on the same amplitude. Therefore, no non-linearity in damping is indicated.

The estimated restoring forces in Fig. 6.5 describe directly the non-linear phenomena of the system. Therefore, an appropriate model can be easily selected and fitted to these forces. The bilinear stiffness coefficients and damping coefficients were found by the fitting of the elastic and dissipative forces, respectively. The results are summarised in Tab. 6.1 in which the relative errors of the estimated coefficients are written in parentheses. The

Method	k_1 [N m^{-1}]	k_2 [N m^{-1}]	c [N s m^{-1}]
original	157.9	631.7	0.2
ZCA	158.30 (0.24 %)	629.79 (−0.29 %)	0.19 (−3.26 %)
HVD	143.75 (−9.85 %)	624.75 (−1.11 %)	0.20 (1.05 %)

Table 6.1 The estimated coefficients of the system with bilinear stiffness (the values in parentheses are the relative errors (in %) between the estimated and original coefficients)

bilinear stiffness coefficients were estimated by the ZCA extremely accurately, having

the error less than 0.5 %. The HVD also estimated the stiffness coefficients quite well, but with slightly lower accuracy than the ZCA with the largest error being close to 10 %. The damping coefficients were estimated by both methods accurately. Again, the ZCA produced slightly higher relative error than the HVD.

Based on the result presented so far it can be stated that the ZCA can obtain the equivalent results with similar or better accuracy compared to the HVD. It is important to note that the HVD required more sophisticated signal processing and additional filtering. Therefore, the ZCA generally needs less effort to achieve the same results. In addition, the detection and characterisation may be generally clearer while using the ZCA, because the measured noise does not influence the results as much as in the HVD.

6.4.2 A system with off-centre clearance

The system is governed by

$$m\ddot{x}(t) + c\dot{x}(t) + kx(t) + f_{\mathrm{nl}}(x) = 0, \tag{6.12}$$

where $m = 1\,\mathrm{kg}$, $c = 0.8\,\mathrm{N\,s\,m^{-1}}$, and $k = (2\pi)^2 \approx 39.5\,\mathrm{N\,m^{-1}}$. The off-centre clearance $f_{\mathrm{nl}}(x)$ is shown in Fig. 6.2(b) and it is described by

$$f_{\mathrm{nl}}(x) = \begin{cases} k_{\mathrm{nl}}(x(t) + b_1), & x(t) < -x_1 \\ 0, & -x_1 \leq x(t) \leq x_2 \\ k_{\mathrm{nl}}(x(t) - b_2), & x > x_2, \end{cases} \tag{6.13}$$

where the off-centre clearance stiffness coefficient was $k_{\mathrm{nl}} = 6000\,\mathrm{N\,m^{-1}}$ and the thresholds of the clearance described by the constants b_1 and b_2 were chosen to be 0.02 m and 0.05 m, respectively. The initial conditions were $x(0) = 0.1\,\mathrm{m}$ and $\dot{x}(0) = 0\,\mathrm{m\,s^{-1}}$, sampling frequency $f_{\mathrm{s}} = 500\,\mathrm{Hz}$ and the response was simulated for time $t = 0 - 10\,\mathrm{s}$. The computed response was again polluted by white noise to simulate more realistic data.

The noisy response was processed using the Whittaker smoother. As the signal is significantly different at the beginning and the end of the time interval, the first ($t \leq 4.5\,\mathrm{s}$) and second parts ($t > 4.5\,\mathrm{s}$) were smoothed separately to improve the performance of the smoother. The smoothing parameter was determined for each part separately using a leave-one-out validation strategy. The performance of the smoother was very similar to the case of bilinear stiffness so only the smoothed signals are shown in Fig. 6.6(a). It can be seen that the signal is not only asymmetric, but also significantly different in frequencies at the beginning and the end. The frequency at the beginning is very high

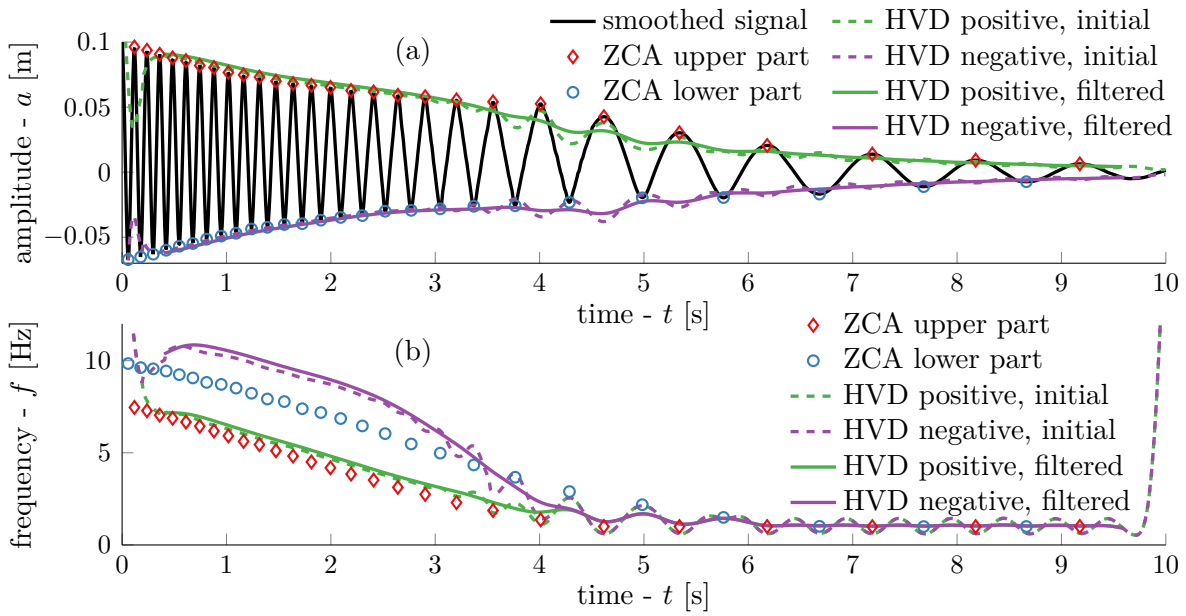

Figure 6.6 Off-centre clearance stiffness: (a) resonant decay response with instantaneous amplitude and (b) instantaneous frequency

due to the presence of the high stiffness caused by the off-centre clearance. In contrast, the frequency at the end of the free decay is very low due to the low stiffness of the underlying linear system.

The ZCA and HVD were applied to the smoothed signal. The resulting IA is shown in Fig. 6.6(a). As for the system with bilinear stiffness, the HVD did not initially produce the smooth estimate of the IA. Therefore, additional smoothing was needed and the end effects had to be excluded. Despite this smoothing, the envelope was badly estimated around the thresholds of the clearance between 4 and 5 s. On the other hand, the ZCA led to accurate estimate of the IA.

The estimated pseudo-modal frequency is shown in Fig. 6.6(b). It can be seen that two different frequencies were estimated in the first half of the time interval. These frequencies are higher at the beginning and merge into a single frequency for lower amplitudes. Unlike for the system with bilinear stiffness, significant differences in the IF occurred between the ZCA and HVD results. Overall, the latter is not so smooth despite the additional smoothing. Nevertheless, both methods were able to estimate the natural frequency of the linear system in the second half of the time interval ($t > 5$ s) correctly.

The estimated pseudo-backbone of the system is shown in Fig. 6.7(a). For the sake of clarity, the initial (without smoothing) results of the HVD are not shown. It can be seen that two pseudo-backbones were estimated by each method. They both start on

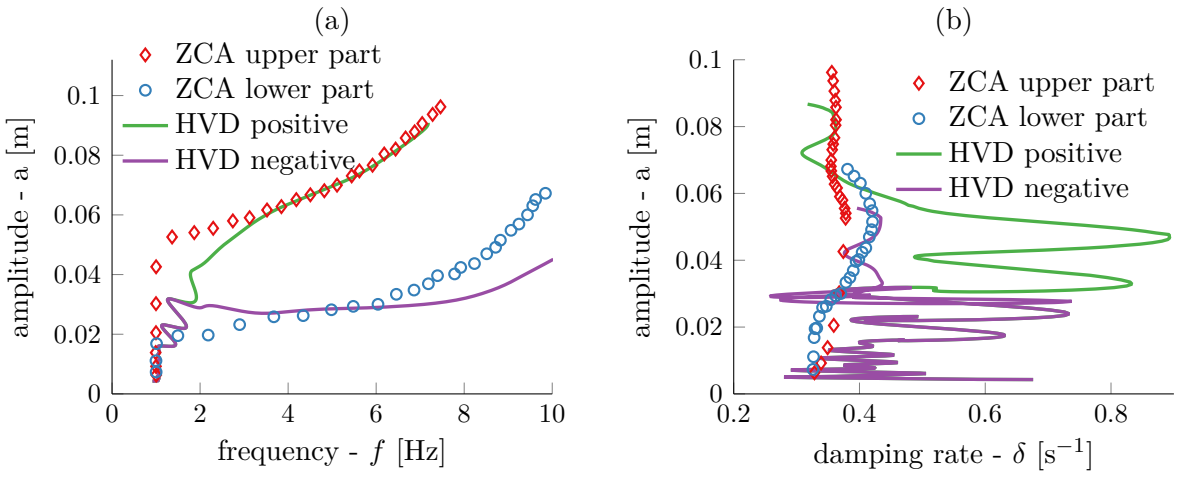

Figure 6.7 Off-centre clearance stiffness: (a) pseudo-backbone and (b) pseudo-damping curve

the natural frequency of the underlying linear system and bend to the right at higher amplitude. The HVD did not estimate the region between linear and non-linear behaviour (for amplitudes $a \in (0.02, 0.05)$m) as well as the ZCA. The thresholds of the off-centre clearance can be clearly determined from the pseudo-backbones estimated by the ZCA whereas they are indistinguishable for the HVD. In addition, the pseudo-backbone for the negative part estimated using the HVD has significantly different slope at higher amplitudes.

The pseudo-damping curves are shown in Fig. 6.7(b). They are not so smooth as the pseudo-backbones due to the numerical derivative used in Eq. (6.9). As for the system with bilinear stiffness, the ZCA appears to estimate smoother characteristics. The pseudo-damping curves estimated by the ZCA are much closer to the correct value of $0.4\,\mathrm{s}^{-1}$ than those estimated by the HVD.

The non-linear elastic restoring force is shown in Fig. 6.8(a). As can be seen, both methods follow the original characteristics qualitatively quite well. Three piece-wise linear regions can be clearly distinguished. From these non-linear restoring forces, the thresholds of non-linearities can be easily established. On the other hand, neither of the method was able to estimate the upper part of clearance stiffness correctly.

The estimated dissipative restoring forces are shown in Fig. 6.8(b). Again, both methods seem to follow the original force quantitatively very well. However, in order to obtain this characteristics by the HVD the end effects were removed.

The detection and characterisation of non-linearity are possible using the pseudo-backbones and pseudo-damping curves as well as the restoring forces. The two pseudo-backbone curves in Fig. 6.7(a) are straight for low amplitudes and bend to the right at

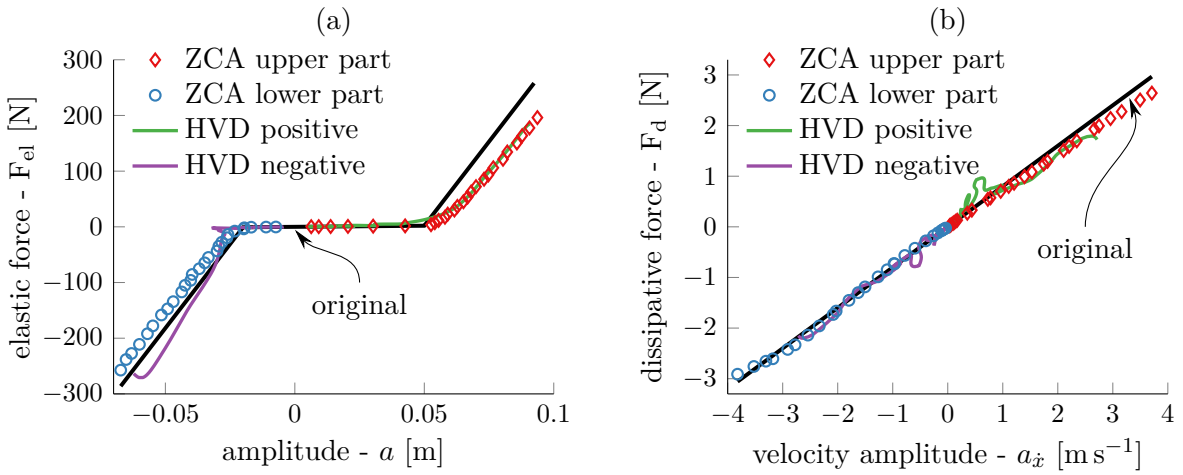

Figure 6.8 Off-centre clearance stiffness: (a) estimated elastic and (b) dissipative restoring forces

higher amplitude. Moreover, each of them divide from the straight line at a different amplitude. This is a clear indication that the dynamics of the system is different for the upper and lower part of the signal. Moreover, piece-wise behaviour can be deduced from these pseudo-backbones. The pseudo-damping curves in Fig. 6.7(b) are not so smooth as the pseudo-backbones, but it is still possible to deduce that they are essentially straight lines. Therefore, there is no non-linearity in damping. The detection and characterisation may be generally clearer while using the ZCA, because the measured noise does not influence the results as much as in the HVD. For example, from the pseudo-damping curves it could wrongly assume that the results of the HVD indicate hardening behaviour in the damping.

The estimated restoring forces in Fig. 6.8 describe directly the non-linear phenomena of the system. Therefore, an appropriate model can be easily selected and fitted to these forces. By doing so, the system if fully qualified. So the off-centre clearance stiffness coefficients and damping coefficients were found by the fitting of the elastic and dissipative forces, respectively. The results are summarised in Tab. 6.2 in which the relative errors of the estimated coefficients are written in parentheses. To avoid significant errors, points around the threshold (corresponding to the amplitude $a \in (-0.3, -0.1) \cup (0.4, 0.6)$) were excluded from the fitting. The upper and lower parts were fitted separately, yielding $k_{\mathrm{nl}}^{(l)}$ and $k_{\mathrm{nl}}^{(u)}$, respectively. In almost all cases the ZCA led to more accurate estimates. The largest error of 15 % was obtained for the non-linear stiffness coefficients of the upper part. In contrast, the largest errors of the HVD was more than 50 %. The ZCA also yielded a slightly better estimates of damping. As for the system with bilinear stiffness,

Method	$k_{\mathrm{nl}}^{(l)}$ [N m^{-1}]	$k_{\mathrm{nl}}^{(u)}$ [N m^{-1}]	k [N m^{-1}]	c [N s m^{-1}]
original	6000	6000	39.5	0.8
ZCA	5795.16 (-3.53)	5194.66 (-15.50)	39.58 (-0.31)	0.76 (-4.83)
HVD	8079.09 (25.73)	5349.13 (-12.17)	86.64 (54.43)	0.75 (-6.25)

Table 6.2 Identified coefficients of the off-centre clearance (the values in parentheses are the relative errors between the estimated and original coefficients)

the results indicate that the ZCA can obtain the same results with similar or better accuracy than the HVD while requiring less effort for signal processing and additional smoothing.

6.4.3 A system with quadratic stiffness

This testing case is described here to not only support the relevance of the ZCA, but to also allow better evaluation of the experimental findings in section 6.5. The same system was used in section 3.4.2 to demonstrate the application of the method for intra-wave frequency modulation estimation. The system with quadratic stiffness is governed by

$$m\ddot{x}(t) + c\dot{x}(t) + kx(t) + k_{\mathrm{nl}}x^2(t) = 0, \tag{6.14}$$

where $m = 1\,\mathrm{kg}$, $c = 0.1\,\mathrm{N\,s\,m^{-1}}$, and $k = (2\pi)^2 \approx 39.5\,\mathrm{N\,m^{-1}}$. The non-linear restoring force is shown in Fig. 6.2(c) and its coefficient is $k_{\mathrm{nl}} = 3\,\mathrm{N\,m^{-2}}$. The initial conditions were $x(0) = 5\,\mathrm{m}$ and $\dot{x}(0) = 0\,\mathrm{m\,s^{-1}}$, sampling frequency $f_{\mathrm{s}} = 50\,\mathrm{Hz}$ and the response was simulated for time $t = 0 - 50\,\mathrm{s}$. The large initial displacement has been chosen to allow reliable demonstration of the proposed method and its comparison with the HVD. The choice of the system parameters does not corrupt the validity of the results. The computed resonant decay response was again polluted by white Gaussian noise to simulate more realistic measured data.

The noisy free decay was processed using the Whittaker smoother with the smoothing parameter evaluated by the leave-one-out procedure. The performance of the smoother was very similar to the case of bilinear stiffness so only the smoothed signals shown in Fig. 6.9(a). It can be seen that the nature of this signal is different than in the two previous cases. This free decay does not have any regions of significantly higher frequencies or significantly different amplitudes of the upper and lower parts. The asymmetry is not so apparent so the signal overall appears to be a free decay of a linear

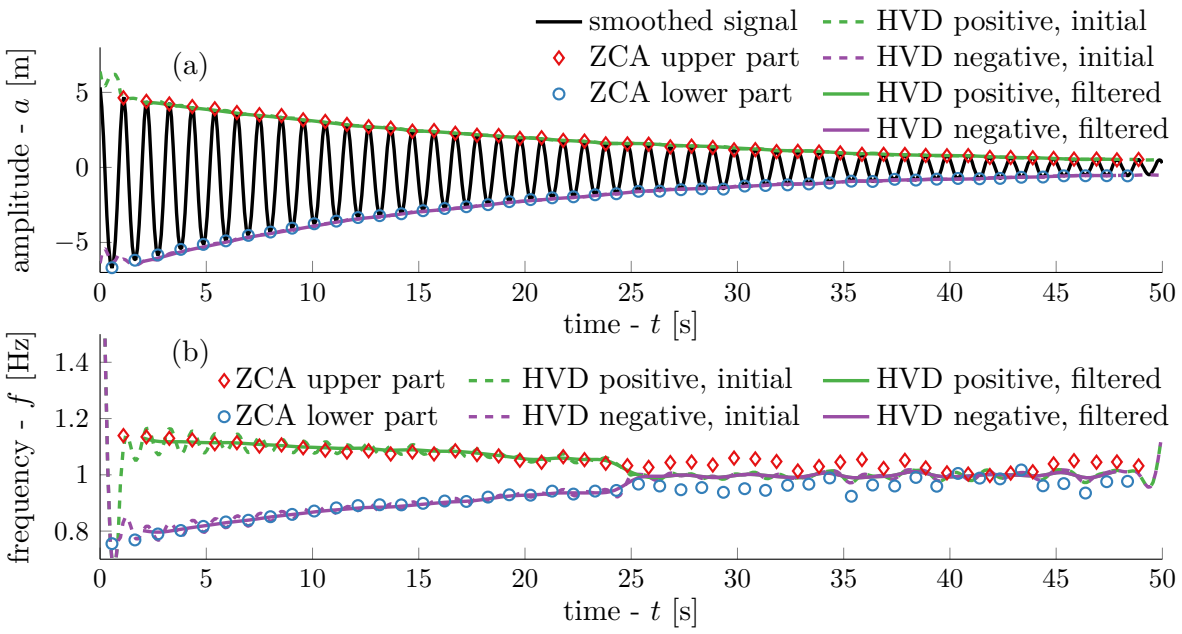

Figure 6.9 Quadratic stiffness: (a) resonant decay response with instantaneous amplitude and (b) instantaneous frequency

SDOF system. In addition, the non-linearity in Eq. (6.14) is smooth whereas the previous non-linearities were piece-wise linear.

The ZCA and HVD were applied to the smoothed signal. The resulting IA is shown is Fig. 6.9(a). It can be seen that the IA estimated using the HVD did not require so strong additional smoothing, but the end effects had to be again removed.

The IF estimated using the ZCA and HVD are shown in Fig. 6.9(b). These two frequencies can be again regarded as pseudo-modal. It can be seen that at the beginning of the signal, two different frequencies were estimated using both methods. Towards the end ($t > 25$) these two frequencies merge for the HVD and stay very close to each other in case of the ZCA. The value of the frequency towards the end of the time interval corresponds to the natural frequency of the underlying linear system. One of the frequencies at the beginning is higher than the natural frequency and the other one is lower, indicating hardening and softening behaviour, respectively. This is in line with the quadratic restoring forces in Fig. 6.2(c).

The pseudo-backbones are shown in Fig. 6.10(a). For the sake of clarity, only the smoothed results of the HVD are shown. Two pseudo-backbones were estimated, corresponding to the softening and hardening behaviour. The results of both methods correspond very well at higher amplitudes ($a > 2\,\mathrm{m}$). In contrast, a single value of the backbones, indicating linear behaviour, was estimated using the HVD at low amplitudes,

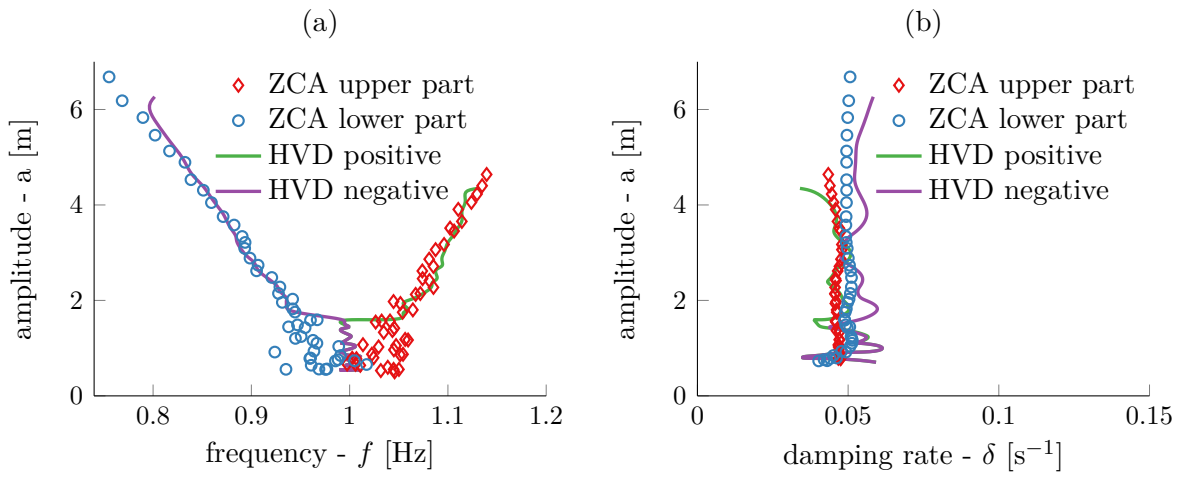

Figure 6.10 Quadratic stiffness: (a) pseudo-backbones and (b) pseudo-damping curve

while the ZCA estimated two separated backbones, albeit slightly distorted and close to each other, at this amplitude level. This finding indicates that the ZCA might be able to qualitatively distinguish weaker non-linear behaviour better than the HVD.

The pseudo-damping curves are shown in Fig. 6.10(b). In this case, both methods were able to produce good estimates although the residual noise still influences the smoothness of the results. Both pseudo-damping curves are close to the correct value of $0.05\,\mathrm{s}^{-1}$.

The elastic and dissipative restoring forces are shown in Fig. 6.11. It can be seen

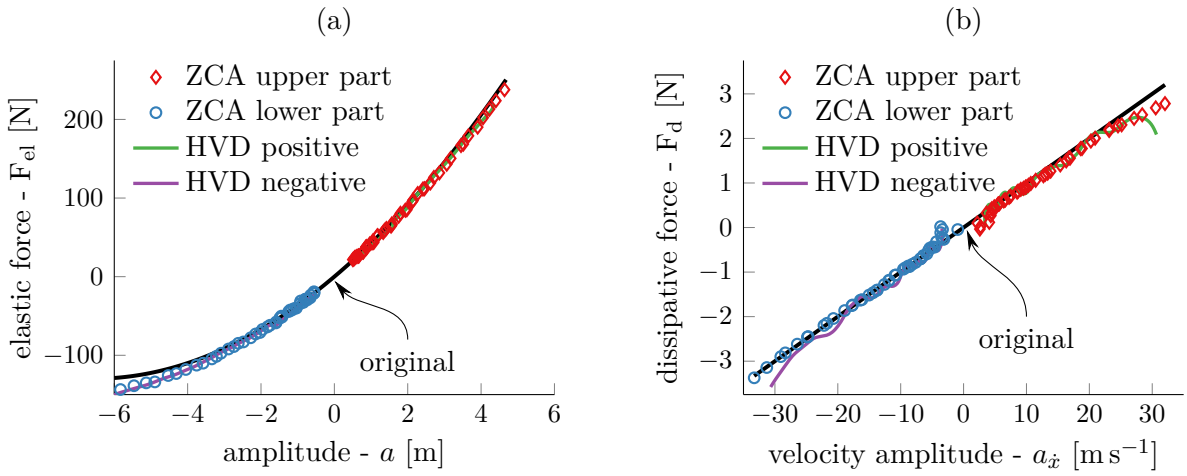

Figure 6.11 Quadratic stiffness: (a) elastic and (b) dissipative restoring forces

that the difference between the methods is minimal. Neither of them was however able to estimate the elastic force very accurately. Although the elastic force is estimated

qualitatively quite well, the absolute values, especially for lower part of the signal, are different.

Again, the detection and characterisation of non-linearity are possible using the pseudo-backbones and pseudo-damping curves as well as the restoring forces. The two pseudo-backbone curves in Fig. 6.10(a) are not straight lines, which immediately eliminates the possibility of the linear system. Moreover, one of them indicates softening and the other hardening behaviour. From these findings, the quadratic stiffness can be deduced. The pseudo-damping curves in Fig. 6.10(b) are straight lines centred around one value. Therefore, there is no non-linearity in damping. In this case, the detection and characterisation are not influenced by the residua noise so much.

The coefficients of the quadratic k_{nl} and linear k stiffness and damping c were found using the fitting of the elastic and dissipative restoring forces. Their determined values are tabulated in Tab. 6.3 with their relative errors in the parentheses. It can be seen from the

Method	$\gamma\,[\mathrm{N\,m^{-2}}]$	$k\,[\mathrm{N\,m^{-1}}]$	$c\,[\mathrm{N\,s\,m^{-1}}]$
original	3	39.5	0.1
ZCA	2.54 (-17.92)	39.43 (-0.11)	0.095 (-4.88)
HVD	2.57 (-16.69)	39.65 (0.43)	0.098 (-1.26)

Table 6.3 Identified coefficients of the quadratic stiffness (the values in parentheses are the relative errors between the estimated and original coefficients)

presented results that both methods were able to estimate the qualitative characteristics very well. In this testing case the accuracy of the ZCA and HVD was almost identical. However, it appears that the ZCA was able to correctly describe non-linear behaviour at lower frequency where the HVD misleadingly identified linear behaviour.

6.4.4 Summary of the application to simulated data

The results obtained by the proposed ZCA have been compared with the results estimated by the HVD. Although the results varied for each simulated case, the proposed ZCA generally estimated the coefficients of non-linearities with higher accuracy. For the system with the bilinear stiffness the ZCA estimated the coefficients with less than 1 % relative error whereas and the HVD obtained the same coefficients with the relative error of almost 10 %. In the case of the off-centre stiffness the difference was even more dramatic. While the ZCA estimated the non-linear coefficients with the maximum relative error of 10 %, the coefficients estimated by the HVD were up to 50 % higher than the correct values. In the third case, in which quadratic stiffness was used, the accuracy of both

methods was almost the same. However, the ZCA was able to qualitatively identify non-linear behaviour even at low amplitudes where the HVD misleadingly indicated linear behaviour (see Fig. 6.10(a)). Based on the investigated simulated cases it can be concluded that the ZCA can identify the coefficients of asymmetric restoring forces with higher accuracy. It may also qualitatively describe weaker non-linearity better than the HVD. Overall, with regards to sophisticated signal processing and the need for additional smoothing in the HVD, the ZCA seems to provide at least the same or better results with much less effort.

6.5 Application to experimental data from a micro-electro-mechanical system

To demonstrate the capabilities of the ZCA, it is used for the identification of elastic and dissipative non-linearities in a double-anchored double-ended-tuning-fork micro-electro-mechanical (MEMS) resonator. The resonator was developed and tested, and the data were kindly provided by Stanford University [206–208, 298]. The resonator, which was designed for time-keeping applications, consists of two micro-mechanical beams (200 µm long, 6 µm wide and 40 µm thick) that are connected on both ends to perforated masses, which are attached to the base. In order to obtain the resonant decay response (ring-down) data, the phase resonance testing was used. The system was driven into the non-linear resonant regime and, once the system reached its steady-state response at a specific amplitude and frequency, the external forcing was turned off and the transient ring-down response recorded. More information about the micro-electro-mechanical resonator and measurement set-up can be found in [206–208, 298].

The voltage linearly proportional to the displacement was measured and the resonant decay acquired with the sampling frequency of $f_s = 50\,\mathrm{MHz}$ for three levels of excitation, leading to maximum initial amplitudes of $a_0 = 125\,\mathrm{mV}$, $165\,\mathrm{mV}$, and $225\,\mathrm{mV}$. The application of the ZCA is shown in detail for $a_0 = 165\,\mathrm{mV}$ and only the most significant results of the two other cases are presented. The data are significantly different than the simulated cases in terms of time and frequency scales. The simulated cases had their pseudo-modal frequencies in order of several hertz, the frequency of the MEMS resonant is in order of megahertz. However, it will be shown that the ZCA can be reliably applied in this case too.

To allow a reliable comparison of the ZCA with the HVD, the Whittaker smoother was used to reduce measured noise. The resulting resonant decay response shown in Fig. 6.12(a) appears to be almost symmetric with respect to the time axis. This apparent

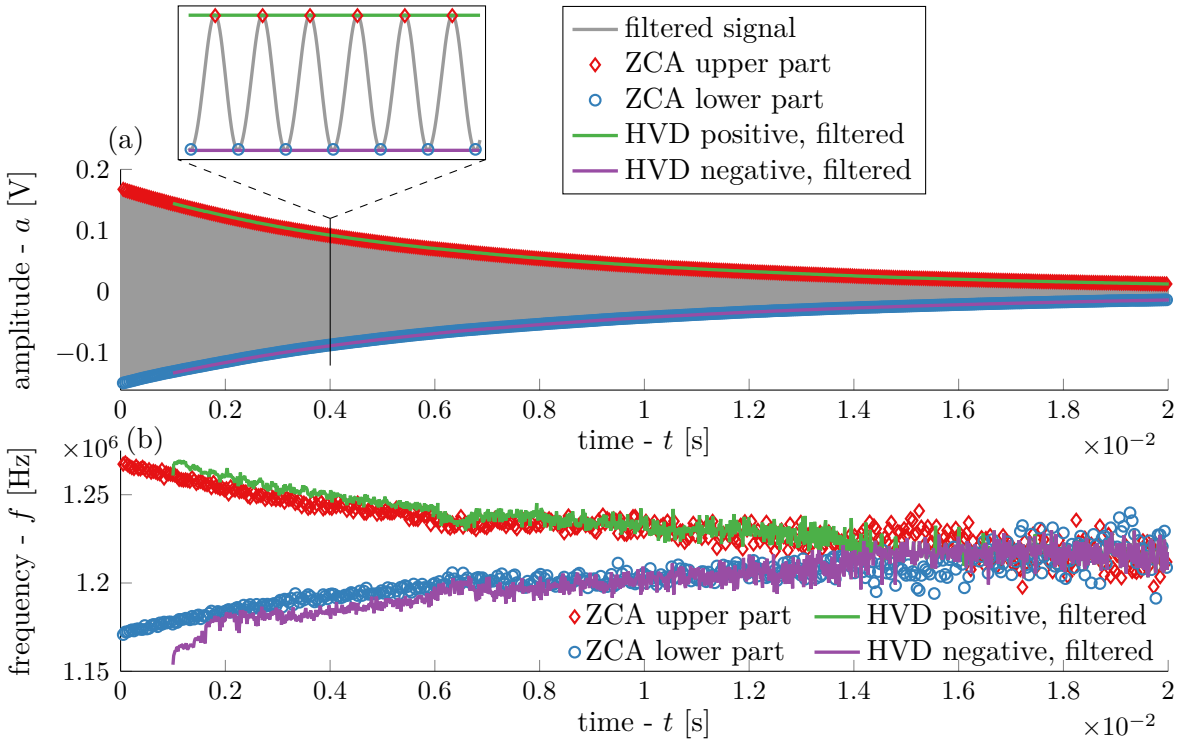

Figure 6.12 Micro-electro-mechanical resonator: (a) ring-down response with instantaneous amplitude and (b) instantaneous frequency

symmetry led to the assumption of symmetric restoring forces and the development of a non-linear vibration model for this MEMS resonator in [206–208]. However, after a closer examination of the free decay in Fig. 6.12(a) and the other two cases for the different initial amplitudes (not shown here), it was observed that some asymmetry exists in the data. This observed asymmetry suggested that the restoring forces might be asymmetric. The presence of the asymmetry was also confirmed by the restoring force surface method in [173]. This asymmetry is more significant at higher amplitudes and almost disappears at lower amplitudes of vibration. The fact that the asymmetry disappears at low amplitudes indicates that the system approaches linear behaviour.

The ZCA and HVD have been applied to the signal and the IA is shown in Fig. 6.12(a). Both ZCA and HVD were influenced by residual noise, especially at lower amplitudes. The HVD also suffered from strong end-effects, which were eventually removed and additional smoothing had to be used to obtain the shown results.

It can be seen in Fig. 6.12(b) that two clearly separated pseudo-modal frequencies are present at high amplitudes at the beginning of the signal. These two frequencies then slowly merge towards the end of the time interval, indicating linear behaviour at lower amplitudes. The results of both methods correspond qualitatively to each other very well,

thereby highlighting the reliability of the proposed ZCA as well as demonstrating that with some careful signal processing the HVD can be used with experimental data. One of the frequencies is lower than the natural frequency, the other one is higher. This indicates that there is hardening behaviour for positive amplitudes and softening behaviour for the negative ones.

Despite the same global qualitative appearance of the pseudo-modal frequencies there are a few differences which are worth mentioning. Firstly, the HVD indicates slightly stronger non-linear behaviour. Secondly, the branches of the IF estimated by the ZCA appear to be smoother than those from the HVD, even though the additional smoothing was not used. Lastly, the HVD produced a strange discontinuity in the IF from the negative part of the free decay (see Fig. 6.12(b) for $t < 0.002\,\mathrm{s}$), whereas the ZCA estimated a smooth frequency in this region.

The extracted pseudo-backbones are shown in Fig. 6.13(a). In order to visualise

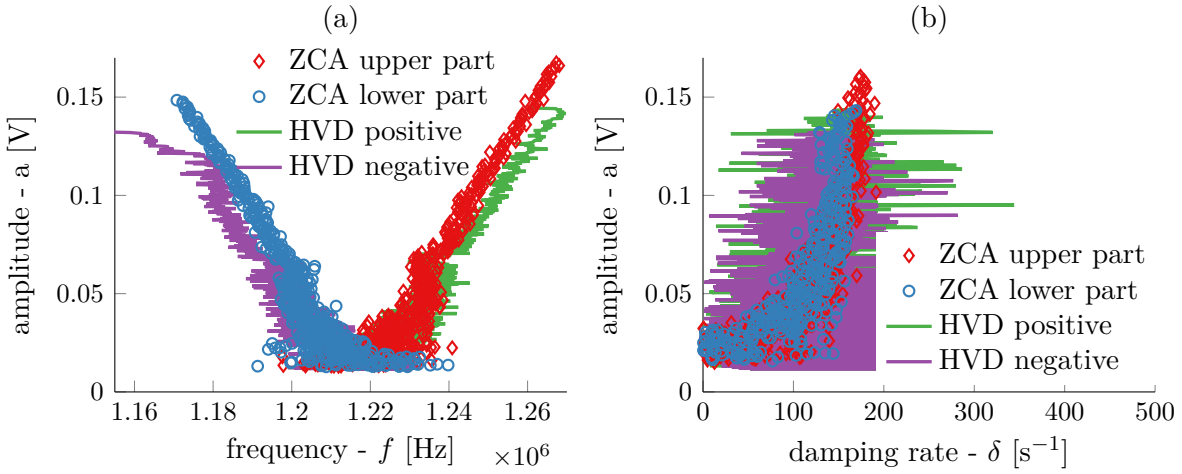

Figure 6.13 Micro-electro-mechanical resonator: (a) pseudo-backbone and (b) pseudo-damping curves

the results clearly, only every 50th point estimated by the ZCA was plotted. Two separated pseudo-backbones were clearly obtained by both methods and they exhibit similar discrepancies as the pseudo-modal frequency. Qualitatively, the results are the same, while quantitatively they are slightly different since the HVD indicates stronger non-linear behaviour. Both sets of results, however, approach the same linear natural frequency at lower amplitudes.

The estimated pseudo-damping curves are shown in Fig. 6.13(b). Again, to allow a better visualisation, only every 50th point estimated by the ZCA was plotted. The both sets of results are highly distorted due to residual measured noise, especially at lower

amplitudes. Even after additional filtering, the HVD produced much more distorted results than the ZCA. The detection of non-linearity could be difficult using the HVD results, because one could argue that this pseudo-damping curve is a straight, highly distorted line. On the other hand, while considering the pseudo-damping curve estimated by the ZCA, the non-linear behaviour is more evident. Moreover, this behaviour is of a hardening type because the damping rate increases with the increasing amplitude.

The estimated elastic and dissipative restoring forces are shown in Fig. 6.14. Unfor-

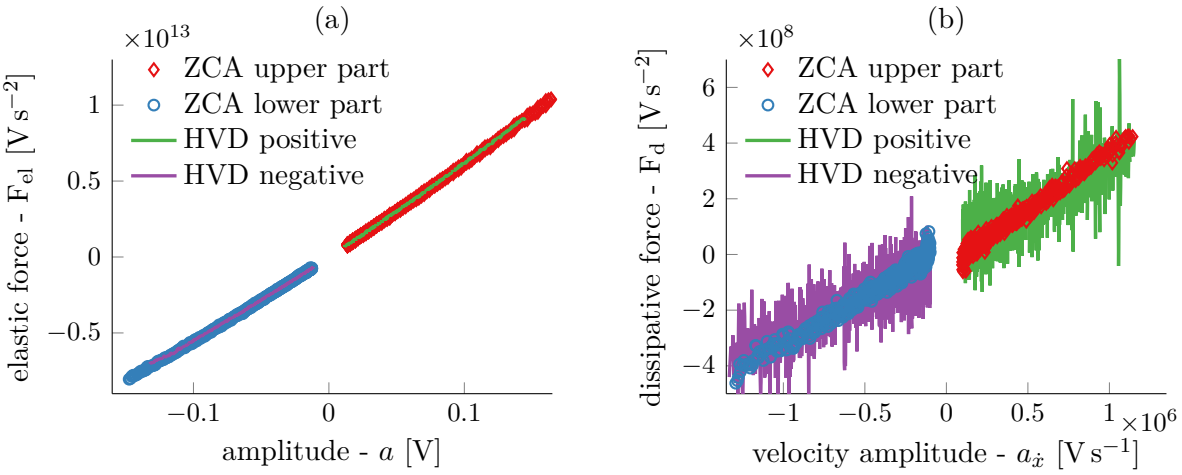

Figure 6.14 Micro-electro-mechanical resonator: (a) elastic and (b) dissipative restoring forces

tunately, due to significantly different orders of magnitude on the x- and y-axis, both restoring forces appear to be almost straight lines. Nonetheless, it can be seen that the difference between the methods is not significant.

The comparison of the experimental results with the results for the system with the quadratic stiffness suggests that the quadratic stiffness could be present in the MEMS resonator. In particular, Fig. 6.9 and Fig. 6.12 exhibit the same features - a signal which is asymmetric at the beginning, but becomes symmetric towards the end and the two different pseudo-frequencies which merge at low vibration amplitudes. The pseudo-backbones in Fig. 6.10(a) and Fig. 6.13(a) are also qualitatively the same, having a V-shape created by the estimates from the upper and lower parts. Both pseudo-backbones suggest the presence of hardening behaviour for the positive amplitudes and softening behaviour for the negative amplitudes. Therefore, it can be concluded that the elastic restoring force of the MEMS can be modelled using quadratic stiffness. This observation was also confirmed in [173] by the use of the restoring force surface (RFS) method.

The pseudo-damping curves indicate that the damping exhibits non-linear behaviour which increases with the increasing amplitude. This finding is also supported by the

theoretical explanation of the possible origin of the non-linear dissipation. Based on the microscopic theory of dissipation, the non-linear dissipative phenomenon can be explained using the non-linear interaction of the primary resonant mode with photons as detailed in [208]. Therefore, it is possible to conclude that the dissipative behaviour can be modelled using a cubic damping model.

All presented results were obtained for the initial amplitude $a_0 = 165\,\mathrm{mV}$. To illustrate that the results are consistent for all three available initial amplitudes, the pseudo-backbones and pseudo-damping curves for all three cases estimated by the ZCA are shown together in Fig. 6.15. For clarity of presentation, several periods were averaged

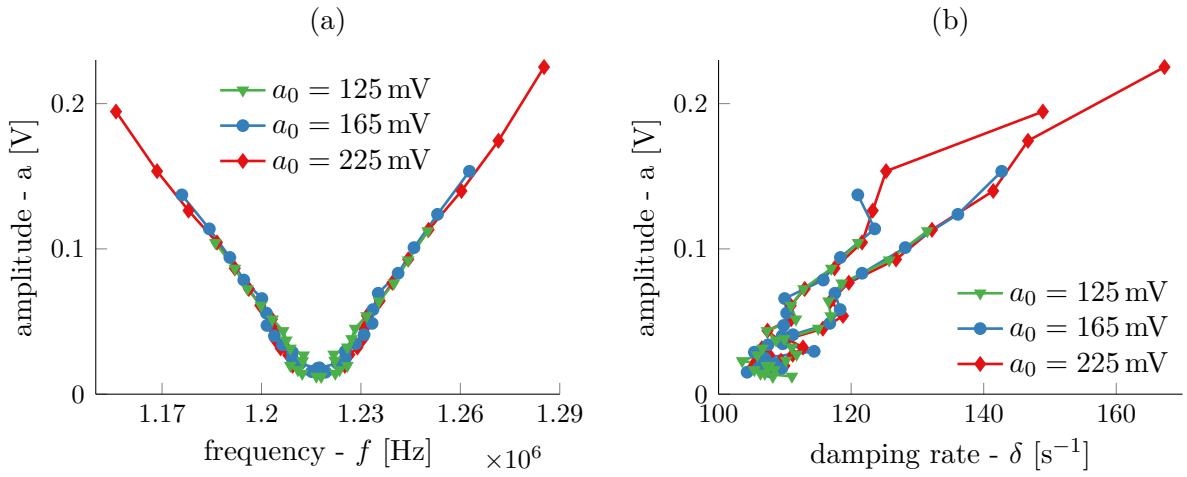

Figure 6.15 Micro-electro-mechanical resonator for different initial amplitudes: (a) pseudo-backbones and (b) pseudo-damping curves

(as described in section 6.3) and the HVD results are not shown. It is clear that the pseudo-backbones for all initial amplitudes are very close to each other, having the matching V-shape with different amplitudes. All of them also approach the same natural linear frequency at low amplitudes. The pseudo-damping curves also overlay well and all of them indicate hardening behaviour.

The previous detection and characterisation have been done in a non-parametric manner and led to the following model

$$\ddot{x}(t) + \underbrace{2\delta\dot{x}(t) + c_{\mathrm{nl}}\dot{x}^3(t)}_{\mathrm{F_d}} + \underbrace{4\pi^2 f_0^2 x(t) + k_{\mathrm{nl}}x^2(t)}_{\mathrm{F_{el}}} = 0, \tag{6.15}$$

where $x(t)$ is a voltage proportional to the displacement, δ is a damping rate, c_{nl} is a cubic hardening damping coefficient, f_0 is a natural frequency, and k_{nl} is a quadratic stiffness coefficient. Since the mass of the MEMS resonator does not have to be considered,

the restoring forces can be evaluated in units of $\mathrm{V\,s^{-2}}$. To quantify all parameters, the restoring forces in Fig. 6.14 were fitted by the expressions outlined in Eq. (6.15). The resulting coefficients are summarised in Tab. 6.4.

Method	a_0 [mV]	k_{nl} [$\mathrm{V^{-1}\,s^{-2}}$]	f_0 [Hz]	c_{nl} [$\mathrm{V^{-2}\,s^{-1}}$]	δ [$\mathrm{s^{-1}}$]
ZCA	125	2.81×10^{13}	1.217×10^{6}	3.13×10^{-11}	112.72
	165	2.82×10^{13}	1.217×10^{6}	3.35×10^{-11}	112.17
	225	2.97×10^{13}	1.217×10^{6}	5.36×10^{-11}	108.01
HVD	125	3.46×10^{13}	1.217×10^{6}	2.64×10^{-11}	131.34
	165	3.43×10^{13}	1.216×10^{6}	3.89×10^{-11}	121.36
	225	3.74×10^{13}	1.220×10^{6}	2.63×10^{-10}	160.26

Table 6.4 Identified coefficients of the micro-electro-mechanical resonator

The coefficients of the quadratic stiffness k_{nl} seems to be increasing with increasing initial amplitude for both methods. The coefficients are not exactly the same for all cases, but they have the same order of magnitude. They also correspond to the quadratic stiffness coefficient estimated by the RFS in [173]. The coefficients identified using the ZCA are slightly lower than those identified by the HVD, which is in line with the previous observation of weaker non-linear behaviour estimated by the ZCA in Fig. 6.12(a) and Fig. 6.13(a).

It can be seen that the natural frequency f_0 is more less the same for all initial amplitudes and both methods. It corresponds to the natural frequency that was estimated using the ZC in [207, 208] and by the restoring force method in [173]. The same natural frequency can also be visually identified in Fig. 6.12(b), Fig. 6.13(a) and Fig. 6.15(a).

The non-linear cubic damping coefficients c_{nl} are very small. This is caused by the significantly different orders of magnitude of the velocity amplitude and dissipative force (see Fig. 6.14(b)). Unfortunately, a comparison with other studies is not possible because none of them has used the same model of damping. Nonetheless, most of the coefficients have the same order of magnitude and the results of both methods are quite close to each other. There is a difference between the ZCA and HVD for the highest initial amplitude ($a_0 = 225\,\mathrm{mV}$). This difference can, however, be explained by the strong distortion of the dissipative forces that have been fitted.

The damping rates δ estimated by the ZCA are almost the same for all investigated cases. Moreover, they match very well to the damping rates estimated in [207, 208]. On the other hand, the damping rates estimated by the HVD are higher and quite

scattered. This, however, is not surprising given the amount of distortion in Fig. 6.13(b) and Fig. 6.14(b).

Overall, with regards to the simulated cases for which the accuracy of the ZCA was often better and due to extensive signal processing used in the HVD, it is likely that the coefficients estimated by the ZCA are more accurate. The comparison of the estimated coefficients with other studies shows that the accuracy of the ZCA is the same as that of the zero-crossing method [207, 208] and restoring force surface method [173]. Based on the presented findings it can be concluded that the newly developed ZCA method can be used reliably for the identification of non-linear systems with asymmetric restoring forces from an experimentally obtained resonant decay response.

6.6 Discussion

The zero-crossing method for systems with asymmetric non-linearities (ZCA) proposed in this chapter is an extension of the ZC methods (see chapter 3). It allows non-parametric identification of pseudo-backbones, pseudo-damping curves, and elastic and dissipative restoring forces from a resonant decay response without any a priori knowledge of the signal or the system parameters. The ZCA is based on the idea that since each signal branch is defined on its half-plane only, it is practically enough to identify matching instantaneous characteristics of each signal branch. To observe the capability of the ZCA and compare it with the Hilbert vibration decomposition in detail, these methods have been applied to three simulated resonant decay responses from the systems with bilinear, off-centre clearance and quadratic stiffness. Before applying the methods, the resonant decay responses obtained by the numerical integration were polluted by white Gaussian noise with signal-to-noise ratio 25 dB to make the data more realistic. Although some noise in the data does not generally prevent either method from estimating the IF and IA, the use of the Whittaker smoother (see appendix C) led to very good noise removal from the vibration signal in all investigated cases and there are several reasons why it seems to be appealing for similar applications.

In order to perform the relevant comparison of the ZCA with the HVD, some known issues of the HVD were avoided beforehand by selecting a relatively high sampling frequency. Generally, the HVD requires the sampling frequency to be twenty to eighty times higher than the highest frequency of interest [71, 72]. In addition, extra smoothing and filtering had to be used in the HVD to obtain the presented results. In contrast, the ZCA does not require the additional smoothing. There is no requirement on the

sampling frequency either. As long as the zero-crossing points, minima and maxima are estimated, the rest of the signal is not important.

To further demonstrate the capabilities of the ZCA as well as the HVD whose application to the experimental data has rarely been reported in literature [71], both methods have been used to investigate the experimentally acquired ring-down response of a micro-electro-mechanical resonator [206–208, 298]. Despite the need for additional smoothing and end-effects removing in the HVD, both methods were eventually able to estimate reasonable results. Although some differences may be observed, they cannot be readily explained based on the data. However, it may be argued that since the ZCA did not require extensive signal processing, was not influenced by any end-effects, and the results were overall smoother, it is likely that the results estimated by the ZCA are more accurate than those obtained by the HVD.

The ZCA is a non-parametric method which can be applied to any resonant decay response that may be described by Eq. (6.6). Such a resonant decay response can be either measured from a SDOF system or using a phase resonance testing [59, 191, 291] for a MDOF system. Similar resonant decay responses can also be obtained by the EMD as discussed in chapter 3 for a MDOF system. If the resonant decay response has been obtained from a SDOF system, the model in Eq. (6.6) with quantified coefficients describes the system completely. Theoretically, this model can be used to predict the response of the system for any range of loading conditions. On the other hand, for a resonant decay response of a MDOF system (obtained either by the phase resonance testing or using the EMD), the model is only valid for the given mode of vibration. Therefore, this model should be used to compute the response of the system only in a close proximity of this mode.

6.7 Conclusion

This chapter proposed a non-parametric method for the identification of systems with asymmetric restoring forces from a resonant decay response. Since the method is based on the zero-crossing method, it is termed zero-crossing methods for systems with asymmetric restoring forces (ZCA). It was demonstrated on the simulated and experimental data that it can provide results of the same or higher accuracy than the Hilbert vibration decomposition. At the same time, however, it is more robust against measured noise and requires less sophisticated signal processing.

Conclusion

This chapter concludes the thesis by summarising the research outcomes, stating the main original contributions and presenting the suggested avenues of future research.

Summary of the thesis

The overall focus of this thesis was on the development of non-linear system identification methods. Two main objectives defined in the introduction were:

1. *Enable robust and fast detection and characterisation of non-linearity from a single frequency response function applicable in an industrial framework.*

2. *Develop an approach to experimental non-linear modal analysis by investigating the use of time-frequency methods based on instantaneous frequency and amplitude and their possible relation to one of the concepts of non-linear modal analysis.*

The first objective of the thesis was motivated by the industrial needs for a practical methodology dedicated to real-life non-linear mechanical systems. This objective was achieved by the method for detection and characterisation of non-linearities proposed in chapter 2. The second objective was motivated by the current research trends in non-linear modal analysis and adaptive data processing. In order to meet this objective, several topics have been addressed, namely the Hilbert-Huang transform was examined in chapter 3, the relation between the Hilbert-Huang transform and recently developed complex non-linear modes was studied in chapter 4 and the approach to experimental non-linear modal analysis was developed in chapter 5. In addition, since the Hilbert-Huang transform cannot analyse systems with asymmetric restoring forces, a new method for this purpose was developed in chapter 6. Therefore, the second objective of the thesis was achieved as well. The rest of this section consists of a more detailed description of each chapter and main outcomes.

The literature review of state-of-the-art was conducted in chapter 1. Firstly, the theoretical modelling, numerical analysis and experimental testing in non-linear structural

dynamics were briefly described to introduce the wider context of the topic. Then, the main focus was on non-linear system identification. In particular, the methods for the detection and characterisation of structural non-linearities in the frequency domain, time-frequency analysis, and theoretical and experimental non-linear modal analysis were reviewed. The purpose of this review was to identify the limitations of the current approaches, which were addressed in the following chapters.

In chapter 2 a new method for detection and characterisation of non-linearities based on the Hilbert transform in the frequency domain and artificial neural networks was proposed. It was demonstrated that the method is robust against measured noise while being able to detect and characterise the non-linear behaviour from a single measured frequency response function. The method was also applied to three different experimental data sets for which it was able to provide reliable results. The method is applicable to a frequency response function of a multi-degree-of-freedom with well spaced vibration modes. Once the network has been trained, the method does not require expertise decision making and is very fast. Overall, it is suitable as an automatised pre-step of the linear modal analysis in an industrial framework to verify the assumption of linear behaviour.

Chapter 3 introduced the concept of time-frequency analysis and discussed the Hilbert-Huang transform (HHT) and its numerical problems in detail. In particular, the mode mixing problem of the empirical mode decomposition was described and it was shown how it can be investigated before applying the EMD. A significant part of chapter 3 was then devoted to the comparison and evolution of the methods for instantaneous frequency and amplitude estimation, namely normalised Hilbert transform, direct quadrature, energy operators and zero-crossing methods. The objective of this part was to determine if the Hilbert transform, which is used to estimate the IF and IA in a vast majority of cases despite being sensitive to numerical issues, can be replaced by one of the other methods. The comparison led to the conclusion that while all methods provide equivalent results after low-pass filtering or other smoothing, each method has unique features that can be used to detect and characterise the non-linearity. These features were summarised in section 3.3.8. In addition, this evaluation motivated the development of the new method for the estimation the intra-wave frequency modulation in section 3.4. The method also provides the ratio of the fundamental frequency and IFM frequency which is subsequently used to determine the type of stiffness non-linearity. Although the proposed method can be used as an additional indicator of the non-linearity type, its practical applicability is very limited due to its sensitivity to measured noise.

The objective of chapter 4 was to investigate a hypothesis that the HHT relates to complex non-linear modes (CNMs) of mechanical systems. The hypothesis was supported by a number of similarities between the methods, but mainly by the existence of the common link which is the slow-flow dynamics. Since the hypothesis cannot be proven mathematically due to the empirical and numerical nature of the HHT and CNMs, respectively, it was investigated using a series of numerical cases and parametric studies. It was concluded that in spite of the fact that the intrinsic mode functions and reduced order model of slow-flow dynamics exhibit the same qualitative features, the quantitative error may be significant in some cases. That means that the computed CNMs do not match to those extracted using the HHT when the response of many modes has been measured. In contrast, if the isolated response of one non-linear mode has been directly measured, i.e. resonant decay responses or slow-sweep harmonic response has been acquired, the extracted and computed modes correspond to each other exactly. These findings limit the accuracy of the quantification proposed in chapter 5.

Chapter 5 described a complete approach to non-linear modal analysis in which the non-linear modes are used to detect, characterise and quantify structural non-linearities. The method firstly detects and characterises the type of structural non-linearity using the HHT. Since the HHT is a non-parametric method, no model of the system is required at this stage. This feature of the proposed method is particularly appealing because it enables to investigate systems based on the experimental data without introducing any assumptions about their character. Once the presence and type of non-linearity have been established, a low-fidelity or full FE model must be selected in order to quantify non-linearity through the optimisation in terms of the CNMs. The final output of the method is a structural model with fully identified linear and non-linear parameters. The detection and characterisation can be performed on virtually any time domain data whereas the accuracy of the quantification is only guaranteed for resonant decay responses due to the only approximative relation between the HHT and CNMs found in chapter 4. The method was applied to experimental data acquired from the ECL benchmark and it was able to successfully extract and characterise first three modes from a single free decay measurement.

The limitation of the Hilbert transform to analyse systems with asymmetric restoring forces was addressed in chapter 6. The new method, named zero-crossing method for systems with asymmetric restoring forces (ZCA), treats the upper and lower part of the resonant decay response separately and allows identification of amplitude-dependent natural frequency, damping and restoring forces. The application of the method was demonstrated on a number of numerical validation cases for which it is shown that the

results are equal or more accurate than the results obtained by the Hilbert vibration decomposition (HVD). The proposed method was applied to the experimental data obtained from a micro-electro-mechanical device. It is found that the ZCA yielded more accurate results then the HVD while requiring much less effort and less sophisticated signal processing.

Main contributions

The main original contributions of the research work presented in this thesis are:

- The new method for detection and characterisation of structural non-linearities based on the Hilbert transform in the frequency domain and artificial neural network described in chapter 2. The method was already published in a journal paper [175].
- The comparison of methods for instantaneous frequency and amplitude estimation conducted in section 3.3 which identified potential features that can provide insight into the presence and character of non-linearity. A similar comparison was already published in a conference paper [173].
- The proposed method for the estimation of intra-wave frequency modulation which can be used for detection and characterisation of stiffness non-linearities presented in section 3.4. The proposed method was briefly described in a conference paper [174].
- The original analysis of the relation between the Hilbert-Huang transform and complex non-linear modes in chapter 4.
- The approach to non-linear modal analysis which uses extracted non-linear modes to detect, characterise and quantify non-linearity described in chapter 5. A journal paper which documents the proposed approach to non-linear modal analysis and includes the findings of chapter 4 is under preparation.
- The new method for the analysis of resonant decay responses of systems with asymmetric restoring forces presented in chapter 6. A journal paper describing this method is being prepared.

Suggested directions of future research

The avenues of future research in non-linear system identification that directly relate to the work presented in this thesis could include the following

- *Development of a method for automatic detection and characterisation of non-linearities based on the extracted non-linear modes.*

  At the moment, the extracted non-linear modes must be visually inspected in order to detect and characterise the non-linearity in chapter 5. However, this inspection may require a good knowledge of the problem and may not be suitable for industrial use where automatised procedures are often preferred. A new method could be similar to the method proposed in chapter 2. Instead of using frequency response functions to create a set of features that are classified by the artificial neural network, the non-linear backbones, damping curves and mode shapes would be used.

- *Definition of non-linearity strength and its assessment*

  It was discussed in section 1.2.1 that it might be beneficial to assess the strength of non-linearity before proceeding further with the identification. If the non-linearity is weak, the non-linear identification is not necessary and the system can be treated as being linear. The assessment of non-linearity strength has not been attempted in the thesis since this quantity cannot be generally defined. However, it might be possible to define the strength of non-linearity for a particular mechanical system based on, for example, a frequency shift, reduction or increase in the amplitude or amount of vibration-induced noise. Provided that the definition of the non-linear strength is available, it can be included in the method proposed in chapter 2 by training the artificial neural network appropriately.

- *Improvement of the proposed approach to non-linear modal analysis*

  New ways for non-linear modal analysis which would allow to obtain correct non-linear structural models even from free decay measurements should be sought. The detection and characterisation as proposed in chapter 5 could remain unchanged. The quantification, which is currently accurate only for resonant decay responses, would not have to be modified either because it was proposed in such a way that it allows to incorporate several measured modes and multiple measured locations. If the modes were correctly estimated, it is anticipated that the quantification procedure would lead to the correct results. In order to achieve significant improvements of the proposed approach, the way to extract non-linear modes must be revised. This could be achieved either by replacing the HHT by other time-frequency analysis method or it might be perhaps possible to modify the extraction of the non-linear modes in section 5.2.2 in such a way that the difference between the HHT and CNMs observed in chapter 4 will be considered and CNMs appropriately corrected.

- *The use of the Holo-Hilbert spectral analysis for non-linear system identification*

  Although the HHT is very popular method for adaptive data processing in many fields, it cannot extract dependencies between the intrinsic mode functions. Therefore, it is likely that it does not allow to study internal resonances. However, an extension of the HHT, called the Holo-Hilbert spectral analysis (HHSA) [100], has been recently proposed. Theoretically, it should allow to recover cross-scale coupling between the IMFs so it may perhaps be possible to study internal resonances using this method. It has never been applied in structural dynamics so its practical feasibility is yet to be determined.

- *Extension of the non-linear modal analysis to industrial cases*

  The dominant focus of this thesis was on resonant and free decay measurements, which are usually used for dynamic testing of non-linear modes due to their prominent properties and short measurement times. However, the forced testing is often used in industry, for instance the commissioning tests of aircraft engines and their components are usually conducted using sweep excitation. Future research could therefore extend the methodology presented in chapter 5 to these cases by incorporating the Forcevib [68] into the extraction of non-linear modes. It was shown in chapter 4 that since the empirical mode decomposition does not have to be applied for this excitation type, the quantification of non-linearity should be exact provided that the non-linear modes have been correctly extracted. Several problems could arise with the processing of data from commissioning test of aircraft engines. The excitation force is not often measured but it is rather estimated with some degree of uncertainly. This fact would need to be considered in a new method. Similarly, the sweep rate can vary significantly so a series of parametric studies would need to assess its effect on estimated non-linear models.

- *Characterisation of spatial location of non-linearity*

  The non-linearity is said to be characterised when its type, spatial location and mathematical form have been found. None of the methods presented in this thesis offers a possibility to characterise the spatial location of the detected non-linearity. Without deep engineering understanding of the problem, the localisation of non-linearity may be very complicated since there are very few methods in literature (a list of methods can be found in appendix A) that can be applied for this purpose. Moreover, most of the available methods are based on machine learning or brute force approaches. Therefore, the future research should attempt to develop a

non-parametric method for localisation of non-linearities which would not require detailed understanding of the system.

- *Assessment of uncertainty in the system and data processing*

  It is known that every mechanical system is influenced by uncertainties. They can originate in imperfections of the manufacturing process, problems during the assembly or arise as a consequence of wear. It is also common that any measured data are polluted by noise and influenced by imperfections of experimental set-ups. As a consequence, many signal processing techniques, such as smoothing and filtering, must be usually applied to obtain the required results. However, the effect of these techniques on the obtained model is not usually taken into account. Even in the computational modelling, the uncertainties are not often considered despite the awareness that a small change in input parameters can significantly alter the response of a non-linear system. Therefore, future research should focus on the assessment of uncertainty in both system identification and simulation in order to obtain more accurate structural models.

Non-linear system identification is still an active research area in which many new methods are constantly being developed. To this day, no method that would be applicable to a wide range of industrial structures has been developed. Out of the great number of approaches, non-linear modal analysis seems to be the one with the greatest progress in recent years. The research effort is probably motivated by the desire to develop a successor of linear modal analysis which could be universally applied to non-linear systems. However, the non-linear modal analysis is yet to reach its full potential. Until then, much research must be conducted to achieve ambitious objectives of non-linear system identification.

References

[1] Adams D. E. Frequency domain ARX model and multi-harmonic FRF estimators for non-linear dynamic systems. *Journal of Sound and Vibration*, 250(5):935–950, 2002. doi:10.1006/jsvi.2001.3965.

[2] Adams D. E. and Allemang R. J. Survey of nonlinear detection and identification techniques for experimental vibrations. In *Proceedings of the International Seminar of Modal Analysis*, pages 269–281, 1998.

[3] Adams D. E. and Allemang R. J. Characterization of nonlinear vibrating systems using internal feedback and frequency response modulation. *Journal of Vibration and Acoustics*, 121(4):495–500, 1999. doi:10.1115/1.2894008.

[4] Adams D. E. and Allemang R. J. A frequency domain method for estimating the parameters of a non-linear structural dynamic model through feedback. *Mechanical Systems and Signal Processing*, 14(4):637–656, 2000. doi:10.1006/mssp.2000.1292.

[5] Adams D. E. and Allemang R. J. Residual frequency autocorrelation as an indicator of non-linearity. *International Journal of Non-Linear Mechanics*, 36(8):1197–1211, 2001. doi:10.1016/S0020-7462(00)00090-1.

[6] Aiordachioaie D., Ceanga E., Keyser R. D., and Naka Y. Detection and classification of non-linearities based on Volterra kernels processing. *Engineering Applications of Artificial Intelligence*, 14(4):497–503, 2001. doi:10.1016/S0952-1976(01)00024-0.

[7] Al-Bender F., Symens W., Swevers J., and Van Brussel H. Theoretical analysis of the dynamic behavior of hysteresis elements in mechanical systems. *International Journal of Non-Linear Mechanics*, 39(10):1721–1735, 2004. doi:10.1016/j.ijnonlinmec.2004.04.005.

[8] Al-hadid M. A. and Wright J. R. Developments in the force-state mapping technique for non-linear systems and the extension to the location of non-linear elements in a lumped-parameter system. *Mechanical Systems and Signal Processing*, 3(3):269–290, 1989. doi:10.1016/0888-3270(89)90053-8.

[9] Allen M. S., Sumali H., and Epp D. S. Piecewise-linear restoring force surfaces for semi-nonparametric identification of nonlinear systems. *Nonlinear Dynamics*, 54(1):123–135, 2008. doi:10.1007/s11071-007-9254-x.

[10] Argoul P. and Le T.-P. Instantaneous indicators of structural behaviour based on the continuous Cauchy wavelet analysis. *Mechanical Systems and Signal Processing*, 17(1):243–250, 2003. doi:10.1006/mssp.2002.1557.

[11] Arora J. S. *Introduction to Optimum Design (Third Edition)*. Academic Press, 2011.

[12] Atkins P. and Worden K. Identification of a multi-degree-of-freedom nonlinear system. In *Proceedings of the International Modal Analysis Conference*, pages 1023–1028, 1997.

[13] Atzberger C. and Eilers P. H. C. Evaluating the effectiveness of smoothing algorithms in the absence of ground reference measurements. *International Journal of Remote Sensing*, 32(13):3689–3709, 2011. doi:10.1080/01431161003762405.

[14] Avramov K. V. and Mikhlin Y. V. Review of applications of nonlinear normal modes for vibrating mechanical systems. *Applied Mechanics Reviews*, 65(2):020801–20, 2013. doi:10.1115/1.4023533.

[15] Aykan M. and Özgüven H. N. Parametric identification of nonlinearity in structural systems using describing function inversion. *Mechanical Systems and Signal Processing*, 40(1):356–376, 2013. doi:10.1016/j.ymssp.2013.03.016.

[16] Barton D. A. W. Control-based continuation: Bifurcation and stability analysis for physical experiments. *Mechanical Systems and Signal Processing*, 84, Part B:54–64, 2017. doi:10.1016/j.ymssp.2015.12.039.

[17] Barton D. A. W. and Burrow S. G. Numerical continuation in a physical experiment: Investigation of a nonlinear energy harvester. *Journal of Computational and Nonlinear Dynamics*, 6(1):011010–6, 2010. doi:10.1115/1.4002380.

[18] Bedrosian E. A product theorem for Hilbert transforms. *Proceedings of the IEEE*, 51(5):868–869, 1963. doi:10.1109/PROC.1963.2308.

[19] Bendat J. S. and Piersol A. G. *Random Data: Analysis and Measurement Procedures*. Wiley Series in Probability and Statistics. Wiley, 2010.

[20] Billings S. A. *Nonlinear System Identification: NARMAX Methods in the Time, Frequency, and Spatio-Temporal Domains*. Wiley-Blackwell, 2013.

[21] Billings S. A., Jamaluddin H. B., and Chen S. Properties of neural networks with applications to modelling non-linear dynamical systems. *International Journal of Control*, 55(1):193–224, 1992. doi:10.1080/00207179208934232.

[22] Boltežar M. and Slavič J. Enhancements to the continuous wavelet transform for damping identifications on short signals. *Mechanical Systems and Signal Processing*, 18(5):1065–1076, 2004. doi:10.1016/j.ymssp.2004.01.004.

[23] Böswald M. and Füllekrug U. Non-linear identification of multi-degree of freedom systems using the restoring force surface method. In *Proceedings of the International Conference on Noise and Vibration Engineering*, pages 2995–3008, Leuven, Belgium, 2014.

[24] Brake M. R. W. *The Mechanics of Jointed Structures*. Springer International Publishing, 2018.

[25] Braun S. and Feldman M. Decomposition of non-stationary signals into varying time scales: Some aspects of the EMD and HVD methods. *Mechanical Systems and Signal Processing*, 25(7):2608–2630, 2011. doi:10.1016/j.ymssp.2011.04.005.

[26] Brincker R. and Ventura C. *Introduction to Operational Modal Analysis*. Wiley, 2015.

[27] Butlin T., Woodhouse J., and Champneys A. R. The landscape of nonlinear structural dynamics: An introduction. *Philosophical Transactions of the Royal Society of London A: Mathematical, Physical and Engineering Sciences*, 373(2051), 2015. doi:10.1098/rsta.2014.0400.

[28] Cafferty S. and Tomlinson G. R. Characterization of automotive dampers using higher order frequency response functions. *Proceedings of the Institution of Mechanical Engineers, Part D: Journal of Automobile Engineering*, 211(3):181–203, 1997. doi:10.1243/0954407971526353.

[29] Cameron T. M. and Griffin J. H. An alternating frequency/time domain method for calculating the steady-state response of nonlinear dynamic systems. *Journal of Applied Mechanics*, 56(1):149–154, 1989. doi:10.1115/1.3176036.

[30] Carrella A. and Ewins D. J. Identifying and quantifying structural nonlinearities in engineering applications from measured frequency response functions. *Mechanical Systems and Signal Processing*, 25(3):1011–1027, 2011. doi:10.1016/j.ymssp.2010.09.011.

[31] Carri A. D. and Ewins D. J. A systematic approach to modal testing of nonlinear structures. In Allemang R., De Clerck J., Niezrecki C., and Wicks A., editors, *Topics in Modal Analysis, Volume 7. Conference Proceedings of the Society for Experimental Mechanics Series*, pages 273–286. Springer, 2014. doi:10.1007/978-1-4614-6585-0_25.

[32] Carri A. D., Weekes B., Di Maio D., and Ewins D. J. Extending modal testing technology for model validation of engineering structures with sparse nonlinearities: A first case study. *Mechanical Systems and Signal Processing*, 84, Part B:97–115, 2017. doi:10.1016/j.ymssp.2016.04.012.

[33] Castellini P., Martarelli M., and Tomasini E. P. Laser Doppler vibrometry: Development of advanced solutions answering to technology's needs. *Mechanical Systems and Signal Processing*, 20(6):1265–1285, 2006. doi:10.1016/j.ymssp.2005.11.015.

[34] Ceravolo R., Erlicher S., and Zanotti Fragonara L. Comparison of restoring force models for the identification of structures with hysteresis and degradation. *Journal of Sound and Vibration*, 332(26):6982–6999, 2013. doi:10.1016/j.jsv.2013.08.019.

[35] Chassiakos A. G. and Marsi S. F. Modelling unknown structural systems through the use of neural networks. *Earthquake Engineering & Structural Dynamics*, 25(2):117–128, 1996. doi:10.1002/(SICI)1096-9845(199602)25:2<117::AID-EQE541>3.0.CO;2-A.

[36] Chatterjee A. and Vyas N. S. Stiffness non-linearity classification through structured response component analysis using Volterra series. *Mechanical Systems and Signal Processing*, 15(2):323–336, 2001. doi:10.1006/mssp.2000.1331.

[37] Chatterjee A. and Vyas N. S. Non-linear parameter estimation in multi-degree-of-freedom systems using multi-input Volterra series. *Mechanical Systems and Signal Processing*, 18(3):457–489, 2004. doi:10.1016/S0888-3270(03)00016-5.

[38] Chen B., Zhao S., and Li P. Application of Hilbert-Huang transform in structural health monitoring: a state-of-the-art review. *Mathematical Problems in Engineering*, 2014:1–22, 2014. doi:10.1155/2014/317954.

[39] Chen H., Kurt M., Lee Y. S., Mcfarland M. D., Bergman L. A., and Vakakis A. F. Experimental system identification of the dynamics of a vibro-impact beam with a view towards structural health monitoring and damage detection. *Mechanical Systems and Signal Processing*, 46(1):91–113, 2014. doi:10.1016/j.ymssp.2013.12.014.

[40] Chen Y. and Feng M. Q. A technique to improve the empirical mode decomposition in the Hilbert-Huang transform. *Earthquake Engineering and Engineering Vibration*, 2(1):75–85, 2003. doi:10.1007/BF02857540.

[41] Chong Y. H. and Imregun M. Use of reciprocal modal vectors for nonlinearity detection. *Archive of Applied Mechanics*, 70(7):453–462, 2000. doi:10.1007/s004199900078.

[42] Chu P. C., Fan C., and Huang N. Derivative-optimized empirical mode decomposition for the Hilbert–Huang transform. *Journal of Computational and Applied Mathematics*, 259:57–64, 2014. doi:10.1016/j.cam.2013.03.046.

[43] Cohen L. *Time-frequency Analysis: Theory and Applications*. Prentice-Hall, 1995.

[44] Collis W. B., White P. R., and Hammond J. K. Higher-order spectra: the bispectrum and trispectrum. *Mechanical Systems and Signal Processing*, 12(3):375–394, 1998. doi:10.1006/mssp.1997.0145.

[45] Colominas M., Schlotthauer G., and Torres M. E. An unconstrained optimization approach to empirical mode decomposition. *Digital Signal Processing*, 40:164–175, 2015. doi:10.1016/j.dsp.2015.02.013.

[46] Colominas M. A., Schlotthauer G., and Torres M. E. Improved complete ensemble EMD: A suitable tool for biomedical signal processing. *Biomedical Signal Processing and Control*, 14:19–29, 2014. doi:10.1016/j.bspc.2014.06.009.

[47] Courtney C. R. P., Neild S. A., Wilcox P. D., and Drinkwater B. W. Application of the bispectrum for detection of small nonlinearities excited sinusoidally. *Journal of Sound and Vibration*, 329(20):4279–4293, 2010. doi:10.1016/j.jsv.2010.04.031.

[48] Crawley E. F. and Aubert A. C. Identification of nonlinear structural elements by force-state mapping. *AIAA Journal*, 24(1):155–162, 1986. doi:10.2514/3.9236.

[49] Darvishan E., Amiri G. G., and Ghaderi P. A study on instantaneous time-frequency methods for damage detection of nonlinear moment-resisting frames. *Shock and Vibration*, 2014:1–14, 2014. doi:10.1155/2014/523675.

[50] Deering R. and Kaiser J. F. The use of a masking signal to improve empirical mode decomposition. *Proceedings of IEEE International Conference on Acoustics, Speech and Signal Processing*, IV:485–488, 2005. doi:10.1109/ICASSP.2005.1416051.

[51] Dempsey E. J. and Westwick D. T. Identification of hammerstein models with cubic spline nonlinearities. *IEEE Transactions on Biomedical Engineering*, 51(2):237–245, 2004. doi:10.1109/TBME.2003.820384.

[52] Desai C. S., Zaman M. M., Lightner J. G., and Siriwardane H. J. Thin-layer element for interfaces and joints. *International Journal for Numerical and Analytical Methods in Geomechanics*, 8(1):19–43, 1984. doi:10.1002/nag.1610080103.

[53] Detroux T., Renson L., and Kerschen G. The harmonic balance method for advanced analysis and design of nonlinear mechanical systems. In Kerschen G., editor, *Nonlinear Dynamics, Volume 2: Proceedings of the 32nd IMAC, A Conference and Exposition on Structural Dynamics, 2014*, pages 19–34. Springer International Publishing, 2014. doi:10.1007/978-3-319-04522-1_3.

[54] Detroux T., Renson L., Masset L., and Kerschen G. The harmonic balance method for bifurcation analysis of large-scale nonlinear mechanical systems. *Computer Methods in Applied Mechanics and Engineering*, 296:18–38, 2015. doi:10.1016/j.cma.2015.07.017.

[55] Di Maio D., Schwingshackl C. W., and Sever I. A. Development of a test planning methodology for performing experimental model validation of bolted flanges. *Nonlinear Dynamics*, 83(1):983–1002, 2016. doi:10.1007/s11071-015-2382-9.

[56] Dossogne T., Noël J. P., and Kerschen G. Identification of complex nonlinearities using cubic splines with automatic discretization. In Kerschen G., editor, *Nonlinear Dynamics, Volume 1: Proceedings of the 35th IMAC, A Conference and Exposition on Structural Dynamics 2017*, pages 51–54. Springer International Publishing, 2017. doi:10.1007/978-3-319-54404-5_5.

[57] Duda R. O., Hard P. E., and Stork D. G. *Pattern Classification (2nd Edition)*. Wiley-Interscience, 2001.

[58] Ehrhardt D. A. *An Experimental and Numerical Investigation of Nonlinear Normal Modes in Geometrically Nonlinear Structures*. PhD thesis, University of Wisconsis-Madison, 2015.

[59] Ehrhardt D. A. and Allen M. S. Measurement of nonlinear normal modes using multi-harmonic stepped force appropriation and free decay. *Mechanical Systems and Signal Processing*, 76–77:612–633, 2016. doi:10.1016/j.ymssp.2016.02.063.

[60] Eilers P. H. C. A perfect smoother. *Analytical Chemistry*, 75(14):3631–3636, 2003. doi:10.1021/ac034173t.

[61] Elliott A. J., Cammarano A., and Neild S. A. Comparing analytical approximation methods with numerical results for nonlinear systems. In Kerschen G., editor, *Nonlinear Dynamics, Volume 1: Proceedings of the 35th IMAC, A Conference and Exposition on Structural Dynamics 2017*, pages 37–49. Springer International Publishing, 2017. doi:10.1007/978-3-319-54404-5_4.

[62] Eriten M., Kurt M., Luo G., McFarland M. D., Bergman L. A., and Vakakis A. F. Nonlinear system identification of frictional effects in a beam with a bolted joint connection. *Mechanical Systems and Signal Processing*, 39(1):245 – 264, 2013. doi:10.1016/j.ymssp.2013.03.003.

[63] Ewins D. J. *Modal Testing: Theory, Practice and Application*. Research studies press Ltd, 2000.

[64] Ewins D. J. Exciting vibrations: The role of testing in an era of supercomputers and uncertainties. *Meccanica*, 51(12):3241–3258, 2016. doi:10.1007/s11012-016-0576-y.

[65] Ewins D. J., Weekes B., and Carri A. D. Modal testing for model validation of structures with discrete nonlinearities. *Philosophical Transactions of the Royal Society of London A: Mathematical, Physical and Engineering Sciences*, 373(2051), 2015. doi:10.1098/rsta.2014.0410.

[66] Fan Y. and Li J. C. Non-linear system identification using lumped parameter models with embedded feedforward neural networks. *Mechanical Systems and Signal Processing*, 16(2-3):357–372, 2002. doi:10.1006/mssp.2001.1466.

[67] Feldman M. Non-linear system vibration analysis using Hilbert transform–I. Free vibration analysis method 'Freevib'. *Mechanical Systems and Signal Processing*, 8(2):119–127, 1994. doi:10.1006/mssp.1994.1011.

[68] Feldman M. Non-linear system vibration analysis using Hilbert transform–II. Forced vibration analysis method 'Forcevib'. *Mechanical Systems and Signal Processing*, 8(3):309–318, 1994. doi:10.1006/mssp.1994.1023.

[69] Feldman M. Time-varying vibration decomposition and analysis based on the Hilbert transform. *Journal of Sound and Vibration*, 295(3-5):518–530, 2006. doi:10.1016/j.jsv.2005.12.058.

[70] Feldman M. Theoretical analysis and comparison of the Hilbert transform decomposition methods. *Mechanical Systems and Signal Processing*, 22(3):509–519, 2008. doi:10.1016/j.ymssp.2007.09.013.

[71] Feldman M. *Hilbert Transform Application in Mechanical Vibration*. John Wiley & Sons Ltd, 2011. doi:10.1002/9781119991656.

[72] Feldman M. Hilbert transform in vibration analysis. *Mechanical Systems and Signal Processing*, 25(3):735–802, 2011. doi:10.1016/j.ymssp.2010.07.018.

[73] Feldman M. Nonparametric identification of asymmetric nonlinear vibration systems with the Hilbert transform. *Journal of Sound and Vibration*, 331(14):3386–3396, 2012. doi:10.1016/j.jsv.2012.02.025.

[74] Feldman M. Mapping nonlinear forces with congruent vibration functions. *Mechanical Systems and Signal Processing*, 37(1-2):315–337, 2013. doi:10.1016/j.ymssp.2013.01.002.

[75] Feldman M. and Braun S. Identification of non-linear system parameters via the instantaneous frequency: application of the Hilbert transform and Wigner-Ville techniques. In *13th International Modal Analysis Conference (IMAC)*, pages 637–642, 1995.

[76] Flandrin P. *Time-frequency/Time-scale Analysis*. Academic Press, 1999.

[77] Franco H. and Pauletti R. M. O. Analysis of nonlinear oscillations by Gabor spectrograms. *Nonlinear Dynamics*, 12(3):215–236, 1997. doi:10.1023/A:1008294918271.

[78] Friswell M. I. and Mottershead J. E. *Finite Element Model Updating in Structural Dynamics*. Springer, 1995. doi:10.1007/978-94-015-8508-8.

[79] Friswell M. I. and Penny J. E. T. Crack modeling for structural health monitoring. *Structural Health Monitoring*, 1(2):139–148, 2002. doi:10.1177/147592170200100202.

[80] Garibaldi L. Application of the conditioned reverse path method. *Mechanical Systems and Signal Processing*, 17(1):227–235, 2003. doi:10.1006/mssp.2002.1564.

[81] Gaul L. and Lenz J. Nonlinear dynamics of structures assembled by bolted joints. *Acta Mechanica*, 125(1):169–181, 1997. doi:10.1007/BF01177306.

[82] Göge D., Sinapius M., Füllekrug U., and Link M. Detection and description of non-linear phenomena in experimental modal analysis via linearity plots. *International Journal of Non-Linear Mechanics*, 40(1):27–48, 2005. doi:10.1016/j.ijnonlinmec.2004.05.011.

[83] Gondhalekar A. C. *Strategies for Non-linear System Identification*. PhD thesis, Imperial College London, 2009.

[84] Goswami J. C. and Hoefel A. E. Algorithms for estimating instantaneous frequency. *Signal Processing*, 84(8):1423 – 1427, 2004. doi:10.1016/j.sigpro.2004.05.016.

[85] Grappasonni C., Noël J. P., and Kerschen G. Subspace and nonlinear-normal-modes-based identification of a beam with softening-hardening behaviour. In Kerschen G., editor, *Nonlinear Dynamics, Volume 2: Proceedings of the 32nd IMAC, A Conference and Exposition on Structural Dynamics, 2014*, pages 55–68. Springer International Publishing, 2014. doi:10.1007/978-3-319-04522-1_6.

[86] Griffel B., Zia M. K., Semmlow J. L., Fridman V., and Saponieri C. Comparison of instantaneous frequency analysis methods for acoustic detection of coronary artery disease. In *Signal Processing in Medicine and Biology Symposium (SPMB), 2011 IEEE*, pages 1–6, 2011. doi:10.1109/SPMB.2011.6120111.

[87] Griffin J. H. Friction damping of resonant stresses in gas turbine engine airfoils. *Journal of Engineering for Power*, 102(2):329–333, 1980. doi:10.1115/1.3230256.

[88] Gross J., Armand J., Lacayo R. M., Reuss P., Salles L., Schwingshackl C. W., Brake M. R. W., and Kuether R. J. A numerical round robin for the prediction of the dynamics of jointed structures. In Allen M., Mayes R. L., and Rixen D., editors, *Dynamics of Coupled Structures, Volume 4: Proceedings of the 34th IMAC, A Conference and Exposition on Structural Dynamics 2016*, pages 195–211. Springer International Publishing, 2016. doi:10.1007/978-3-319-29763-7_20.

[89] Guckenheimer J. and Holmes P. J. *Nonlinear Oscillations, Dynamical Systems, and Bifurcations of Vector Fields*. Springer, 1983. doi:10.1007/978-1-4612-1140-2.

[90] Ha N. S., Vang H. M., and Goo N. S. Modal analysis using digital image correlation technique: An application to artificial wing mimicking beetle's hind wing. *Experimental Mechanics*, 55(5):989–998, 2015. doi:10.1007/s11340-015-9987-2.

[91] Hagan M. T., Demuth H. B., and Beale M. H. *Neural Network Design*. PWS Publishing Co., 1996.

[92] Haroon M., Adams D. E., Luk Y. W., and Ferri A. A. A time and frequency domain approach for identifying nonlinear mechanical system models in the absence of an input measurement. *Journal of Sound and Vibration*, 283(3-5):1137–1155, 2005. doi:10.1016/j.jsv.2004.06.008.

[93] Hartwigsen C. J., Song Y., McFarland D. M., Bergman L. A., and Vakakis A. F. Experimental study of non-linear effects in a typical shear lap joint configuration. *Journal of Sound and Vibration*, 277(1-2):327–351, 2004. doi:10.1016/j.jsv.2003.09.018.

[94] Haykin S. *Neural Networks: A Comprehensive Foundation*. Prentice Hall, 2nd edition, 1998.

[95] Hemez F. M. and Doebling S. W. Review and assessment of model updating for non-linear, transient dynamics. *Mechanical Systems and Signal Processing*, 15(1):45–74, 2001. doi:10.1006/mssp.2000.1351.

[96] Hill T. L., Green P. L., Cammarano A., and Neild S. A. Fast Bayesian identification of a class of elastic weakly nonlinear systems using backbone curves. *Journal of Sound and Vibration*, 360:156–170, 2016. doi:10.1016/j.jsv.2015.09.007.

[97] Hosseini S. M., Johansen T. A., and Fatehi A. Comparison of nonlinearity measures based on time series analysis for nonlinearity detection. *Modeling, Identification and Control*, 32(4):123–140, 2011. doi:10.4173/mic.2011.4.1.

[98] Hot A., Kerschen G., Foltête E., and Cogan S. Detection and quantification of nonlinear structural behavior using principal component analysis. *Mechanical Systems and Signal Processing*, 26(1):104–116, 2012. doi:10.1016/j.ymssp.2011.06.006.

[99] Huang B. and Kunoth A. An optimization based empirical mode decomposition scheme. *Journal of Computational and Applied Mathematics*, 240:174 – 183, 2013. doi:10.1016/j.cam.2012.07.012.

[100] Huang N. E., Hu K., Yang A. C. C., Chang H.-C., Jia D., Liang W.-K., Yeh J. R., Kao C.-L., Juan C.-H., Peng C. K., Meijer J. H., Wang Y.-H., Long S. R., and Wu Z. On Holo-Hilbert spectral analysis: A full informational spectral representation for nonlinear and non-stationary data. *Philosophical Transactions of the Royal Society of London A: Mathematical, Physical and Engineering Sciences*, 374(2065), 2016. doi:10.1098/rsta.2015.0206.

[101] Huang N. E. and Shen S. S. P. *Hilbert-Huang Transform and Its Applications*. World Scientific, 2005.

[102] Huang N. E., Shen Z., and Long S. R. A new view of nonlinear water waves: The Hilbert spectrum. *Annual Review of Fluid Mechanics*, 31(1):417–457, 1999. doi:10.1146/annurev.fluid.31.1.417.

[103] Huang N. E., Shen Z., Long S. R., Wu M. C., Shih H. H., Zheng Q., Yen N.-C., Tung C. C., and Liu H. H. The empirical mode decomposition and the Hilbert spectrum for nonlinear and non-stationary time series analysis. *Proceedings of the Royal Society of London A: Mathematical, Physical and Engineering Sciences*, 454(1971):903–995, 1998. doi:10.1098/rspa.1998.0193.

[104] Huang N. E., Wu Z., Long S. R., Arnold K. C., Chen X., and Blank K. On instantaneous frequency. *Advances in Adaptive Data Analysis*, 1(2):177–229, 2009. doi:10.1142/S1793536909000096.

[105] Ismail M., Ikhouane F., and Rodellar J. The hysteresis Bouc-Wen model, A survey. *Archives of Computational Methods in Engineering*, 16(2):161–188, 2009. doi:10.1007/s11831-009-9031-8.

[106] Iwan W. D. A distributed-element model for hysteresis and its steady-state dynamic response. *Journal of Applied Mechanics*, 33(4):893–900, 1966. doi:10.1115/1.3625199.

[107] Jaumouillé V., Sinou J.-J., and Petitjean B. An adaptive harmonic balance method for predicting the nonlinear dynamic responses of mechanical systems—application to bolted structures. *Journal of Sound and Vibration*, 329(19):4048–4067, 2010. doi:10.1016/j.jsv.2010.04.008.

[108] Josefsson A., Magnevall M., Ahlin K., and Broman G. Spatial location identification of structural nonlinearities from random data. *Mechanical Systems and Signal Processing*, 27:410–418, 2012. doi:10.1016/j.ymssp.2011.07.020.

[109] Juang J.-N. and Pappa R. S. An eigensystem realization algorithm for modal parameter identification and model reduction. *Journal of Guidance, Control, and Dynamics*, 8(5):620–627, 1985. doi:10.2514/3.20031.

[110] Juditsky A., Hjalmarsson H., Benveniste A., Delyon B., Ljung L., Sjöberg J., and Zhang Q. Nonlinear black-box models in system identification: Mathematical foundations. *Automatica*, 31(12):1725–1750, 1995. doi:10.1016/0005-1098(95)00119-1.

[111] Kaliakin V. N. and Li J. Insight into deficiencies associated with commonly used zero-thickness interface elements. *Computers and Geotechnics*, 17(2):225–252, 1995. doi:10.1016/0266-352X(95)93870-O.

[112] Karkar S., Cochelin B., and Vergez C. A comparative study of the harmonic balance method and the orthogonal collocation method on stiff nonlinear systems. *Journal of Sound and Vibration*, 333(12):2554–2567, 2014. doi:10.1016/j.jsv.2014.01.019.

[113] Kerschen G. *On the Model Validation in Non-linear Structural Dynamics*. PhD thesis, University of Liege, 2002.

[114] Kerschen G. and Golinval J.-C. A model updating strategy of non-linear vibrating structures. *International Journal for Numerical Methods in Engineering*, 60(13):2147–2164, 2004. doi:10.1002/nme.1040.

[115] Kerschen G., Lenaerts V., and Golinval J.-C. Identification of a continuous structure with a geometrical non-linearity. Part I: Conditioned reverse path method. *Journal of Sound and Vibration*, 262(4):889–906, 2003. doi:10.1016/S0022-460X(02)01151-3.

[116] Kerschen G., Lenaerts V., and Golinval J.-C. VTT benchmark: Application of the restoring force surface method. *Mechanical Systems and Signal Processing*, 17(1):189–193, 2003. doi:10.1006/mssp.2002.1558.

[117] Kerschen G., Peeters M., Golinval J.-C., and Vakakis A. F. Nonlinear normal modes, Part I: A useful framework for the structural dynamicist. *Mechanical Systems and Signal Processing*, 23(1):170–194, 2009. doi:10.1016/j.ymssp.2008.04.002.

[118] Kerschen G., Vakakis A. F., Lee Y. S., Mcfarland M. D., and Bergman L. A. Toward a fundamental understanding of the Hilbert-Huang transform in nonlinear structural dynamics. *Journal of Vibration and Control*, 14(1-2):77–105, 2008. doi:10.1177/1077546307079381.

[119] Kerschen G., Worden K., Vakakis A. F., and Golinval J.-C. Past, present and future of nonlinear system identification in structural dynamics. *Mechanical Systems and Signal Processing*, 20(3):505–592, 2006. doi:10.1016/j.ymssp.2005.04.008.

[120] Kim J., Yoon J.-C., and Kang B.-S. Finite element analysis and modeling of structure with bolted joints. *Applied Mathematical Modelling*, 31(5):895–911, 2007. doi:10.1016/j.apm.2006.03.020.

[121] Kim W.-J. and Park Y.-S. Non-linearity identification and quantification using an inverse Fourier transform. *Mechanical Systems and Signal Processing*, 7(3):239–255, 1993. doi:10.1006/mssp.1993.1011.

[122] Kinkaid N. M., O'Reilly O. M., and Papadopoulos P. Automotive disc brake squeal. *Journal of Sound and Vibration*, 267(1):105–166, 2003. doi:10.1016/S0022-460X(02)01573-0.

[123] Kirshenboim J. and Ewins D. J. A method for recognizing structural nonlinearities in steady-state harmonic testing. *Journal of Vibration, Acoustics, Stress, and Reliability in Design*, 106(1):49–52, 1984. doi:10.1115/1.3269151.

[124] Kohonen T. *Self-Organizing Maps*. Springer, 1997.

[125] Koyuncu A., Cigeroglu E., Yumer M. E., and Özgüven H. N. Localization and identification of structural nonlinearities using neural networks. In Kerschen G., Adams D. E., and Carrella A., editors, *Topics in Nonlinear Dynamics, Volume 1: Conference Proceedings of the Society for Experimental Mechanics Series*, pages 103–112. Springer, 2013. doi:10.1007/978-1-4614-6570-6_9.

[126] Koyuncu A., Cigeroglu E., and Özgüven H. N. Localization and identification of structural nonlinearities using cascaded optimization and neural networks. *Mechanical Systems and Signal Processing*, 95:219–238, 2017. doi:10.1016/j.ymssp.2017.03.030.

[127] Krack M., Panning-Von Scheidt L., and Wallaschek J. A method for nonlinear modal analysis and synthesis: Application to harmonically forced and self-excited mechanical systems. *Journal of Sound and Vibration*, 332(25):6798–6814, 2013. doi:10.1016/j.jsv.2013.08.009.

[128] Krack M., Panning-Von Scheidt L., and Wallaschek J. On the computation of the slow dynamics of nonlinear modes of mechanical systems. *Mechanical Systems and Signal Processing*, 42(1-2):71–87, 2014. doi:10.1016/j.ymssp.2013.08.031.

[129] Krack M., Salles L., and Thouverez F. Vibration prediction of bladed disks coupled by friction joints. *Archives of Computational Methods in Engineering*, pages 1–48, 2016. doi:10.1007/s11831-016-9183-2.

[130] Kragh K. A., Thomsen J. J., and Tcherniak D. Experimental detection and quantification of structural nonlinearity using homogeneity and Hilbert transform methods. In *Proceedings of the International Conference on Noise and Vibration Engineering*, pages 3173–3188, 2010.

[131] Kuether R. J. and Brake M. R. W. Instantaneous frequency and damping from transient ring-down data. In Allen M., Mayes R. L., and Rixen D., editors, *Dynamics of Coupled Structures, Volume 4: Proceedings of the 34th IMAC, A Conference and Exposition on Structural Dynamics 2016*, pages 253–263. Springer International Publishing, 2016. doi:10.1007/978-3-319-29763-7_24.

[132] Lacy S. L. and Bernstein D. S. Subspace identification for non-linear systems with measured-input non-linearities. *International Journal of Control*, 78(12):906–926, 2005. doi:10.1080/00207170500214095.

[133] Lang Z. Q. and Peng Z. K. A novel approach for nonlinearity detection in vibrating systems. *Journal of Sound and Vibration*, 314(3-5):603–615, 2008. doi:10.1016/j.jsv.2008.01.043.

[134] Laxalde D., Salles L., Blanc L., and Thouverez F. Non-linear modal analysis for bladed disks with friction contact interfaces. In *ASME Turbo Expo: Power for Land, Sea, and Air, Volume 5: Structures and Dynamics, Parts A and B*, pages 457–467, Berlin, Germany, 2008. doi:10.1115/GT2008-50860.

[135] Laxalde D. and Thouverez F. Complex non-linear modal analysis for mechanical systems: Application to turbomachinery bladings with friction interfaces. *Journal of Sound and Vibration*, 322(4-5):1009–1025, 2009. doi:10.1016/j.jsv.2008.11.044.

[136] Le T.-P. and Argoul P. Continuous wavelet transform for modal identification using free decay response. *Journal of Sound and Vibration*, 277(1–2):73–100, 2004. doi:10.1016/j.jsv.2003.08.049.

[137] Lee Y. S., Tsakirtzis S., Vakakis A. F., Bergman L. A., and McFarland D. M. A time-domain nonlinear system identification method based on multiscale dynamic partitions. *Meccanica*, 46(4):625–649, 2011. doi:10.1007/s11012-010-9327-7.

[138] Lee Y. S., Tsakirtzis S., Vakakis A. F., Bergman L. A., and McFarland M. D. Physics-based foundation for empirical mode decomposition. *AIAA Journal*, 47(12):2938–2963, 2009. doi:10.2514/1.43207.

[139] Lenaerts V., Kerschen G., and Golinval J.-C. Identification of a continuous structure with a geometrical non-linearity. Part II: Proper orthogonal decomposition. *Journal of Sound and Vibration*, 262(4):907–919, 2003. doi:10.1016/S0022-460X(02)01132-X.

[140] Li Z. and Crocker M. J. A study of joint time-frequency analysis-based modal analysis. *IEEE Transactions on Instrumentation and Measurement*, 55(6):2335–2342, 2006. doi:10.1109/TIM.2006.884137.

[141] Lin R. M. and Ewins D. J. Location of localised stiffness non-linearity using measured modal data. *Mechanical Systems and Signal Processing*, 9(3):329–339, 1995. doi:10.1006/mssp.1995.0027.

[142] Londoño J. M., Neild S. A., and Cooper J. E. Identification of backbone curves of nonlinear systems from resonance decay responses. *Journal of Sound and Vibration*, 348:224–238, 2015. doi:10.1016/j.jsv.2015.03.015.

[143] Luzzato E. Approximate computation of non-linear effects in a vibrating cracked beam. *Journal of Sound and Vibration*, 265(4):745–763, 2003. doi:10.1016/S0022-460X(02)01562-6.

[144] Magnevall M., Josefsson A., Ahlin K., and Broman G. Nonlinear structural identification by the reverse path spectral method. *Journal of Sound and Vibration*, 331(4):938–946, 2012. doi:10.1016/j.jsv.2011.10.029.

[145] Makki Alamdari M., Li J., and Samali B. FRF-based damage localization method with noise suppression approach. *Journal of Sound and Vibration*, 333(14):3305–3320, 2014. doi:10.1016/j.jsv.2014.02.035.

[146] Marchesiello S. and Garibaldi L. A time domain approach for identifying nonlinear vibrating structures by subspace methods. *Mechanical Systems and Signal Processing*, 22(1):81–101, 2008. doi:10.1016/j.ymssp.2007.04.002.

[147] Marple S. L. Computing the discrete-time analytic signal via FFT. *IEEE Transactions on Signal Processing*, 47(9):2600–2603, 1999. doi:10.1109/78.782222.

[148] Masri S. F. and Caughey T. K. A nonparametric identification technique for nonlinear dynamic problems. *Journal of Applied Mechanics*, 46(2):433–447, 1979. doi:10.1115/1.3424568.

[149] McIntyre M. E. and Woodhouse J. Friction and the bowed string. *Wear*, 113(1):175–182, 1986. doi:10.1016/0043-1648(86)90067-0.

[150] Mertens M. The complex stiffness method to detect and identify non-linear dynamic behaviour of SDOF systems. *Mechanical Systems and Signal Processing*, 3(1):37–54, 1989. doi:10.1016/0888-3270(89)90021-6.

[151] Meyer S. and Link M. Modelling and updating of local non-Linearities using frequency response residuals. *Mechanical Systems and Signal Processing*, 17(1):219–226, 2003. doi:10.1006/mssp.2002.1563.

[152] Mikhlin Y. V. and Avramov K. V. Nonlinears normal modes for vibrating mechanical systems. Review of rheoretical developments. *Applied Mechanics Reviews*, 63(6):060802–21, 2011. doi:10.1115/1.4003825.

[153] Mohammad K. S., Worden K., and Tomlinson G. R. Direct parameter estimation for linear and non-linear sturctures. *Journal of Sound and Vibration*, 152(3):471–499, 1992. doi:10.1016/0022-460X(92)90482-D.

[154] Moon F. C. *Chaotic Vibrations: An Introduction for Applied Scientists and Engineers*. Wiley, 2004.

[155] Moore K. J., Kurt M., Eriten M., McFarland D. M., Bergman L. A., and Vakakis A. F. Wavelet-bounded empirical mode decomposition for measured time series analysis. *Mechanical Systems and Signal Processing*, 99:14–29, 2018. doi:10.1016/j.ymssp.2017.06.005.

[156] Nacivet S., Pierre C., Thouverez F., and Jezequel L. A dynamic Lagrangian frequency–time method for the vibration of dry-friction-damped systems. *Journal of Sound and Vibration*, 265(1):201–219, 2003. doi:10.1016/S0022-460X(02)01447-5.

[157] Nagarajaiah S. and Basu B. Output only modal identification and structural damage detection using time frequency & wavelet techniques. *Earthquake Engineering and Engineering Vibration*, 8(4):583–605, 2009. doi:10.1007/s11803-009-9120-6.

[158] Nayhef A. H. and Mook D. T. *Nonlinear oscillations*. John Wiley & Sons, Inc., 1979.

[159] Naylor S., Platten M. F., Wright J. R., and Cooper J. E. Identification of multi degree of freedom systems with nonproportional damping using the resonant decay method. *Journal of Vibration and Acoustics*, 126(2):298, 2004. doi:10.1115/1.1687395.

[160] Nehete D. V., Modak S. V., and Gupta K. Structural FE model updating of cavity systems incorporating vibro-acoustic coupling. *Mechanical Systems and Signal Processing*, 50-51:362–379, 2015. doi:10.1016/j.ymssp.2014.05.028.

[161] Neild S. A., McFadden P. D., and Williams M. S. A review of time-frequency methods for structural vibration analysis. *Engineering Structures*, 25(6):713–728, 2003. doi:10.1016/S0141-0296(02)00194-3.

[162] Noël J.-P. *A Frequency-domain Approach to Subspace Identification of Nonlinear Systems Application to Aerospace Structures*. PhD thesis, University of Liege, 2014.

[163] Noël J.-P. and Kerschen G. Frequency-domain subspace identification for nonlinear mechanical systems. *Mechanical Systems and Signal Processing*, 40(2):701–717, 2013. doi:10.1016/j.ymssp.2013.06.034.

[164] Noël J.-P. and Kerschen G. Nonlinear system identification in structural dynamics: 10 more years of progress. *Mechanical Systems and Signal Processing*, 83:2–35, 2017. doi:10.1016/j.ymssp.2016.07.020.

[165] Noël J.-P., Kerschen G., Foltête E., and Cogan S. Grey-box identification of a nonlinear solar array structure using cubic splines. *International Journal of Non-Linear Mechanics*, 67:106–119, 2014. doi:10.1016/j.ijnonlinmec.2014.08.012.

[166] Noël J.-P., Kerschen G., and Newerla A. Application of the restoring force surface method to a real-life spacecraft structure. In Adams D., Kerschen G., and Carrella A., editors, *Topics in Nonlinear Dynamics, Volume 3: Conference Proceedings of the Society for Experimental Mechanics Series*, pages 1–19. Springer, New York, NY, 2012. doi:10.1007/978-1-4614-2416-1_1.

[167] Noël J.-P., Marchesiello S., and Kerschen G. Subspace-based identification of a nonlinear spacecraft in the time and frequency domains. *Mechanical Systems and Signal Processing*, 43(1-2):217–236, 2014. doi:10.1016/j.ymssp.2013.10.016.

[168] Noël J.-P., Renson L., Grappasonni C., and Kerschen G. Identification of nonlinear normal modes of engineering structures under broadband forcing. *Mechanical Systems and Signal Processing*, 74:95–110, 2016. doi:10.1016/j.ymssp.2015.04.016.

[169] Noël J.-P., Renson L., and Kerschen G. Complex dynamics of a nonlinear aerospace structure: Experimental identification and modal interactions. *Journal of Sound and Vibration*, 333(12):2588–2607, 2014. doi:10.1016/j.jsv.2014.01.024.

[170] Norton H. N. *Handbook of Transducers*. Prentice Hall, 1989.

[171] Nuttall A. H. and Bedrosian E. On the quadrature approximation to the Hilbert transform of modulated signals. *Proceedings of the IEEE*, 54(10):1458–1459, 1966. doi:10.1109/PROC.1966.5138.

[172] Ondra V. *Creation of Modal Parameter Estimation Application for Experimental Modal Analysis*. Master's thesis, Brno University of Technology, 2014.

[173] Ondra V., Riethmueller R., Brake M. R. W., Schwingshackl C. W., Polunin P. M., and Shaw S. W. Comparison of nonlinear system identification methods for free decay measurements with application to MEMS devices. In Wee Sit E., Walber C., Walter P., and Seidlitz S., editors, *Sensors and Instrumentation, Volume 5. Conference Proceedings of the Society for Experimental Mechanics Series*, Los Angeles, California, USA, 2017. doi:10.1007/978-3-319-54987-3_5.

[174] Ondra V., Sever I. A., and Schwingshackl C. W. Non-parametric identification of asymmetric signals and characterization of a class of non-linear systems based on frequency modulation. In *ASME International Mechanical Engineering Congress and Exposition, Volume 4B: Dynamics, Vibration, and Control*, page V04BT05A010, Phoenix, Arizona, USA, 2016. doi:10.1115/IMECE2016-65229.

[175] Ondra V., Sever I. A., and Schwingshackl C. W. A method for detection and characterisation of structural non-linearities using the Hilbert transform and neural networks. *Mechanical Systems and Signal Processing*, 83:210–227, 2017. doi:10.1016/j.ymssp.2016.06.008.

[176] Oppenheim A. V., Schafer R. W., and Buck J. R. *Discrete-time Signal Processing (2nd Ed.)*. Prentice-Hall, 1999.

[177] Özer M. B., Özgüven N. H., and Royston T. J. Identification of structural non-linearities using describing functions and the Sherman-Morrison method. *Mechanical Systems and Signal Processing*, 23(1):30–44, 2009. doi:10.1016/j.ymssp.2007.11.014.

[178] Padmanabhan C. and Singh R. Analysis of periodically excited non-linear systems by a parametric continuation technique. *Journal of Sound and Vibration*, 184(1):35–58, 1995. doi:10.1006/jsvi.1995.0303.

[179] Pai P. F. *Highly Flexible Structures: Modeling, Computation, and Experimentation*. AIAA Education Series, 2007.

[180] Pai P. F. Nonlinear vibration characterization by signal decomposition. *Journal of Sound and Vibration*, 307(3-5):527–544, 2007. doi:10.1016/j.jsv.2007.06.056.

[181] Pai P. F. Time–frequency characterization of nonlinear normal modes and challenges in nonlinearity identification of dynamical systems. *Mechanical Systems and Signal Processing*, 25(7):2358–2374, 2011. doi:10.1016/j.ymssp.2011.02.013.

[182] Pai P. F. Time-frequency analysis for parametric and non-parametric identification of nonlinear dynamical systems. *Mechanical Systems and Signal Processing*, 36(2):332–353, 2013. doi:10.1016/j.ymssp.2012.12.002.

[183] Pai P. F., Nguyen B.-A., and Sundaresan M. J. Nonlinearity identification by time-domain-only signal processing. *International Journal of Non-Linear Mechanics*, 54:85–98, 2013. doi:10.1016/j.ijnonlinmec.2013.04.002.

[184] Pai P. F. and Palazotto A. N. Detection and identification of nonlinearities by amplitude and frequency modulation analysis. *Mechanical Systems and Signal Processing*, 22(5):1107–1132, 2008. doi:10.1016/j.ymssp.2007.11.006.

[185] Pai P. F. and Palazotto A. N. HHT-based nonlinear signal processing method for parametric and non-parametric identification of dynamical systems. *International Journal of Mechanical Sciences*, 50(12):1619–1635, 2008. doi:10.1016/j.ijmecsci.2008.10.001.

[186] Panayotoukanos D. E., Panayotounakou N. D., and Vakakis A. F. On the solution of the unforced damped duffing oscillator with no linear stiffness term. *Nonlinear Dynamics*, 28(1):1–16, 2002. doi:10.1023/A:1014925032022.

[187] Parloo E. *Application of Frequency-Domain System Identification Techniques in the Field of Operational Modal Analysis*. PhD thesis, University in Brussels, 2003.

[188] Peeters B., Van Der Auweraer H., Guillaume P., and Leuridan J. The PolyMAX frequency-domain method: A new standard for modal parameter estimation? *Shock and Vibration*, 11(3–4):395–409, 2004. doi:10.1155/2004/523692.

[189] Peeters M. *Theoretical and Experimental Modal Analysis of Nonlinear Vibrating Structures using Nonlinear Normal Modes*. PhD Thesis, University of Liege, 2010.

[190] Peeters M., Kerschen G., and Golinval J.-C. Dynamic testing of nonlinear vibrating structures using nonlinear normal modes. *Journal of Sound and Vibration*, 330(3):486–509, 2011. doi:10.1016/j.jsv.2010.08.028.

[191] Peeters M., Kerschen G., and Golinval J.-C. Modal testing of nonlinear vibrating structures based on nonlinear normal modes: Experimental demonstration. *Mechanical Systems and Signal Processing*, 25(4):1227–1247, 2011. doi:10.1016/j.ymssp.2010.11.006.

[192] Peeters M., Viguié R., Sérandour G., Kerschen G., and Golinval J.-C. Nonlinear normal modes, Part II: Toward a practical computation using numerical continuation techniques. *Mechanical Systems and Signal Processing*, 23(1):195–216, 2009. doi:10.1016/j.ymssp.2008.04.003.

[193] Pegram G. G. S., Peel M. C., and McMahon T. A. Empirical mode decomposition using rational splines: An application to rainfall time series. *Proceedings of the Royal Society of London A: Mathematical, Physical and Engineering Sciences*, 464(2094):1483–1501, 2008. doi:10.1098/rspa.2007.0311.

[194] Peifer M., Timmer J., and Voss H. U. Non-parametric identification of non-linear oscillating systems. *Journal of Sound and Vibration*, 267(5):1157–1167, 2003. doi:10.1016/S0022-460X(03)00361-4.

[195] Peng Z. K., Tse P. W., and F. L. An improved Hilbert-Huang transform and its application in vibration signal analysis. *Journal of Sound and Vibration*, 286(1-2):187–205, 2005. doi:10.1016/j.jsv.2004.10.005.

[196] Pesaresi L. *On the Validation of Nonlinear Dynamic Models for Structures with Frictional Joints*. PhD thesis, Imperial College London, 2017.

[197] Pesaresi L., Salles L., Elliott R., Jones A., Green J., and Schwingshackl C. W. Numerical and experimental investigation of an under-platform damper test rig. *Applied Mechanics and Materials*, 849:1–12, 2016. doi:10.4028/www.scientific.net/AMM.849.1.

[198] Pesaresi L., Salles L., Jones A., Green J. S., and Schwingshackl C. W. Modelling the nonlinear behaviour of an underplatform damper test rig for turbine applications. *Mechanical Systems and Signal Processing*, 85:662–679, 2017. doi:10.1016/j.ymssp.2016.09.007.

[199] Pesaresi L., Stender M., Ruffini V., and Schwingshackl C. W. DIC measurement of the kinematics of a friction damper for turbine applications. In Allen M. S., Mayes R. L., and Rixen D. J., editors, *Dynamics of Coupled Structures, Volume 4: Proceedings of the 35th IMAC, A Conference and Exposition on Structural Dynamics 2017*, pages 93–101. Springer International Publishing, 2017. doi:10.1007/978-3-319-54930-9_9.

[200] Pesheck E., Boivin N., Pierre C., and Shaw S. W. Nonlinear modal analysis of structural systems using multi-mode invariant manifolds. *Nonlinear Dynamics*, 25(1):183–205, 2001. doi:10.1023/A:1012910918498.

[201] Petrov E. P. and Ewins D. J. Analytical formulation of friction interface elements for analysis of nonlinear multi-harmonic vibrations of bladed disks. *Journal of Turbomachinery*, 125(2):364–371, 2003. doi:10.1115/1.1539868.

[202] Petrov E. P. and Ewins D. J. State-of-the-art dynamic analysis for non-linear gas turbine structures. *Proceedings of the Institution of Mechanical Engineers, Part G: Journal of Aerospace Engineering*, 218(3):199–211, 2004. doi:10.1243/0954410041872906.

[203] Petrov E. P. and Ewins D. J. Effects of damping and varying contact area at blade-disk joints in forced response analysis of bladed disk assemblies. *Journal of Turbomachinery*, 128(2):403, 2006. doi:10.1115/1.2181998.

[204] Pierre C., Jiang D., and Shaw S. Nonlinear normal modes and their application in structural dynamics. *Mathematical Problems in Engineering*, 2006:1–15, 2006. doi:10.1155/MPE/2006/10847.

[205] Platten M., Wright J., Dimitriadis G., and Cooper J. Identification of multi-degree of freedom non-linear systems using an extended modal space model. *Mechanical Systems and Signal Processing*, 23(1):8–29, 2009. doi:10.1016/j.ymssp.2007.11.016.

[206] Polunin P., Yang Y., Atalaya J., Ng E., Strachan S., Shoshani O., Dykman M., Shaw S., and Kenny T. Characterizing MEMS nonlinearities directly: The ring-down measurements. In *2015 Transducers - 2015 18th International Conference on Solid-State Sensors, Actuators and Microsystems (TRANSDUCERS)*, pages 2176–2179, 2015. doi:10.1109/TRANSDUCERS.2015.7181391.

[207] Polunin P. M. *Nonlinearities and Noise in Micromechanical Resonators: From Understanding to Characterization and Design Tools*. PhD thesis, Michigan State University, 2016.

[208] Polunin P. M., Yang Y., Dykman M. I., Kenny T. W., and Shaw S. W. Characterization of MEMS resonator nonlinearities using the ringdown response. *Journal of Microelectromechanical Systems*, 25(2):297–303, 2016. doi:10.1109/JMEMS.2016.2529296.

[209] Pustelnik N., Borgnat P., and Flandrin P. A multicomponent proximal algorithm for empirical mode decomposition. In *Proceedings of the 20th European Signal Processing Conference (EUSIPCO)*, pages 1880–1884, 2012.

[210] Qin S., Wang Q., and Kang J. Output-only modal analysis based on improved empirical mode decomposition method. *Advances in Materials Science and Engineering*, 2015:1–12, 2015. doi:10.1155/2015/945862.

[211] Rato R. T., Ortigueira M. D., and Batista A. G. On the HHT, its problems, and some solutions. *Mechanical Systems and Signal Processing*, 22(6):1374–1394, 2008. doi:10.1016/j.ymssp.2007.11.028.

[212] Rauch A. Corehence: a powerful estimator of nonlinearity, theory and application. In *Proceedings of the 10th International Modal Analysis Conference (IMAC)*, pages 784–795, 1992.

[213] Reid J. D. and Hiser N. R. Detailed modeling of bolted joints with slippage. *Finite Elements in Analysis and Design*, 41(6):547–562, 2005. doi:10.1016/j.finel.2004.10.001.

[214] Renson L., Gonzalez-Buelga A., Barton D. A. W., and Neild S. A. Robust identification of backbone curves using control-based continuation. *Journal of Sound and Vibration*, 367:145–158, 2016. doi:10.1016/j.jsv.2015.12.035.

[215] Renson L., Kerschen G., and Cochelin B. Numerical computation of nonlinear normal modes in mechanical engineering. *Journal of Sound and Vibration*, 364, 2016. doi:10.1016/j.jsv.2015.09.033.

[216] Reynders E. and De Roeck G. Reference-based combined deterministic–stochastic subspace identification for experimental and operational modal analysis. *Mechanical Systems and Signal Processing*, 22(3):617–637, 2008. doi:10.1016/j.ymssp.2007.09.004.

[217] Rice H. J. and Fitzpatrick J. A. A generalised technique for spectral analysis of non-linear systems. *Mechanical Systems and Signal Processing*, 2(2):195–207, 1988. doi:10.1016/0888-3270(88)90043-X.

[218] Richards C. M. and Singh R. Feasibility of identifying non-linear vibration systems consiting of unknown polynomial forms. *Journal of Sound and Vibration*, 220(3):413–450, 1999. doi:10.1006/jsvi.1998.1918.

[219] Richards C. M. and Singh R. Characterization of rubber isolator nonlinearities in the context of single- and multi-degree-of-freedom experimental systems. *Journal of Sound and Vibration*, 247(5):807–834, 2001. doi:10.1006/jsvi.2001.3759.

[220] Rilling G. and Flandrin P. One or two frequencies? The empirical mode decomposition answers. *IEEE Transactions on Signal Processing*, 56(1):85–95, 2008. doi:10.1109/TSP.2007.906771.

[221] Rilling G., Flandrin P., and Gonçalves P. On empirical mode decomposition and its algorithms. In *Proceedings of IEEE-EURASIP Workshop on Nonlinear Signal and Image Processing NSIP-03*, Grado, Italy, 2003.

[222] Rosenberg R. M. On nonlinear vibrations of systems with many degrees of freedom. *Advances in Applied Mechanics*, 9:155–242, 1966. doi:10.1016/S0065-2156(08)70008-5.

[223] Rother A., Mohieddine J., and Söffker D. A brief review and a first application of time-frequency-based analysis methods for monitoring of strip rolling mills. *Journal of Process Control*, 35:65–79, 2015. doi:10.1016/j.jprocont.2015.08.010.

[224] Ruffini V., Schwingshackl C. W., and Green J. S. LDV measurement of local nonlinear contact conditions of flange joint. In Kerschen G., Adams D., and Carrella A., editors, *Topics in Nonlinear Dynamics, Volume 1: Proceedings of the 31st IMAC, A Conference on Structural Dynamics, 2013*, pages 159–168, 2013. doi:10.1007/978-1-4614-6570-6_14.

[225] Ruzzene M., Fasana A., Garibaldi L., and Piombo B. Natural frequencies and dampings identification using wavelet transform: Application to real data. *Mechanical Systems and Signal Processing*, 11(2):207–218, 1997. doi:10.1006/mssp.1996.0078.

[226] Sainsbury M. G. and Ho Y. K. Application of the time domain fourier filter output (TDFFO) method to the identification of a lightly damped non-linear system with an odd-spring characteristic. *Mechanical Systems and Signal Processing*, 15(2):357–366, 2001. doi:10.1006/mssp.2000.1308.

[227] Salles L., Blanc L., Thouverez F., Gouskov A. M., and Jean P. Dual time stepping algorithms with the high order harmonic balance method for contact interfaces with fretting-wear. *Journal of Engineering for Gas Turbines and Power*, 134(3):032503, 2012. doi:10.1115/1.4004236.

[228] Salles L., Staples B., Hoffmann N., and Schwingshackl C. Continuation techniques for analysis of whole aeroengine dynamics with imperfect bifurcations and isolated solutions. *Nonlinear Dynamics*, 86(3):1897–1911, 2016. doi:10.1007/s11071-016-3003-y.

[229] Salzenstein F., Boudraa A.-O., and Cexus J.-C. Generalized higher-order nonlinear energy operators. *Journal of Optical Society of America A*, 24(12):3717–3727, 2007. doi:10.1364/JOSAA.24.003717.

[230] Sanliturk K. Y., Imregun M., and Ewins D. J. Harmonic balance vibration analysis of turbine blades with friction dampers. *Journal of Vibration and Acoustics*, 119(1):96–103, 1997. doi:10.1115/1.2889693.

[231] Schmidt A. and Gaul L. Finite element formulation of viscoelastic constitutive equations using fractional time derivatives. *Nonlinear Dynamics*, 29(1):37–55, 2002. doi:10.1023/A:1016552503411.

[232] Schmidt R. Updating non-linear components. *Mechanical Systems and Signal Processing*, 8(6):679–690, 1994. doi:10.1006/mssp.1994.1048.

[233] Scholz M. Validation of nonlinear PCA. *Neural Processing Letters*, 36(1):21–30, 2012. doi:10.1007/s11063-012-9220-6.

[234] Schoukens J., Pintelon R., Rolain Y., and Dobrowiecki T. Frequency response function measurements in the presence of non-linear distortions. A general framework and practical advices. In *Proceedings of the International Conference on Noise and Vibration Engineering*, pages 459–464, Leuven, Belgium, 2001.

[235] Schwingshackl C. W., Di Maio D., Sever I. A., and Green J. S. Modeling and validation of the nonlinear dynamic behavior of bolted flange joints. *Journal of Engineering for Gas Turbines and Power*, 135(12):122504, 2013. doi:10.1115/1.4025076.

[236] Segalman D. J. Modelling joint friction in structural dynamics. *Structural Control and Health Monitoring*, 13(1):430–453, 2006. doi:10.1002/stc.119.

[237] Senroy N., Suryanarayanan S., and Ribeiro P. F. An improved Hilbert-Huang method for analysis of time-varying waveforms in power quality. *IEEE Transactions on Power Systems*, 22(4):1843–1850, 2007. doi:10.1109/TPWRS.2007.907542.

[238] Sever I. A. Nonlinear vibration phenomena in aero-engine measurements. In Allen M., Mayes R. L., and Rixen D., editors, *Dynamics of Coupled Structures, Volume 4: Proceedings of the 34th IMAC, A Conference and Exposition on Structural Dynamics 2016*, pages 241–252. Springer International Publishing, 2016. doi:10.1007/978-3-319-29763-7_23.

[239] Seydel R. *Practical Bifurcation and Stability Analysis*. Springer, 2010. doi:10.1007/978-1-4419-1740-9.

[240] Sharma K. G. and Desai C. S. Analysis and implementation of thin-layer element for interfaces and joints. *Journal of Engineering Mechanics*, 118(12):2442–2462, 1992. doi:10.1061/(ASCE)0733-9399(1992)118:12(2442).

[241] Shaw S. W. and Pierre C. Normal modes for non-linear vibratory systems. *Journal of Sound and Vibration*, 164(1):85–124, 1993. doi:10.1006/jsvi.1993.1198.

[242] Shin K. and Hammond J. *Fundamentals of Signal Processing for Sound and Vibration Engineers*. Wiley-Blackwell, 2008.

[243] Sieber J., Gonzalez-Buelga A., Neild S. A., Wagg D. J., and Krauskopf B. Experimental continuation of periodic orbits through a fold. *Physical Review Letters*, 100:244101, 2008. doi:10.1103/PhysRevLett.100.244101.

[244] Siller H. R. E. *Non-linear Modal Analysis Methods for Engineering Structures*. PhD thesis, Imperial College London, 2004.

[245] Simon M. and Tomlinson G. R. Use of the Hilbert transform in modal analysis of linear and non-linear structures. *Journal of Sound And Vibration*, 96(4):421–436, 1984. doi:10.1016/0022-460X(84)90630-8.

[246] Singh R., Davies P., and Bajaj A. K. Identification of nonlinear and viscoelastic properties of flexible polyurethane foam. *Nonlinear Dynamics*, 34(3):319–346, 2004. doi:10.1023/B:NODY.0000013511.07097.87.

[247] Sivaselvan M. V. and Reinhorn A. M. Hysteretic models for deteriorating inelastic structures. *Journal of Engineering Mechanics*, 126(6):633–640, 2000. doi:10.1061/(ASCE)0733-9399(2000)126:6(633).

[248] Sjöberg J., Zhang Q., Ljung L., Benveniste A., Delyon B., Glorennec P.-Y., Hjalmarsson H., and Juditsky A. Nonlinear black-box modeling in system identification: unified overview. *Automatica*, 31(12):1691–1724, 1995. doi:10.1016/0005-1098(95)00120-8.

[249] Song Y., Hartwigsen C. J., McFarland D. M., Vakakis A. F., and Bergman L. A. Simulation of dynamics of beam structures with bolted joints using adjusted Iwan beam elements. *Journal of Sound and Vibration*, 273(1-2):249–276, 2004. doi:10.1016/S0022-460X(03)00499-1.

[250] Spina D., Valente C., and Tomlinson G. R. A new procedure for detecting nonlinearity from transient data using the Gabor transform. *Nonlinear Dynamics*, 11(3):235–254, 1996. doi:10.1007/BF00120719.

[251] Stanbridge A. B. and Ewins D. J. Modal testing using a scanning laser Doppler vibrometer. *Mechanical Systems and Signal Processing*, 13:255–270, 1999. doi:10.1006/mssp.1998.1209.

[252] Stanbridge A. B., Martarelli M., and Ewins D. J. Measuring area vibration mode shapes with a continuous-scan LDV. *Measurement*, 35(2):181–189, 2004. doi:10.1016/j.measurement.2003.07.005.

[253] Staszewski W. J. Identification of non-linear systems using multi-scale ridges and skeletons of the wavelet transform. *Journal of Sound and Vibration*, 214(4):639–658, 1998. doi:10.1006/jsvi.1998.1616.

[254] Staszewski W. J. Analysis of non-linear systems using wavelets. *Proceedings of the Institution of Mechanical Engineers, Part C: Journal of Mechanical Engineering Science*, 214(11):1339–1353, 2000. doi:10.1243/0954406001523317.

[255] Stickel J. J. Data smoothing and numerical differentiation by a regularization method. *Computers and Chemical Engineering*, 34(4):467–475, 2010. doi:10.1016/j.compchemeng.2009.10.007.

[256] Storer D. M. and Tomlinson G. R. Recent developments in the measurement and interpretation of higher order transfer functions from non-linear structures. *Mechanical Systems and Signal Processing*, 7(2):173–189, 1993. doi:10.1006/mssp.1993.1006.

[257] Stoykov S. and Margenov S. Numerical computation of periodic responses of nonlinear large-scale systems by shooting method. *Computers & Mathematics with Applications*, 67(12):2257–2267, 2014. doi:10.1016/j.camwa.2014.01.023.

[258] Strogatz S. H. *Nonlinear Dynamics and Chaos: With Applications to Physics, Biology, Chemistry, and Engineering*. Westview Press, 2014.

[259] Süß D. and Willner K. Investigation of a jointed friction oscillator using the multiharmonic balance method. *Mechanical Systems and Signal Processing*, 52-53:73–87, 2015. doi:10.1016/j.ymssp.2014.08.003.

[260] Tan K. C., Li Y., Murray-Smith D. J., and Sharman K. C. System identification and linearisation using genetic algorithms with simulated annealing. In *First International Conference on Genetic Algorithms in Engineering Systems: Innovations and Applications*, pages 164–169, 1995. doi:10.1049/cp:19951043.

[261] Thouverez F. Presentation of the ECL benchmark. *Mechanical Systems and Signal Processing*, 17(1):195–202, 2003. doi:10.1006/mssp.2002.1560.

[262] Thouverez F. and Jezequel L. Identification of NARMAX models on a modal base. *Journal of Sound and Vibration*, 189(2):193–213, 1996. doi:10.1006/jsvi.1996.0015.

[263] Tomlinson G. R. Development in the use of the Hilbert transform for detectiong and quantifying non-linearity associated with frequency response functions. *Mechanical Systems and Signal Processing*, 1(2):151–171, 1987. doi:10.1016/0888-3270(87)90068-9.

[264] Trendafilova I., Lenaerts V., Kerschen G., Golinval J.-C., and Brussel H. V. Detection, localisation and identification of nonlinearities in structural dynamics. In *Proceedings of the International Seminar on Modal Analysis (ISMA)*, Leuven, Belgium, 2000.

[265] Tsakirtzis S., Lee Y. S., Vakakis A. F., Bergman L. A., and Mcfarland M. D. Modelling of nonlinear modal interactions in the transient dynamics of an elastic rod with an essentially nonlinear attachment. *Communications in Nonlinear Science and Numerical Simulation*, 15(9):2617–2633, 2010. doi:10.1016/j.cnsns.2009.10.014.

[266] Vakakis A. F. Non-linear normal modes (NNMs) and their applications in vibration theory: An overview. *Mechanical Systems and Signal Processing*, 11(1):3–22, 1997. doi:10.1006/mssp.1996.9999.

[267] Vakakis A. F. *Normal Modes and Localization in Nonlinear Systems*. Springer, 2001. doi:10.1007/978-94-017-2452-4.

[268] Vakakis A. F. and Ewins D. J. Effects of weak non-linearities on modal analysis. *Mechanical Systems and Signal Processing*, 8(2):175–198, 1994. doi:10.1006/mssp.1994.1015.

[269] Vanhoenacker K., Schoukens J., Swevers J., and Vaes D. Summary and comparing overview of techniques for the detection of non-linear distortions. In *Proceeding of the International Seminal on Modal Analysis*, pages 1241–1256, 2002.

[270] Verboven P. *Frequency-Domain System Identification For Modal Analysis*. PhD thesis, University in Brussels, 2002.

[271] Verhulst F. *Nonlinear Differential Equations and Dynamical Systems*. John Wiley & Sons Ltd, 1996. doi:10.1007/978-3-642-61453-8.

[272] Vestroni F. and Noori M. Hysteresis in mechanical systems—modeling and dynamic response. *International Journal of Non-Linear Mechanics*, 37(8):1261–1262, 2002. doi:10.1016/S0020-7462(02)00059-8.

[273] Virgin L. N. *Introduction to Experimental Nonlinear Dynamics: A Case Study in Mechanical Vibration*. Cambridge University Pres, 2000.

[274] von Groll G. and Ewins D. J. The harmonic balance method with arc-lenght continuation in rotor/stator contact problems. *Journal of Sound and Vibration*, 241(2):223–233, 2001. doi:10.1006/jsvi.2000.3298.

[275] Wang G., Chen X.-Y., Qiao F.-L., Wu Z., and Huang N. E. On intrinsic mode function. *Advances in Adaptive Data Analysis*, 2(3):277–293, 2010. doi:10.1142/S1793536910000549.

[276] Wang W., Mottershead J. E., Ihle A., Siebert T., and Schubach H. R. Finite element model updating from full-field vibration measurement using digital image correlation. *Journal of Sound and Vibration*, 330(8):1599–1620, 2011. doi:10.1016/j.jsv.2010.10.036.

[277] Wang Y.-H., Yeh C.-H., Young H.-W. V., Hu K., and Lo M.-T. On the computational complexity of the empirical mode decomposition algorithm. *Physica A: Statistical Mechanics and its Applications*, 400(300):159–167, 2014. doi:10.1016/j.physa.2014.01.020.

[278] Wang Z.-C., Xin Y., and Ren W.-X. Nonlinear structural model updating based on instantaneous frequencies and amplitudes of the decomposed dynamic responses. *Engineering Structures*, 100:189–200, 2015. doi:10.1016/j.engstruct.2015.06.002.

[279] Wardle R., Worden K., and King N. Classification of nonlinearites using neural networks. In *Proceeding of the International Modal Analysis Conference*, pages 980–986, 1997.

[280] White S. W., Kim S. K., Bajaj A. K., Davies P., Showers D. K., and Liedtke P. E. Experimental techniques and identification of nonlinear and viscoelastic properties of flexible polyurethane foam. *Nonlinear Dynamics*, 22(3):281–313, 2000. doi:10.1023/A:1008302208269.

[281] Wiggins S. *Introduction to Applied Nonlinear Dynamical Systems and Chaos*. Springer, 2003. doi:10.1007/b97481.

[282] Worden K. and Becker W. E. On the identification of hysteretic systems. Part II: Bayesian sensitivity analysis and parameter confidence. *Mechanical Systems and Signal Processing*, 29:213–227, 2012. doi:10.1016/j.ymssp.2012.01.005.

[283] Worden K. and Green P. L. A machine learning approach to nonlinear modal analysis. *Mechanical Systems and Signal Processing*, 84, Part B:34 – 53, 2017. doi:10.1016/j.ymssp.2016.04.029.

[284] Worden K. and Hensman J. J. Parameter estimation and model selection for a class of hysteretic systems using Bayesian inference. *Mechanical Systems and Signal Processing*, 32:153–169, 2012. doi:10.1016/j.ymssp.2012.03.019.

[285] Worden K. and Manson G. On the identification of hysteretic systems. Part I: Fitness landscapes and evolutionary identification. *Mechanical Systems and Signal Processing*, 29:201–212, 2012. doi:10.1016/j.ymssp.2012.01.004.

[286] Worden K., Staszewski W. J., and Hensman J. J. Natural computing for mechanical systems research: A tutorial overview. *Mechanical Systems and Signal Processing*, 25(1):4–111, 2011. doi:10.1016/j.ymssp.2010.07.013.

[287] Worden K. and Tomlinson G. R. Modeling and classification of non-linear systems using neural networks - I. Simulation. *Mechanical Systems and Signal Processing*, 8(3):319–356, 1994. doi:10.1006/mssp.1994.1024.

[288] Worden K. and Tomlinson G. R. Nonlinearity in experimental modal analysis. *Philosophical Transactions of the Royal Society A: Mathematical, Physical and Engineering Sciences*, 359(1778):113–130, 2001. doi:10.1098/rsta.2000.0716.

[289] Worden K. and Tomlinson G. R. *Nonlinearity in Structural Dynamics: Detection, Identification and Modelling*. Institute of Physics Publishing, Bristol and Philadelphia, 2001.

[290] Wright J. P. and Pei J.-S. Solving dynamical systems involving piecewise restoring force using state event location. *Journal of Engineering Mechanics*, 138(8):997–1020, 2012. doi:10.1061/(ASCE)EM.1943-7889.0000404.

[291] Wright J. R., Cooper J. E., and Desforges M. J. Normal-mode force appropriation - theory and application. *Mechanical Systems and Signal Processing*, 13(2):217 – 240, 1999. doi:10.1006/mssp.1998.1214.

[292] Wu Z. and Huang N. E. Ensemble Empirical Mode Decomposition: a noise-assisted data analysis method. *Advances in Adaptive Data Analysis*, 1(1):1–41, 2009. doi:10.1142/S1793536909000047.

[293] Wu Z., Yang N., and Yang C. Identification of nonlinear structures by the conditioned reverse path method. *Journal of Aircraft*, 52(2):373–386, 2015. doi:10.2514/1.C032424.

[294] Xun J. and Yan S. A revised Hilbert-Huang transformation based on the neural networks and its application in vibration signal analysis of a deployable structure. *Mechanical Systems and Signal Processing*, 22(7):1705–1723, 2008. doi:10.1016/j.ymssp.2008.02.008.

[295] Yang J. N., Lei Y., Pan S., and Huang N. E. System identification of linear structures based on Hilbert-Huang spectral analysis. Part 1: normal modes. *Earthquake Engineering & Structural Dynamics*, 32(9):1443–1467, 2003. doi:10.1002/eqe.287.

[296] Yang J. N., Lei Y., Pan S., and Huang N. E. System identification of linear structures based on Hilbert-Huang spectral analysis. Part 2: Complex modes. *Earthquake Engineering & Structural Dynamics*, 32(10):1533–1554, 2003. doi:10.1002/eqe.288.

[297] Yang L., Yang Z., Zhou F., and Yang L. A novel envelope model based on convex constrained optimization. *Digital Signal Processing*, 29:138–146, 2014. doi:http://dx.doi.org/10.1016/j.dsp.2014.02.017.

[298] Yang Y., Ng E., Polunin P., Chen Y., Strachan S., Hong V., Ahn C. H., Shoshani O., Shaw S., Dykman M., and Kenny T. Experimental investigation on mode coupling of bulk mode silicon MEMS resonators. In *2015 28th IEEE International Conference on Micro Electro Mechanical Systems (MEMS)*, pages 1008–1011, 2015. doi:10.1109/MEMSYS.2015.7051132.

[299] Yeh J. R., Shien J.-S., and Huang N. E. Complementary ensemble empirical mode decomposition: A novel noise enhanced data analysis method. *Advances in Adaptive Data Analysis*, 2(2):135–156, 2010. doi:10.1142/S1793536910000422.

[300] Zhang G. P. Neural networks for classification: A survey. *IEEE Transactions on Systems, Man, and Cybernetics, Part C (Applications and Reviews)*, 30(4):451–462, 2000. doi:10.1109/5326.897072.

[301] Zhang M. W., Peng Z. K., Dong X. J., Zhang W. M., and Meng G. A forward selection reverse path method for spatial location identification of nonlinearities in MDOF systems. *Nonlinear Dynamics*, 82(3):1379—-1391, 2015. doi:10.1007/s11071-015-2244-5.

[302] Zhou S.-D., Heylen W., Sas P., and Liu L. Parametric modal identification of time-varying structures and the validation approach of modal parameters. *Mechanical Systems and Signal Processing*, 47(1-2):94–119, 2014. doi:10.1016/j.ymssp.2013.07.021.

Appendix A

Methods for non-linear system identification

Non-linear system identification is a vast field in which many methods and approaches have been developed. This appendix complements the literature review in chapter 1 by providing a more complete list of methods with a basic indication of their function (detection, characterisation or quantification) and a few (by far not all) references. It should be noted that the categorisation of the methods can be misleading because the limitations and assumptions are not mentioned. Therefore, even if a method provides all functions, it does not automatically mean that it should be the method of choice in every situation.

Besides the references given, several books and review papers have been published [2, 20, 30, 31, 97, 119, 164, 269, 289]. In the following table over 70 different methods can be found. Some methods have a number of variants and minor modifications, but these are not listed. The methods are color-coded according to their function as:

D : *Detection* - These methods can determine the presence of a structural non-linearity.

S : *Strength of non-linearity* - The strength of non-linearity can be assessed by the visual inspection of the difference between the characteristics of non-linear systems and their linear counter-pairs. This category does not include the methods based on the visual inspection because they are usually very subjective, but it rather focuses on the methods that provide a numerical indication of the non-linearity strength.

T : *Type characterisation* - This category includes methods that allow characterisation of a non-linearity type either by visual inspection or by more sophisticated (potentially automatic) procedures.

L : *Location characterisation* - These methods can assist to decide about the spatial location of the non-linearity within the structure.

F : *Functional (mathematical) form characterisation* - The mathematical expression must often be selected based on the non-linearity type and with the physical understanding of the problem. The possible models of non-linearities are summarised in section 1.1.1. If a method can improve the selection of this model, it is included in this category. Many brute force (trial-error) approaches can be found here as well.

Q : *Quantification* - All the methods that belong to this category can quantify the coefficients of structural non-linearities or obtain a model of the structure without considering the non-linearities explicitly. After the application of these methods the identification procedure is finished.

U : *Uncertainty quantification* - The experimental testing and processing of measured data are subjected to many uncertainties. Although uncertainties are not yet often considered in non-linear dynamics, their quantification is important. The methods in this category attempt to take into account the effect of uncertainty while identifying non-linear behaviour.

NP : *Non-parametric methods* - This marks the methods that do not require a great amount of information to be known or assumed before the identification process. In particular, no specific knowledge of the non-linearity is needed and the estimation of under-lying linear system is not required.

Method	Function						References
Amplitude and frequency modulation	D		T			NP	[180, 184, 185], section 3.4
Bayesian scheme				Q	U		[282, 284, 285]
Bicoherence	D	S				NP	[44, 97]
Bispectrum	D	S	T			NP	[47]
Carpet plot	D		T				[63]
Coherence	D	S				NP	[19, 26, 63, 97, 242]
Conditioned reverse path (CRP)			L	Q			[108, 144, 217, 301]
Corehence	D					NP	[212]
Correlation-based indication functions	D	S				NP	[289]
Correlation coefficient	D	S				NP	[130], section 2.2.3
Complex stiffness method	D		T	Q			[150]
Complexification-averaging (CxA)				Q			[118], section 4.2.3
Conjugate-pair decomposition	D		T	Q			[181, 184]
Control-based continuation	D		T			NP	[16, 17, 243]
Damage localisation techniques			L				[145]
Describing function inversion	D		T	L	Q		[15, 177]
Distortion of frequency response functions	D		T			NP	[63, 234, 268], chapter 2
Direct parameter estimation				Q			[31, 153]
Direct quadrature (DQ)	D		T			NP	[86, 102], section 3.3.4
Equivalent linearisation				Q			[286]
Energy operators	D						[49, 104, 229], section 3.3.5
Footprint libraries	D		T				[83]
Forcevib	D		T	Q		NP	[68]
Formap identification method	D		T	Q		NP	[74]
Freevib	D		T	Q		NP	[67], section 5.2.2

Frequency-domain ARX model				Q		[1]
Frequency domain non-linear subspace identification (FNSI)				Q		[163]
Gabor transform	D		T	Q	NP	[77, 250]
Genetic algorithm			T	Q		[83]
Generalised zero-crossing	D		T	Q	NP	[104], section 3.3.7
Harmonic detection	D				NP	[150]
Harmonic distortion	D				NP	[289]
Higher-order frequency response functions	D		T		NP	[28, 256]
Higher-order spectra	D	S	T		NP	[44]
Hilbert transform describes	D	S				[263], section 2.2.3
Hilbert transform in the frequency domain	D		T		NP	[71, 263, 289], chapter 2
Hilbert transform in the time domain	D		T	Q	NP	[71, 104, 181], chapter 3
Hilbert-Huang transform (HHT)	D		T	Q	NP	[103, 292], chapter 3
Hilbert vibration decomposition (HVD)	D		T	Q	NP	[71, 73], section 6.2
Homogeneity test	D				NP	[31, 130, 289]
Identification based on multi-scale dynamic partition	D		T	Q		[39, 62, 137], section 5.1
Kalman filters				Q		[20, 286]
Linearity J-factor factor	D	S			NP	[123]
Linearity plots	D		T			[82]
Machine learning				Q	U NP	[66, 194, 286]
NARMAX models				Q		[20]
Neural networks for classification	D		T	L		[125, 126, 279], chapter 2
Nearest neighbour approach			T	L		[264]
Non-causal power ratio (NPR)	D				NP	[121]
Non-linearity indexes (NLIs)	D	S	T		NP	reviewed in [97], section 2.2.3
Non-linear identification through feedback of the outputs (NIFO)				Q		[3, 4, 92]
Non-linear modal grade	D	S				[244]

Non-linear output FRFs	D		T		Q		[133]
Non-linear resonant decay (force appropriation)	D		T		Q		[159, 205]
Normal non-linear modes (NNMs)	D		T			NP	[117, 191, 192, 266]
Normalised Hilbert transform (NHT)	D		T		Q	NP	[104], section 3.3.3
Pattern recognition or classification			T				[83, 264]
Principal component analysis	D		T		Q	NP	[113, 289]
Reciprocal modal vectors	D						[41]
Reciprocity test	D					NP	[289]
Residual autocorrelation functions	D					NP	[5]
Restoring force surface (RFS)	D		T	L	Q	NP	[8, 23, 48, 148, 166]
Sig-function	D	S				NP	[150]
Significance factor				F			[12]
Stabilisation diagram	D						[146, 162, 163, 169]
Structural model updating and upgrading			T	L	F	Q	[32, 65, 78, 160]
Superposition principle	D					NP	[289]
Short-time Fourier transform (STFT)	D		T		Q	NP	[76, 161, 173]
Time domain Fourier filter output (TDFFO)					Q		[226]
Time domain non-linear subspace identification (TNSI)					Q		[146, 167]
Type-analysis correlation	D		T	L			[141]
Volterra kernels processing	D		T			NP	[6]
Volterra series	D		T			NP	[36, 37, 289]
Wavelet transform (WT)	D		T		Q	NP	[10, 76, 161, 189]
Wigner-Ville distribution	D		T		Q	NP	[75, 161]
Zero-crossing methods (ZC)	D		T		Q	NP	[104, 207], section 3.3.6

Appendix B

Numerical implementation of complex non-linear modes

The theory of the complex non-linear modes (CNMs) of mechanical systems was described in section 4.2.1 and their relation to the Hilbert-Huang transform was investigated in chapter 4. They were also used in chapter 5 to develop an approach to non-linear modal analysis. This appendix aims to complement section 4.2.1 by providing a description of the numerical implementation. The implementation is very similar to the conventional harmonic balance method described, for example in [29, 54, 156, 202, 227]. The use of the CNMs has been demonstrated on a number of systems in this thesis and one more verification example created by a two-degree-of-freedom system with Coulomb friction from [128, 134, 135] is given in the second part of this appendix.

B.1 Numerical implementation

An autonomous general dynamic system is considered

$$\mathbf{M}\ddot{\mathbf{x}} + \mathbf{C}\dot{\mathbf{x}} + \mathbf{K}\mathbf{x} + \mathbf{f}_{\mathrm{nl}}(\mathbf{x}, \dot{\mathbf{x}}) = \mathbf{0} \tag{B.1}$$

where $\mathbf{M}$, $\mathbf{C}$ and $\mathbf{K}$ are $n \times n$ mass, damping and stiffness matrices, respectively, and $\mathbf{x} = \mathbf{x}(t)$ is an $n \times 1$ vector of generalised coordinates. The $n \times 1$ vector $\mathbf{f}_{\mathrm{nl}}(\mathbf{x}, \dot{\mathbf{x}})$ comprises all non-linear effects, which depend on the displacement and velocity. In line with the definition of the complex non-linear mode in Eq. (4.2), the solution is numerically sought

in a form of generalised Fourier series

$$\mathbf{x}(t) = q \left\{ \mathbf{c}_0 + \sum_{k=1}^{N_h} \mathrm{e}^{-k\delta t} \left(\mathbf{s}_k \sin(k\omega t) + \mathbf{c}_k \cos(k\omega t) \right) \right\}, \tag{B.2}$$

where $\mathbf{c}_0$, $\mathbf{s}_k$ and $\mathbf{c}_k$ are the vectors $(n \times 1)$ of the Fourier coefficients related to zeroth harmonic, sine and cosine terms of k-th harmonic, N_h is the total number of harmonics and q is a modal amplitude. Equation (B.2) is equivalent to Eq. (4.2) with the difference that the former is written using the real coefficients whereas the latter using the complex representation which is better for a theoretical description, but unsuitable for the numerical implementation.

The eigenvalue of the mode is defined using the natural angular frequency ω_0 and modal damping ratio ζ as $\lambda = -\delta + \mathrm{i}\omega = -\zeta\omega_0 + \mathrm{i}\omega_0\sqrt{1-\zeta^2}$, where δ is a damping rate and ω is a damped natural angular frequency. The Fourier coefficients, which represent the eigenvector of the complex mode in the frequency domain, are organised into $(2N_h + 1)n \times 1$ vector as

$$\mathbf{z} = \left[\mathbf{c}_0,\ \mathbf{s}_1,\ \mathbf{c}_1,\ \mathbf{s}_2,\ \mathbf{c}_2,\ \ldots,\ \mathbf{s}_{N_h},\ \mathbf{c}_{N_h} \right]. \tag{B.3}$$

For the evaluation of the non-linear effects that are velocity dependent, the velocity can be expressed using

$$\dot{\mathbf{z}} = \nabla(\lambda)\mathbf{z}, \tag{B.4}$$

where the differential operator $\nabla(\lambda)$ is given by

$$\nabla(\lambda) = \mathrm{diag}\left[\mathbf{0},\ \nabla_1,\ \ldots,\ \nabla_k,\ \ldots,\ \nabla_{N_h} \right], \quad \text{with} \quad \nabla_k = \nabla_k(\lambda) = k \begin{bmatrix} -\delta & -\omega \\ \omega & -\delta \end{bmatrix}. \tag{B.5}$$

It should be noted that this operator is one of the main differences between the CNM and HBM in which it reads

$$\nabla_k(\omega) = k \begin{bmatrix} 0 & -\omega \\ \omega & 0 \end{bmatrix}. \tag{B.6}$$

Using the operator $\nabla(\lambda)$ it is possible to define the dynamic stiffness matrix of the underlying linear system [54] as

$$\mathbf{A}(\lambda) = \nabla(\lambda)^2 \otimes \mathbf{M} + \nabla(\lambda) \otimes \mathbf{C} + \mathbb{I}_{2N_h+1} \otimes \mathbf{K}, \tag{B.7}$$

where $\otimes$ is the Kronecker tensor product and $\mathbb{I}_{2N_h+1}$ is an identity matrix of the size $2N_h+1$. The dynamic stiffness matrix $\mathbf{A}(\lambda)$ has the size $(2N_h+1)n \times (2N_h+1)n$.

The non-linear term $\mathbf{f}_{\mathrm{nl}}(\mathbf{x}, \dot{\mathbf{x}})$ which depends on the displacement and velocity cannot be usually evaluated analytically in the frequency domain. Therefore, an alternating frequency-time domain procedure (AFT) [29] is very often used:

$$\mathbf{z} \xrightarrow{\mathrm{FFT}^{-1}} \mathbf{x} \longrightarrow \mathbf{f}(\mathbf{x}, \dot{\mathbf{x}}) \xrightarrow{\mathrm{FFT}} \mathbf{b}(\mathbf{z}) \tag{B.8}$$

The unknown coefficients $\mathbf{z}$ are transformed from the frequency domain to the time domain using the inverse Fourier transform, the non-linear (and in the case of the HBM also the excitation) forces are evaluated in the time domain and transformed back to the frequency domain by means of the direct Fourier transform. As emphasised in section 4.2.1 the periodic representation of the displacement and the velocity must be used in the AFT procedure. The direct and inverse Fourier transform can be computed effectively using the operator $\mathbf{\Gamma}(\omega)$. The inverse Fourier transform can be written as a linear operation

$$\mathbf{x}^{\dagger} = \mathbf{\Gamma}(\omega)\mathbf{z}q \tag{B.9}$$

with the $nN_t \times (2N_h+1)n$ operator given by

$$\mathbf{\Gamma}(\omega) = \begin{bmatrix} \mathbb{I}_n \otimes \begin{bmatrix} 1 \\ 1 \\ \vdots \\ 1 \end{bmatrix}, & \mathbb{I}_n \otimes \begin{bmatrix} \sin(\omega t_1) \\ \sin(\omega t_2) \\ \vdots \\ \sin(\omega t_{N_t}) \end{bmatrix}, & \mathbb{I}_n \otimes \begin{bmatrix} \cos(\omega t_1) \\ \cos(\omega t_2) \\ \vdots \\ \cos(\omega t_{N_t}) \end{bmatrix}, \\ \dots, & \mathbb{I}_n \otimes \begin{bmatrix} \sin(N_h\omega t_1) \\ \sin(N_h\omega t_2) \\ \vdots \\ \sin(N_h\omega t_{N_t}) \end{bmatrix}, & \mathbb{I}_n \otimes \begin{bmatrix} \cos(N_h\omega t_1) \\ \cos(N_h\omega t_2) \\ \vdots \\ \cos(N_h\omega t_{N_t}) \end{bmatrix} \end{bmatrix}, \tag{B.10}$$

where N_t is the number of time samples used to approximate a single period of oscillation. The vector of the size $nN_t \times 1$ containing these time samples will be organised as

$$\mathbf{x}^{\dagger} = [x_1(t_1),\ \dots,\ x_1(t_{N_t}),\ \dots,\ \ x_n(t_1),\ \dots,\ x_n(t_{N_t})]^T \tag{B.11}$$

and must be appropriately used to evaluate the non-linear restoring forces $\mathbf{f}_{\mathrm{nl}}(\mathbf{x}, \dot{\mathbf{x}})$. The evaluated non-linear forces $\mathbf{f}^{\dagger}$ are transformed back to the frequency domain using the

direct Fourier transform as

$$\mathbf{b}(\mathbf{z}) = \mathbf{\Gamma}(\omega)^{+}\mathbf{f}^{\dagger}, \tag{B.12}$$

where $(\bullet)^{+}$ denotes the Moore-Penrose pseudo-inverse. The AFT procedure must be repeated in each iteration of the solver.

In order to find the unknown Fourier coefficients $\mathbf{z}$ and modal properties ω and δ for a given modal amplitude q the following system of non-linear algebraic equations needs to be solved

$$\mathbf{A}(\lambda)\mathbf{z}q + \mathbf{b}(\mathbf{z}) = \mathbf{0}. \tag{B.13}$$

However, as mentioned in section 4.2.1 two equations are missing so the mode normalisation must be introduced. The normalisation with respect to the selected degree-of-freedom can be used

$$s_1 = q_s, \quad c_1 = q_c. \tag{B.14}$$

where q_s and q_c are the defined modal amplitudes of the sine and cosine part of the first harmonic of the selected degree-of-freedom. Although the above normalisation is easier to numerically implement, the mass normalisation has been used in this thesis, because the reduced order model in chapter 4 required mass normalised non-linear modes. Two normalisation conditions must be enforced

$$\mathbf{\Psi}_1^H \mathbf{M} \mathbf{\Psi}_1 = 1, \quad \Re\{\mathbf{t}^{\mathrm{H}} \mathbf{\Psi}_1\} = 0, \tag{B.15}$$

where $\mathbf{t}$ is a complex vector and $\mathbf{\Psi}_1$ is the first harmonic of a mode shape. The first condition represents an amplitude constrain while the second provides a phase normalisation.

Equation (B.13) subjected to either the coordinate normalisation (Eq. (B.14)) or to the mass normalisation (Eq. (B.15)) can now be solved for $\mathbf{z}$, ω and δ. The solution for a very low modal amplitude can be obtained by a Newton-like solver with the linear modal properties as a starting guess. However, since the modal properties are amplitude-dependent, it is beneficial to use a continuation procedure on the modal amplitude $q \in (q_{\min}, q_{\max})$.

There are many continuation schemes available in literature [239]. Every continuation method has three basic steps, namely predictor, corrector and the step length adaptation. The prediction using a secant method and the correction via arc-length continuation worked very well for the systems considered in this thesis. The continuation procedure consisted of

1. The prediction of the next solution point using a secant method as

$$\mathbf{y}^{(i+2)} = \mathbf{y}^{(i+1)} + s[\mathbf{y}^{(i+1)} - \mathbf{y}^{(i)}], \tag{B.16}$$

   where s is a step length, $\mathbf{y} = [q, \omega, \delta, \mathbf{z}]^T$ is an extended vector of unknowns, $\mathbf{y}^{(i+1)}$ and $\mathbf{y}^{(i)}$ are the last two converged solutions and $\mathbf{y}^{(i+2)}$ is a new starting point which will be updated in the correction step to obtain the correct solution.

2. The correction was performed using an extended system of equations

$$\begin{bmatrix} ||\mathbf{y} - \mathbf{y}^{(i+1)}|| - s \\ \mathbf{A}(\lambda)\mathbf{z}q - \mathbf{b}(\mathbf{z}) \end{bmatrix} = \begin{bmatrix} 0 \\ \mathbf{0} \end{bmatrix}. \tag{B.17}$$

   The first equation represents the arc-length continuation and the second one is Eq. (B.13) in which the coordinate normalisation given by Eq. (B.14) has been considered or the mass normalisation given by Eq. (B.15) enforced via a constrained optimisation using the Lagrange multipliers. In the harmonic balance method the normalisation is not necessary so the correlation step is much simpler.

3. The step length adaptation was based on the number of iterations of the corrector. By changing the step adaptation conditions, the performance of the continuation can be influenced. Typically, the step s was doubled when the corrector converged in less than 5 iterations, remained unchanged when the convergence was reached in 5 to 10 iterations and was halved when the number of correction iterations exceeded 10.

The continuation procedure with an adaptive step length has a very good performance because if the solution changes rapidly with the modal amplitude, the length can be shorten to avoid convergence issues. On the other hand, if the solution does not change, the step can be longer. This leads to the time-efficient computation and unstable solutions can be also tracked. If the results are required in equidistant steps, for instance, for the computation of the reduced order model in chapter 4, the results must be appropriately interpolated.

The described numerical procedure has been implemented and used throughout this thesis. However, it should be noted that it is suitable only for smaller systems because it omits the condensation of the equations of motion [156, 202] into the non-linear degrees-of-freedom and can be therefore time-consuming for large systems.

B.2 Numerical verification case

A two-degree-of-freedom system with a Coulomb friction element is considered as a verification case of the numerical implementation of the CNMs. The same system was used in a number of studies, including [128, 134, 135], because it is a numerically challenging example of a system with strong non-linear behaviour.

The system consists of two masses connected by two linear springs as depicted in Fig. B.1. The non-linear behaviour is introduced by Coulomb friction between the right

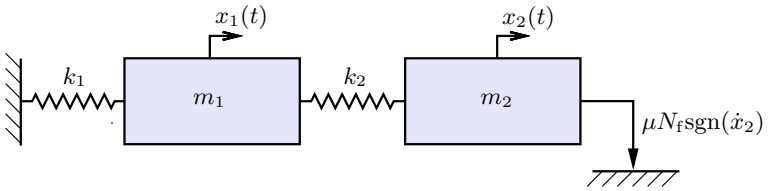

Figure B.1 Two-degree of freedom system with friction

mass and the ground. The system is allowed to vibrate only in the horizontal direction. This system can be described by Eq. (B.1) in which

$$\mathbf{M} = \begin{bmatrix} m_1 & 0 \\ 0 & m_2 \end{bmatrix}, \quad \mathbf{K} = \begin{bmatrix} k_1 + k_2 & -k_2 \\ -k_2 & k_2 \end{bmatrix}, \quad \mathbf{f}_\mathrm{nl}(\mathbf{x}, \dot{\mathbf{x}}) = \begin{bmatrix} 0 \\ \mu N_\mathrm{f} \tanh\left(\frac{\dot{x}_2}{\epsilon}\right) \end{bmatrix}, \tag{B.18}$$

where $m_1 = 1\,\mathrm{kg}$, $m_2 = 0.02\,\mathrm{kg}$, $k_1 = 600\,\mathrm{N\,m^{-1}}$, $k_2 = 40\,\mathrm{N\,m^{-1}}$ and linear damping equivalent to the modal damping ratio of 0.1 % was also introduced. Although the Coulomb friction is theoretically described by the signum function, it is usually approximated using an hyperbolic tangent due to improved numerical properties. The friction coefficient was $\mu = 0.2$, normal force $N_\mathrm{f} = 10\,\mathrm{N}$ and a small parameter $\epsilon = 0.01$. Generally, a smaller ϵ leads to a better approximation of the signum function.

The computed backbones and a set of frequency response functions (computed using the harmonic balance method implemented based on a similar procedure as the CNMs) can be seen in Fig. B.2. Thirteen harmonics were used in both non-linear modal analysis and harmonic balance method to capture strong non-linear behaviour of the system.

Two limit states can be recognised from the backbone in Fig. B.2(a). For the very low amplitudes (less than 0.07 m) the friction element is fully stuck so the displacement of the right mass is equal to zero. For very high amplitudes, on the other hand, the friction contact is fully slipping, so the modal properties approach the modal properties of the underlying linear system. As the modal amplitude increases between these two limit states the transition zone of the partial slip occurs. As seen in Fig. B.2(c) and

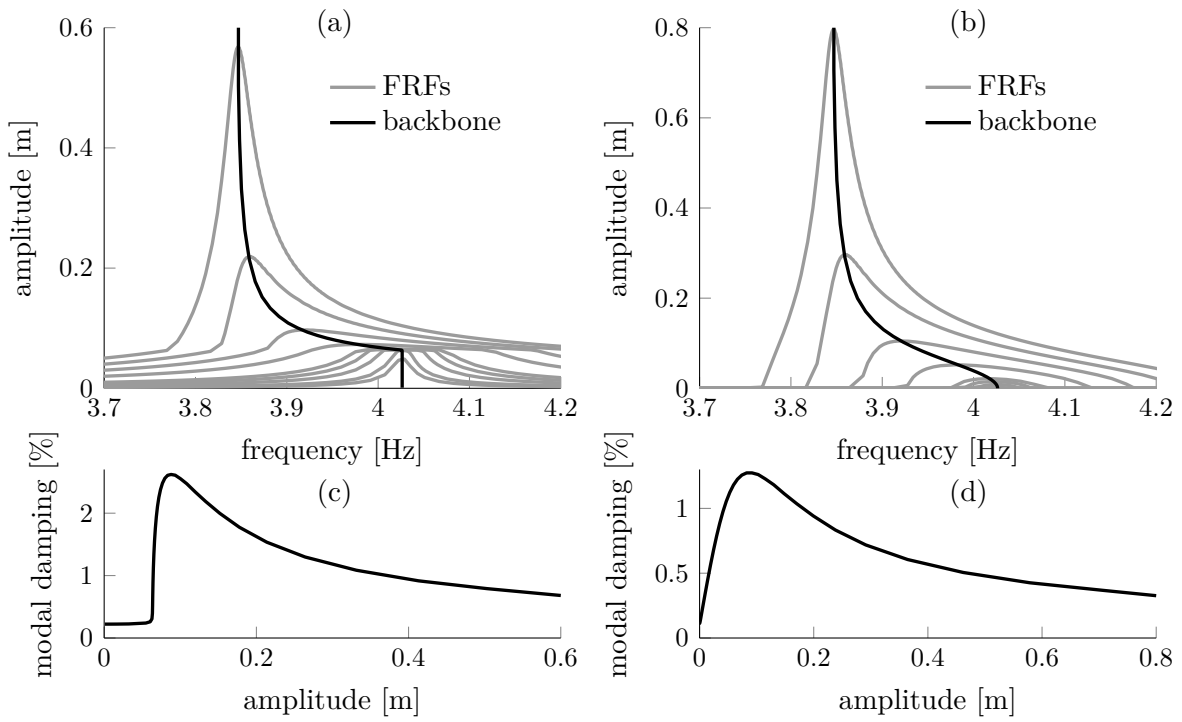

Figure B.2 The first vibration mode of the system with the Coulomb friction: (a) backbones and frequency response functions of the first mass, (b) backbones and frequency response functions of the second mass, (c) modal damping ratio of the first mass, and (d) modal damping ratio of the second mass

Fig. B.2(d) the modal damping reaches its maximum value in the region of the partial slip. Therefore, as also discussed in [129], the friction joints should be ideally designed in such a way that they operate in this region of the maximum dissipation.

Since the presented results are in accordance with similar studies [128, 134, 135], the numerical procedure used to compute the CNMs in this thesis has been verified.

Appendix C

Whittaker smoother

The Whittaker smoother [60] is a data smoothing method that fits the data using the penalty least square method by balancing the fidelity of the data and their roughness:

$$\min_{y} \left[\sum_{i} \underbrace{(x_i - y_i)^2}_{\text{fidelity}} + \lambda_{\mathrm{W}} \sum_{i} \underbrace{(y_i - 2y_{i-1} + y_{i-2})^2}_{\text{smoothness}} \right], \tag{C.1}$$

where $x_i = x(t_i)$ is an initial (noisy) signal, $y_i = y(t_i)$ is a smoothed signal and λ_{W} is a smoothing parameter. The smoothing parameter weights the fidelity and the smoothness of the data. The requirement of the smoothness is stronger for larger values of λ_{W}. Therefore, while y becomes smoother for larger λ_{W}, the fit of the original data x becomes worse. The appropriate λ_{W} might be chosen by tuning it until the resulting series y is visually satisfying. However, this parameter can be also determined automatically (and more objectively) based on the leave-one-out cross validation strategy combined with minimum search optimisation.

The leave-one-out cross validation strategy is one of many cross validation procedures used in a machine learning community [255, 286]. In case of the Whittaker smoother, this strategy consists of removing one element of the series x, smoothing the remaining data, and evaluating the error of the prediction for the removed element. After repeating this process for all elements in x, the total standard error can be calculated [60, 255]. Then, the smoothing parameter λ_{W} for which this total standard error is at its minimum is taken as the optimal value.

The Whittaker smoother was originally proposed in chemical engineering [60], but it has many attractive properties for the non-linear system identification as well:

- It is very quick even if the cross validation procedure is used.

- It handles missing data and adapts to boundaries automatically, so it does not suffer from any end effects.
- The smoothness is controlled using a single parameter which can be selected automatically.
- It does not assume any particular form (polynomial or sinusoidal) of the signal [13].
- Since the smoothness of the derivative is required, the methods that use this derivative, such as the Freevib algorithm in section 5.2.2 or the zero-crossing method for systems with asymmetric restoring forces (ZCA) in section 6.3, can benefit from the use of the Whittaker smoother.

The Whittaker smoother used in this thesis has been implemented based on the pseudo-code provided in [60] and complemented by an optimisation procedure to determine the smoothing parameter λ_W automatically using the leave-one-out cross validation strategy.

Index